AN INVESTIGATION INTO THE PUNCHING SHEAR FAILURE IN R.C. WAFFLE SLABS SUBJECTED TO CONCENTRATED LOAD

Shuangxi Pei

A Thesis submitted in partial fulfilment
of the requirements of the
University of Abertay Dundee
for the degree of Doctor of Philosophy

November 1994

I certify that this thesis is the true and accurate version of the thesis approved by the examiners

Signed..... Date.....23/1/95.....

Director of Studies

ACKNOWLEDGEMENT

The author would like to express his sincere gratitude to his Supervisor Prof. Susanta Sarkar, Head of Department of Civil Engineering, Building & Surveying, for his encouragement, guidance and supervision given to the author throughout the course of this research which have been invaluable and have made this research possible.

The author is indebted to his external supervisor Dr S L Ho, a Consultant Engineer in Ove Arup & Partners, Scotland, for the valuable advice received through frequent meetings with the author. Thanks are also due to my second supervisor Mr M Khalid, Lecturer in the Department of Civil Engineering, Surveying & Building, for his helpful discussion and advice.

Grateful thanks are given to the entire technical staff of the Department of Civil Engineering, Surveying & Building for their practical assistance, preparing and testing the models and especially to Mr. J. Galloway for organising the preparation work. Thanks are also due to the staff of the Computer Centre particularly Mr S L Gardner for his help in using the computer.

The Author would like to record his thanks to University of Abertay Dundee for providing the research studentship which enabled him to carry out the work.

Finally, the author would like to take this opportunity to express his greatest appreciation and gratitude to his wife, parents and family members, for their patience and support throughout this work.

AN INVESTIGATION INTO THE PUNCHING SHEAR FAILURE IN R.C. WAFFLE SLABS SUBJECTED CONCENTRATED LOAD

Shuangxi Pei, B. Eng., M. Eng.

ABSTRACT

The existence of recesses (hollow pots) in hollow ribbed (waffle) reinforced concrete slabs makes the slab more vulnerable when subjected to concentrated loads. The punching shear failure inside waffle slabs has not been thoroughly investigated and this is also reflected in the current code of practice, which, in the main, relates the design of punching shear in waffle slabs to that in solid slabs. In this study, both experimental and theoretical studies have been conducted to investigate the failure pattern and ultimate failure load of punching shear failure of waffle slabs.

Twelve model waffle slabs, 1/3 scale, were tested to failure to study the failure pattern, the influence of the local configuration of the ribs and presence of local solid area, and the effectiveness of the stirrups supplied inside the ribs. The experimental results were compared with the calculated results by following the provisions of BS8110.

The theoretical study was carried out in parallel; the Upper Bound Analysis and Non-linear Finite Element Analysis were employed to predict the ultimate punching load and also to serve the purpose of investigating the failure mechanism. Alternative methods, modified from the methods recommended by the code, are proposed to predict the punching load.

From the comparison of punching loads obtained by tests and calculation using BS8110, it was found that the punching capacity of waffle slabs without stirrups was under-estimated and the shear resistance of stirrups was over-estimated.

By the experimental study and theoretical study, it was found that the punching capacity of waffle slabs were not sensitive to the loading directions nor to the local configuration of the ribs in the vicinity of the loading pad; the punching load was dissipated to a larger area than the loading pad and resisted by both the orthogonal ribs and deck of the slab. The use of local solid area in the waffle slabs can increase the punching shear capacity more efficiently than the use of shear reinforcements; the upper bound analysis revealed that the dimension of the punching perimeter would be reduced by the supplement of the stirrups and resulted in less strength of the stirrups being mobilised than expected.

By comparing the results obtained from tests with those obtained employing various analytical methods two methods are recommended for the prediction of the punching shear capacity of R.C. waffle slabs with a degree of confidence because of their inherent simplicity and accuracy, which are the **Upper Bound Analysis** and the **Alternative Method using the Affine Solid Slabs**.

LIST OF TABLES

LIST OF FIGURES

NOTATIONS

a side dimension of the square recess;
a_{sv} cross section area of a leg of a stirrup;
A area of the nominal failure surface;
A_{rib} area of a rib;
A_{deck} area of the deck of the section in a recess;
A_{sv} cross section area of all legs in a stirrup;
b width of rib;
B dimension of nominal punching perimeter;
C cohesion factor; or
dimension of the rectangular loaded area;
d effective depth of the slab; or
dimension of the inner perimeter of the failure surface in upper bound analysis;
d_1 dimension of the outer perimeter of the failure surface in upper bound analysis;
d_{aff} equivalent depth of the affine solid slab converted from a waffle slab;
E elastic modulus;
f_c compressive strength of concrete cylinder;
f_c' plastic (effective) compressive strength of concrete;
f_{cu} compressive strength of concrete cube;
f_t tensile strength of concrete;
f_t' plastic (effective) tensile strength of concrete; or
uniaxial tensile (fracture) strength of concrete for finite element analysis;
f_{sv} strength of stirrups;
F_k coefficient relating to the plastic compressive strength of concrete;
F_{sv} strength reduction factor for stirrups considering the poor anchorage;
h total depth of slab;
$\overline{h}$ depth of the deck;
m ratio between plastic compressive and tensile strengths;
n_1 coefficient factor converting depth of waffle slab into the affine solid slab;
N number of ribs intersected with the nominal punching perimeter;
P_B punching failure load of waffle slab in deck-bottom case — downward loading;
P_c shear resistance of concrete;
P_{DB} deck's shear resistance of waffle slabs in deck-bottom case;
P_{DT} deck's shear resistance of waffle slabs in deck-top case;
P_{rib} shear resistance of the ribs in waffle slabs;
P_s punching failure load of solid slab;
P_{sv} shear resistance of stirrups;

P_T punching failure load of waffle slab in deck-top case — downward loading;
S total area nominal failure surface;
S_{deck} total area of the deck intersected with the nominal punching perimeter;
S_{rib} total area of the ribs intersected with the nominal punching perimeter;
S_{sv} total area of the stirrups inside the failure zone;
t depth of deck of waffle slab;
U periphery of the critical (nominal) punching perimeter;
U_o periphery of the loading pad;

$\overline{\alpha}$ average inclination angle of the failure surface in relative to vertical plane;
ε_{uc} maximum tensile strain at which the shear retention and tensile stiffening will become zero.
φ internal friction angle of material;
ρ flexural steel ratio;
ρ_x, ρ_y directional void ratio of recess;
ρ_{xy} void (area) ration of the recess;
ρ_{sv} steel content of the stirrups inside ribs;
υ_c, ν_c effective compressive strength factor; or
critical (nominal) shear strength of concrete;
ν_{sv} critical (nominal) shear strength provided by stirrups;
υ_t strength effective factor for tension;

CONTENTS

CHAPTER 1

INTRODUCTION

1.1 INTRODUCTION

Reinforced concrete waffle slab construction has been used to improve the efficiency of concrete slab systems since 1950's. With advances in the fabrication of formwork and concrete handling and placing, waffle slabs are now widely used in industrial and public buildings, multi-storey car parks and highway bridges, owing to their structural, architectural and economic benefits. A reinforced concrete waffle slab consists essentially of a relatively thin top slab, acting compositely with an orthogonal grid of beams. The recesses in the slab, often cast using either removable or expendable forms, decrease the weight of the slab and allow the use of large effective depth without the accompanying dead weight; this leads to the structural benefits of small deflection and construction economics in slabs with spans larger than 10m. The architectural benefits are the long spans providing large uninterrupted floor space and special architectural effect created by the recesses in the slabs.

Waffle slabs are usually designed as either flat slabs or two-way slabs, depending on where recesses are avoided to form the solid areas. In the flat slab configuration, the solid areas are near the column and are comparable to a drop panel or column capital, as they provide a path for the shear transfer and the extra compression area in the highly stressed negative-moment regions surrounding the columns. In the two-way slab configuration, the solid areas are along the column lines and considered as beams since they are areas of concentrated flexural stiffness, even though they do not extend below the soffit of the slabs.

The relatively close spacing of ribs in waffle slabs is considered to produce a response to loads which is closer to that of a solid slab, rather than to a series of inter-connecting beams. Current British Standard[12] recommends ultimate load design of waffle slabs using the provisions for the design of solid slabs, provided certain requirements in respect of the structural dimensions, rib spacing and suitable reinforcement are satisfied. However, the actual behaviour of this type of structure is rather complicated due to the interaction between the top slab and the grillage of monolithically cast beams.

Since the initial interest in waffle slabs in 1950's there have been only a few research investigations into the behaviour of R.C. waffle slabs. Helal[30], Testa and Levy[60], Resissm and Skoal[54], Tebbet[61] worked on elastic analysis of the flexural behaviour of slabs under uniform load; Ajdukiewicz and Kliszczewics[5] on the ultimate flexural load of slabs under uniform load; Marshall[44] on the ultimate flexural load of two-way slabs under uniform load; Ho[31] on the ultimate flexural load of both two-way and flat slabs under both uniform and concentrated loads. These researchers were mainly engaged in the study of the flexural capacity of a full panel or multi panels of slabs; the results from these studies showed that the flexural capacity of waffle slabs was close to that of solid slabs although the distribution of moment in the span and support varied between a solid slab and a waffle slab; the methods to calculate the flexural load of solid slabs can be applied to waffle slabs by modifying the section properties of the waffle slabs; the compressive membrane action in R.C. waffle slabs is effective and can substantially increase the flexural capacity of the slabs.

In the design of R.C. waffle slabs, especially in the type of flat slab configuration, the shear capacity is equally of major concern as the flexural capacity. Large shear forces exist in the vicinity of the slab-column connections; concentrated loads may exist in the middle of a slab panel due to temporary supports employed during construction stage. Large concentrated loads can lead to brittle failure by punching shear in slabs. Waffle slabs, with the recesses inside slab, use less volume of concrete compared to solid slabs, and they are more vulnerable to large shear forces. Three tests[40] of different load patterns on a building floor, constructed of multi-panel waffle slabs, in the USA showed that all the tests were characterised by the punching shear failure near the slab-column connections, even though local solid areas were provided in slab-column connections.

Research investigations into the shear behaviour of R.C. waffle slabs are almost non-existed; this is obviously inappropriate given the increasing popularity of R.C waffle slabs. The proper design of the waffle slabs can only be achieved by considering not only the flexural capacity but also the shear capacity, and in some sense the latter is more critical as the former is less affected by the recesses and is also enhanced by the compressive membrane enhancement.

The shear failure in R.C beams and slabs is an interesting but fairly complicated subject. Moe[45] conducted a series of experiments on the punching shear failure on R.C. solid slabs, which laid the foundation for the provisions in the codes of practice regarding the shear design of flat slabs. Elstner and Hognestad[26] also did the

experimental and theoretical study on the punching shear phenomena. In recent years, experimental studies by Regan[50] and other researchers lead to the update of the provisions relating to shear design of slabs during the revision of CP110[13] to BS8110[12].

A lot of effort has been made by numerous researchers to study the mechanism of punching shear failure and various failure models have been proposed. Braestup[11] used the plastic theory (upper bound method) with the modified Mohr-Columnb failure criteria; Jiang[34] simplified the method by using a parabolic Mohr-Columnb criteria; and Bortolotti[10] further improved the method by considering the strain softening in the concrete. Broms[14] used the equilibrium method and Gonzalez-Vidosa[29] used the non-linear finite element method. From the various theoretical studies, it appears that the proper failure model is still not clear, the results of theoretical analysis being not as accurate as those obtained by empirical methods. This is one of the reasons why the theoretical approach on the punching shear has not been adopted in the various codes of practice.

In the code of practice BS8110[12], the method adopted for the punching shear design of R.C. waffle slabs is a mixture of the methods for beams and solid slabs, with some special requirements for the geometric configuration and reinforcement detail. The principal concept is that a concentrated load is equally distributed to a group of ribs which intersect with the critical (nominal) punching perimeter; the shear capacity of each rib is the same as that of beams. Such a design method has certainly simplified the work for engineers; however, its applicability needs to be examined because of the following reasons:

First, a waffle slab is a composite between the orthogonal ribs and the top deck; how they respond to the punching shear is not clear and therefore the simplification employed in the codes of practice has to be examined. Second, the design formulae in the code were obtained from studies on solid slabs and most of the related parameters had empirical characteristics and these were determined from experiments on solid slabs; their application to waffle slabs has not been validated. Third, the code suggests counting the number of ribs intersecting with the critical perimeters to calculate the shear resistance; this could lead to large variation in results, as the same size of nominal perimeter can intersect with different number of ribs depending on the position of the nominal perimeter on the slab and the configuration of the ribs near the loading position; this needs to be justified.

With the problems mentioned above, it appears necessary to conduct an experimental/theoretical research on the shear behaviour of waffle slabs under concentrated load and then evaluate the methods in the current codes of practice on the shear capacity of R.C. waffle slabs by comparing the test results with the calculated ones.

1.2 AIM OF THE PROJECT

As mentioned before, the current research is to investigate the shear behaviour of the waffle slabs and to evaluate the methods recommended by the codes in calculating the shear capacity of waffle slabs, and if necessary, either to find new methods or to modify existing methods for calculating the punching capacity of waffle slabs. These aims can be broken down into the following specific objectives of the project:

a) Study on the Punching Shear Behaviour of Waffle Slabs

(i) the failure process and cracking development in the slab during the loading;
(ii) the final crack pattern in the slab; the difference and similarity between waffle slab and solid slab;
(iii) do the ribs and deck act compositely to resist the applied load or do the ribs mainly react?
(iv) the difference of the punching shear resistance on different parts of the waffle slab; the difference of the resistance for upwards and downward loading;
(v) the effectiveness of the local solid area in enhancing the shear capacity, and the effectiveness of the stirrups in increasing the load capacity.

(b) Evaluation of BS8110's Method of Predicting the Punching Shear Load

(i) the evaluation of BS8110's method for waffle slabs without shear reinforcements;
(ii) the evaluation of BS8110's method for waffle slabs with shear reinforcements;
(iii) if necessary, to modify the design method.

Two aspects of the investigation were conducted in parallel, viz.:

(a) experimental investigation using 1/3 scale model waffle slabs considering the following influences:

(i) different loading directions or the punching locations; two cases are considered, one is in the vicinity of slab-column connection area (upward loading) and the other in the middle of a slab panel (downward loading);
(ii) different configuration of the ribs in the area near the loading pad;
(iii) slabs with and without local solid area;
(iv) slabs with and without stirrups.

(b) analytical investigation into the load capacity of the waffle slabs using the following methods:

(i) the ultimate load analysis based on the plastic theory employing a modified Mohr-Coulomb criteria for concrete;
(ii) non-linear finite element analysis employing both the Mohr-Coulomb criteria and the concrete crack model for concrete;
(iv) alternative methods are proposed and examined in calculating the load capacity.

The test results are compared with the computed results obtained by various methods. By conducting this programme of investigation, it was expected that it would be possible to postulate a set of design criteria for the punching shear on reinforced concrete waffle slabs, and this has been achieved.

CHAPTER 2
LITERATURE REVIEW

Study of reinforced concrete waffle slabs started in the 1960's as this type of slab was becoming popular. Previous researchers were mainly concerned with the flexural behaviour of RC. waffle slabs; Marshall was on the uniformly distributed load of a single panel, Ajdukiewicz and Kilszcewicz[4] on the limit state of the slabs of multi-panel, Ho[31] on the uniform and concentrated load on single panel. Just as in solid slabs, waffle slabs may fail by either flexure or shear. Punching shear failure in slabs is characterised by the punching out of part of the slab under the load. This form of failure is more dangerous because of its brittle nature.

Study of punching shear capacity of R.C. waffle slab is limited, while there are many references on punching shear on solid slabs. Moe[45], Regan[52] have suggested different design formulae. The research on solid slabs can be divided into two main groups: first, the experimental studies, which are mainly dependent on experimental results giving simple formulae for the design. The current codes of various countries are based mainly on the results from these studies. Second, the theoretical studies, which include equilibrium model, plastic model, and the finite element model. Although there exist several reports on the holed[55] or sandwich slabs under concentrated load, the study on the waffle slab under concentrated load has been limited to a specific number.

In the design codes adopted by different countries, the punching shear strength of a concrete slab is usually checked by considering a cylindrical or prismatic surface around the loaded area (column section) at a distance from the column surface as the critical punching section — the average shear stress over this control surface is normally limited.

The methods of design by using codes are simple and convenient for practical design; however, they are more or less empirical. The actual failure surface is by no means cylindrical, as observed from experiments.

In this literature review, first, a survey of the configuration of waffle slab floor is presented; second, experimental study on the solid slab and waffle slab are described; third, a theoretical study on the punching shear; and fourth the provision in the codes of practices for punching shear design of solid slabs and waffle slabs are considered.

2.1 TYPES AND SURVEY OF RC WAFFLE SLABS

2.1.1 TYPES OF THE CONFIGURATION OF WAFFLE SLAB FLOORS

R.C. waffle slabs can be divided basically into two types, the flat slabs and two-way slabs, according to where recesses are omitted to provide larger solid areas. Fig. 2.1 and Fig. 2.2 show two possible arrangements. In the flat-slab type of configuration, solid areas, the dimensions of which vary a lot depending on the total load, are provided near the column; this is comparable to a drop panel or column capital providing a path for shear transfer and the extra compression area in the highly stressed negative-moment regions surrounding the column. In the two-way-slab type of configuration, the recesses along the column lines have been omitted to form solid areas which are equivalent to beams since they are the areas of concentrated flexural stiffness, even though they do not extend below the lower surface of the slab.

In practice, R.C. waffle slabs are usually designed as one of the above two types or as a hybrid. In some flat-slab type of configuration, the local solid area around the column is provided by an extra column capital to enhance the shear resistance.

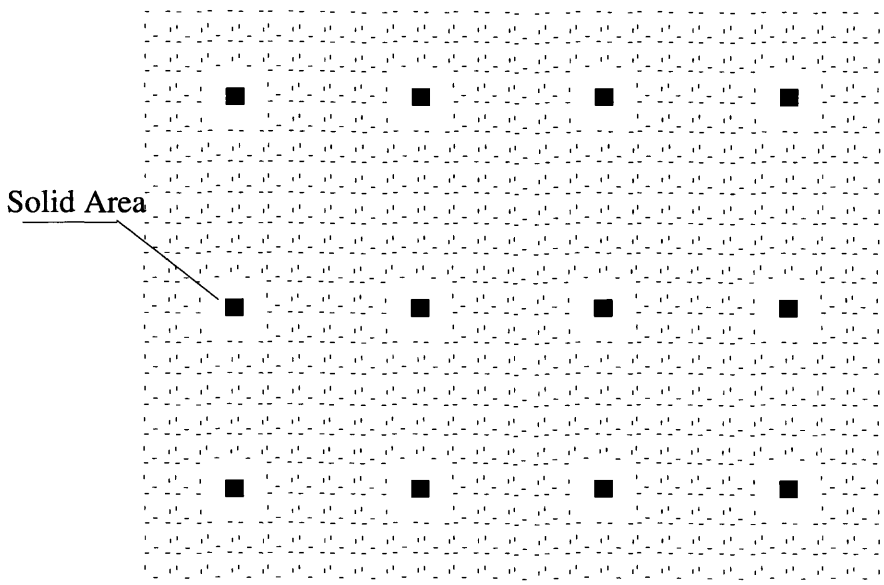

Fig. 2.1 Flat-Slab Type of Configuration of R.C. Waffle Slabs

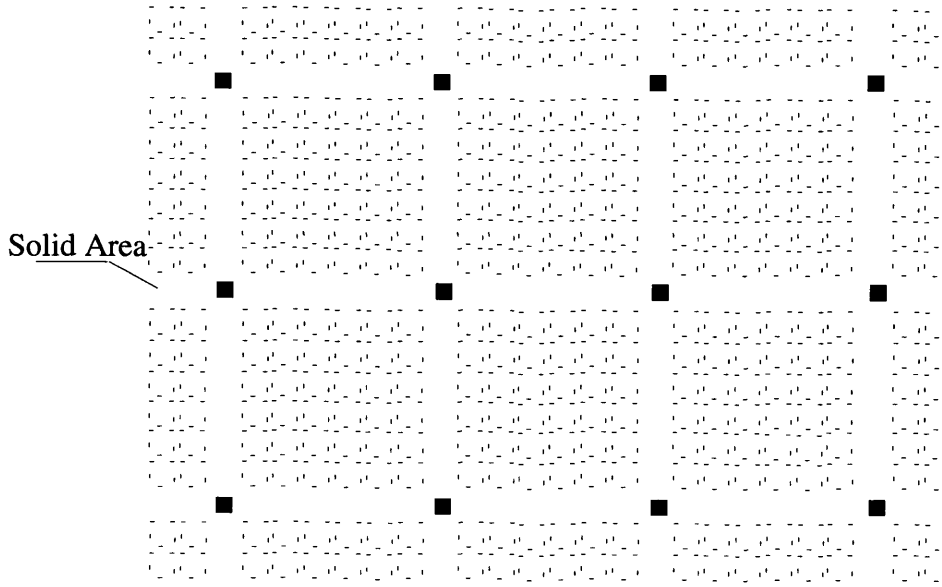

Fig. 2.2 Two-Way-Slab Type of Configuration of R.C. Waffle Slabs

2.1.2 SURVEY OF EXISTING WAFFLE SLABS

In a survey by Matthew and Bennett[42], 40 office buildings with long-span concrete floors were reviewed, of which 6 buildings used waffle slabs. They are listed bellowed.

Table 2.1 Key data of six building floors of waffle slabs

Building No.	No. of floors	Column spacing	Depth	Span/Depth ratio	Materials/m² of floor area			Design Load	Stabi-lity	Prestr-essed	Notes
					Concrete	Re-Bar	Strand				
		m	mm		m³	kg	kg	kN/m²			
1	5	6.6×7.43	350	21.2	0.245	24.0	-	6.0	Frame action	no	Grade C35 BS8110
2	3	7.5×10.5	525	20.0	0.450	67.0	-	6.0	Frame action	no	Grade C35 BS8110
3	3	10.18 ×10.18	550	18.5	0.396	37.0	-	9.0	Shear walls	no	Grade C35 BS8110
4	1	12.0 ×12.0	500	24.0	0.349	15.9	2.52	6.0	Shear walls	yes	Grade C40 BS8110
5	2	12.7 ×12.7	500	25.4	0.341	12.2	5.60	6.0	Shear walls	yes	Grade C35 BS8110
6	2	15.0 ×15.0	680	22.1	0.480	20.4	9.26	7.0	Frame action	yes	Grade C40 BS8110

The sections of these slabs are shown in Fig.2.3 (a)~(f).

From Table 2.1, it is seen that the span/depth ratio is about 20 for RC slabs, and 24 for prestressed slabs. In comparison with the solid slabs, the amount of concrete used is reduced byabout 30%, and this also means the dead load of the slabs is reduced by 30%.

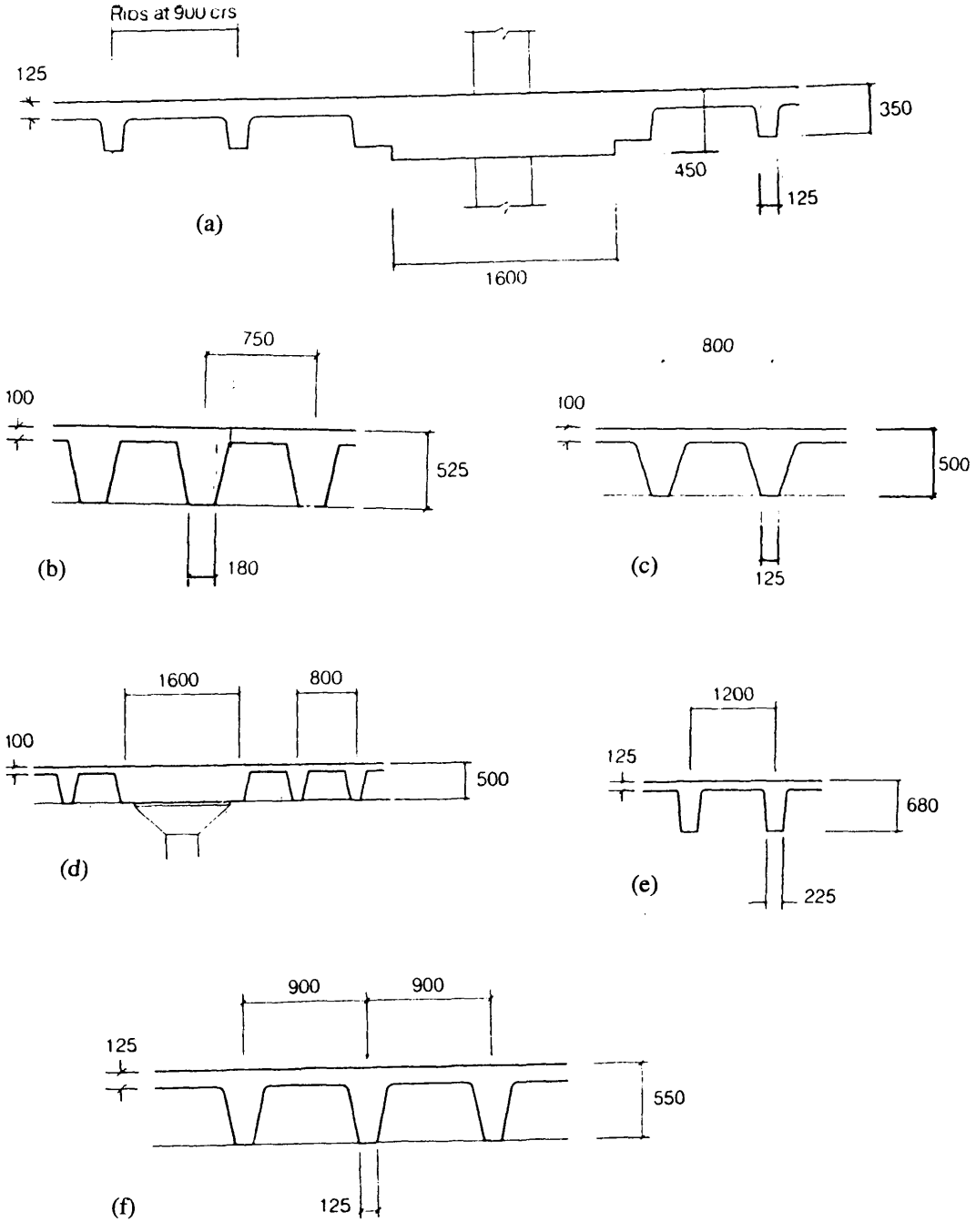

Fig. 2.3 Sections of the waffle slabs surveyed

2.2 EXPERIMENTAL STUDY ON PUNCHING SHEAR OF RC SLABS

2.2.1 EXPERIMENTAL STUDY ON RC SOLID SLABS

In this section, the results of several groups of tests conducted by previous researchers are summarised and their methods to calculate punching shear capacity are described. The slabs are reinforced with flexural reinforcements only. Slabs with shear reinforcement will be discussed in later sections.

2.2.1.1 Moe's[45] Study

Moe conducted a large number of experiments on solid flat slabs of various configuration and proposed a formula for the punching shear analysis. The current design codes of various countries are more or less influenced by his work. His test included five series studying the punching load capacity and its influence from i)holes in slabs; ii)concentration of tensile reinforcement; iii)special type of shear reinforcement; iv)extremely large column size, and; v)eccentric column loads.

The conclusions from Moe's work are listed below:

i) The deflections of slabs were not influenced by the presence of the holes.
ii) Concentration of the reinforcement did not increase the shearing strength, but rather caused a moderate reduction in strength and decreased central deflections.
iii) Slabs with shear reinforcement failed much more gradually than those without shear reinforcement, and there was indication that the shear reinforcement was not fully effective due to the tearing off from the compression zone. In the slabs embedded with steel plate above the column stub to extend the loading area, the failure was sudden and noisy with the punching taking place along the edge of the steel plate.
iv) Large column was not as effective as the small ones in terms of punching capacity per unit column area.

Based on his and other people's experimental results, Moe proposed the formulae to calculate the punching shear capacity of solid slabs. He used the concept of nominal shear stress and the critical perimeter to simplify the calculation for design purposes. The critical perimeter was assumed to be a cylinder around the loading area, and the uniform shear stresses distributed on the surface of the cylinder. When the shear stress reached a certain amount, i.e., the nominal shear strength, the slab would be punched through.

The nominal shear strength was defined as

$$v_{cr} = \frac{P_{pun}}{bd} \tag{2.1}$$

where, b the perimeter of the loading area or column;

d the effective depth of the slab;

P_{pun} the punching load.

The nominal shear strength was achieved by considering the parameters which influenced the punching shear capacity, and are given as below.

$$\frac{v_{cr}}{\sqrt{f_{cu}}} = \frac{P_{pun}}{bd\sqrt{f_{cu}}} = \frac{A(1-Cd/r)}{12\left(1+B\dfrac{bd\sqrt{f_{cu}}}{P_{flex}}\right)} \tag{2.2}$$

The constants A, B and C of Eq.(2.2) had been determined on the basis of a statistical analysis of the available test data. Eq.(2.3) is the final form.

$$P_{pun} = \frac{(1.25bd\sqrt{f_{cu}})(1-0.075r/d)}{1+0.44bd\sqrt{f_{cu}}/P_{flex}} \tag{2.3}$$

where,

P_{pun} punching failure load, in *N*.

b effective periphery around the loaded area (around the face of the column), *mm*.

d effective depth of slab, *mm*.

f_{cu} compressive strength of concrete cube, *MPa*.

r the side length of column, *mm*.

P_{flex} shear force at which flexural failure occurs in a solid slab, *N*.

The term P_{flex} is calculated in accordance with the following equation derived by Elster and Hognestad[26] using yield line theory:

$$P_{flex} = 8m\left(\frac{1}{1-r/a} - 3 + 2\sqrt{2}\right) \tag{2.4}$$

where,

m ultimate flexural moment capacity per unit width of a solid slab;

a width of square slab;

r column dimension.

The value of m can be determined from:

$$m = \rho f_y d^2 (1-0.59q) = q f_{cu} d^2 (1-0.59q) \qquad (2.5)$$

where

A_s total area of tensile reinforcement;

ρ ratio of tensile steel area to concrete area, A_s / ad;

f_y yield strength of reinforcement;

q tension reinforcement index, $\rho f_y / f_{cu}$.

The formula for slabs with shear reinforcement is as Eq.(2.6).

$$\frac{P_{pun}}{bd\sqrt{f_{cu}}} = \frac{1.25\left(1-0.075\frac{r}{d}\right)+\left(\frac{12P_s}{bd\sqrt{f_{cu}}}-3.0\right)}{1+0.44\frac{bd\sqrt{f_{cu}}}{V_{flex}}} \qquad (2.6)$$

$$P_s = A_v f_v \sin\theta' \qquad (2.7)$$

where

P_s the shear resistance provided by links and bent up bars;

A_v the area of the links or bent up bars;

f_v the yield strength of links and bars;

θ' inclination angle between bent bars and horizontal.

The test results were compared with the calculation results by Eqs. (2.3) and (2.6), it was reported that they agreed quite well.

2.2.1.2 Yitzhaki's[65] Study

Based on Moe and other researchers' tests Yitzhaki did some more tests and proposed new formulae which considered the transition of the flexural failure to punching failure. His new definition of the nominal shear strength had assigned this parameter some physical meaning. He assumed that the effective depth of slab and the material parameter, $q = \rho f_y / f_{cu}$, had similar effect on both the flexural failure and the punching shear failure, all the other influential parameters being determined by the experimental data. The proposed formula is as following,

$$P_{pun} = 8(1-q/2)d^2 (1.03+0.164\rho f_y)(1+0.5r/d) \qquad (2.8)$$

In the above formula, all the parameters have similar meaning as those in section 2.2.1.1. Yitzhaki defined the critical perimeter at a distant d from the face of the column or loading pad, and also put an extra part, $\left(1-q/2\right)$, to modify the definition of the nominal shear strength. His formula was

$$v_{cr} = \frac{P_{pun}}{\left(1-q/2\right)d(4r+8d)} = 1.03 + 0.164\rho f_y \qquad (2.9)$$

By this definition, it appears that the nominal shear strength is dependent on the reinforcement strength only. It should be noted that the influence of f_{cu} on shear strength is rather implicit; the parameter q reflects the influence of f_{cu}. The results of tests were in good agreement with Eq.(2.9).

2.2.1.3 Regan's[52] Study

Regan tested 28 RC slabs which were divided into five series primarily concerned with the effects of the arrangement of flexural reinforcement, absolute size or depth, concrete strength and ratio of reinforcement, boundary restraint and the size of the loaded area. The tests were designed to assess the provisions of four Codes of Practice — *BS8110*[12], *CP110*[13], *ACI 318-83*[1] and *CEB-FIP Model Code*[16].

The tests about the effect of the arrangement of flexural reinforcement showed that the concentration of reinforcement toward the loaded area had no significant beneficial effect in terms of punching resistance. When using the formula to calculate the punching capacity, it was considered appropriate to calculate steel ratio for column strips, i.e. width of load area plus *3h* to each side instead of *1.5d* each side. As to the influence of steel ratio on the punching capacity, the provision in BS8110, $\propto \sqrt[3]{100\rho}$ was satisfactory.

The tests regarding the size or depth of slabs showed that the size effect was not linear as that assumed by Moe, the size factor ($\zeta \propto \sqrt[4]{1/d}$) given in BS8110 gave good correction to the experimental result.

As to the influence of concrete strength on the nominal shear strength, the expression, $v_{cr} \propto \sqrt[3]{f_{cu}}$, adopted by British Standard is appropriate while the CEB use of compressive strength to the power of the two thirds causes significant errors.

Another two series of tests showed that the punching resistance of slabs can be appreciably enhanced when the boundary of the slabs were restrained; when the loaded area was very small (side dimension less than about 0.75d), the BS8110 general expression for punching resistance could give very significant overestimation of strength.

2.2.1.4 Comments on the Above Research

A comparison of experimental and analytical results has enabled the factors affecting the punching load capacity of a slab to be established. The principal factors in the order of importance are as follows:

a) Strength of Concrete.
b) Proportion of column cross-section (area of loading) to the effective depth of slab, i.e. c/d.
c) Distribution and amount of horizontal reinforcement.

The secondary factors with less influence are:

a) The shape of the column cross-section.
b) The condition of the fixing of the slab and its loading outside the support zone considered.
c) The loading process, particularly the speed rate at which the load increases.

Further factors are considered separately, such as:

a) Shear reinforcement, its distribution and intensity.
b) Shear head in the support zone.
c) The effect of prestressing.
d) Opening in the support zone.

Many formulae have been proposed to reflect the above factors influencing the punching shear capacity. As can been seen from the above survey, it does not appear that a great deal of agreement between the test results and the formulae proposed by various authors, which is reflected in the provision in the codes of different countries. The problems relating to the discrepancy which may need further consideration are listed below.

1. **The Failure Surface of the Punching Shear**

   All the experiments reported that the failure surface is a truncated cone or pyramid starting from the column face (exceptional to slabs with shearheads).

The outer limit of the failure zone, or the inclination angles of truncated cone varies significantly, from 40° to 20° or even smaller. This resulted in a very different critical section, or assumed failure zone. For example, in BS8110, the critical section is 1.5d from the column face; in ACI and CEB, the failure zone is 0.5d from the column surface. As mentioned before, the shear strength used for different codes is also different to compensate the use of different perimeters of the failure zone; the final result for the punching load can be expected not to vary too much for a slab without shear reinforcement. While, the problem arises from the design and detailing of the shear reinforcement. BS8110 checks the failure perimeter which is 1.5d from the face of the column; if shear reinforcement is required, stirrups are put at two perimeters (one is 0.75d from the column surface, the other is 1.5d from the column surface). ACI and CEB check the failure perimeter which is 0.5d from the column surface, and if shear reinforcement is required, stirrups are put at this critical surface and only one layer of stirrups is put. Because the exact failure zone is not known, the stirrups are put around an imagined failure zone; the shear reinforcement may not be fully effective, because in the case of punching shear, the stirrups placed away from the column surface (still within the real failure zone) may be more effective than those near the column surface.

From the above analysis, it is still of importance to establish as close as possible the location of the failure zone to the real situation.

2. Relationship Between concrete Strength f_{cu} and the Nominal Shear Strength

In the above experiments all the researchers paid attention to the relationship between the nominal shear strength v_{cr} and the concrete strength f_{cu}, but the conclusions were different. Moe's conclusion was $v_{cr} \propto \sqrt{f_{cu}}$; Regan's $v_{cr} \propto (f_{cu})^{1/3}$; Yitzhaki's was $v_{cr} \propto (1-2\rho f_y/f_c)$.

These opinions are reflected in the design codes; BS8110 is $v_{cr} \propto (f_{cu})^{1/3}$; ACI $v_{cr} \propto \sqrt{f_{cu}}$; CEB is $v_{cr} \propto (f_{cu})^{2/3}$.

It appears that the question is what causes punching failure; is it the tensile failure, or the compression failure or the diagonal tensile failure?

3. Relationship Between Flexural Reinforcement ratio and the nominal Shear Strength

From the reports of the experiments mentioned before, it was found that there were radial and circumferential cracks on the slabs, and part of the steel near to the column also yielded. It is not surprising to note that in a practical slab, the punching failure is always a combination of shear and flexural failure. As described by Yitzhaki, the slab's failure can transfer from a flexural failure to a punching shear failure depending on the flexural reinforcement ratio. This conclusion can be further extended to state that P_{pun} may also be a function of the flexural capacity, depending on the reinforcement ratio ρ, span-depth ratio l/d, and the condition of the boundary of the slab. This can be supported by the experiments conducted by Moe, Regan etc. Moe studied this problem, his formula was based on the empirical method, so the application was limited to slabs with a certain amount of steel and a certain range of spans.

The current codes deal with this problem differently: BS8110 gives $v_{cr} \propto (\rho)^{1/3}$; ACI states ρ has no influence on v_{cr} and CEB states $v_{cr} \propto \rho$.

2.2.2 EXPERIMENTAL STUDY ON THE RC WAFFLE SLABS

Magura and Corley[40] conducted a full-scale test on a building which was purpose-built for the New York World's Fair and was used for destructive tests before demolition. The building was a one story structure with 6×4 continuous panels of R.C. waffle slabs as roof. The layout of the roof is shown in Fig.2.4 and Fig.2.5. The slabs had the longest span of 10.23m and the depth 0.61m. The configuration of the roof was a hybrid between flat slab and two-way slab, solid area being provided in the local areas near columns and also along the column lines.

Three sets of test were conducted on different panels. The first test was on 2×2 continuous panels surrounded by the column lines B, D, 3 and 5; the second was on 1×3 continuous panels surrounded by column lines D, E, 2 and 5; the third was a single panel surrounded by column lines C, D, 5 and 6. Numerous jacks were used to simulate the uniform live load.

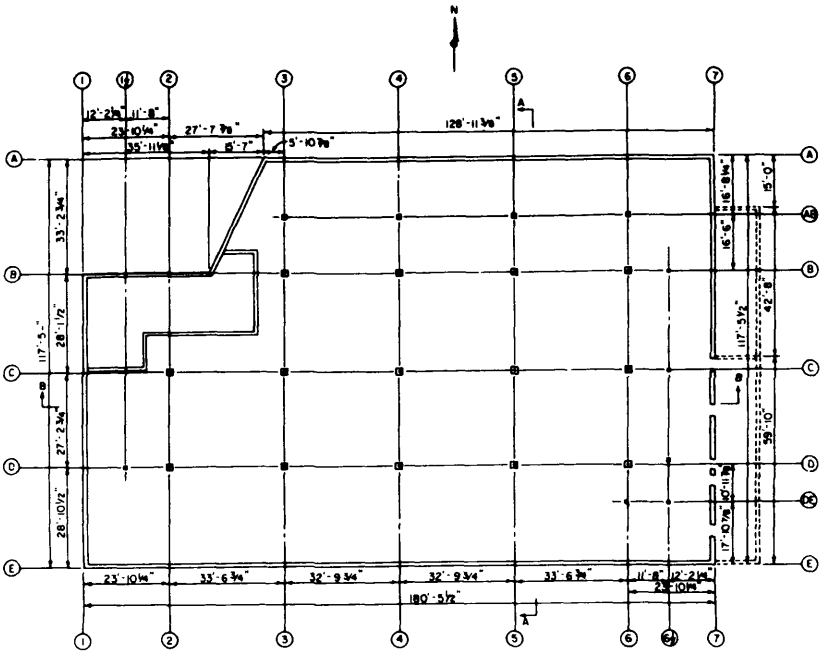

Fig.2.4 Plan of the Roof

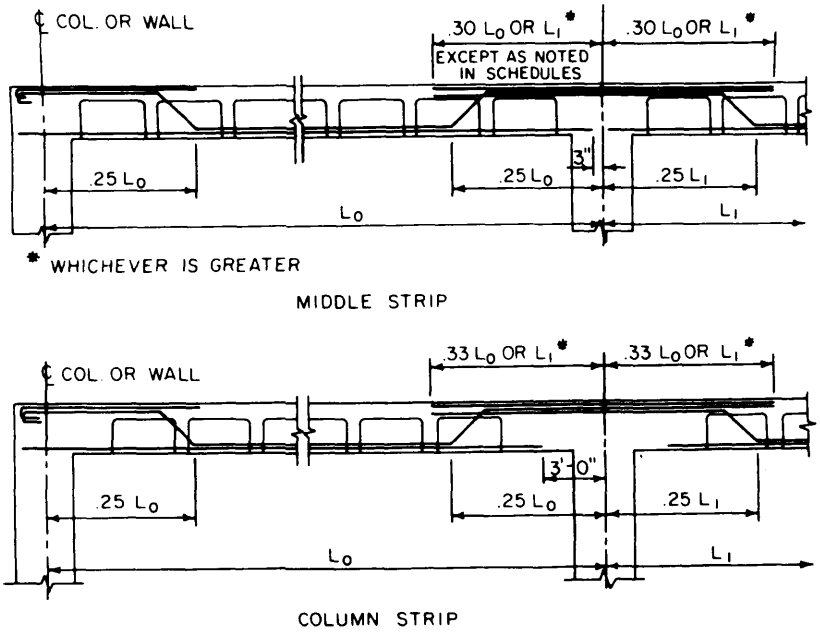

Fig.2.5 Elevation of R.C. Waffle slab

The four panels in Test I responded in an essentially elastic manner under the applied load until ultimate strength was reached when Column C4 punched through. The ultimate load intensity was equal to added dead plus 2.8 live loads.

Test II was divided into two parts. In Part A, the three panels along the edge of the building between column Lines 2 and 5 were loaded. This part of the test ended with a shear failure at Column E3. In Part B, panel 4,5-D,E and the adjacent half of panel 3,4-D,E were loaded. Part B was terminated after the slab failed in shear at Column E4. In

Test III Column C5 was punched through first, then after some further continued load(at reduced load level), column D5 was also punched through.

It is seen that shear failure occurred in all three tests although all the columns were enhancement by local solid areas around the columns and along the column lines. Only in Test III was there evidence of flexural distress; reinforcement in the positive moment region began to yield before punching. None of the measured reinforcement strains approached yield in Test I and II when the first shear failure occurred. Maximum applied load was substantially below the flexural capacity of the slab in each test.

Table 2.2 and 2.3 list the test result against calculation results, and the parameters used for the analysis.

Table 2.2 Shear Strength of Slab

Location	Test No.	Frame Analysis	Test P_{test}	Moe P_{Moe}	ACI* P_{ACI}	ACI Beam P_{Beam}	$\frac{P_{test}}{P_{Moe}}$	$\frac{P_{test}}{P_{ACI}}$	$\frac{P_{test}}{P_{Beam}}$
			KN	KN	KN	KN			
Column C4	I	C	5028	6319	4316	-	0.81	1.16	-
		4a	5117	6319	4316	-	0.81	1.19	-
Column E3	IIA	3	1736	3560	4138	2047	0.49	0.42	0.85
		E	1958	3872	4138	2047	0.51	0.47	0.96
Column E4	IIB	3	1736	3160	3560	1914	0.55	0.49	0.91
		E	2047	3426	3560	1914	0.60	0.57	1.07
Column C5	III	C	3115	4850	5251	-	0.64	0.59	-
		5	3248	4984	5251	-	0.65	0.62	-

* 1963 ACI Code.

Table 2.3 Parameters used for Punching Calculation

			Moe's Method			ACI Method	Moe's and ACI methods		
Location	Test No.	Column Size	Perimeter Dim B	Column Dim C	P_{flex}	Perimeter Dim B	Slab Depth d	$\sqrt{f_c'}$	Unbalanced Moment
		mm×mm	mm	mm	KN	mm		MPa	KN-m
Column C4	I	660×660	2642	660	9746	4547	478	0.50	-
					9968				
Column E3	IIA	305×142	1422	676*	2759	2870	719	0.50	59.9
					3293				
Column E4	IIB	305×610	1219	508*	2759	2591	688	0.50	71.2
					3293				
Column C5	III	660×660	2642	660	5073	546	546	0.50	509.8
					5340				

* Equivalent value of C for a rectangular column was taken as $(x^2+y^2)/(x+y)$, where x and y are the column dimensions.

The above is the only investigation available regarding the punching shear on R.C. waffle slabs. Although the solid areas around the columns are quite large, the slabs still failed by punching. It can be seen that the punching shear is a very important issue to be considered in the design of waffle slabs, and it may be the governing factor in the load capacity.

2.3 METHODS OF THEORETICAL ANALYSIS OF PUNCHING ON SLABS WITHOUT SHEAR REINFORCEMENT

Concrete is the material which is very complicated compared to other materials, the punching shear is more complicated due to the tri-axial stress status near the loading area. In the past several decades, a lot of effort has been made to explain the mechanism of and predict the resistance of the punching shear failure. In this section, the plastic theory, equilibrium method and finite element method employed by previous researchers are reviewed.

2.3.1 UPPER BOUND ANALYSIS METHOD

Concrete is a material which shows plastic character before failure occurs. Barestrup[11] applied the plastic flow theory to solve the problem of punching shear, the material failure criteria being the modified Mohr-Columnb criteria. Based on the plastic method, Jiang[34] used a parabolic Mohr-Columnb criteria, the formulae being simplified and the punching angle smaller than the angle of friction of the concrete material being made possible. The method was further improved by Bortolotti[10] who considered the softening of the strength of the concrete under large stresses. Here Barestrup's method is reviewed as it gives better understanding of the basic failure mechanism, although the limitation exists in using the derived formulae.

2.3.1.1 Formulation

Barestrup assumed that concrete was a perfectly plastic material, this was supported by using a plastic strength of concrete which could be converted from the actual strength of concrete based on statistics of experimental data.

Consider a concrete slab annularly supported and loaded by a circular load pad. The slab was reinforced in such a way that flexural failure was prevented. It was assumed that a failure mechanism consisting of the punching out of a solid of revolution and the rest of the slab remaining rigid, Fig.2.6, would occur.

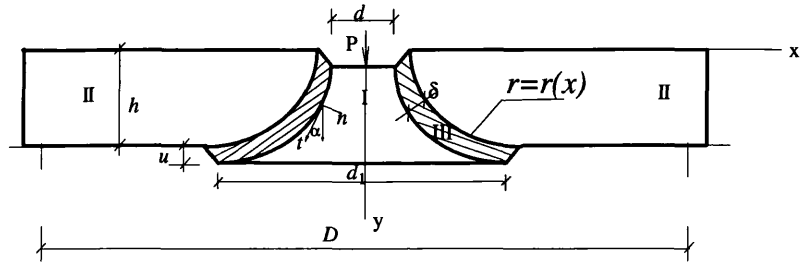

Fig.2.6 Failure surface in punching shear

The relative displacement of the failure surface was assumed to be perpendicular to the main reinforcement; hence the main reinforcement did not contribute to the load-carrying capacity, dowel action being neglected. The justification for assuming a punching failure mechanism without yielding of the main reinforcement lay in the fact that if the main reinforcements were yielding, the slab would fail in flexure at a lower load, since flexural failure did not involve the dissipation of energy in a failure surface in the concrete passing through the whole depth of the slab.

The generatrix of the axisymmetric failure surface was described by the function $r = r(x)$ and sketched in Fig.2.6. Punching diameter and slab depth were termed d and h, respectively. The relative displacement was u, directed at angle α to the generatrix.

By the assumed failure mechanism, the strain in the circumferential direction was zero; hence the generatrix might be regarded as a yield line in plane strain. The normality condition then required that $\alpha \geq \varphi$ (φ was the friction angle of concrete). Thus the analysis was valid only for $D \geq d + 2h\tan\varphi$, D being the diameter of the annular support.

Once the failure mechanism was assumed, the derivation of the equation was done based on the virtual work equation: the energy dissipated on the failure surface (by integration over the failure surface--zone of the strain discontinuity) should be equal to the virtual work done by load P on the virtual displacement u. The stress and strain relation was based on the status of plasticity: normality condition was applied using the associated flow rule. The yield function was Mohr-Coulomb criteria.

The failure surface generatrix was obtained as consisting of a straight line in combination with the catenary curve, as sketched in Fig.2.7.

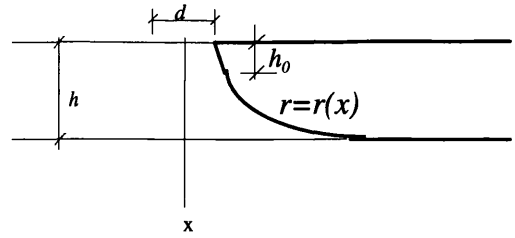

Fig. 2.7 Failure surface generatrix with a straight line in combination with a catenary curve.

The total punching load P was obtained as the sum of two parts:

$$P = P_1 + P_2 \tag{2.10}$$

where P_1 and P_2 are the contributions from the conical surface and the catenary of revolution, respectively.

P_1 and P_2 were found as

$$P_1 = \pi f_c' \frac{h_o}{2} \frac{(d\cos\varphi + h_o \sin\varphi)(1-\sin\varphi)}{\cos^2\varphi} \tag{2.11}$$

$$P_2 = \frac{1}{2}\pi f_c'[lc(h-h_o) + l(\frac{d_1}{2}\sqrt{(\frac{d_1}{2})^2 - c^2} - ab) - m((\frac{d_1}{2})^2 - a^2)] \tag{2.12}$$

where,

h_o	the depth of the changing point of the genetrix from a straight line to catenary curve,
h	depth of slab,
d	diameter of the loading pad,
d_1	diameter of the punching perimeter,
φ	internal friction angle of concrete,
f_c'	plastic compressive strength of concrete cylinder,
f_t'	plastic tensile strength of concrete,
m	ratio between plastic compressive strength and tensile strength,
l	a constant, $l = 1 - 2\frac{f_t'}{f_c'}\frac{\sin\varphi}{1-\sin\varphi}$

2.3.1.2 Conclusions

a) The punching diameter d_1 always reaches the support, if $f_t = 0$.
b) The larger the span D, the smaller is the punching load.

c) When the punching diameter is not too large compared with the support diameter, the load parameter is fairly independent of the relative punching diameter.
d) The introduction of a finite tensile strength leads to a finite value of the optimum opening diameter d_l. When the support diameter is larger than the optimum opening diameter, the ultimate load becomes independent of the support diameter.
e) The tensile strength has a considerable influence on the load-carrying capacity.

2.3.2 EQUILIBRIUM METHOD

In this section, the method employed is based on the equilibrium of forces. This method does not consider the compatibility of the deflection, although the equilibrium equation is satisfied. This method is somehow equivalent to the lower bound limit analysis. This method had been employed by quite a lot of researchers[14,26], while it differed substantially in the detailed assumption of the failure mechanism. In the following, the work by Broms is reviewed.

The slab outside the inclined shear crack was divided into sectors ---elements between radial cracks. Each element was assumed to act as a rigid body supported by an imaginary conical shell in the part of a slab immediately above the column (see Fig.2.8). Failure was assumed to occur when the stress in the conical shell or the compression strain in the tangential direction reached critical values. The height of the compression zone x was determined by iteration, so the two failure conditions coincided.

In a flat plate, inclined shear cracks usually form at a load level of less than 70 percent of the ultimate load. Although these cracks can completely surround the column, the slab is nevertheless stable, and can be unloaded and reloaded without any decrease of the ultimate load. It is therefore evident that the failure mechanism is not normally a pure "shear failure" governed by the diagonal tensile strength of the concrete.

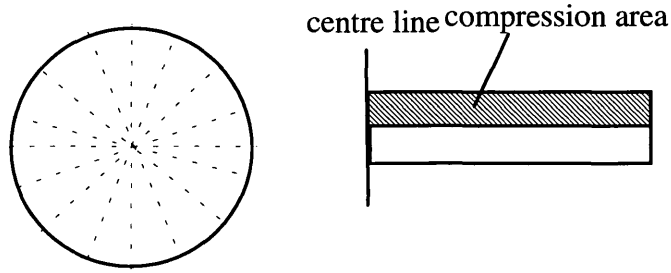

(a) Yield Line on slab **(b) Compression zone**

Fig.2.8 The assumed failure model

After finding out the forces to causes the distresses by high stress or strain, the punching load was finally found based to the equilibrium in the vertical direction.

2.3.3 ANALYTICAL INVESTIGATION BASED ON NON-LINEAR FINITE ELEMENT MODELLING

The mathematical theory of finite element is by now well be established, it is powerful in solving almost any type of problems provided the equations governing the concerned problem is accurate. In the application of FEA to reinforced concrete members or structures, specially problems are encountered. This complexity may be summarised as following:

a) the mechanical properties of concrete can vary widely depending upon the particular conditions of mixing, placing, curing, nature and rate of loading, and environmental influences;
b) the behaviour of concrete under multi-axial stress status is not fully known; the criteria defining the fracture and yielding of concrete is still not comprehensive; the concrete behaviour after cracking needs more investigation.

Due to the complexity of the material characteristics of concrete, the success of applying FEA to reinforced concrete members or structure depends on the complexity of the problem under concern and what exactly is expected from the analysis.

The literature on the application of FEA to the punching on RC slabs is very limited. Geozalez-Vidosa[29] studied punching in axisymmetrical cases and looked into the failure mechanism and compared his analysis results with the experimental results of previous researchers. He indicated that the key to the understanding of the mechanics of punching failure was the proper modelling of triaxial conditions that govern the behaviour of slabs under punching; the high principal stresses (often well in excess of f_c), achieved through triaxial conditions, were capable of equilibrating the applied load at failure.

2.3.4 COMMENTS ON THE ANALYSIS MODELS

In the above sections, we have looked through the existing methods to model the punching shear failure in RC slabs. Each of the methods has its own advantages and also has its shortfalls, they are discussed below:

a) Upper bound method

The upper bound method is based on the plastic theory; it is able to consider the span and depth of the slab, gives the curve of the failure surface and ultimate load. The analysis procedure is rather simple compared to FEA, and also easily been adopted for practical use, or lay the foundation for empirical method.

The problem in the method is the material strength, the plastic strength of concrete is used instead of the actual strength f_c' and f_t'. The relationship between the plastic strength and the test strength is empirical. Another problem is the assumption that the failure surface is through the whole depth and failure occurs at the same time thought the slab. Actually, it was observed from the experiments that the punching process was: the diagonal crack first appeared on part of the failure surface (near to the tensile side of the slab) at a load of about half or 3/4 of the ultimate load and this crack was visible. Some researchers reported that if the slab was unloaded and reloaded again, the ultimate load was the same as that of a slab loaded to failure directly. In this sense, the plastic theory is not compatible with the experimental phenomena.

The disadvantage of the plastic method is that it can not reflect the influences from the flexural reinforcement, the boundary condition, or the influence from the flexural capacity of the slab.

b) Equilibrium Method

- Advantage: considering the flexural capacity of slabs which failed by punching; the deformation at the ultimate can be estimated.
- Problem: The failure model is an assumed one which may be suitable for slabs which has small flexural reinforcement. Some of the assumption, e.g., the strength and strain of concrete at tri-axial cases are hardly realistic.

c) Finite Element Method

The advantage of FEA is that it can, in theory, calculates all the mechanical responses like stress, strain, displacement for every point in the slab and shows the crack pattern.

The problem is that the determination of the input data for the FEA, or more precisely the fundamental behaviour of concrete. As this is still under investigation by numerous researchers, the problems may be overcome some day.

d) Suggestion for Modelling the Punching Shear

A possible model of the punching shear failure may be a combination of the plastic model and the equilibrium model. The slab under concentrated load cracks first under the combination of the bending and shear force. After the crack has occurred, further loading will cause the uncracked part to 'yield' (or crash); the ultimate load may be found by considering the cracked slab using the plastic method. The possible steps are as following.

- Find the crack depth of a slab under concentrated load. The stress in the steel and the stress in the concrete can be estimated.
- The uncracked part of the slab will support most part of the ultimate load and the plastic theory will be used to find this load. There are two other parts of shear resistance, one is the contribution from the friction on the cracked part of the failure zone and the other is from the dowel effect.

2.4 CODES OF PRACTICE OF VARIOUS COUNTRIES

The provisions of current codes of practice of various countries are based on the experimental study of previous researchers, the concept of the nominal shear strength and the critical perimeters are used for the simplicity. Four codes are considered here to compare their provisions to punching shear ------- **BS8110**[12], **CP110**[13], **ACI318-83**[1] and **CEB-FIP**[16] CODE.

2.4.1 SLABS WITHOUT SHEAR REINFORCEMENT

2.4.1.1 Analysis Formulae of the Four Codes

The assumed failure surface for different codes are shown in Fig.2.9.

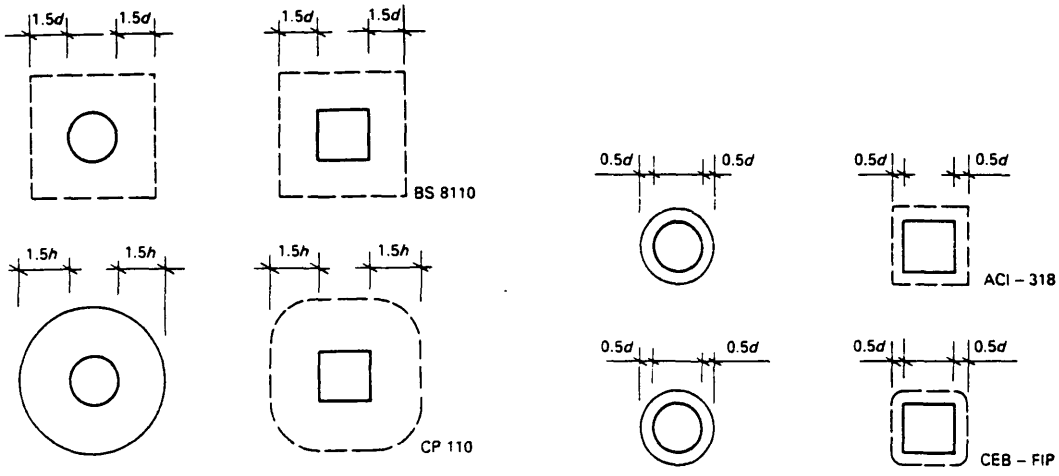

d: effective depth of slab; *h*: total depth of slab.

Fig. 2.9 Control perimeters for the punching shear

1) BS8110

In order to compare different codes of practice, the safety factors are not considered here and they are dealt with separately. In BS8110 the partial safety factor for materials γ_m=1.25.

Nominal shear strength of concrete

$$v_{cr} = 0.79\sqrt[3]{100\rho}\sqrt[3]{f_{cu}/25}\sqrt[4]{400/d} \qquad (2.13)$$

Where, ρ flexural steel ratio calculated for a width equal to *(B + 3d)* or *(b + 3d)*;

B diameter of the loaded area;

b dimension of the rectangular loaded area;

f_{cu} cube crushing strength of concrete;

d effective depth of the slab.

Perimeter of the assumed failure surface (1.5d from the column face)

$u = 4\ (B + 3d)$ for circular loaded areas.

$u = 4\,(b + 3d)$ for square loaded areas.

Shear resistance

$$P = \nu_{cr} u d \tag{2.14}$$

Upper limit of shear resistance

$$P \le 0.8\sqrt{f_{cu}}\, u_o d \quad \text{or } 5\text{N/mm} \tag{2.15}$$

where u_o length of periphery of loaded area = πB or 4b;

f_{cu} cube crushing strength of concrete;

In the check of the upper limit of P, γ_m has been assumed to be 1.5.

2) CP110

With partial safety factor for materials removed, the formulae are.

$$\nu_{cr} = 0.27\sqrt{100\rho f_{cu}} \tag{2.16}$$

$$P = \zeta_s \nu_{cr} u d \tag{2.17}$$

where, $\zeta_s = 1.6 - 0.002h \ge 1.0$ (size factor)

$u = \pi(B + 3h)$ for circular loaded areas.

$u = 4b + 3\pi h$ for square loaded areas.

ρ: flexural steel ratio calculated for a width equal to (B + 6h) or (b+ 6h).

3) ACI 318-83 (with capacity reduction ϕ omitted)

$$\nu_{cr} = 0.332\sqrt{f_c} \tag{2.18}$$

$$P = \nu_{cr} u d \tag{2.19}$$

where $u = \pi(B + d)$ for circular loaded areas.

$u = 4(B + d)$ for square loaded areas.

f_c is the concrete cylinder strength =0.8 f_{cu}

4) CEB - FIP (with partial safety factor r_m=1.5 removed)

$$\nu_{cr} = 0.084(1 + 50\rho) f_c^{2/3} \tag{2.20}$$

$$P = \zeta_s \nu_{cr} u d \tag{2.21}$$

where, $\zeta_s = 1.6 - 0.001d$

$u = \pi(B+d)$ for circular loaded areas.

$u = 4b+\pi d$ for square loaded areas.

with r calculated for a width equal to (B + 5d) or (b + 5d).

2.4.1.2 Comparison of BS8110 and CP110

Both BS8110 and CP110 work in terms of control perimeters at relatively large distance from the loaded area (Fig.2.9) and use the same limiting shear stresses as for one-way and two-way spanning slabs. The difference between the basic limiting stresses in the two Codes are small. The significant differences between the two codes are:

1) In BS8110 the ratio of flexural reinforcement is calculated for a width of slab equal to that of the loaded area plus 1.5d to either side of it, while in CP110 the width is that of the loaded area plus 3h each side.

2) In BS8110 the control perimeter at a distance 1.5d from the load has square corners no matter the loaded area is square or circular; in CP110 the perimeter at a distance of 1.5h from the load, has round corners in all cases.

3) The range of slab depths over which a size effect is taken to affect the punching resistance in BS8110 is $100mm \leq d \leq 400mm$ while in CP110 this is 150mm$\leq d \leq$ 300mm.

4) BS8110 introduces a specific upper limit to the resistance expressed in terms of the nominal shear stresses at the periphery of the loaded area which is related to the strength of the concrete.

2.4.1.3 Comparison of ACI 318 and CEB78

The control perimeters of the ACI and CEB Codes are much closer to the loaded area (0.5d) than those of British Codes, and the limiting nominal shear stresses for relatively small loaded areas are higher than the values for one-way slabs. The main difference between these two codes are:

1) In ACI 318 the control perimeter is taken to have the same shape as the loaded area, but in CEB 78 the perimeter always has rounded corners (see Fig. 2.9).

2) In ACI 318 the limiting shear stress depends only on the concrete strength while in CEB 78 it is also a function of the ratio of the flexural reinforcement and of the slab depth.

2.4.1.4 Comparison of British Codes with Others

1) The distance of the critical perimeter from the load differs considerably in the various codes: in BS8110, it is 1.5d, whereas in ACI and CEB-FIP it is 0.5d. However, undue importance should not be attached to these differences, because the allowable stresses acting over the assumed failure surface also differ considerably to compensate for the differences in the surface areas of the perimeters; for example, the ACI stresses are of the order of twice the BS8110 values.

2) In BS8110 and CEB, the same allowable stresses are used for punching shear as those used for flexural shear, while in ACI, the allowable stresses are distinguished between the two case; the allowable stress for punching being twice that of the flexural shear.

2.4.1.5 SAFETY FACTORS BY THE FOUR CODES

Safety Factors: $\gamma_m \gamma_f = \gamma$

where γ_m is the partial safety factor for material; γ_f is the partial safety factor for load.

BS8110 and CP110	1.25×1.4 = 1.75
ACI 318	1.18×1.4 = 1.65
CEB-FIP	1.5×1.35 = 2.02

2.4.2 SLABS WITH SHEAR LINKS OR BENT-UP BARS

If the punching shear force to be resisted exceeds the capacity provided by the concrete, it is necessary to provide shear reinforcement in the form of stirrups, bent-up bars or specially fabricated shear heads.

2.4.2.1 BS8110 & CP110

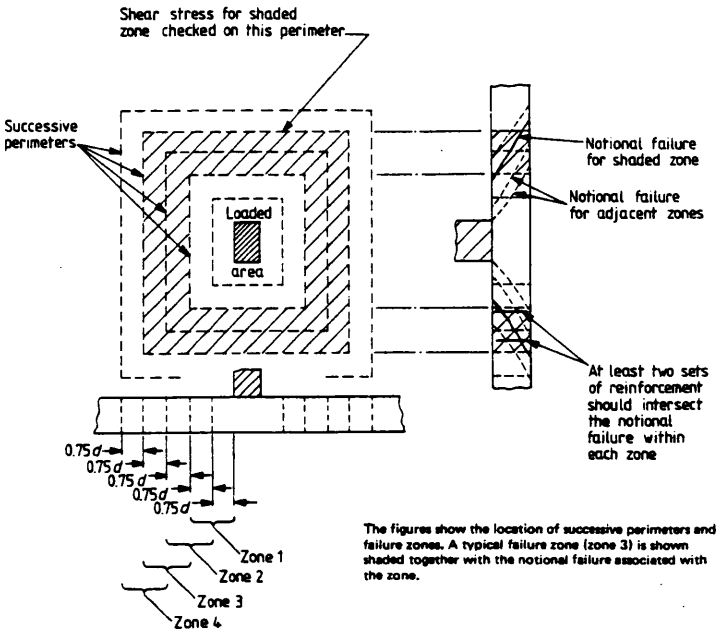

Fig. 2.10 Possible punching failure zone.

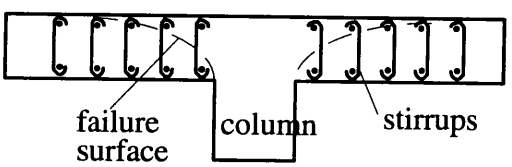

Fig.2.11 The layout of the shear reinforcement.

BS8110 and CP110 have the following requirements:

1) The shearing reinforcements are only applicable for slab thickness greater than 200mm.
2) The possible successive failure zones should be checked as shown in Fig.2.10.
3) The distance between the links should not be more than *0.75d* (Fig.2.11); the shear reinforcement should be distributed evenly around the zone on at least two perimeters; the spacing around the perimeter should not exceed *1.5d*. In assessing the reinforcement required, shear reinforcement within the zone provided to reinforce other zone may be taken into account.
4) The area of shear reinforcement required is

$$\sum A_{sv} \sin\alpha = \frac{(v - v_{cr})ud}{0.87 f_{yv}} \qquad (2.22)$$

$(\nu - \nu_{cr})$ should not be taken as less than 0.4N/mm.

where A_{sv} the area of the required shear reinforcement, including bent-bars and stirrups.

α the angle between the shear reinforcement and the plane of the slab.

f_{yv} the characteristic strength of the shear reinforcement

u the length of the perimeter which has a distance of 1.5d from the face of the column.

ν the nominal shear stress at the punching periphery.

ν_{cr} the nominal shear strength.

5) Upper strength limit: no matter what amount of shear reinforcement is provided, the shear strength on the column face should be limited to that:

$$\nu_{cr} \leq 0.8\sqrt{f_{cu}} \text{ or } 5 \text{ N/mm}, \text{ whichever is less.}$$

2.4.2.2 ACI-318

When shear reinforcement is provided, the shear force carried by the concrete is assumed to be equal to the shear force at which the shear stress in the concrete is equal to the stress at which diagonal tension cracks form. The shear reinforcement is assumed to carry all of the shear force in excess of that to cause diagonal cracking. The shear stress to cause diagonal cracking is given as a function of concrete strength and, depending upon the aspect ratio of the load area, is up to 50% less than the allowable shear stress in the absence of shear reinforcement. Hence, the shear force carried by the concrete when shear reinforcement is present is ϕP_c where $0.5 \leq \phi \leq 1$. Thus, the American code combines P_C and P_S as follow:

$$P = \phi P_c + P_s \tag{2.23}$$

$$\phi P_c = 0.166\sqrt{f_c}ud \tag{2.24}$$

$$P_s = A_v f_y \frac{d}{s} + A_v f_y \sin\alpha \tag{2.25}$$

where,

u the assumed perimeter of the failure surface which is 0.5d from the column face;

s the spacing of the stirrups.

The maximum nominal ultimate shear stress on the assumed failure surface that can be carried by the concrete and shear reinforcement is not permitted to exceed $0.5\sqrt{f_c}$, no matter how much shear reinforcement is provided.

2.4.2.4 CEB-FIP

If the shear resistance of the concrete alone is insufficient then the shear reinforcement should be provided such that the reinforcement resists 75% of the total shear force. However the stress in the shear reinforcement should not be assumed to exceed $30N/mm^2$. The governing equations are

$$P = \beta P_s \tag{2.26}$$

$$1.0 \leq \beta \leq 1.33 \tag{2.27}$$

$$P \leq 1.6 P_c \tag{2.28}$$

2.4.3 PUNCHING SHEAR DESIGN OF WAFFLE SLABS BY BS8110

1) In order to ensure that the normal punching shear clauses for flat slabs adjacent to the column can be applied, the solid section should extend for a distance at least 2.5 times the slab effective depth from each column face.
2) Shear perimeters which lie outside the solid area should be considered. In such cases, the applied force should be distributed equally among all ribs.

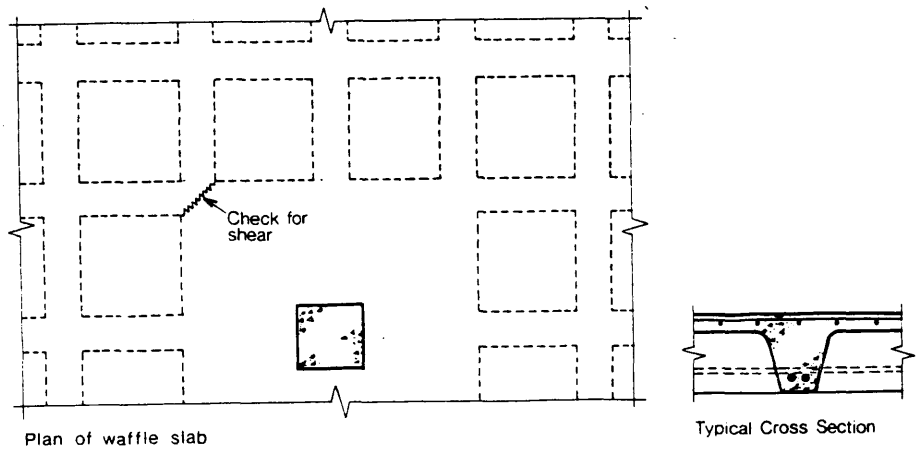

Fig.2.12 The punching in waffle slab

3) Where two ribs at right angles to each other meet at a corner of the solid section, there is a section at 45^o, the width of which is only equal to $\sqrt{2}$ times the width of

the rib although the shear force is equal to the reactions from the two ribs (see Fig.2.12).

4) If shear reinforcement is required, this should be extended an effective depth distance into the solid slab.

The formula for calculating the shear capacity is similar to that of solid slabs. The code does not provide a method to calculate the shear capacity of the waffle slab under a concentrated load.

2.5 CONCLUSIONS

In this chapter, we have reviewed the previous research and current codes of practice of various countries on the subject of punching shear in reinforced concrete slabs. As little work has been done towards punching shear in RC waffle slabs and the natural link between solid slabs and waffle slabs, this chapter has reviewed previous research on solid slab, understanding the existing study methods and achievement of previous people, expecting to extend the previous finding on solid slabs to waffle slabs.

The study methods applied to the punching, like in any other subject, included the experimental study and theoretical study. As to the code of practice, it is based on a rational study: using the theoretical study to establish the factors which mostly influence the results, and then these parameters are verified and determined by the statistics of the test results. The factors mostly influencing the punching load capacity were summarised and listed in section 2.2.1.4.

Several pioneer experimental study, described in section 2.2, has formed the bases of the provisions regarding the punching shear in codes of practice. They all used the concept of nominal shear strength and the critical perimeter to define the punching capacity. Due to the numerous factors influencing the punching capacity of slabs, the test results were interpreted in various manners; and these were reflected in adopting different punching perimeter and different nominal shear strength by their proposed analysis formulae. The more detailed discussion of these experimental studies was given in section 2.2.2.

The approach of theoretical modelling of punching shear started at about the same time as the experimental study, although the limit analysis and equilibrium analysis are

earlier that the finite element analysis. In the three methods of analysis, the limit analysis and equilibrium analysis are less sophisticated, easier to be converted into practical use; their disadvantage is that they also depend on the experimental results. The application of FEA to punching analysis has not been intensively conducted, although the FEA may be capable of giving the crack pattern, deflection as well as the punching load; the results are sensitive to the input data -- the parameters governing the behaviour of the concrete under multi-axial stress status, which itself is by now still not very clear and under investigation. The three analysis methods and the comments on them were described in section 2.3.

Due to the complexity of the punching problem, the previous study shows that the best prediction is from formulae obtained through experimental study. The codes of practice are more or less based on these formulae; as they are empirical, their extension applying to waffle slabs has to be verified, this is one of the objectives of our study.

CHAPTER 3

LIMIT ANALYSIS ON PUNCHING SHEAR FAILURE

3.1 INTRODUCTION

Limit analysis has been extensively applied to the analysis of RC slabs in flexure; this method has the advantage of simplicity and acceptability to engineers. The application of this upper-bound method to the punching shear analysis of slabs has been investigated by a few researchers (Braestrup[46], Jiang[34], and Bortolli[10]), and formulae to predict the punching shear load in solid axisymmetrical slabs have been recommended.

In this chapter, the upper bound method is applied to rectangular solid slabs with rectangular loading pad, and then the method is further applied to RC waffle slabs. Using the formulae developed for waffle slabs, a study is made to show the proportion of the shear resistance between the ribs and decks; the punching perimeter in solid slabs, and waffles slabs; the influence of the dimension of the recess on the punching load; the change of the punching load and punching perimeter by the use of vertical shear reinforcement.

Combining the above study with the current code of practice BS8110, three methods to predict the punching load on RC waffle slabs are proposed.

3.2 MODIFIED COULOMB CRITERIA AND ITS APPROXIMATION

3.2.1 MODIFIED COULOMB CRITERIA

In 1775, Coulomb proposed the frictional hypothesis which is based on the observation that failure often occurs along certain sliding planes, and the resistance to the sliding is determined by the cohesion, c, and the internal friction of the material, μ. The magnitude of the resistance depends on the normal stress in the sliding plane and the expression for the Coulomb criteria is

$$\tau = c \pm \mu\sigma \qquad (3.1)$$

where σ is considered positive for tensile stress. Fig.3.1a shows the criteria in a $\sigma \sim \tau$ co-ordinate system, and Fig.3.1b in a principal stress co-ordinate system. The internal friction can be further expressed as

$$\mu = \tan\varphi \qquad (3.2)$$

where φ is called internal friction angle. The magnitudes of c and φ vary for different materials and can be determined from experiments on the material concerned.

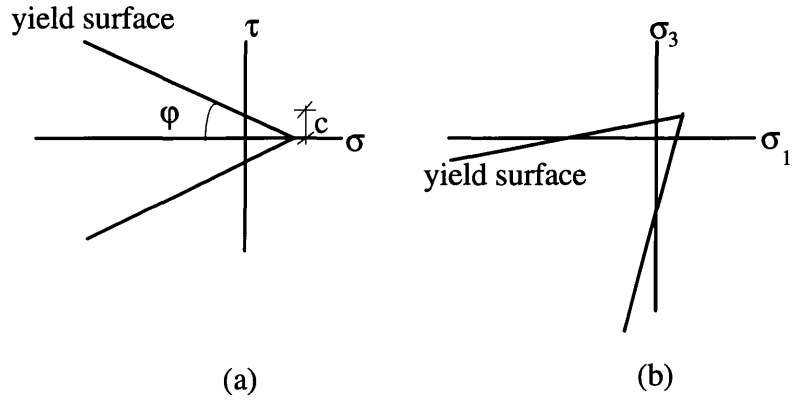

Fig.3.1 Coulomb Criterion

Coulomb criterion considers only the sliding failure, while, there actually exists another type of material failure, i.e., the separation or tension failure. The coulomb criteria can be modified to cover the tension failure, i.e., a tension-cutoff is imposed on the material.

The tension-cutoff is expressed as

$$\sigma = f_t \qquad (3.3)$$

where f_t is the separation resistance.

Fig.3.2a & 3.2b shows the modified Coulomb criteria on the $\sigma \sim \tau$ co-ordinate and principal co-ordinate systems.

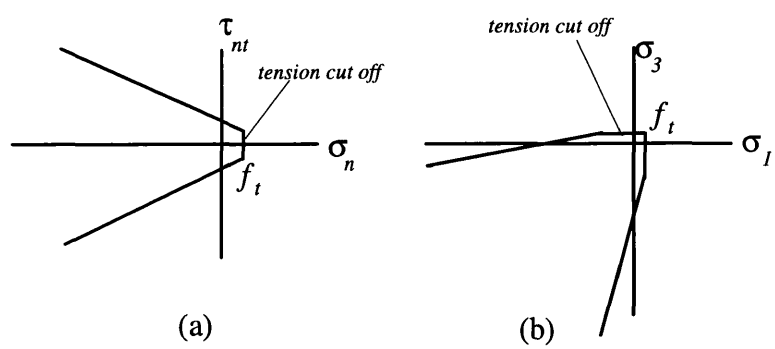

Fig.3.2 Modified Coulomb Criterion

3.2.2 APPROXIMATION OF MOHR-COULOMB CRITERIA BY PARABOLIC CURVES

The modified Mohr-Coulomb criteria consists of several segments of straight lines (several pieces of planes in the 3-D space) when drawn on 2-D plane. Although the equations look simple and have proved reasonably good to define the failure characteristics of material a few problems exist with this criteria, as stated below when applied to concrete.

First, difficulties are encountered when they are employed in the analysis, as the failure curve (surface) is not smooth and the stress status has to be checked constantly to find the proper equation. Second, the failure stress in high compression stress status may be over-estimated and experiments showed that the limit stress would not increase linearly with the increase of the compressive stress. Third, straight line on the failure curve leads to single ratio of plastic strains ε_n and γ_{nt} (according to the associate flow theory) and this further leads to a straight line of the generatrix of the failure surface; this is contrary to the experiment result.

In order to overcome the shortcomings of the modified Coulomb-Mohr criteria, various strength criteria have been proposed in the past years[19], recently by Jiang[43] and Bortolotti[10] in their paper on punching on reinforced concrete slabs. Jiang proposed a parabolic failure curve to replace the modified Coulomb-Mohr curves. The parabolic curve has the advantage of smoothed curves and reflecting the drop of the limit stress under high compression, and allowing the occurrence of various ratios of plastic strains ε_n and γ_{nt}.

In this study, the upper limit analysis will be applied to the punching on RC waffle slabs, employing the strength criteria expressed by parabolic curves. The following sections describe the determination of the parameters used and compared it with the modified Coulomb-Mohr criteria.

In comparison with Eq.(3.1), a parabolic equation is used to express the relationship between the normal stress σ_n and τ_{nt} on a plane

$$\frac{\sigma_n}{f_t'} + \frac{m^2}{4K}\left(\frac{\tau_{nt}}{f_c'}\right)^2 = 1 \qquad (3.4)$$

where f_t' is the plastic (or effective) tensile strength of concrete, f_c' is the plastic compressive strength,

$$f_t' = \upsilon_t f_t \qquad (3,5a)$$

$$f_c' = \upsilon_c f_c \qquad (3.5b)$$

$$m = f_c'/f_t' \qquad (3.6)$$

f_t and f_c are the tensile and compressive strength of concrete. υ_t and υ_c are the effective factors, which can be determined from experiments on various types of structures[46]. K is a factor defined by Eq.3.7.

In Eq.3.4, the plastic strengths were used instead of the compressive or tensile strength, the reason was that this formula would be used later on for the plastic analysis. In the plastic analysis, the RC concrete is considered as perfect-plastic, while, in reality it is not; therefore a reduction to f_t and f_c are necessary. This is shown schematically in Fig.3.3a and 3.3b.

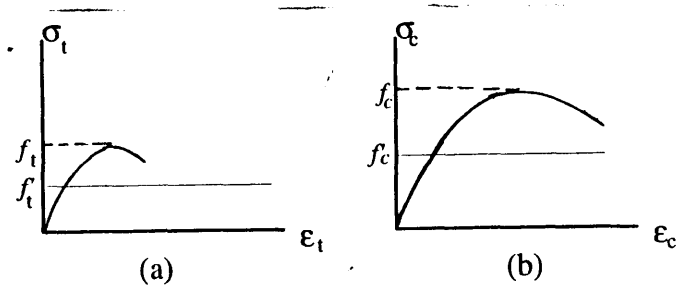

Fig.3.3 Plastic (effective) Strength

The parameter K is determined by allowing the parabolic failure curve tangent to the Mohr circle for uniaxial tension and compression states respectively, as shown in Fig.3.4.

$$K = \frac{1}{4}\left[m + 2\left(1 - \sqrt{m+1}\right)\right] \qquad (3.7)$$

In Fig.3.4, the modified Coulomb-Mohr criteria is also shown by thinner lines for comparison.

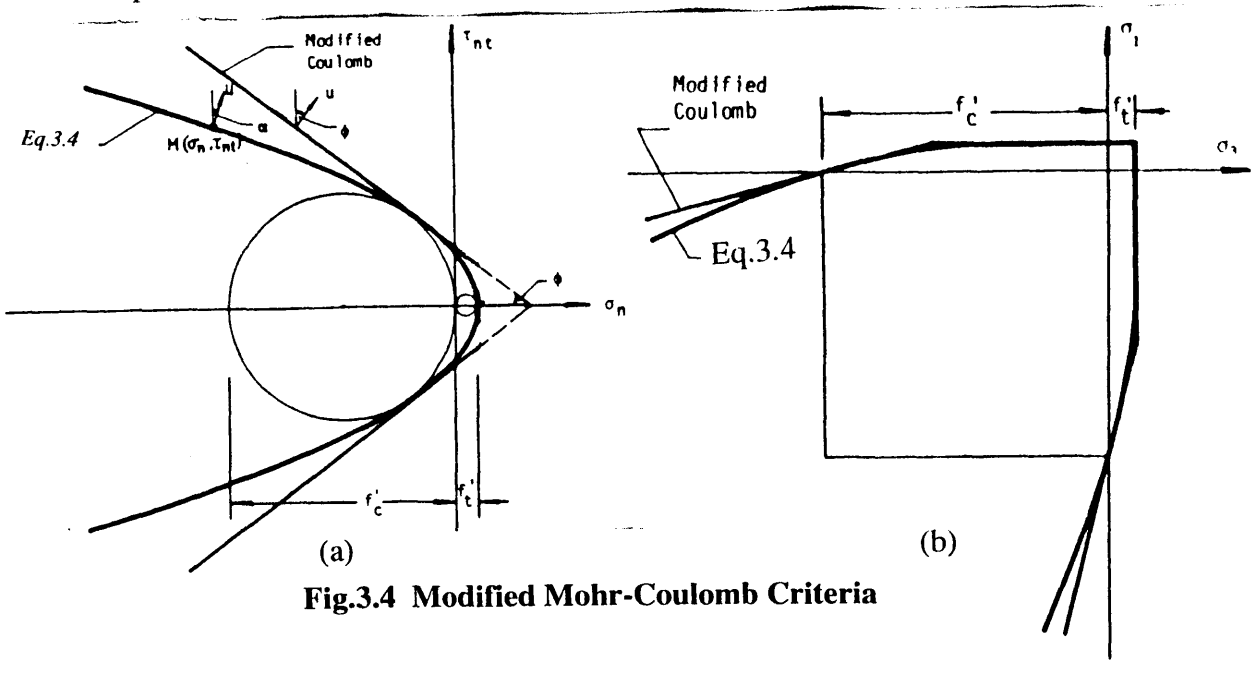

Fig.3.4 Modified Mohr-Coulomb Criteria

3.3 FORMULATION FOR RC SOLID SLABS WITH SQUARE LOADING AREA

Previous researchers[1] have used upper bound analysis to model the axisymmetrical punching in RC solid slabs — circular loading pad and circular slabs. In this section, this method is extended to punching in rectangular slabs — squared loading pad and squared slabs.

The parabolic equation, Eq.3.4, is employed as the failure criteria for concrete; the associated flow theory is assumed to be applicable to concrete material. Although there have been long argument as to whether or not the associate flow theory is applicable to RC concrete, it is still commonly used. The reason is that there are not many other choices.

Associated Flow — Normality Condition

When a certain stress state $M(\sigma_n, \tau_{nt})$ reaches the parabolic curve the material yields. The co-ordinates σ_n and τ_{nt} must satisfy Eq.3.4 The normality condition requires the direction of plastic flow be normal to the yield surfaces. Thus

$$\tan\alpha = 2K\frac{f_t'}{\tau_{nt}} \qquad (3.8)$$

The direction of plastic strain being known, the values of the shear and normal stresses on the yield surface can be uniquely determined.

$$\sigma_n = (1 - K\cot^2\alpha) f_t' \qquad (3.9)$$

$$\tau_{nt} = 2K\cot\alpha f_t' \qquad (3.10)$$

Work Equation

For deriving an upper-bound solution, a collapse mechanism has to be assumed and a work equation established.

The assumed failure mechanism is that, as shown in Fig.3.5, a solid of revolution I is punched out of the remaining part II of the slab. Both parts I and II are rigid and are connected by a plastic region III in the form of a shell of revolution with a thickness δ. The generatrix of the failure surface remains to be determined.

The central cone undergoes a vertical virtual displacement u, inducing plastic strain in the plastic region III only, since parts I and II are both rigid. The displacement is directed at an angle α to the yield surface, allowing the plastic region to extend in the direction n and also shear at an angle γ_{nt}.

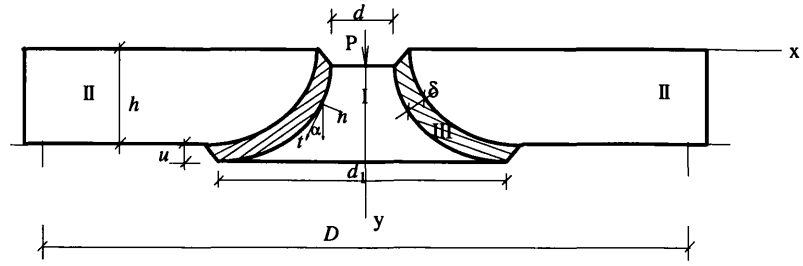

Fig.3.5 Assumed Failure Mechanism

The tensile and shear plastic strain are, respectively:

$$\varepsilon_n = \frac{u\sin\alpha}{\delta} \tag{3.11}$$

$$\gamma_{nt} = \frac{u\cos\alpha}{\delta} \tag{3.12}$$

There is no deformation in the tangential direction *t*. The strain in the horizontal direction parallel to the plan of the slab is small and may be neglected in the analysis, this assumption can be justified by comparing to the case of punching with a circular loading area, where the strain in the circumferential direction is zero.

The internal energy of dissipation in the plastic region

$$W_I = \int_A W_A dA \tag{3.13}$$

where, W_A is the dissipation per unit volume of the plastic region having a thickness of δ.

$$W_A = \delta(\sigma_n\varepsilon_n + \sigma_t\varepsilon_t + \sigma_\theta\varepsilon_\theta + \tau_{nt}\gamma_{nt} + \tau_{t\theta}\gamma_{t\theta} + \tau_{\theta n}\gamma_{\theta n}) = \delta(\sigma_n\varepsilon_n + \tau_{nt}\gamma_{nt})$$

$$W_A = uf_t'(1+K\cot^2\alpha)\sin\alpha \tag{3.14}$$

$$W_I = u\int_A f_t'(1+K\cot^2\alpha)\sin\alpha dA \tag{3.15}$$

The external work done by the applied load is

$$W_E = P\cdot u \tag{3.16}$$

The external work should be equal to the internal work, then

$$P = f_t'\int_A (1+K\cot^2\alpha)\sin\alpha dA \tag{3.17}$$

In the case of a square loading pad, the revolution of the punching out could be in the shape of a pyramid or a pyramid with rounded corner, as shown in Fig.3.6a and Fig.3.6b. Different solutions will be derived for these two cases.

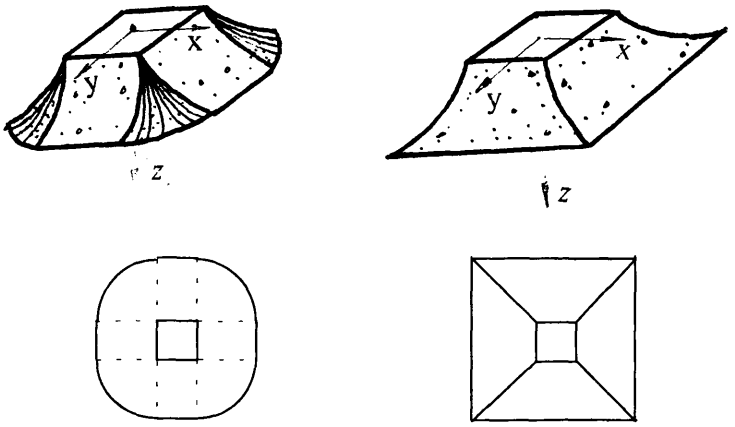

(a) Round Corner Surface (b) Rectangular Surface

Fig.3.6 Geometry of Punching Failure Surface

1. Rectangular Failure Surface

In the case of a rectangular pyramid, it can be further assumed that the pyramid is symmetric about x and y axes, the edge of the intersection of the two sides can be expressed as

$$x = \pm y = f(z), \tag{3.18}$$

where, $f(z)$ is the equation for the generatrix of the failure surface.

The punching load can be expressed as

$$P = 4 f_t' \int_{A1} (1 + K \cot^2 \alpha) \sin \alpha \, dA \tag{3.19}$$

where, A1 is a quarter of the failure surface, located in the positive x direction.

$$dA = \frac{1}{\cos \alpha} dy dz \tag{3.20}$$

Substituting Eq.3.20 into Eq.3.19 will give

$$P = 4 f_t' \iint_{A1} (\tan \alpha + K \cot \alpha) dy dz = 4 f' \int_0^h \left(\int_{-y1}^{y1} \left(x' + \frac{K}{x'} \right) dy \right) dz \tag{3.21}$$

$$P = 8 f_t' \int_o^h y_1 \left(x' + \frac{K}{x'} \right) dz \tag{3.22}$$

where, y_1 represents the edge of the pyramid. As the edge has the equation

$$x_1 = f(z) \tag{3.23a}$$

$$y_1 = f(z) \tag{3.23b}$$

and the generatrix of the surface has the equation

$$x = f(z) \tag{3.24}$$

so $x_1 = x$, and substituting this into Eq.3.22 gives

$$P = 8 f_t' \int_o^h x\left(x' + \frac{K}{x'}\right) dz \tag{3.25}$$

Denoting $F(x, x') = x(x' + \frac{K}{x'})$

we get $$P = 8 f_t' \int_o^h F\left(x' + \frac{K}{x'}\right) dz \tag{3.26}$$

The lowest value to the upper bound solution is determined by calculus of variation. By using Euler's equation $F - x'F_{x'}' = C$, we have

$$x\left(x' + \frac{K}{x'}\right) - x'x\left(1 - \frac{K}{(x')^2}\right) = C \tag{3.27}$$

which gives $x' = C_1 x$, where $C_1 = 2K/C$. Solving Eq.3.27 gives

$$x = C_2 e^{C_1 z} \tag{3.28}$$

This is the required generatrix which gives a minimum value of the collapse load when a pyramid failure surface is assumed. The constants C_1 and C_2 are determined from the following boundary conditions: $x(0) = d/2$ and $x(h) = d_1/2$, which gives $C_2 = d/2$ and

$$C_1 = \ln\left(d_1/2\right) / h$$

Hence

$$x = \frac{d}{2}\left(\frac{d_1}{d}\right)^{z/h} \tag{3.29}$$

in which d_1 is the dimension at the base of the failure pyramid.

The lowest upper bound can be obtained by substituting Eq.3.29 into Eq.3.26,

$$P = f_t'\left(d_1^2 - d^2 + \frac{Kh^2}{\ln d_1 - \ln d}\right) \tag{3.30}$$

For different d_1 there would be different values of P, the critical one can be derived from

$$\frac{\partial P}{\partial d} = 0$$

or $$\left(\frac{d_1}{d}\right)^{d_1/d} = e^{2\sqrt{K}h/d} \tag{3.31}$$

If the span of the slab, D, is larger than d_1, then use d_1 derived from Eq.3.31; while, if $D < d_1$, use D instead of d_1 in Eq.3.31 to get P.

2. Rounded Corner Failure Surface

In this case the pyramid has round-corners, the edge is replaced by a round corner — a quarter of the circular with the radius r. It is assumed the generatrix of the side failure surface is the same as that of the corner, so

$$x = \frac{d}{2} + f(z) \tag{3.32a}$$

$$r = f(z) \tag{3.32b}$$

The failure load is

$$P = 4f_t'\left[\int_{S1}\left(1 + K\cot^2\alpha\right)\sin\alpha dA + \int_{P1}\left(1 + K\cot^2\alpha\right)\sin\alpha dA\right] \tag{3.33}$$

where, S_1 is the side failure surface located in the positive x direction, P_1 is the corner surface located in the first quadrant. Eq.3.33 can be further expressed as

$$P = 4f_t'\left[\int_0^h\int_{-d/2}^{d/2}(\tan\alpha + K\cot\alpha)dydz + \int_0^h\int_0^{\pi/2}(\tan\alpha + K\cot\alpha)rd\theta dz\right]$$

$$P = 4f_t'\left[d\int_0^h\left(x' + \frac{K}{x'}\right)dz + \frac{\pi}{2}\int_0^h r\left(r' + \frac{K}{r'}\right)dz\right] \tag{3.34}$$

Assume $x = \frac{d}{2} + t$ and $r = t$, then Eq.3.34 becomes

$$P = 4f_t'\int_0^h\left(d + \frac{\pi}{2}t\right)\left(t' + \frac{K}{t'}\right)dz \tag{3.35}$$

Denoting $F(t,t') = \left(d + \frac{\pi}{2}t\right)\left(t' + \frac{K}{t'}\right)$

$$P = 4f_t'\int_0^h F(t,t')dz \tag{3.36}$$

The lowest upper bound is derived by using Euler equation, $F - t'F_{t'}' = C$. We have

$$\left(d + \frac{\pi}{2}t\right)\left(t' + \frac{K}{t'}\right) - t'\left(d + \frac{\pi}{2}t\right)\left(1 - \frac{K}{(t')^2}\right) = C \tag{3.37}$$

or $$\left(d + \frac{\pi}{2}t\right)\frac{2K}{t'} = C$$

$$t' = \frac{2K}{C}\left(d + \frac{\pi}{2}t\right) = C_1\left(d + \frac{\pi}{2}t\right) \tag{3.38}$$

where, $C_1 = \frac{2K}{C}$

Solution to Eq.3.38 is

$$t = \frac{2d}{\pi}\left(C_2 e^{C_1 z} - 1\right) \tag{3.39}$$

The boundary conditions are

when $z=0$, $x=d/2$, $t=0$, hence $C_2 = d$

when $z=h$, $x = {}^{d_1}\!/_{2}$, $t = {}^{(d_1 - d)}\!/_{2}$,

$$C_1 = \frac{1}{h}\ln\left(\frac{\pi}{4}\left(\frac{d_1 - d}{d}\right)+1\right)$$

then

$$P = 4 f_t' \left[\frac{\pi}{16}(d_1 - d)^2 + \frac{d(d_1 - d)}{2} + \frac{K\pi h^2}{2\ln\left(\frac{\pi}{4}\frac{(d_1 - d)}{d}+1\right)}\right] \tag{3.40}$$

The lowest upper bound solution is obtained by

$$\frac{\partial P}{\partial d_1} = 0,$$

which gives

$$S^S = e^{\frac{\pi h\sqrt{K}}{2d}}, \tag{3.41}$$
$$S = \frac{\pi}{4}\frac{(d_1 - d)}{d}+1$$

3.4 FORMULATION FOR RC WAFFLE SLABS WITH SQUARE LOADING PAD

Because of the existence of recesses on the waffle slabs, the area on the failure surface is reduced. The equations of the punching failure in waffle slabs will be formulated in this section. As the exact solutions are not easy to get, a numerical solution is sought and the results will be compared with those of solid slabs. Before the formulation on the waffle slabs is attempted, it is necessary to define a few parameters expressing the dimension of the recesses and the contents of the recesses inside the slabs.

3.4.1 DEFINITION OF PARAMETERS RELATING TO WAFFLE SLABS

The waffle slabs consist of two parts, the top solid deck and the ribs in the orthogonal directions. In the second part of the slab, there are recesses among the ribs. When calculating the area in an inclined surface, it is convenient to use the parameter of recess ratio (or void ratio) as defined bellow:

The plane view of ribs of a waffle slab is shown in Fig.3.7a, the x and y dimensional void ratio is

x direction void ratio: $\rho_x = \dfrac{a_x}{a_x + b_x}$ (3.42a)

y direction void ratio: $\rho_y = \dfrac{a_y}{a_y + b_y}$ (3.42b)

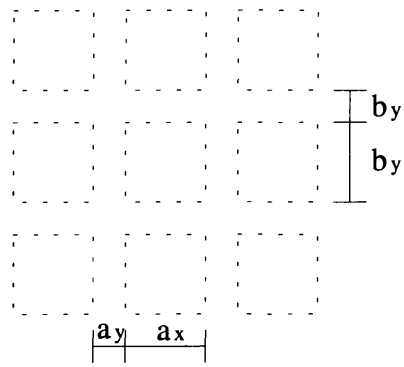

Fig.3.7a Plane View of Waffle Slabs

the void area ratio is

$$\rho_{xy} = \rho_x \rho_y \qquad (3.43)$$

Table 3.1 lists the void ration for a few configuration of waffle slabs with squared recesses.

Table 3.1 Example values of void ratio and area void ratio

ρ_x	0.39	0.50	0.59	0.67	0.74	0.81	0.87	0.92
ρ_{xy}	0.15	0.25	0.35	0.45	0.55	0.65	0.75	0.85

In a rectangular area with dimensions x and y, the void area and the filled area are

$$V_{xy} = \rho_x \cdot \rho_y \cdot x \cdot y$$

$$A_{xy} = x \cdot y - V_{xy} = (1 - \rho_{xy}) \cdot x \cdot y$$

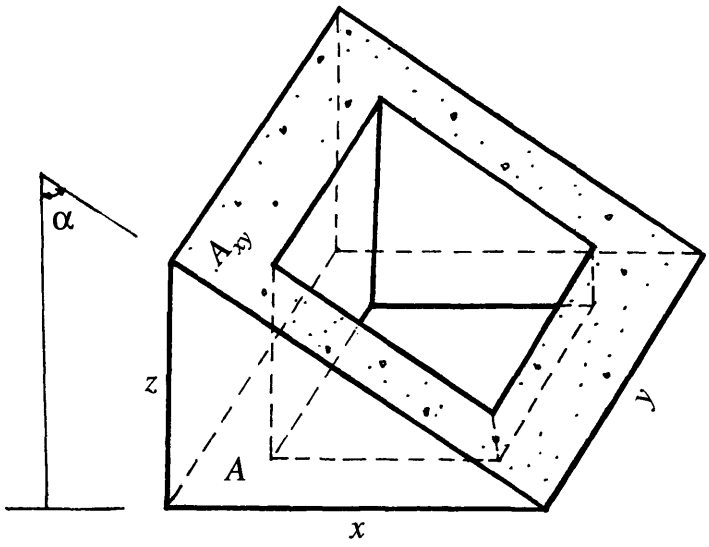

Fig. 3.7b The Inclined surface

The area of an inclined surface as shown in Fig.3.7b is

$$A = A_{xy} / \sin\alpha = (1-\rho_{xy}) \cdot x \cdot y / \sin\alpha \qquad (3.44)$$

and

$$x = z \tan\alpha \qquad (3.44b)$$

Substituting Eq.3.44b into Eq.3.44 will get

$$A = (1-\rho_{xy}) yz / \cos\alpha \qquad (3.45)$$

3.4.2 FORMULATION FOR RC WAFFLE SLABS WITHOUT SHEAR REINFORCEMENTS

Here the formulae for RC solid slabs will be extended to RC waffle slabs, and the geometry of the recesses will be reflected in the formulae by the parameters defined in section 3.4.1. Both the rectangular and the rounded-corner failure surfaces will be studied.

In a waffle slab, the punching position might be in the middle of a slab panel or at the slab-column connection area. In the former case, the deck is under compression; and in the latter case the deck is under tension. These two cases will also be dealt with separately, and we refer the former as deck-top punching case, and the latter as deck-bottom punching case. In the following, the rectangular failure surface for both deck-top and deck-bottom cases will be studied first, and then followed by punching with the assumed rounded-corner failure surface.

3.4.2.1 Rectangular Failure Surface

From Eq.3.19, we get

$$P = 4f_t' \int_{A1} (1 + K\cot^2\alpha)\sin\alpha dA$$

If the area A is divided into the deck part A_d and the rib part A_r, so

$$P = 4f_t' \left(\int_{A_{d1}} (1 + K\cot^2\alpha)\sin\alpha dA + \int_{A_{r1}} (1 + K\cot^2\alpha)\sin\alpha dA \right) \quad (3.46)$$

1. Deck-Top Case

Substituting Eq.3.45 into Eq.3.46 we get

$$P = 4f_t' \left(\int_0^{\bar{h}} \int_{-y_1}^{y_1} (\tan\alpha + K\cot\alpha) dy dz + (1 - \rho_{xy}) \int_{\bar{h}}^{h} \int_{-y_1}^{y_1} (\tan\alpha + K\cot\alpha) dy dz \right) \quad (3.47)$$

where h is the depth of the slab, $\bar{h}$ is the depth of the solid deck. Substituting $x' = \tan\alpha$ and $y_1 = x$ into Eq.3.47, we get

$$P = 8f_t' \left(\int_0^{\bar{h}} x\left(x' + \frac{K}{x'}\right) dz + (1 - \rho_{xy}) \int_{\bar{h}}^{h} x\left(x' + \frac{K}{x'}\right) \right)$$

then

$$P = 8f_t' \left(\int_0^{h} x\left(x' + \frac{K}{x'}\right) dz - \rho_{xy} \int_{\bar{h}}^{h} x\left(x' + \frac{K}{x'}\right) \right) \quad (3.48a)$$

or

$$P = 8f_t' \left((1 - \rho_{xy}) \int_0^{h} x\left(x' + \frac{K}{x'}\right) dz + \rho_{xy} \int_0^{\bar{h}} x\left(x' + \frac{K}{x'}\right) \right) \quad (3.48b)$$

In Eq.3.48b, the first part is the shear resistance of the grillage system which is through the whole depth of the slab; the second part is the resistance provided by the part of the deck concrete, the projection of which coincide with the recesses.

From Eq 3.48b it is seen that the solution to the first part of the equation is also the solution to the second part of the equation, as the two parts are of the same form. Furthermore the equation is the two parts added together, so two minimum answers for each will make the addition minimum.

Comparison between the first part of Eq.3.48b and Eq.3.25 shows that they have the same form and will yield the same solution, so Eq.3.48 can be expressed as

$$P = 8f_t'\left\{\left(\frac{{d_1}^2 - d^2}{8} + \frac{kh^2}{\ln d_1 - \ln d}\right) - \rho_{xy}\left[\frac{d^2}{8}\left(\left(\frac{d_1}{d}\right)^2 - \left(\frac{d_1}{d}\right)^{2\bar{h}/h}\right) + \frac{k(h-\bar{h})h}{\ln d_1 - \ln d}\right]\right\} \tag{3.49}$$

the lowest value of P is obtained by getting the most critical punching perimeter d_1 and then substitute the d_1 into Eq.3.49 to get the most critical load P. d_1 is obtained by

$$\frac{\partial P}{\partial d_1} = 0$$

$$\left(\frac{d_1}{d}\right)^{\sqrt{(1-\rho_{xy})\left(\frac{d_1}{d}\right)^2 + \rho_{xy}\frac{\bar{h}}{h}\left(\frac{d_1}{d}\right)^{2\bar{h}/h}}} = e^{\frac{2\sqrt{kh\left[(1-\rho_{xy})h + \rho_{xy}\bar{h}\right]}}{d}} \tag{3.50}$$

Solving Eq.3.50 will give d_1.

2. Deck-Bottom Case

Similarly in the case of deck-top, we get the equations as below.

$$P = 8f_t'\left(\int_0^h x\left(x' + \frac{K}{x'}\right)dz - \rho_{xy}\int_0^{h-\bar{h}} x\left(x' + \frac{K}{x'}\right)\right) \tag{3.51}$$

The minimum solution to the above equation is obtained as

$$P = 8f_t'\left\{\left(\frac{{d_1}^2 - d^2}{8} + \frac{kh^2}{\ln d_1 - \ln d}\right) - \rho_{xy}\left[\frac{d^2}{8}\left(\left(\frac{d_1}{d}\right)^{2(h-\bar{h})/h} - 1\right) + \frac{k(h-\bar{h})h}{\ln d_1 - \ln d}\right]\right\} \tag{3.52}$$

$$\frac{\partial P}{\partial d_1} = 0$$

$$\left(\frac{d_1}{d}\right)^{\sqrt{\left(\frac{d_1}{d}\right)^2 - \rho_{xy}\frac{h-\bar{h}}{h}\left(\frac{d_1}{d}\right)^{2(h-\bar{h})/h}}} = e^{\frac{2\sqrt{kh\left[(1-\rho_{xy})h + \rho_{xy}\bar{h}\right]}}{d}} \tag{3.53}$$

3.4.2.2 Pyramid revolution with round corner

1. Deck-Top Case

Following the same procedures as the type of rectangular failure surface, the equation for punching shear in a waffle slab with the deck in compression is

$$P = 4f_t'\left[\int_0^h \left(d+\frac{\pi}{2}t\right)\left(t'+\frac{K}{t'}\right)dz - \rho_{xy}\int_{\bar{h}}^{h}\left(d+\frac{\pi}{2}t\right)\left(t'+\frac{K}{t'}\right)dz\right] \quad (3.54a)$$

$$\text{or } P = 4f_t'\left[(1-\rho_{xy})\int_0^h \left(d+\frac{\pi}{2}t\right)\left(t'+\frac{K}{t'}\right)dz + \rho_{xy}\int_0^{\bar{h}}\left(d+\frac{\pi}{2}t\right)\left(t'+\frac{K}{t'}\right)dz\right] \quad (3.54b)$$

The minimum load is given by

$$P = 4f_t'\left\{\left[\frac{\pi}{16}(d_1-d)^2+\frac{1}{2}d(d_1-d)+\frac{\pi kh^2}{2\ln\left(\frac{\pi}{4}\frac{(d_1-d)}{d}+1\right)}\right]-\right.$$
$$\left.\rho_{xy}\left[\frac{d}{\pi}\left(\left(\frac{\pi}{4}\frac{(d_1-d)}{d}+1\right)^2-\left(\frac{\pi}{4}\frac{(d_1-d)}{d}+1\right)^{2\bar{h}/h}\right)+\frac{\pi kh(h-\bar{h})}{2\ln\left(\frac{\pi}{4}\frac{(d_1-d)}{d}+1\right)}\right]\right\} \quad (3.55)$$

The lowest value of P is obtained by

$$\frac{\partial P}{\partial d_1}=0$$

$$\left(\frac{\pi}{4}\frac{d_1-d}{d}+1\right)^{\sqrt{\frac{(1-\rho_{xy})}{\pi}\left(\frac{\pi}{4}\frac{d_1-d}{d}+1\right)^2+\frac{\rho_{xy}\bar{h}}{\pi h}\left(\frac{\pi}{4}\frac{d_1-d}{d}+1\right)^{2\bar{h}/h}}} = e^{\frac{\sqrt{\pi kh\left[(1-\rho_{xy})+\rho_{xy}\bar{h}\right]}}{2d}} \quad (3.56)$$

2. Deck-Bottom Case

When the deck is under tension, the equation becomes

$$P = 4f_t'\left[\int_0^h \left(d+\frac{\pi}{2}t\right)\left(t'+\frac{K}{t'}\right)dz - \rho_{xy}\int_0^{h-\bar{h}}\left(d+\frac{\pi}{2}t\right)\left(t'+\frac{K}{t'}\right)dz\right] \quad (3.57)$$

and the solution is

$$P = 4f_t' \left\{ \left[\frac{\pi}{16}(d_1 - d)^2 + \frac{1}{2}d(d_1 - d) + \frac{\pi k h^2}{2\ln\left(\frac{\pi}{4}\frac{(d_1 - d)}{d} + 1\right)} \right] - \rho_{xy}\left[\frac{d}{\pi}\left(\left(\frac{\pi}{4}\frac{(d_1 - d)}{d} + 1\right)^{2(h-\bar{h})/h} - 1 \right) + \frac{\pi k h(h - \bar{h})}{2\ln\left(\frac{\pi}{4}\frac{(d_1 - d)}{d} + 1\right)} \right] \right\} \tag{3.58}$$

with the lowest value of P obtained by

$$\frac{\partial P}{\partial d_1} = 0$$

$$\left(\frac{\pi}{4}\frac{d_1 - d}{d} + 1\right)^{\sqrt{\left(\frac{\pi}{4}\frac{d_1 - d}{d} + 1\right)^2 + \rho_{xy}\left(\frac{\pi}{4}\frac{d_1 - d}{d} + 1\right)^{2(h-\bar{h})/h}}} = e^{\frac{\pi\sqrt{kh\left[(1-\rho_{xy}) + \rho_{xy}\bar{h}\right]}}{2d}} \tag{3.59}$$

3.4.3 FORMULATION FOR RC WAFFLE SLABS WITH SHEAR REINFORCEMENT

In a slab, the vertical shear reinforcements (stirrups) intersecting with the failure surface participate in the resistance to the punching. These shear reinforcements lie inside the area compounded between the inner punching perimeter and the outside perimeter, as shown by the shaded area in Fig.3.8

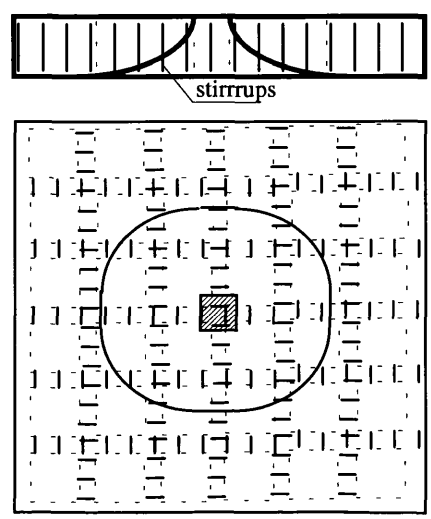

Fig.3.8 Stirrups Participating in Shear Resistance

The steel content can be expressed by the shear steel ratio

$$\rho_{sv} = \frac{A_{sv}}{A(1-\rho_{xy})} \tag{3.60}$$

where, A_{sv} the total shear steel area inside the shaded area,

A the shaded area.

The shaded area can be calculated for the two types of geometry of the revolution, rectangular and the round-corner ones.

Rectangular: $A = d_1{}^2 - d^2$ (3.61)

Round-corner $A = 2d(d_1 - d) + \frac{\pi(d_1 - d)^2}{8}$ (3.62)

The punching load capacity of slabs with shear reinforcement is the resistance of the shear steel, P_{sv}, in addition to that of the concrete, P_c, as following

$$P_{stl} = P_c + P_{sv}$$

The yield stress of the steel is f_{sv}, Since the anchorage of the shear reinforcement is poor, the full strength of shear reinforcement can not be fully exploited, and a reduction to the yield strength is necessary. Therefore, instead of using f_{sv} in the analysis, the strength of shear reinforcements should be taken as $F_{sv}f_{sv}$ in the analysis. F_{sv} is the reduction factor for the yield strength of shear reinforcement, and should taken as less than 1.0. Based on Eq.3.48, 3.52,3.55 and 3.58, the formulae will be

3.4.3.1 Rectangular Surface

1. Deck-Top Case

$$P_{stl} = 8f_t'\left\{\left(\frac{d_1{}^2 - d^2}{8} + \frac{kh^2}{\ln d_1 - \ln d}\right) - \rho_{xy}\left[\frac{d^2}{8}\left(\left(\frac{d_1}{d}\right)^2 - \left(\frac{d_1}{d}\right)^{2\bar{h}/h}\right) + \frac{k(h-\bar{h})h}{\ln d_1 - \ln d}\right]\right\} + \rho_{sv}F_{sv}f_{sv}(1-\rho_{xy})(d_1{}^2 - d^2) \tag{3.63}$$

2. Deck-Bottom Case

$$P_{stl} = 8f_t'\left\{\left(\frac{d_1{}^2 - d^2}{8} + \frac{kh^2}{\ln d_1 - \ln d}\right) - \rho_{xy}\left[\frac{d^2}{8}\left(\left(\frac{d_1}{d}\right)^{2(h-\bar{h})/h} - 1\right) + \frac{k(h-\bar{h})h}{\ln d_1 - \ln d}\right]\right\} + \rho_{sv}F_{sv}f_{sv}(1-\rho_{xy})(d_1{}^2 - d^2) \tag{3.64}$$

3.4.3.2 Round-corner revolution

1. Deck-Top Case

$$P_{stl} = 4f_t' \left\{ \begin{array}{l} \left[\frac{\pi}{16}(d_1-d)^2 + \frac{1}{2}d(d_1-d) + \frac{\pi k h^2}{2\ln\left(\frac{\pi}{4}\frac{(d_1-d)}{d}+1\right)} \right] - \\ \rho_{xy}\left[\frac{d}{\pi}\left(\left(\frac{\pi}{4}\frac{(d_1-d)}{d}+1\right)^2 - \left(\frac{\pi}{4}\frac{(d_1-d)}{d}+1\right)^{2\bar{h}/h} \right) + \frac{\pi k h(h-\bar{h})}{2\ln\left(\frac{\pi}{4}\frac{(d_1-d)}{d}+1\right)} \right] \end{array} \right\} + \rho_{sv}F_{sv}f_{sv}(1-\rho_{xy})\left[2d(d_1-d) + \frac{\pi(d_1-d)^2}{8} \right]$$

(3.65)

2. Deck-Bottom Case

$$P_{stl} = 4f_t' \left\{ \begin{array}{l} \left[\frac{\pi}{16}(d_1-d)^2 + \frac{1}{2}d(d_1-d) + \frac{\pi k h^2}{2\ln\left(\frac{\pi}{4}\frac{(d_1-d)}{d}+1\right)} \right] - \\ \rho_{xy}\left[\frac{d}{\pi}\left(\left(\frac{\pi}{4}\frac{(d_1-d)}{d}+1\right)^{2(h-\bar{h})/h} - 1 \right) + \frac{\pi k h(h-\bar{h})}{2\ln\left(\frac{\pi}{4}\frac{(d_1-d)}{d}+1\right)} \right] \end{array} \right\} + \rho_{sv}F_{sv}f_{sv}(1-\rho_{xy})\left[2d(d_1-d) + \frac{\pi(d_1-d)^2}{8} \right]$$

(3.66)

3.5 DETERMINATION OF THE GEOMETRY OF THE FAILURE SURFACES

In the above sections, we have derived the formulae for the punching failure in RC waffle slabs. For the failure surface, we have assumed two types of geometry: the rectangular failure surface and the rounded-corner failure surfaces. Bearing in mind that the method employed is the upper bound analysis, we have to find out which failure surface is the critical one. Between the two type of failure surfaces, the one gives the lower punching load is the one we want.

In this section, we'll compare the results obtained by using the two types of failure surfaces. The analysis will be conducted on three slabs: a solid slab; a waffle slab of deck-top punching; a waffle slab with deck-bottom punching. The three slabs have the same depth and material parameter. The dimension of the recesses of the two waffle slabs will be varied to consider a wide range of configuration. The parameters of the slabs are given below.

slab depth $h=150mm$
dimension of the square load pad $d=150mm$
uniaxial concrete compressive strength, $f_c = 42.5N/mm^2$
effective factor, $v_c = 2/\sqrt{f_c} = 0.3068$
ratio between plastic compressive strength and tensile strength, $m = f_c'/f_t' = 20$
effective compressive strength, $f_c' = \upsilon_c f_c = 13.04N/mm^2$
effective tensile strength, $f_t' = f_c'/m = 0.652N/mm^2$
the void ration of waffle slab, $\rho_{xy} = 0.15 \sim 0.85$
the deck depth, $\bar{h} = h/5; 2h/5; 3h/5$

Each of the slab will be analysed by formulae based on the two geometric types of failure surface. Solid slab is by Eq.3.30 and 3.40; waffle slabs of deck-top punching by Eq.3.49 and Eq.3.55; and waffle slabs of deck-bottom punching by Eq.3.52 and Eq.3.58.

3.5.1 COMPARISON BETWEEN THE RECTANGULAR FAILURE SURFACE AND THE ROUNDED CORNER FAILURE SURFACE

The punching loads of the three slabs based on the two types of failure geometry are listed in Table 3.2. The abbreviation used in the table are explained below.

P_{s1}: solid slab with rectangular revolution,
P_{s2}: solid slab with round-corner revolution,
P_{T1}: deck-top waffle slab with rectangular revolution,
P_{T2}: deck-top waffle slab with round-corner revolution,
P_{B1}: deck-bottom waffle slab with rectangular revolution,
P_{B2}: deck-bottom waffle slab with round-corner revolution.

The values of Table 3.2 are plotted in Fig.3.9a~c, where the load ratio P/P_{s2} is used instead of the absolute value of the punching load. P_{s_2} is the punching load of the solid slab based on the round-corner revolution.

Table 3.2 Punching Load of Different Failure Geometry and Loading Direction

		Rectangular Revolution			Round-Corner Revolution		
	ρ_{xv}	P_{s1}(KN)	P_{T1}(KN)	P_{B1}(KN)	P_{s2}(KN)	P_{T2}(KN)	P_{B2}(KN)
$\bar{h} = h/5$	0.15	459.04	401.32	407.93	414.9	362.77	368.48
	0.25	459.04	362.8	373.74	414.9	327.98	337.46
	0.35	459.04	324.23	339.45	414.9	293.15	306.35
	0.45	459.04	285.59	305.02	414.9	258.26	275.13
	0.55	459.04	246.84	270.42	414.9	223.28	243.78
	0.65	459.04	207.91	235.6	414.9	188.14	212.24
	0.75	459.04	168.64	200.48	414.9	152.72	180.46
	0.85	459.04	128.59	164.92	414.9	116.64	148.33
$\bar{h} = 2h/5$	0.15	459.04	413.16	422.8	414.9	373.55	381.94
	0.25	459.04	382.45	398.49	414.9	345.89	359.86
	0.35	459.04	351.6	374.05	414.9	318.11	337.66
	0.45	459.04	320.57	349.46	414.9	290.18	315.34
	0.55	459.04	289.27	324.7	414.9	262.02	292.88
	0.65	459.04	257.55	299.75	414.9	233.53	270.26
	0.75	459.04	225.14	274.56	414.9	204.48	247.45
	0.85	459.04	191.39	249.1	414.9	174.38	224.4
$\bar{h} = 3h/5$	0.15	459.04	426.19	435.9	414.9	385.42	393.87
	0.25	459.04	404.12	420.38	414.9	365.64	379.77
	0.35	459.04	381.88	404.78	414.9	345.72	365.6
	0.45	459.04	359.43	389.1	414.9	325.62	351.37
	0.55	459.04	336.67	373.32	414.9	305.3	337.05
	0.65	459.04	313.52	357.44	414.9	284.66	322.65
	0.75	459.04	289.79	341.45	414.9	263.58	308.16
	0.85	459.04	265.14	325.35	414.9	241.82	293.56

P_{s1} & P_{s2}: Solid Slab; P_{T1} & P_{T2}: Deck on Top; P_{B1} & P_{B2}: Deck on Bottom

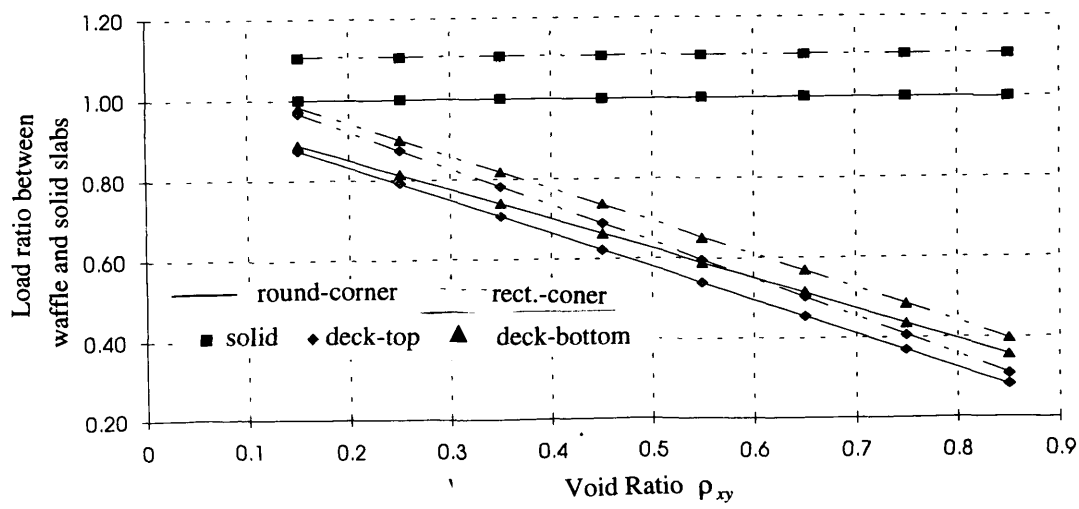

(a) $\bar{h} = h/5$

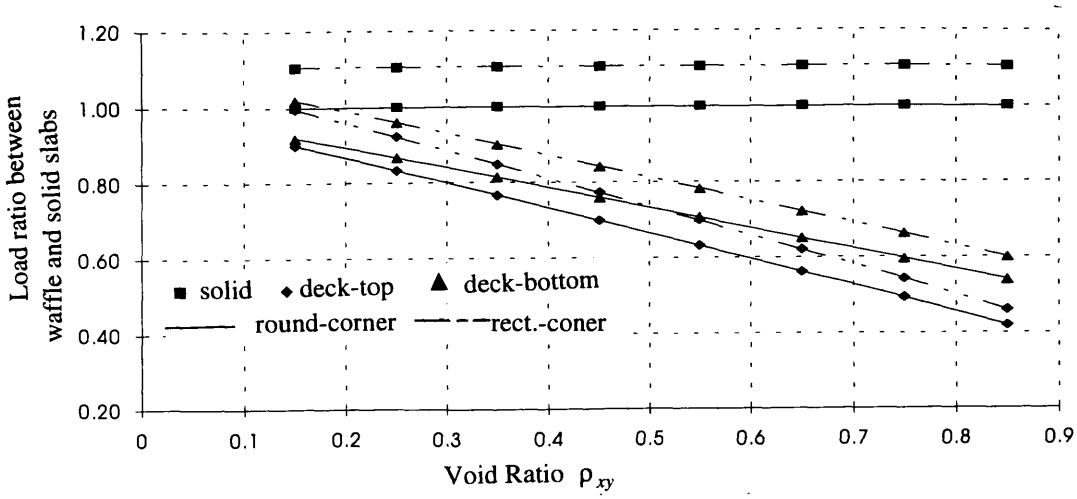

(b) $\bar{h} = 2h/5$

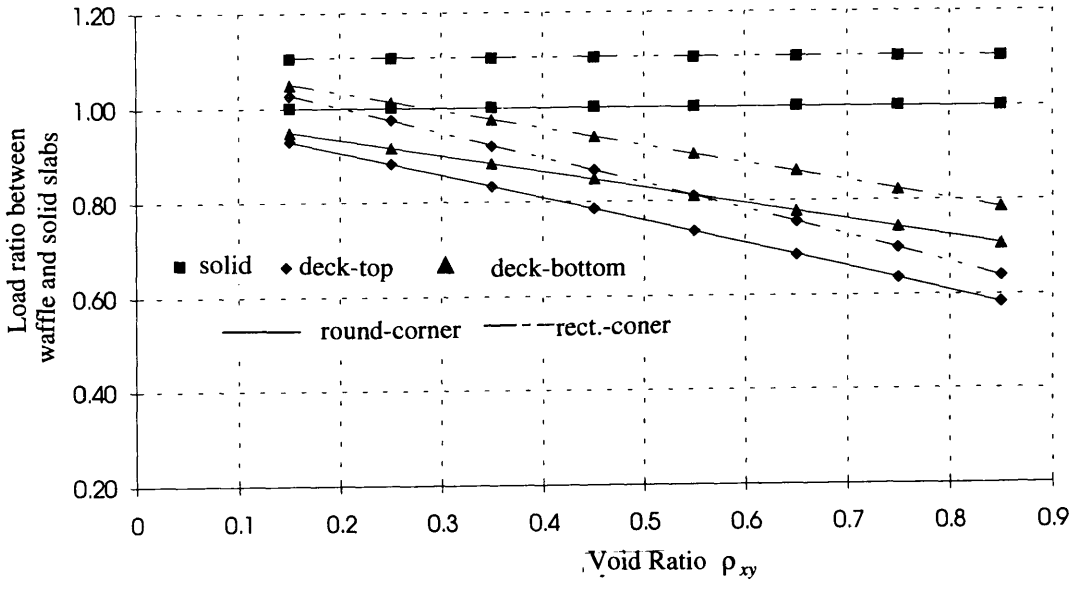

(c) $\bar{h} = 3h/5$

Fig 3.9 Punching Load of Two Types of punching Geometry

From Fig.3.9(a)~(c), it is seen that the results based on the rounded-corner punching surfaces are smaller than those based on the rectangular revolution regardless of the slab type and the depth of the deck. Bearing in mind that the analysis here is the upper limit analysis and the minimum load is the desired one, so the formula based on the round-corner revolution should be used in the analysis of the punching load. This is also in conformation with experiments which gave the rounded-corner failure surface.

From Fig. 3.9(a)-(c), it is also observed that, for the waffle slabs, the load of deck-bottom punching is larger than that of deck-top punching. This means that the punching load differs with the loading direction in a waffle slab, higher value for upward and

lower for downward. This is the result of using the total depth of slab and we'll see in the later section that the effective depth should be used for practical analysis.

Conclusions can be drawn that the round-corner punching surface is more critical, so the upper bound analysis should be based on the rounded-corner punching failure surface.

3.5.2 COMPARISON OF PUNCHING PERIMETERS BETWEEN SOLID SLAB AND WAFFLE SLAB

The punching failure surface intersects with the top and bottom surface of the slab. The intersection with the top surface is normally the perimeter of the loading pad, and the intersection with the bottom surface is referred as the punching perimeter. Normally the average inclination of the failure surface is referred as the punching angle $\bar{a}$, which is show in Fig. 3.10. $\bar{a}$ is defined as

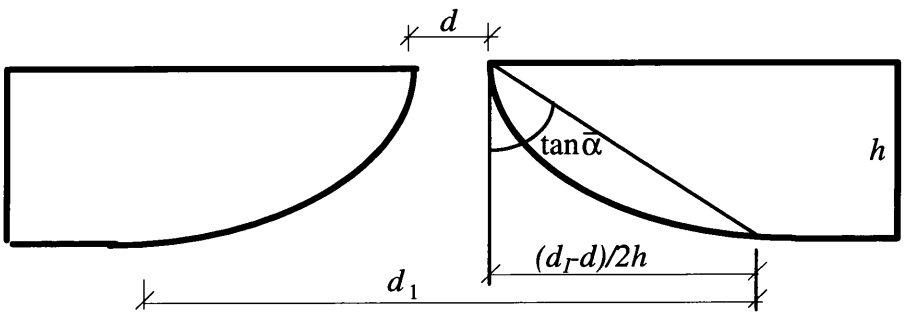

Fig.3.10 Average punching angle

$$\tan\bar{\alpha} = \frac{d_1 - d}{2h}$$

where, d is the dimension of the inner perimeter of the failure surface; d_1 is the dimension of the outer punching perimeter; h is the depth of the slab.

The results of $\tan\bar{\alpha}$ for the solid slab and waffle slabs analysed in the above section are listed in Table 3.3 and plotted in Fig.3.11 for both the two types of failure surface. The abbreviations are as below.

$\tan\bar{\alpha}_{S1}$: solid slab with rectangular failure surface,
$\tan\bar{\alpha}_{S2}$: solid slab with rounded-corner failure surface
$\tan\bar{\alpha}_{T1}$: waffle slabs of deck-top punching with rectangular failure surface,
$\tan\bar{\alpha}_{T2}$: waffle slabs of deck-top punching with round-corner failure surface,

$\tan\overline{\alpha}_{B1}$: waffle slabs of deck-bottom punching with rectangular failure surface,
$\tan\overline{\alpha}_{B2}$: waffle slabs of deck-bottom punching with round-corner failure surface.

Table 3.3 Punching Angles of Solid & Waffle Slabs

		Rectangular Revolution			Round-Corner Revolution		
	ρ_{xv}	$\tan\overline{\alpha}_{S1}$	$\tan\overline{\alpha}_{T1}$	$\tan\overline{\alpha}_{B1}$	$\tan\overline{\alpha}_{S2}$	$\tan\overline{\alpha}_{T2}$	$\tan\overline{\alpha}_{B2}$
$\overline{h} = h/5$	0.15	1.067	1.08	1.047	1.123	1.137	1.103
	0.25	1.067	1.09	1.033	1.123	1.147	1.09
	0.35	1.067	1.103	1.013	1.123	1.16	1.073
	0.45	1.067	1.123	0.993	1.123	1.18	1.053
	0.55	1.067	1.147	0.97	1.123	1.203	1.03
	0.65	1.067	1.183	0.943	1.123	1.24	1
	0.75	1.067	1.243	0.907	1.123	1.303	0.967
	0.85	1.067	1.363	0.867	1.123	1.423	0.923
$\overline{h} = 2h/5$	0.15	1.067	1.09	1.043	1.123	1.147	1.1
	0.25	1.067	1.107	1.027	1.123	1.163	1.083
	0.35	1.067	1.13	1.01	1.123	1.187	1.067
	0.45	1.067	1.157	0.99	1.123	1.213	1.047
	0.55	1.067	1.197	0.967	1.123	1.253	1.023
	0.65	1.067	1.25	0.943	1.123	1.303	1
	0.75	1.067	1.33	0.92	1.123	1.383	0.977
	0.85	1.067	1.47	0.89	1.123	1.517	0.947
$\overline{h} = 3h/5$	0.15	1.067	1.093	1.05	1.123	1.15	1.103
	0.25	1.067	1.113	1.037	1.123	1.17	1.09
	0.35	1.067	1.137	1.02	1.123	1.193	1.077
	0.45	1.067	1.167	1.007	1.123	1.22	1.063
	0.55	1.067	1.203	0.993	1.123	1.257	1.047
	0.65	1.067	1.25	0.977	1.123	1.3	1.033
	0.75	1.067	1.313	0.96	1.123	1.36	1.017
	0.85	1.067	1.407	0.943	1.123	1.447	1

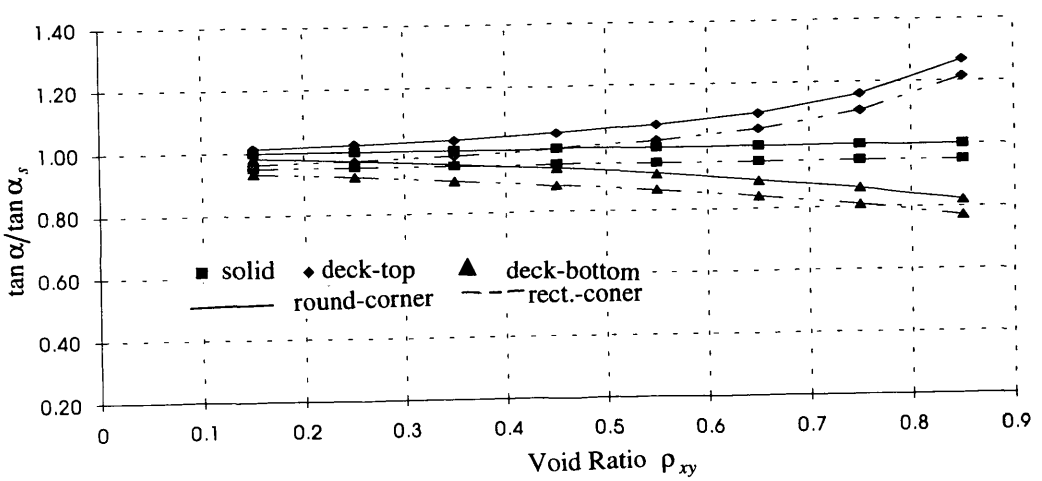

(a) $(\overline{h} = h/5)$

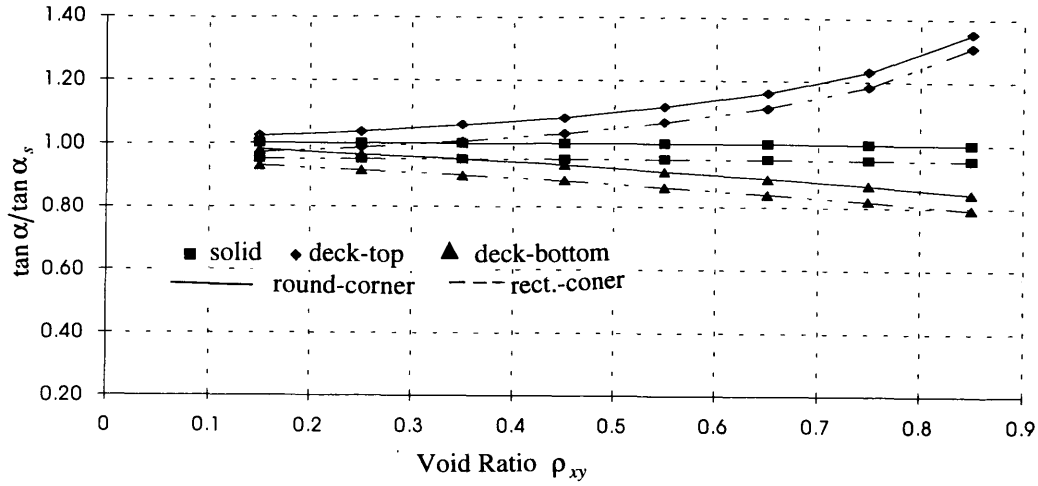

(b) $(\bar{h} = 2h/5)$

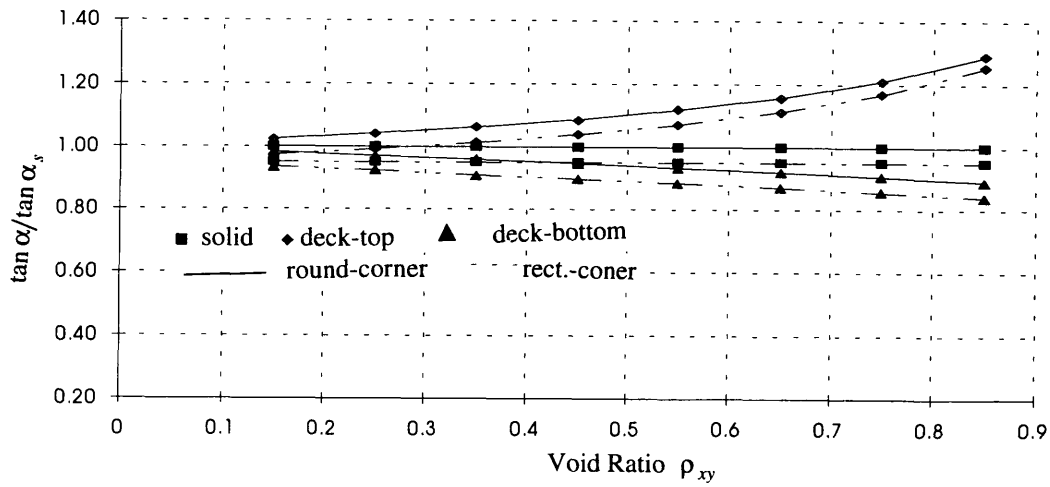

(c) $(\bar{h} = 3h/5)$

Fig.3.11 Punching Diameter of Two Types of Punching Geometry

From Fig.3.11a~c, it is seen that the punching angles obtained from formula based on the round-corner failure surface are larger than those of the rectangular failure surface, i.e., the former has larger punching perimeters than those of the latter. The punching angle, $\tan\bar{\alpha}$, is 1.123 for solid slab, varies from 1.137 to 1.519 for deck-top waffle slabs, and 0.923 to 1.113 for deck-bottom waffle slabs. So the distance from the edge of the loading pad to the perimeter of the punching failure surface is about *1.0h* to *1.5h*, which is close to the *1.5h* suggested in BS8110 and further away from the ACI's value of *0.5h*. From the experiments by previous researchers, it was reported that the above distance was larger than *1.5h*, and the explanation for this was the dowel action of the flexural reinforcements in the slabs, which was not taken into account in the limit analysis conducted in this chapter.

3.6 INFLUENCES OF RECESSES ON THE PUNCHING SHEAR OF WAFFLE SLABS

In this section, we'll look through the recesses in the waffle slabs on the punching load by comparing the proportion of shear resistance between ribs and deck, and dimensions of the recesses on the punching load.

3.6.1 PROPORTION OF THE SHEAR RESISTANCE BETWEEN RIBS AND THE DECK

The shear resistance of the RC waffle slabs consist two parts, the ribs which makes up a grillage system with the same depth as that of the total slab, and the solid concrete of the deck, the projection of which onto the xy plane coincide with the recesses. These two parts are show in Fig3.12.

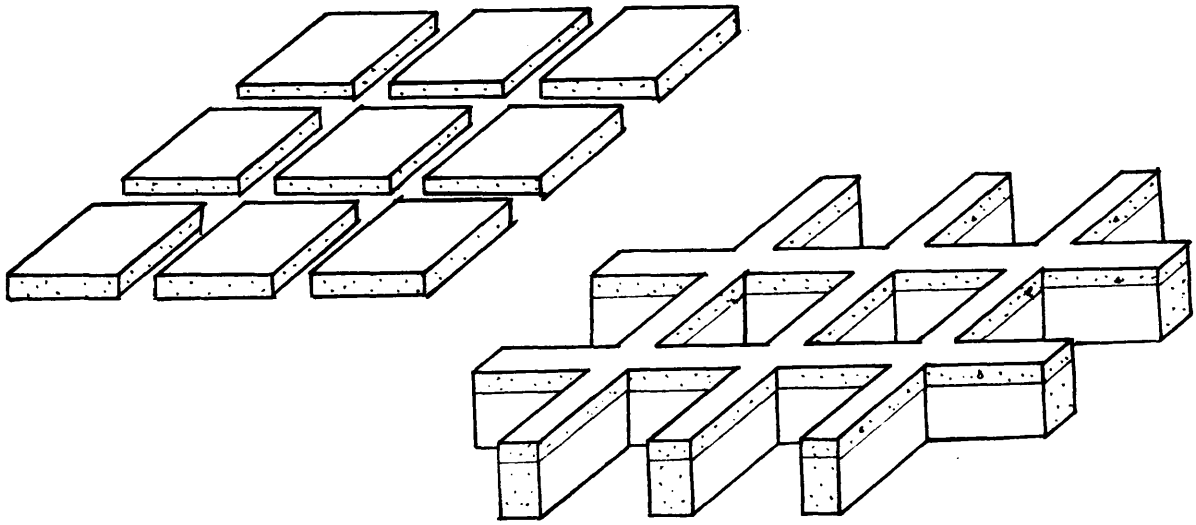

Fig. 3.12 Ribs and Deck Slabs of the Waffle Slab

From the analysis in section 3.5, we have already seen that punching with a geometry of the round corner revolution is more critical; therefore the limit analysis from now on will be based on this type of failure.

The formulae to calculate the shear resistance of the ribs and deck can be derived from the formula of section 3.4, as given below.

Deck-top waffle slabs

Shear resistance of the ribs can be considered as the resistance of the grillage system consisting of the ribs only. The dimension of the punching surface of the grillage system is the same as that of the solid slab. So

$$P_{rib} = (1-\rho_{xy})\left[\frac{\pi}{16}(d_1{}^2 - d^2) + \frac{1}{2}d(d_1 - d) + \frac{\pi k h^2}{2\ln\left(\frac{\pi}{4}\frac{d_1 - d}{d} + 1\right)}\right] \quad (3.68)$$

$$P_{DT} = P_T - P_{rib} \quad (3.69)$$

where,

P_{rib} shear resistance of a grillage system consisting of the ribs only,

P_{DT} shear resistance of the deck in the case of deck-top punching,

P_T the resistance of the waffle slabs in the case of deck-top punching.

Deck-Bottom waffle slabs

Similarly as above, there are

$$P_{rib} = (1-\rho_{xy})\left[\frac{\pi}{16}(d_1{}^2 - d^2) + \frac{1}{2}d(d_1 - d) + \frac{\pi k h^2}{2\ln\left(\frac{\pi}{4}\frac{d_1 - d}{d} + 1\right)}\right] \quad (3.70)$$

$$P_{DB} = P_B - P_{rib} \quad (3.71)$$

where,

P_{rib} shear resistance of a grillage system consisting of the ribs only,

P_{DT} shear resistance of the deck in the case of deck-bottom punching,

P_T the resistance of the waffle slabs in the case of deck-bottom punching.

Using Eqs. 3.68~3.71, the analysis was done on the waffle slabs used in section 3.5. The shear resistance of the ribs, decks, and waffle slabs are calculated.

In the following section, the results will be compared.

Table 3.4 lists the ratio between the shear resistance of the deck and the ribs, they are also plotted in Fig.3.13.

Table 3.4 Ratio of the Shear Resistance between Deck and Ribs in Waffle Slabs

	$\bar{h} = h/5$		$\bar{h} = 2h/5$		$\bar{h} = 3h/5$		$\bar{h} = 4h/5$	
ρ_{xy}	P_{DT}/P_{rib}	P_{DB}/P_{rib}	P_{DT}/P_{rib}	P_{DB}/P_{rib}	P_{DT}/P_{rib}	P_{DB}/P_{rib}	P_{DT}/P_{rib}	P_{DB}/P_{rib}
0.15	0.03	0.04	0.06	0.08	0.09	0.12	0.13	0.15
0.25	0.05	0.08	0.11	0.16	0.17	0.22	0.25	0.28
0.35	0.09	0.14	0.18	0.25	0.28	0.36	0.40	0.45
0.45	0.13	0.21	0.27	0.38	0.43	0.54	0.61	0.68
0.55	**0.20**	**0.31**	**0.40**	**0.57**	0.64	0.80	0.90	1.02
0.65	**0.29**	**0.46**	**0.61**	**0.86**	0.96	1.22	1.37	1.55
0.75	0.47	0.74	0.97	1.38	1.54	1.97	2.22	2.51
0.85	0.87	1.39	1.80	2.61	2.89	3.72	4.17	4.73

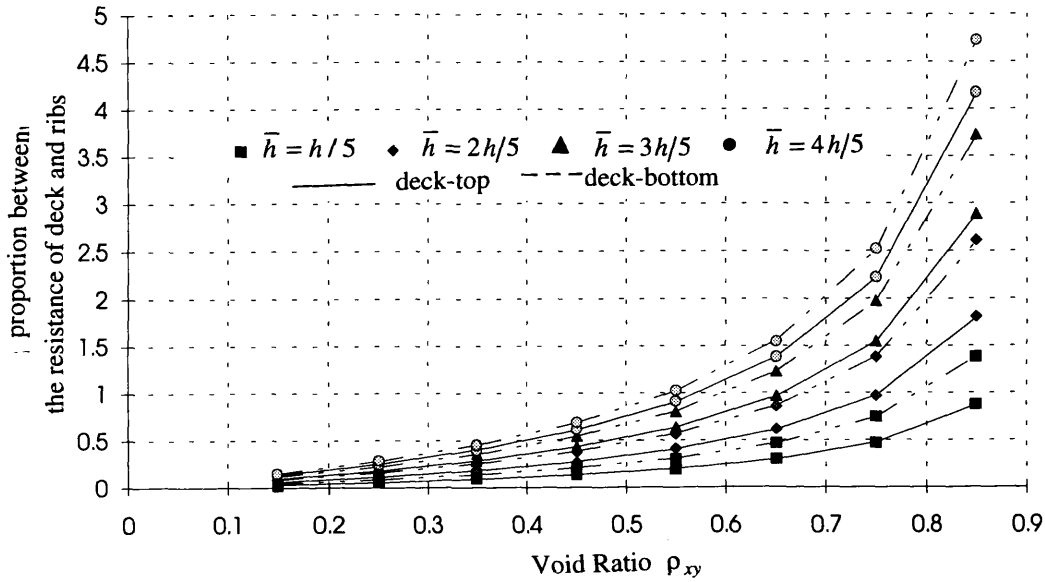

Fig.3.13 Ratio of Shear Resistance between Deck and Ribs

From Fig.3.13, it is seen that the ratio increases with the increase of the void ratio and the depth of deck. This means that the contribution of the deck towards the shear resistance becomes larger if the dimension of the recesses increase or the depth of the deck increases. The latter is obvious, the former is because that deck will have larger proportion of concrete volume in relative to ribs as there are less ribs if the distance between the ribs gets bigger.

In Fig.3.13, it is observed that the proportion ratio between deck and ribs is bigger for deck-bottom punching case than that of the deck-bottom case. This is because that, when the deck is on the tension side, more deck will intersect with the failure surface, so deck is more effective in participating in shear. This does not count the cracks in the

cover of the tension surface of the slab, if this is accounted, not much difference exists as will be proved by the experimental results described later.

A typical case of waffle slab configuration with the void ratio of 0.55, $\overline{h} = 3h/10$, from Table 3.4, the proportion ratio is 0.3, which means the deck contributed to about 30% the total shear resistance. So it is conservative to neglect the deck's shear contribution.

3.6.2 INFLUENCE OF RECESSES DIMENSION ON PUNCHING LOAD

In this section, we will compare the shear resistance of waffle slabs in relation to a solid slab to see how the recess reduces the shear capacity of slabs.

For the slabs calculated in section 3.5, the ratios of the shear resistance between waffle slabs and solid slabs are listed in Table 3.5 and plotted in Fig.3.14, where

P_s shear resistance of solid slab,
P_T shear resistance of waffle slabs with deck-top punching,
P_B shear resistance of waffle slabs with deck-bottom punching.

From Fig.3.14, we see that the shear resistance decreases with the increase of the void ratio (reflecting the space between ribs) and increases with the depth of deck.

A typical case of waffle slab configuration with the void ratio of 0.55, $\overline{h} = 3h/10$, from Table 3.5, the ratio is 0.59, which means the existence of the recesses reduced the shear resistance by 41%.

From Table 3.1, it is known that a void ratio of 0.55 is equivalent to a directional void ratio of 0.74. If following the concept of BS8110 for punching in waffle slabs, it would get a reduction of 74% by the existence of recesses; this is too conservative.

Table 3.5 Ratio of Shear Resistance between Waffle Slabs & Solid Slabs

	$\bar{h} = h/5$		$\bar{h} = 2h/5$		$\bar{h} = 3h/5$		$\bar{h} = 4h/5$	
ρ_{xy}	P_T/P_S	P_B/P_S	P_T/P_S	P_B/P_S	P_T/P_S	P_B/P_S	P_T/P_S	P_B/P_S
0.15	0.87	0.89	0.90	0.92	0.93	0.95	0.96	0.98
0.25	0.79	0.81	0.83	0.87	0.88	0.92	0.94	0.96
0.35	0.71	0.74	0.77	0.81	0.83	0.88	0.91	0.94
0.45	0.62	0.66	0.70	0.76	0.79	0.85	0.88	0.93
0.55	0.54	0.59	0.63	0.71	0.74	0.81	0.86	0.91
0.65	0.45	0.51	0.56	0.65	0.69	0.78	0.83	0.89
0.75	0.37	0.44	0.49	0.60	0.64	0.74	0.80	0.88
0.85	0.28	0.36	0.42	0.54	0.58	0.71	0.78	0.86

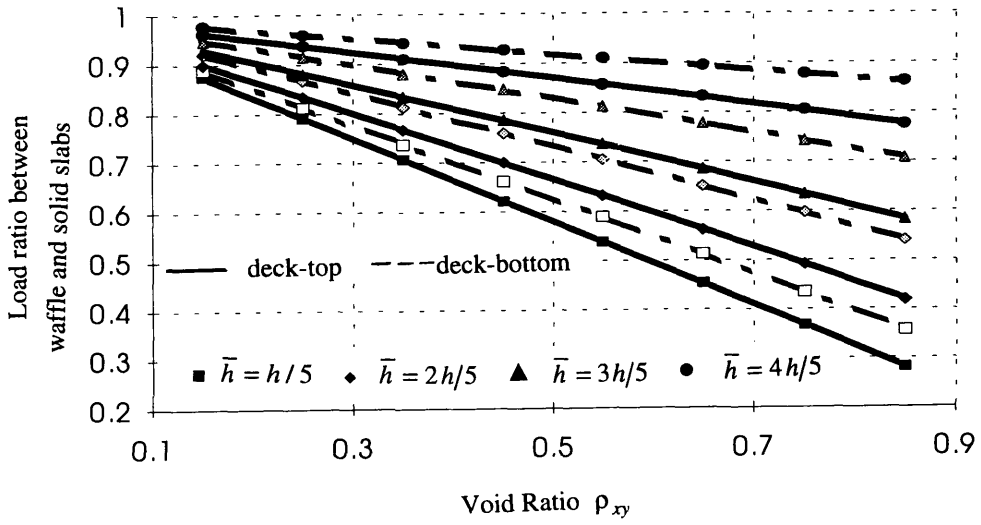

Fig. 3.14 Comparison between waffle slabs and solid

3.7 INFLUENCE OF SHEAR STEEL IN RC SOLID AND WAFFLE SLABS

It is well known that the supplement of shear reinforcements, e.g., stirrups, can increase the shear capacity of slabs and also make the slabs more ductile. A lot of previous researchers[1] have investigated the effectiveness of the stirrups or other types of shear reinforcements, and reported the ineffectiveness of the stirrups. The ineffectiveness was mainly attributed to the poor anchorage of the stirrups inside slabs, especially in relative shallow slabs. Here in this section, we will use the upper bound analysis method to study this problem, and to see how effective the stirrups will be and is there any other reason causing the ineffectiveness apart from the poor anchorage.

A series of slabs with shear steel ratios ranging from 0.1% to 3.0% are analysed using Eq.3.65 & 3.66 derived in section 3.4.3. The slabs used here are the same as those described in section 3.5, except the slabs are reinforced with stirrups.

The yield strength of the reinforcements are taken as $250 N/mm^2$. The poor anchorage of the stirrups is neglected, although this affects the absolute value of the analysis, it does not affect the relative value between the slabs. Therefore the reduction factor for the yield strength of the stirrups is taken as F_{sv}=1.0. Putting this in another way, the neglect of the poor anchorage is equivalent to using stirrups of higher yield strength.

3.7.1 INCREASE OF PUNCHING LOAD BY SHEAR REINFORCEMENTS

The ratios of the punching loads between slabs with and without stirrups are given in Table.3.6 and plotted in Fig.3.15a & b.

From Fig. 3.15a & b, it is seen that

- although the punching load increases with the increase of shear steel ratio, it is not in a linear proportion, the load increase rate is far less than the steel increase ratio. For example, in deck-top punching case with void ratio of 0.55, the steel ratio increases from 0.5% to 3% (six times), while the load ratio increases only from 1.59 to 2.87 (less than two times). This means that some amount of the strength of the shear steel is not in use when the steel ratio increases;
- the load increase in solid slabs is the highest compared with the waffle slabs; the larger the void ratio is, the less effective the shear steel will be.
- For the deck-top and top-bottom cases, the load increase by steel is very similar for both cases;
- stirrups seem slightly more effective for slabs with shallow deck.

From the above analysis, conclusions can be drawn that the stirrups is not very effective in waffle slabs, and less effective than in solid slabs. This conclusion was drawn not considering the anchorage condition of stirrups, which may be worse off in waffle slabs as the stirrups are inside ribs where limited spaced is provided for the anchorage.

Table 3.6 Ratio of Punching Load between Slabs with and without Shear Steel

Slab Type	Steel Void	$\bar{h} = h/5$					$\bar{h} = 2h/5$				
		0.5%	1.0%	1.5%	2.0%	3.0%	0.5%	1.0%	1.5%	2.0%	3.0%
Deck	0.35	1.62	1.99	2.28	2.53	2.94	1.59	1.95	2.23	2.47	2.87
---	0.55	1.59	1.95	2.23	2.47	2.87	1.55	1.88	2.14	2.36	2.73
Top	0.75	1.55	1.88	2.14	2.35	2.72	1.46	1.75	1.98	2.17	2.49
Deck	0.35	1.56	1.91	2.19	2.42	2.82	1.52	1.85	2.11	2.33	2.71
---	0.55	1.49	1.81	2.06	2.27	2.64	1.42	1.71	1.93	2.13	2.46
Bottom	0.75	1.37	1.63	1.84	2.02	2.32	1.29	1.50	1.67	1.82	2.08
Solid	0	1.64	2.02	2.32	2.58	3.00	1.64	2.02	2.32	2.58	3.00

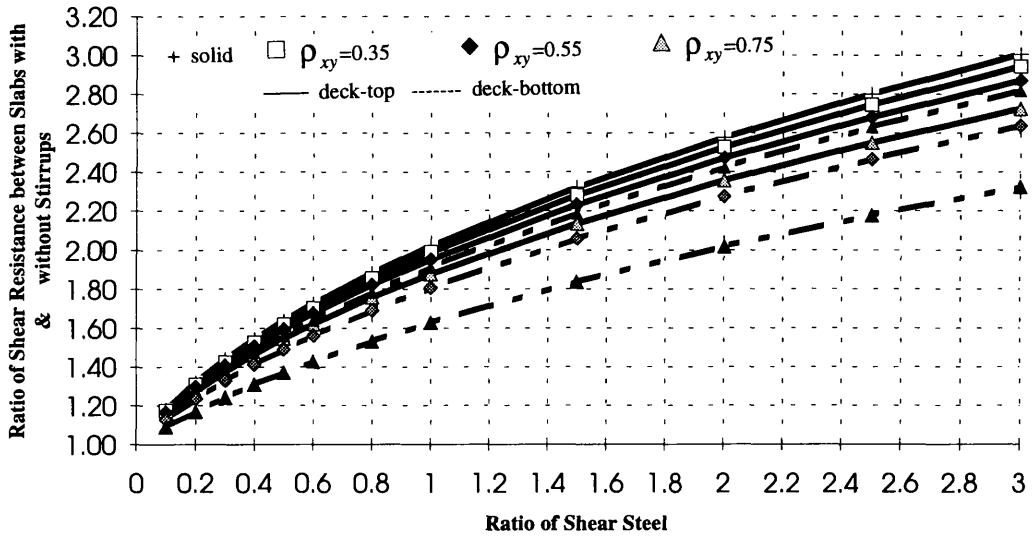

Fig.3.15a Load Increment by the Use of Shear Steel $(\bar{h} = h/5)$

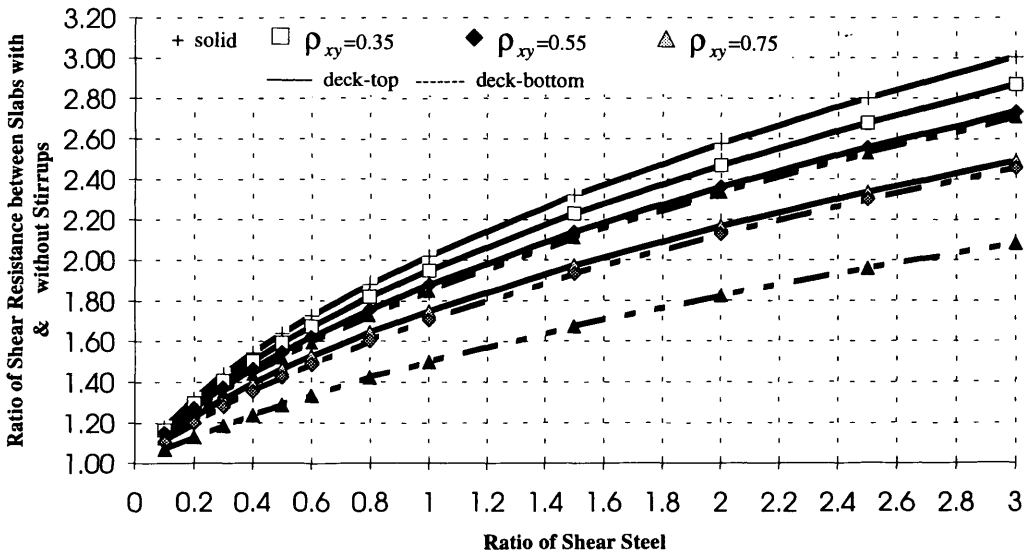

Fig.3.15b Load Increment by the Use of Shear Steel $(\bar{h} = 2h/5)$

3.7.2 Reduction in Punching Perimeter by Supplement of Shear Reinforcements

Table 3.7 lists the punching angles (measuring the size of the punching perimeter) of the slabs which was analysed in previous section; the perimeters are also plotted in Fig.3.16a & b.

Table 3.7 Punching Angle of Slabs with Shear Steel

Slab Type	Steel Void	$\bar{h} = h/5$					$\bar{h} = 2h/5$				
		0.5%	1.0%	1.5%	2.0%	3.0%	0.5%	1.0%	1.5%	2.0%	3.0%
Deck	0.35	0.64	0.50	0.43	0.43	0.33	0.66	0.52	0.45	0.45	0.34
---	0.55	0.67	0.53	0.45	0.45	0.34	0.71	0.56	0.49	0.49	0.37
Top	0.75	0.73	0.58	0.50	0.50	0.38	0.81	0.65	0.56	0.56	0.43
Deck	0.35	0.63	0.50	0.43	0.43	0.33	0.64	0.51	0.44	0.44	0.34
---	0.55	0.64	0.52	0.45	0.45	0.34	0.67	0.55	0.48	0.48	0.37
Bottom	0.75	0.67	0.56	0.49	0.49	0.38	0.73	0.61	0.54	0.54	0.42
Solid	0	0.61	0.48	0.41	0.41	0.31	0.61	0.48	0.41	0.41	0.31

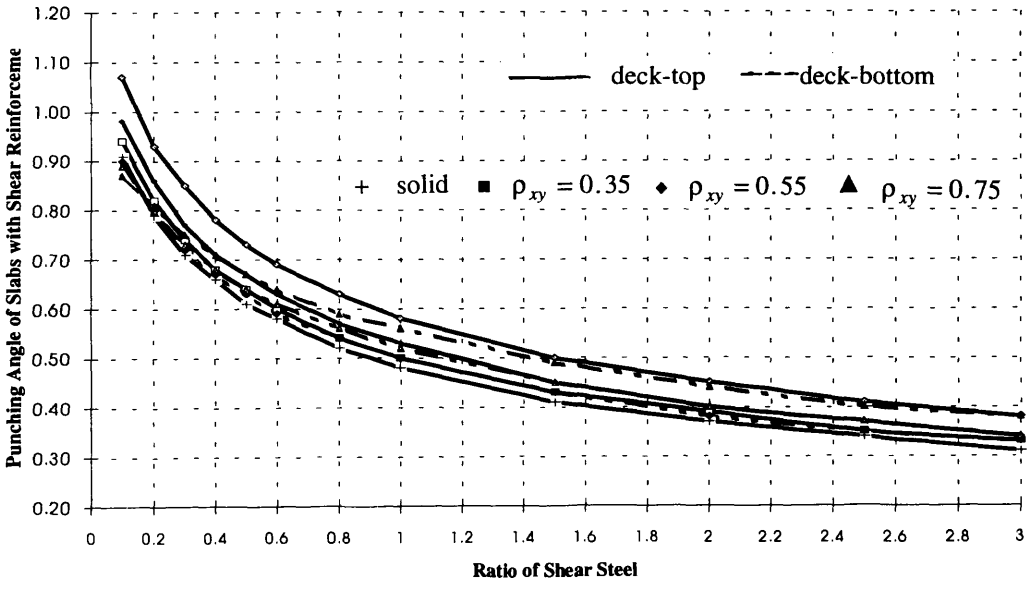

Fig.3.16a The Punching Angle in Slabs with Shear Steel $(\bar{h} = h/5)$

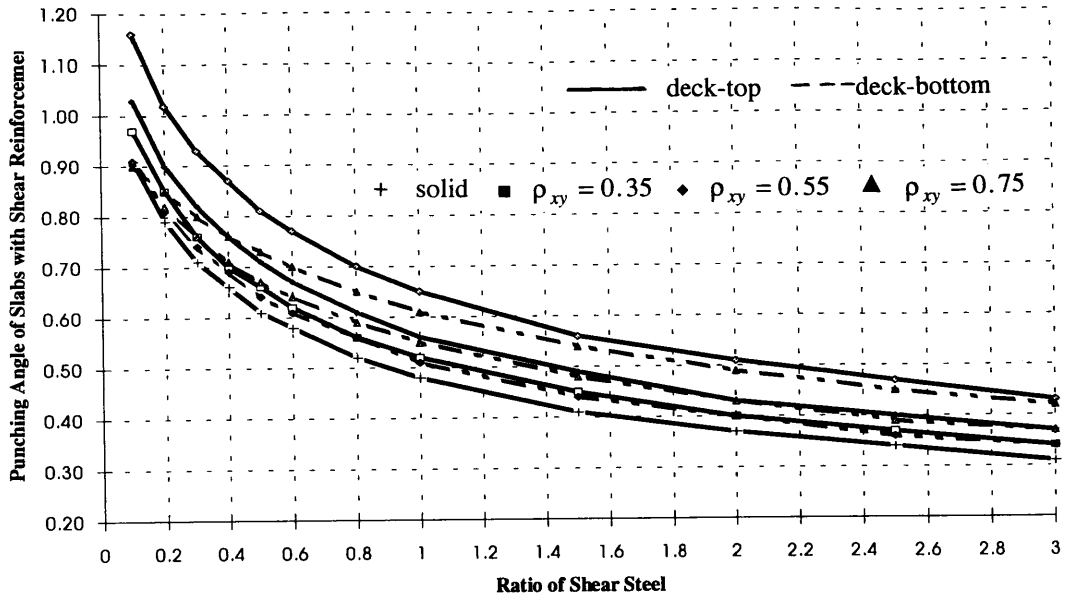

Fig.3.16b The Punching Angle in Slabs with Shear Steel $(\overline{h} = 2h/5)$

From Fig.3.16a & b, it is seen that the punching angle $\tan\overline{\alpha}$ (or the punching perimeters) decreases with the increase of the shear steel ratio; the punching angle $\tan\overline{\alpha}$ is reduced from about 1.0 to 0.4 when the steel ratio increased from 0.1% to 3%. The trend is that the failure surface will become a cylinder around the punching pad if the shear reinforcement is increased to ultimate, this is easy to understand as the slab will become a steel plate if shear reinforcement content increases to infinitee. The solid slabs seem to have smaller punching perimeter compared with the waffle slabs.

Table 3.8 and Fig.3.17a&b give the ratio of the punching angles between slabs with and without shear reinforcement.

Table 3.8 Ratio of Punching Angle of Slabs with & without Shear Steel

Slab Type		$\overline{h} = h/5$					$\overline{h} = 2h/5$				
	Steel Void	0.5%	1.0%	1.5%	2.0%	3.0%	0.5%	1.0%	1.5%	2.0%	3.0%
Deck	0.35	0.55	0.43	0.37	0.37	0.28	0.55	0.44	0.38	0.38	0.29
---	0.55	0.56	0.44	0.38	0.38	0.28	0.57	0.45	0.39	0.39	0.30
Top	0.75	0.56	0.45	0.38	0.38	0.29	0.59	0.47	0.41	0.41	0.31
Deck	0.35	0.59	0.47	0.40	0.40	0.31	0.60	0.48	0.41	0.41	0.32
---	0.55	0.62	0.50	0.44	0.44	0.33	0.66	0.54	0.47	0.47	0.36
Bottom	0.75	0.69	0.58	0.51	0.51	0.39	0.74	0.62	0.55	0.55	0.43
Solid	0	0.54	0.43	0.37	0.37	0.28	0.54	0.43	0.37	0.37	0.28

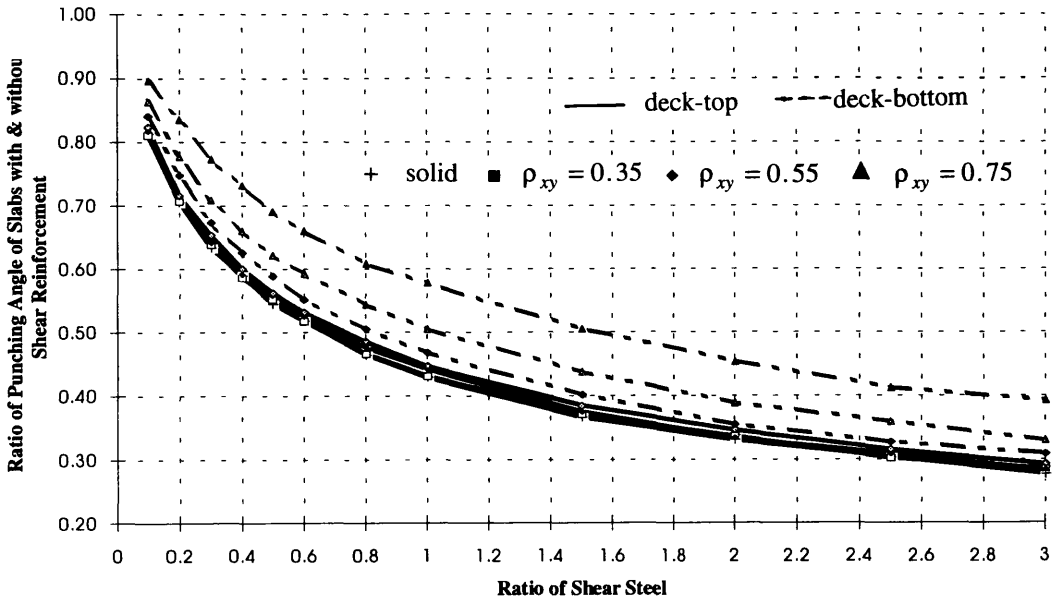

Fig.3.17a Ratio of the Punching Perimeter in Slabs with & without Shear Reinforcements $(\bar{h} = h/5)$

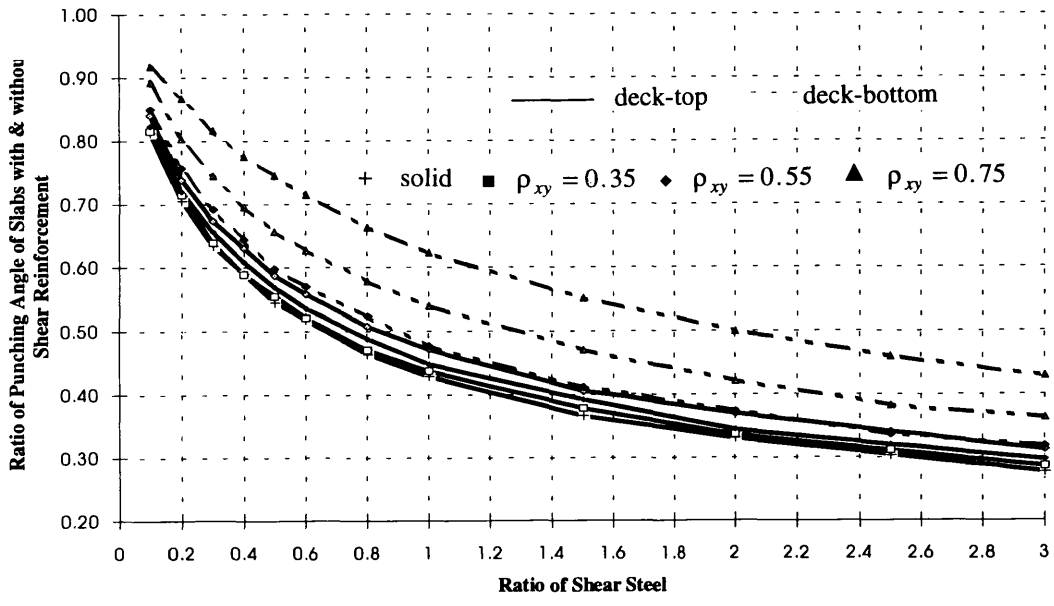

Fig.3.17b Ratio of the Punching Perimeter in Slabs with & without Shear Reinforcements $(\bar{h} = 2h/5)$

From Fig. 3.17a&b, it is seen that the change of the punching perimeter for slabs with shear reinforcements decreases fast along with the increase of the steel ratio.

The decrease of the punching perimeter along with the increase of the shear steel ratio can be explained by the following reason. In a slab with out shear reinforcement, the variation of the shear resistance along with the punching perimeter is shown by the curve S_c in Fig.3.18, there is the lowest point on the curve corresponding to d_{1c}, which is the punching perimeter of the most critical load. When the slabs is reinforced with stirrups, the stirrups will provide the shear resistance which is shown by curve S_{sv}. The total resistance of the slabs is the sum up of curves S_c and S_{sv}, shown by curve S. On the curve S, the lowest point is reduced to d'_{1c}, i.e., the punching perimeter is reduced.

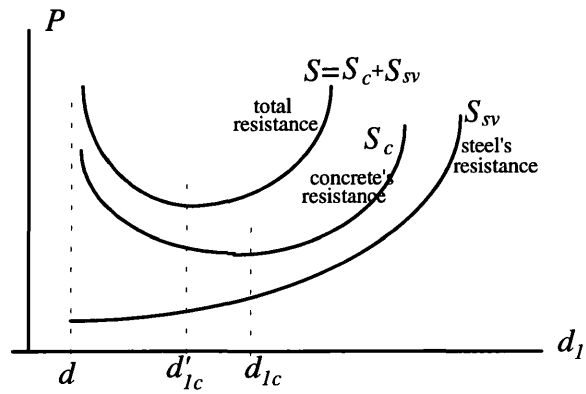

Fig.3.18 Variation of Shear Resistance against the Punching Perimeter

The above analysis gives some idea why the rate of punching load increase is less than the rate of steel ratio increase. The reason is that, when large steel ratio is provided, the shear resistance per unit area of concrete is increased, but the punching perimeter is reduced and leads to less area participating in the shear resistance. Therefore, apart from the poor anchorage preventing the full use of the strength of stirrups, there are intrinsic problems relating to the use of stirrups.

3.7.3 EFFECTIVE FACTOR MEASURING THE EFFECTIVENESS OF THE SHEAR REINFORCEMENTS

From the above analysis, we have know that the shear reinforcement can not develop its full capacity due to the decrease of punching perimeter, apart from the anchorage problem. We'll introduce a factor which can measure effectiveness of the stirrups in resisting punching shear.

In BS8110, the nominal punching perimeter is used which is *1.5d* away from the edge of the loading pad. We'll use this nominal punching perimeter: how much the strength of stirrups, which fall inside the failure zone between loading pad and the nominal punching perimeter, is used for the shear resistance.

The area of the failure zone is

$$A_{bs} = (d+3h)^2 - d^2; \qquad (3.71)$$

the effective factor is defined as

$$\lambda_{eff} = \frac{P - P_c}{f_{sv}\rho_{sv}(1-\rho_{xy})A_{bs}} \qquad (3.72)$$

where,

d	dimension of the loading pad;
h	depth of slab;
P	the punching capacity of slabs with shear reinforcement;
P_c	the punching capacity of the slab without shear reinforcement;
ρ_{sv}	the shear steel ratio as defined by Eq.3.60;
ρ_{xy}	the void (area) ratio of the waffle slab, defined in section 3.4.1, is 1.0 for solid slab;
f_{sv}	the yield strength of stirrups.

Using Eq.3.71 & 3.72, the analysis was done on slabs previously used in section 3.7.2. The results of the analysis, and plotted in Fig.3.19a & b.

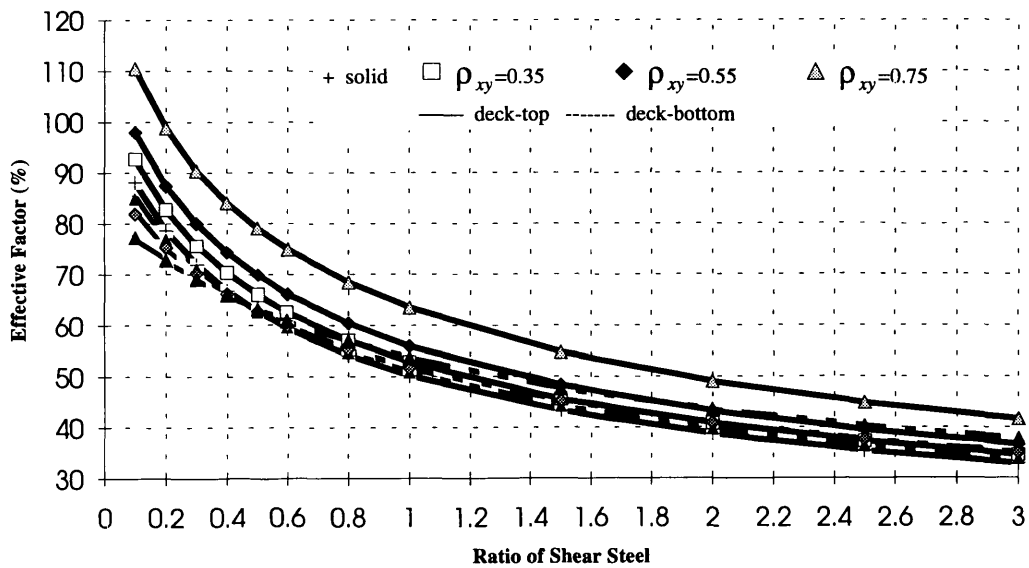

Fig.3.19a Effectiveness of the Shear Steel in RC Slabs $(\bar{h} = h/5)$

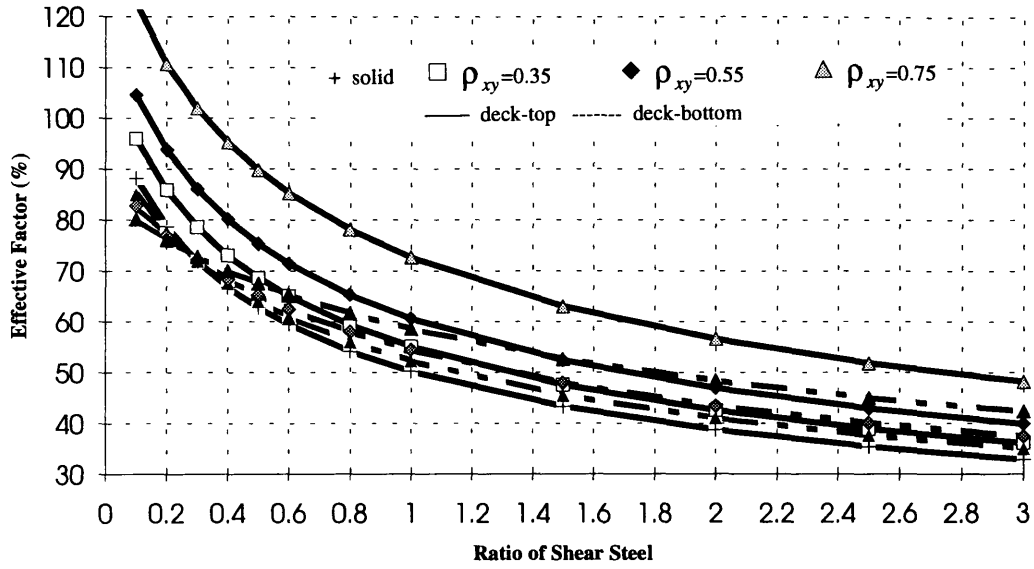

Fig.3.19b Effectiveness of the Shear Steel in RC Slabs $\left(\bar{h} = 2h/5\right)$

From Fig.3.19a & b, it is seen that the effective factor is quite small when the ratio of the stirrups is large; the reason has been explained before, i.e., the reduction of the failure perimeter due to the higher steel content.

3.8 PROPOSED ALTERNATIVE METHODS FOR PUNCHING IN RC WAFFLE SLABS

BS8110 employs a method based on the nominal punching perimeter and the nominal shear strength, shown in Fig.3.20, and described in Chapter 2. The dimension of the punching perimeter and the nominal shear strength are basically determined by experiments on RC solid slabs. For RC waffle slabs, the resistance of the deck of waffle slabs is neglected, and then the principle for solid slabs are applied on the remaining grillage system (or ribs only); the nominal perimeter and the shear strength are taken to be the same for solid slabs and the grillage system.

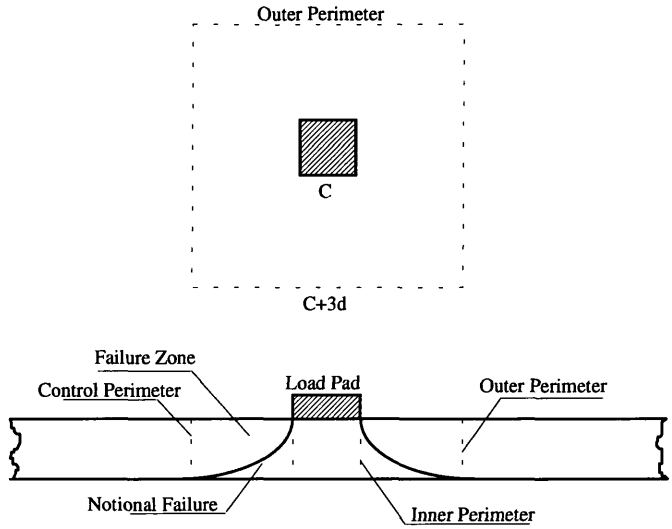

Fig3.20 Punching Failure inside Solid Slabs

In this section, three alternative methods are proposed, which are based on similar concept used in BS8110 but considering the shear contribution of the deck of the waffle slabs and the punching perimeter being modified. They are described as below.

3.8.1 METHOD ONE

This method is similar to that of BS8110 using the nominal punching perimeter, counting number of ribs and the nominal shear strength, but the top slabs are also considered as taking part in the shear resistance.

In BS8110, the ratio of flexural steel is calculated based on the section of the rib, which results in a substantially large steel ratio and hence a high nominal shear strength. Here the steel ratio is calculated based on the T section shown in Fig. 3.21.

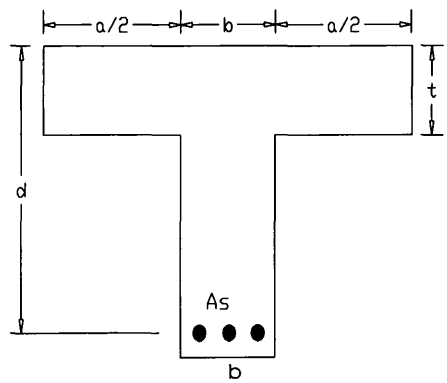

Fig 3.21 T Section Dimension

1. Slabs without Shear Reinforcements

The control perimeter is the same as that suggested by BS8110, the number of ribs taken into account are those intersected with the control perimeter; the area of the top slab which is thought to contribute to the shear resistance is that part cut by the control perimeter. The formulae are

nominal shear strength of concrete: $$\upsilon_c = \frac{0.79}{\gamma_m}\sqrt[3]{100\rho}\sqrt[3]{f_{cu}/25}\sqrt[4]{400/d} \quad (3.73)$$

dimension of nominal punching perimeter: $B=C+3d$ (3.74)

length of the punching perimeter: $U=4(C+3d)$ (3.75)

area of rib: $A_{rib} = bd$ (3.76)

area of deck: $A_{deck} = a \cdot t$ (3.77)

total area of nominal failure surface: $S = N \cdot (A_{rib} + A_{deck})$ (3.78)

punching load: $P=P_c=S\cdot \nu_c$ (3.79)

limit of nominal strength: $\nu_{max}= P/(U_o d)$ (3.80)

length of loading pad: $U_o=4Cd$ (3.81)

where,

- γ_m is the safety factor of the material;
- ρ is the ratio of flexural steel inside the slab;
- f_{cu} is the cube strength of concrete;
- a dimension of the squared recesses;
- b width of rib;
- t depth of deck of waffle slab;
- N number of ribs intersected with punching perimeter;
- d is the effective depth of the slab;
- P_c is the part of the punching resistance provided by concrete, flexural steel;

The steel ratio is calculated as shown in Fig3.21 and Eq.3.82. The same nominal shear strength of concrete is used for the top slab and the ribs.

$$\rho = \frac{A_s}{at + bd} \quad (3.82)$$

2. Slabs with Shear Reinforcements

The shear resistance provided by the shear links are calculated by treating the shear reinforcements as in beams. The formulae are as follows.

$$P = P_c + P_{sv} \tag{3.83}$$

$$\nu_{sv} = \frac{1}{\gamma_{sv}} \frac{f_{sv} A_{sv}}{b l_{sv}} \tag{3.84}$$

$$P_{sv} = S_{rib} \nu_{sv} \tag{3.85}$$

where,

P_{sv} shear resistance provided by shear reinforcements;

ν_{sv} is the nominal shear strength provided by the links.

γ_{sv} partial safety factor for shear reinforcements;

f_{sv} yield strength of shear reinforcements;

A_{sv} area of all legs of a stirrup;

b width of ribs;

l_{sv} distance along the ribs between stirrups or bent-up bars.

3.8.2 METHOD TWO

This method is very similar to method one except that the ratio of the flexural steel is based on the imagined rectangular section as show in Fig 3.22 by the dashed line. The reason behind the use of rectangular section is that when the compression area of the T section during bending is within the flange, a rectangular section is used for the analysis of the bending capacity.

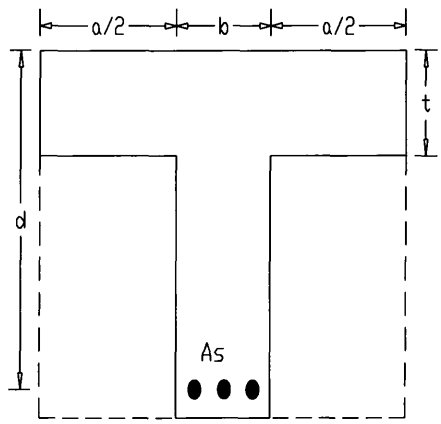

Fig 3.22 Rectangular Section Dimension

$$\rho = \frac{A_s}{bd} \tag{3.86}$$

All the other formulae are the same as those of method one.

3.7.3 METHOD THREE

In this method, the calculation is based on an affine solid slab. The section of the waffle slab can be modelled as a solid section with a depth

$$d_{aff} = n_1 d \qquad (3.87)$$

$$n_1 = \frac{(a+b)^2 d - a^2 (d-t)}{(a+b)^2 d} \qquad (3.88)$$

where,

d_{aff} is the equivalent depth of the affine slab;

n_1 is the coefficient, the physical meaning is the content ratio of the concrete;

d effective depth of slab;

a dimension of the squared recesses;

b width of rib;

t depth of deck of the waffle slab.

1. Waffle Slabs with Shear Reinforcements

The flexural steel ratio and the control perimeter are calculated based on the affine solid slab, but the original depth d is used to include the scale effect when calculating the nominal shear strength.

dimension of nominal punching perimeter: $B = C + 3d_{aff}$ (3.89)

length of the punching perimeter: $U = 4(c + 3d_{aff})$ (3.90)

area of nominal failure surface: $A = U \cdot d_{aff}$ (3.91)

punching load: $P=P_c=Av_c$ (3.92)

2. Waffle Slabs with Shear Reinforcements

The shear resistance of the shear reinforcements are based on the formulae for solid slabs, but the shear reinforcements are counted based on the control perimeter for the affine slab. Therefore less shear reinforcement will be counted compared to BS8110.

$$P_{sv} = \frac{1}{\gamma_{ms}} f_{sv} \sum^{n} a_{sv} \qquad (3.93)$$

where,

γ_{ms} is the partial safety factor for links, 1.15;

f_{sv} is the characteristic strength of steel;

n number of legs of stirrups inside the nominal punching perimeter;

a_{sv} is the section area of the stirrups fall into the nominal failure zone.

3.9 Conclusions

In this chapter, we have applied the upper bound analysis to the punching shear analysis of RC waffle slabs. The formulae for the RC solid slabs and waffle slabs with rectangular loading pad were derived first, then the formulae for slabs with shear reinforcements were obtained. Based on the formulae, we did the study on the influences of the dimension of the recesses on the punching slabs; the shear resistance contribution of the deck; the effectiveness of reinforcements in RC slabs. Based on the study and the concept of BS8110, three alternative methods to calculate the punching shear capacity of RC waffle slabs were proposed.

The main conclusions are

- among the two types of failure surfaces - rectangular surface and rounded-corner surface, the latter one is more critical and should be used for the upper bound analysis;
- the punching perimeter is measured by the punching angle, $\tan\overline{\alpha}$, which is about 1.0~1.5 for slabs without shear reinforcements; this punching perimeter will be substantially reduced if the slabs are supplied with shear reinforcements;
- the deck contributes substantially to the shear resistance and it's too conservative to neglect this source of contribution;
- the existence of the recesses in waffle slabs reduces the punching capacity, but not as much as what BS8110 indicates;
- although stirrups increase the shear capacity of waffle slabs, the load increase is rather small in comparison to their potential strength; the increase rate of the load is far smaller than the increase rate of the shear reinforcements, making shear reinforcements less effective for slabs with large steel content;
- the causes of the ineffectiveness of stirrups is that, apart from the poor anchorage inside slabs, there is an intrinsic problem in using stirrups: the increase of the stirrups can increase the shear resistance per unit area of

concrete, but the punching perimeter is reduced at the same time, so the total area participating in the resistance is reduced resulting in the waste of material.

The formulae derived in this section using upper bound analysis have several parameters to be determined by experimental results if wishing to put them in practical use. This work is done in Chapter 6 and the calculation results are also compared with the test results in Chapter 7. The proposed alternative methods will be examined by applying to the model waffle slabs; the calculations are done in Chapter 6 and the comparison in Chapter 7.

CHAPTER 4

NON-LINEAR FINITE ELEMENT ANALYSIS

4.1 INTRODUCTION

Finite element method has been extensively used in structural analysis; it offers a powerful and general analytical tool for reinforced concrete members and structures. Although there are numerous articles on the application of FEA to reinforced concrete structures not many have been found on the punching shear analysis in RC slabs. Punching shear in slabs has the following characteristics: small deflection of the slab before the failure; the failure is sudden and the load drops substantially; there are major cracks inside the slab that form the failure surface. Because of the these characteristics, the application of FEA to punching problems will need more work.

A finite element software package LUSAS[69] is available for structural analysis, but it is applicable only to 2-D or axisymmentrical concrete structure or members. The problem of punching shear in RC waffle slabs is a 3D problem and can not even be approximated by a 2D or axisymmentrical analysis as the recesses inside the slab are distributed in a pattern of neither 2 dimensional nor axisymmentrical. Furthermore, the punching shear problem is very much related to the local failure of the material, the geometry of the slab is vital to the analysis.

Having the above problems in mind, the following efforts have been made.

1. Use the Mohr-Coulomb criteria to simulate concrete behaviour: LUSAS provides this type of failure criteria and can be applied to 3D problems;

2. Employ the concrete's failure criteria — fracture under tension, non-linear elastic and plastic failure for shear and compression; implement this model by writing a program in combination with LUSAS to do the 3D analysis.

In this chapter, the essential formulation of FEA is described first, then the constitutive relationship of concrete — plasticity and fracture are discussed, followed by the description of the programming for the numerical implementation of the concrete failure model. Finally the analysis model for the waffle slab is described.

4.2 ESSENTIAL THEORY

4.2.1 NUMERICAL DISCRETIZATION

If a body is subjected to a set of body forces $\boldsymbol{b}$ then using the Virtual Work Principle there will be

$$\int_{\Omega}[\delta\varepsilon]^{T}\sigma d\Omega-\int_{\Omega}[\delta u]^{T}bd\Omega-\int_{\Gamma_t}[\delta u]^{T}td\Gamma=0 \qquad (4.1)$$

where σ is the vector of the stresses, $\boldsymbol{t}$ is the vector of boundary traction, δu is the vector of virtual displacement, $\delta\varepsilon$ is the vector of associated virtual strain, Ω is the domain of interest, Γ_t is that part of the boundary on which boundary tractions are prescribed and Γ_u is that of the boundary on which displacement are prescribed.

In a finite element representation, the displacements and strains and their virtual counterparts may be expressed by the relations

$$u=\sum_{i=1}^{n}N_i d_i \qquad \delta u=\sum_{i=1}^{n}N_i\delta d_i \qquad (4.2)$$

$$\varepsilon=\sum_{i=1}^{n}B_i d_i \qquad \delta\varepsilon=\sum_{i=1}^{n}B_i\delta d_i \qquad (4.3)$$

where, for node $\boldsymbol{i}$, d_i is the vector of nodal variables, δd_i is the vector of the virtual nodal variables, $N_i = I\cdot N_i$ is the matrix of global shape functions and B_i is the global strain-displacement matrix. The total number of nodes in the whole mesh is $\boldsymbol{n}$.

If Eqs.4.2 and 4.3 are substituted into the virtual work expression Eq.4.1, then

$$\sum_{i=}^{n}[\delta d_i]^{T}\left\{\int_{\Omega}[B_i]^{T}\sigma d\Omega-\int_{\Omega}[N_i]^{T}bd\Omega-\int_{\Gamma_t}[N_i]^{T}td\Gamma\right\}=0 \qquad (4.4)$$

and since Eq.4.4 must be true for an arbitrary set of virtual displacements, δd_i then we have for each node $\boldsymbol{i}$ an equation of the form

$$\int_{\Omega}[B_i]^{T}\sigma d\Omega-\int_{\Omega}[N_i]^{T}bd\Omega-\int_{\Gamma_t}[N_i]^{T}td\Gamma=0 \qquad (4.5)$$

For the 3D isoparametric finite element, we can evaluate contributions to Eq.4.5 separately from each element. The displacements can be expressed as

$$u^{(e)}=\sum_{i=1}^{r}N_i^{(e)}d_i^{(e)} \qquad (4.6)$$

where, for node $\boldsymbol{i}$ of element $\boldsymbol{e}$, $N_i^{(e)} = IN^{(e)}$ is the matrix of shape function and $d_i^{(e)}$ the vector of variables. There are $\boldsymbol{r}$ local nodes in each element $\boldsymbol{e}$.

The shape functions of 20-node isoparametric quantratic element are as below in local co-ordinate system

Corner nodes: $N_i = \frac{1}{8}(1+\xi_0)(1+\eta_0)(1+\varsigma_0)(\xi_0+\eta_0+\varsigma_0-2)$ *(4.7a)*

Typical mid-side node: $\xi_i = 0 \quad \eta_i = \pm 1 \quad \varsigma_i = \pm 1$

$$N_i = \frac{1}{4}(1-\xi^2)(1+\eta_0)(1+\varsigma_0) \qquad (4.7b)$$

The strain displacement relationships are expressed as

$$\varepsilon^{(e)} = \sum_{i=1}^{r} B_i^{(e)} d_i^{(e)} \qquad (4.8)$$

$$B^{(e)}{}_i = \begin{bmatrix} \frac{\partial N_i}{\partial x} & 0 & 0 \\ 0 & \frac{\partial N_i}{\partial y} & 0 \\ 0 & 0 & \frac{\partial N_i}{\partial z} \\ \frac{\partial N_i}{\partial y} & \frac{\partial N_i}{\partial x} & 0 \\ 0 & \frac{\partial N_i}{\partial z} & \frac{\partial N_i}{\partial y} \\ \frac{\partial N_i}{\partial z} & 0 & \frac{\partial N_i}{\partial x} \end{bmatrix} \qquad (4.9)$$

in which $B_i^{(e)}$ is the strain matrix.

In Eq.4.9 shape function derivatives are in Cartesian axes x, y, and z , while the shape functions are presented in the local axes ξ, η, and ζ. The transformation of the derivatives for the two co-ordinates systems can be done as follows:

$$\frac{\partial N_i^{(e)}}{\partial \xi} = \frac{\partial N_i^{(e)}}{\partial x}\frac{\partial x}{\partial \xi} + \frac{\partial N_i^{(e)}}{\partial y}\frac{\partial y}{\partial \xi} + \frac{\partial N_i^{(e)}}{\partial z}\frac{\partial z}{\partial \xi} \qquad (4.10a)$$

$$\frac{\partial N_i^{(e)}}{\partial \eta} = \frac{\partial N_i^{(e)}}{\partial x}\frac{\partial x}{\partial \eta} + \frac{\partial N_i^{(e)}}{\partial y}\frac{\partial y}{\partial \eta} + \frac{\partial N_i^{(e)}}{\partial z}\frac{\partial z}{\partial \eta} \qquad (4.10b)$$

$$\frac{\partial N_i^{(e)}}{\partial \varsigma} = \frac{\partial N_i^{(e)}}{\partial x}\frac{\partial x}{\partial \varsigma} + \frac{\partial N_i^{(e)}}{\partial y}\frac{\partial y}{\partial \varsigma} + \frac{\partial N_i^{(e)}}{\partial z}\frac{\partial z}{\partial \varsigma} \qquad (4.10c)$$

$$\begin{Bmatrix} \partial N_i/\partial \xi \\ \partial N_i/\partial \eta \\ \partial N_i/\partial \varsigma \end{Bmatrix} = J \begin{Bmatrix} \partial N_i/\partial x \\ \partial N_i/\partial y \\ \partial N_i/\partial z \end{Bmatrix} \qquad (4.11)$$

$$\begin{Bmatrix} \partial N_i/\partial x \\ \partial N_i/\partial y \\ \partial N_i/\partial z \end{Bmatrix} = J^{-1} \begin{Bmatrix} \partial N_i/\partial \xi \\ \partial N_i/\partial \eta \\ \partial N_i/\partial \varsigma \end{Bmatrix} \qquad (4.12)$$

where, J is the Jacobian matrix. Also note that in an isoparametric representation we may use the following representation for the x and y co-ordinates within the element

$$\begin{Bmatrix} x^{(e)} \\ y^{(e)} \\ z^{(e)} \end{Bmatrix} = \sum_{i=1}^{r} \begin{bmatrix} N_i^{(e)} & 0 & 0 \\ 0 & N_i^{(e)} & 0 \\ 0 & 0 & N_i^{(e)} \end{bmatrix} \begin{Bmatrix} x_i^{(e)} \\ y_i^{(e)} \\ z_i^{(e)} \end{Bmatrix} \qquad (4.13)$$

in which $N_i^{(e)}$ are the same shape functions used in the displacement representation.

The Jacobian matrix may be presented as

$$J^{(e)} = \begin{bmatrix} \frac{\partial x}{\partial \xi} & \frac{\partial y}{\partial \xi} & \frac{\partial z}{\partial \xi} \\ \frac{\partial x}{\partial \eta} & \frac{\partial y}{\partial \eta} & \frac{\partial z}{\partial \eta} \\ \frac{\partial x}{\partial \varsigma} & \frac{\partial y}{\partial \varsigma} & \frac{\partial z}{\partial \varsigma} \end{bmatrix} = \begin{bmatrix} \sum_{i=1}^{r} \frac{\partial N_i^{(e)}}{\partial \xi} x_i^{(e)} & \sum_{i=1}^{r} \frac{\partial N_i^{(e)}}{\partial \xi} y_i^{(e)} & \sum_{i=1}^{r} \frac{\partial N_i^{(e)}}{\partial \xi} z_i^{(e)} \\ \sum_{i=1}^{r} \frac{\partial N_i^{(e)}}{\partial \eta} x_i^{(e)} & \sum_{i=1}^{r} \frac{\partial N_i^{(e)}}{\partial \eta} y_i^{(e)} & \sum_{i=1}^{r} \frac{\partial N_i^{(e)}}{\partial \eta} z_i^{(e)} \\ \sum_{i=1}^{r} \frac{\partial N_i^{(e)}}{\partial \varsigma} x_i^{(e)} & \sum_{i=1}^{r} \frac{\partial N_i^{(e)}}{\partial \varsigma} y_i^{(e)} & \sum_{i=1}^{r} \frac{\partial N_i^{(e)}}{\partial \varsigma} z_i^{(e)} \end{bmatrix} \qquad (4.14)$$

The discretised element volume is given as

$$d\Omega^{(e)} = dxdydz = \det J d\xi d\eta d\varsigma \qquad (4.15)$$

For each element, the relationship between the stress and strain has the form

$$\sigma^{(e)} = D^{(e)} \varepsilon^{(e)} = D^{(e)} \left(\sum_{j=1}^{r} B_j^{(e)} d_j^{(e)} \right) \qquad (4.16)$$

where, $D^{(e)}$ is the matrix of elastic modulus, which is constant for ideally elastic material, and in most other cases varies with the displacement (or strain) of the material.

The contribution from element e to the first term in Eq.(4.5) is given as

$$\sum_{i=1}^{r} K_{ij}^{(e)} d_j^{(e)} \equiv \int_{\Omega^{(e)}} \left[B_i^{(e)}\right]^T D^{(e)} \left(\sum_{i=1}^{r} B_j^{(e)} d_j^{(e)} \right) d\Omega \qquad (4.17)$$

with $$K_{ij}^{(e)} = \int_{\Omega^{(e)}} \left[B_i^{(e)}\right]^T D^{(e)} B_j^{(e)} d\Omega \qquad (4.18)$$

where, K_{ij} is also called the element stiffness matrix.

The contribution from element ***e*** to the second term in *(4.5)* is given as

$$f_{B_i}^{(e)} = \int_{\Omega^{(e)}} \left[N_i^{(e)}\right]^T b^{(e)} d\Omega \qquad (4.19)$$

For the third term, the contribution from element ***e*** is

$$f_{T_i}^{(e)} = \int_{\Gamma_t^{(e)}} \left[N_i^{(e)}\right]^T t^{(e)} d\Gamma \qquad (4.20)$$

The evaluation of the above three terms is performed in the local co-ordinate system and formulated to be as below

$$\begin{aligned} K_{ij}^{(e)} &= \int_{-1}^{+1}\int_{-1}^{+1}\int_{-1}^{+1} \left[B_i^{(e)}\right]^T D^{(e)} B_j^{(e)} \det J^{(e)} d\xi d\eta d\varsigma \\ &= \int_{-1}^{1}\int_{-1}^{1}\int_{-1}^{1} T_{ij}^{(e)} d\xi d\eta d\varsigma = \sum_{p=1}^{n}\sum_{q=1}^{n}\sum_{s=1}^{n} T(\bar{\xi}_p, \bar{\eta}_q, \bar{\varsigma}_s)_{ij} W_p W_q W_s \end{aligned} \qquad (4.21)$$

where ***n*** is the sampling points, $W_p$and W_q are the weighting factors and $(\bar{\xi}_p, \bar{\eta}_q, \bar{\varsigma}_s)$ is a sampling position.

The consistent nodal forces at node ***i*** caused by body forces are

$$\begin{aligned} f_{B_i}^{(e)} &= \int_{-1}^{+1}\int_{-1}^{+1}\int_{-1}^{+1} \left[N_i^{(e)}\right]^T b^{(e)} \det J^{(e)} d\xi d\eta d\varsigma \\ &= \int_{-1}^{1}\int_{-1}^{1}\int_{-1}^{1} g_i^{(e)} d\xi d\eta d\varsigma = \sum_{p=1}^{n}\sum_{q=1}^{n}\sum_{s=1}^{n} g(\bar{\xi}_p, \bar{\eta}_q, \bar{\varsigma}_s)_i^{(e)} W_p W_q W_s \end{aligned} \qquad (4.22)$$

Here the distributed boundary load is evaluated. The consistent node forces for node ***i*** can be shown to be

$$p_{xi}^{(e)} = \int_{\Gamma^{(e)}} N_i^{(e)} \left(p_t \frac{\partial x}{\partial \xi} - p_n \frac{\partial y}{\partial \xi} \right) d\xi \qquad (4.23a)$$

$$p_{yi}^{(e)} = \int_{\Gamma^{(e)}} N_i^{(e)} \left(p_n \frac{\partial x}{\partial \xi} + p_t \frac{\partial y}{\partial \xi} \right) d\xi \qquad (4.23b)$$

where p_n and p_t are the normal and tangential distributed loads respectively.

By using the above Equations, Eq.4.5 can be rewritten as

$$\sum_{i=1}^{r} K_{ij}^{(e)} d_j^{(e)} - \sum_{i=1}^{r} f_{B_i} - \sum_{i=1}^{r} f_{T_i} = 0 \qquad (4.24)$$

or $$Kd - f = 0 \qquad (4.25)$$

and $$f = \sum_{i=1}^{r} f_{B_i} + \sum_{i=1}^{r} f_{T_i} \qquad (4.26)$$

Solving the simultaneous equations, Eq.4.25, we get the displacement under the applied load, and then use the displacement to calculate the strain and stress.

4.2.2 SOLUTION TO NON-LINEAR PROBLEMS

In a linear problem, the relationship between the stress and strain is constant and the stiffness matrix, K, is therefore constant, so Eq.4.19 can be solved directly. If the problem is non-linear, the stiffness, K, is a function of the unknown variable, displacement, the solution will not generally be satisfied at any stage of the computation, there are some residual forces. If the stiffness at an instant is expressed as K_T, Eq.4.19 is converted into Eq.4.27.

$$\psi = K_T d - f \neq 0 \qquad (4.27)$$

Iteration is necessary in order to reduce the residual force near-zero. Different methods have been proposed to solve Eq.4.27.

Newton-Raphson Method

The residual forces ψ in Eq.4.27 can be interpreted as a measure of the departure of Eq.4.25 from equilibrium. Since K_T is a function of d and possibly its derivatives, then at any stage of the process, $\psi = \psi(d)$.

If the true solution to the problem exists at $d^r + \Delta d^r$, then the Newton-Raphson approximation for the general term of the residual force vector, ψ^r corresponding to solution d^r is

$$\psi_i{}^r = -\sum_{j=1}^{N} \left(\frac{\partial \psi_i}{\partial d_j} \right) \Delta d_j{}^r \qquad (4.28)$$

in which N is the total number of variables in the system and the superscript r denotes r^{th} approximation to the true solution. Substituting for ψ_i from Eq.4.26, the complete

expression for all the residual components can be written in matrix form as

$$\psi(d^r) = -JJ(d^r)\Delta d^r \qquad (4.29)$$

in which a typical term of the Jacobian matrix JJ is

$$JJ_{ij} = \left(\frac{\partial \psi_i}{\partial d_j}\right) = \left(k_T{}^r\right)_{ij} + \sum_{l=1}^{N}\left(\frac{\partial (k_T)_{iK}}{\partial d_j}\right)^r d_k{}^r \qquad (4.30)$$

$$JJ(d) = K_T(d) + K_T'(d)$$

where $(k_T)_{ij}$ is the general term of matrix K_T. The last term in (4.30) gives rise to non-symmetric terms in Jacobian matrix.

The Newton-Raphson process can finally be written, using Eq.4.29 and Eq.4.30, in the form

$$\Delta d^r = -\left[JJ\left(d^r\right)\right]^{-1}\psi\left(d^r\right) = -\left[K_T\left(d^r\right) + K_T'\left(d^r\right)\right]^{-1}\psi\left(d^r\right) \qquad (4.31)$$

$$d^{r+1} = d^r + \Delta d^r \qquad (4.32)$$

This process is continued until convergence has occurred.

Modified Newton-Raphson Method

In Newton-Raphson method, the Jacobia matrix has to be modified and reversed for every iteration, which is time consuming. The modified method is to retain the Jacobia matrix the same for the second and later iterations; such a method reduces the time used for calculating the reverse of the matrix, but the speed of convergence is slowed down as more iterations are required.

Incremental Analysis Using Either NR or MNR

In the Newton-Raphson Method (**NR**) and Modified Newton-Raphson Method (**MNR**), the solution sought is for the whole loading f; this is sometimes unacceptable as the stiffness of the structure K_T may depend on the loading history as well as the displacement d. Therefore the analysis for a non-linear problem should be proceeded in an incremental manner.

In the incremental method, the loading f is divided into subloading Δf_i, and

$$f = \sum_{i=1}^{l} \Delta f_i \qquad (4.33)$$

The corresponding equation of Eq.4.25 in the incremental form is

$$\Theta\psi = K_T \Theta d - \Theta f \neq 0 \qquad (4.34)$$

with $$\Theta f = \int_{\Omega} \left[N_i\right]^T \Theta b d\Omega + \int_{\Gamma_t} \left[N_i\right]^T \Theta t d\Gamma \qquad (4.35)$$

Eq.(4.34) can be solved by either NR or MNR method as explained before. The total solution is

$$d = \sum_{i=1}^{l} \Theta d_i \qquad (4.36)$$

4.3 MODELLING OF CONCRETE FAILURE AND POST FAILURE BEHAVIOUR

4.3.1 GENERAL BEHAVIOUR OF CONCRETE

Concrete is a complex material which has a high compressive strength and a low tensile strength, shown in Fig.4.1; the failure mode has the characteristics of non-linear, plastic, fracture and crushing behaviour. In the past, a lot of efforts have been made to find the constitutive relation of concrete[7]. Normally concrete is modelled as a brittle material under tension, non-linear plastic under compression, as shown in Fig.4.2 and 4.3.

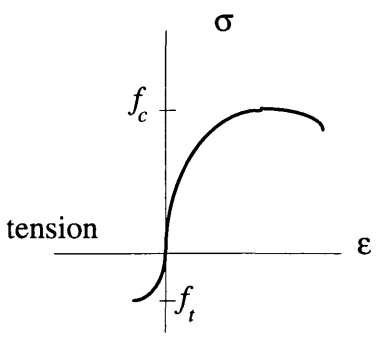

Fig. 4.1 Uniaxial Behaviour of Concrete

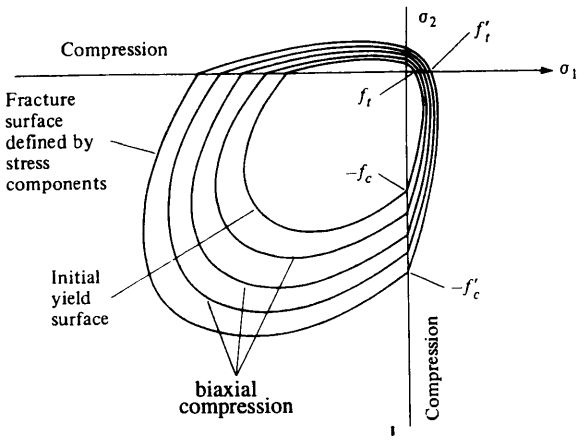

Fig.4.2 Concrete Failure Criteria in Plane Stress

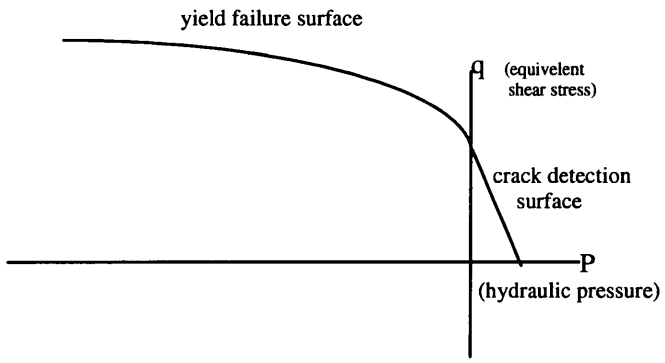

Fig.4.3 Concrete Failure Criteria in *P-q* Co-ordinate

The precise definition of concrete failure criteria — the equations governing the failure surface shown in Fig.4.2 and 4.3 and the behaviour of concrete after yield or crack, have been the interest of many researchers[19]. In the early times, the concrete's failure criteria had been developed based on the strength theory used for plastic mechanics[17] and various models have been proposed. In the past decades, the fracture mechanics has been found more suitable for concrete material, and is still under investigation.

In this study, some simple failure criteria have been applied to the concrete, i.e., the Mohr Coulomb criteria and the fracture failure criteria based on the maximum tensile stress. The reason for using the Mohr-Coulomb criteria is that it is the closest one to simulate concrete behaviour among a few material models supported by the LUSAS package. It is obvious that these two criteria have quite a history, but as the main objective of this study is on the structural behaviour of RC waffle slabs and no other software package based on more advanced failure criteria is available, regrettably compromise has to be made. In the following the above mentioned two criteria will be briefly discussed and their merits and shortcoming are also highlighted.

4.3.2 Mohr-Coulomb Criteria

The general expression of the Mohr-Coulomb criteria is

$$F = \frac{1}{3} I_1 \sin\varphi + \sqrt{J_2}\left(\cos\theta - \frac{1}{\sqrt{3}} \sin\theta \sin\varphi \right) - C\cos\varphi = 0 \qquad (4.37)$$

where,

I_1 the first stress invariant;

J_2 the second invariant of stress deviator;

θ a variable determined by the stress status,

C cohesion factor of the material concerned;

φ the frictional angle of the material.

The material factors C and φ can be determined from experimental tests on material samples and they may be taken as functions of the plastic strain or plastic work in order to consider the strain hardening or work hardening of the material.

Eq 4.37 is a conical surface if expressed in the principal stress space, as shown in Fig.4.4; if expressed in the $\sigma_n \sim \tau_{nt}$ co-ordinate system, it is as in Fig.4.5.

In using the Mohr-Coulomb criteria, the material at a point is considered as yield if its stress status reaches the failure surface defined by Eq.4.37. In the elastic-plastic analysis, the material is considered as elastic before yield has taken place so the stiffness matrix is calculated using the elastic modulus E; once the material reaches yield the plastic strain will exist, which is calculated using the associated flow theory, and the stiffness matrix has to be modified as the elastic-plastic stiffness matrix. The material may be considered as either isotropic or anisotropic before and after the yield of the material, but for the application to concrete the isotropic characteristic is usually assumed for simplicity.

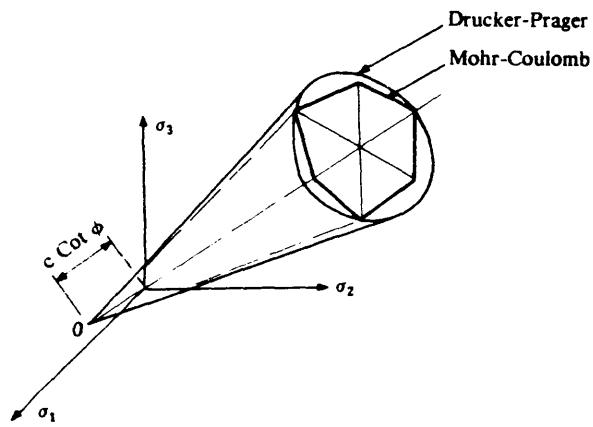

Fig. 4.4 Geometric representation of the Mohr-Coulomb yield surface in the principal stress space

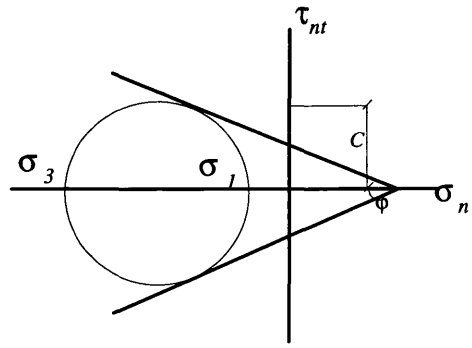

Fig. 4.5 Geometric representation of the Mohr-Coulomb yield surface in the $\sigma_n \sim \tau_{nt}$ co-ordinate system

In applying the Mohr-Coulomb criteria to concrete, the factors C and φ have to be determined first, this is usually done using the tests results of the compressive strength of concrete cylinders. In reference 46, it was found that the frictional angle of concrete doess not vary with the strength of concrete and is almost constant at 37°; the factor *C* varied with the compressive strength of concrete; the modified Mohr-Coulomb criteria with the tension cut-off surface should be used for the concrete. Here the conflict arises in simulating both the tensile failure and compressive failure of concrete by using the unmodified Mohr-Coulomb criteria with the frictional angle remaining at $\varphi = 37°$. This can be explained as below.

If the friction angle is maintained at a value of 37°, the corresponding cohesion factor C_{37} can be obtained from Eq.4.38, which is derived by substituting $\sigma_1 = 0$ and $\sigma_3 = -f_c$ into Eq.4.37; the corresponding tensile strength f_{t37} is obtained from Eq.4.39 which is derived by substituting Eq.4.38, $\sigma_3 = 0$ and $\sigma_1 = f_{t37}$ into Eq.4.37.

$$C_{37} = \frac{f_c}{2}\frac{\cos 37}{1+\sin 37} \approx 0.25 f_c \qquad (4.38)$$

$$f_{t37} = 2C_{37}\frac{\cos 37}{1+\sin 37} \approx C_{37} = 0.25 f_c \qquad (4.39)$$

From Eq.4.39, it is seen that the tensile strength of concrete is 25% of the compressive strength and this is obviously too high.

In order to use the unmodified Mohr-Coulomb criteria for concrete and also reasonably reflect the true characteristics of concrete under both tension and compression, the frictional angle is not retained as$\varphi = 37°$, instead, making both the Mohr circles of uniaxial tension and compression of concrete tangent to the failure surface, as shown in Fig.4.6. Following such an approximation, the material factors can be obtained by Eq.4.40 and 4.41 using the tensile and compressive strengths of concrete.

$$C = \frac{\sqrt{f_c \cdot f_t}}{2} \qquad (4.40)$$

$$\tan\varphi = \frac{C}{f_t} - \frac{f_t}{4C} \qquad (4.41)$$

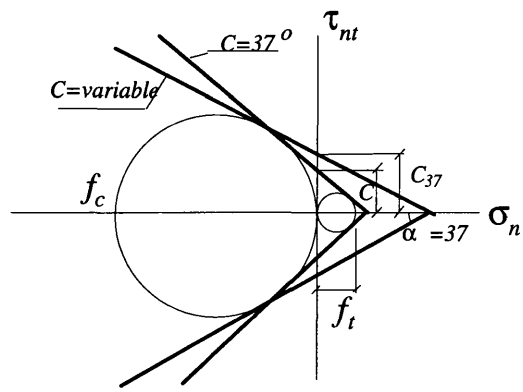

Fig.4.6 Difference in Mohr-Coulomb Curves with φ=37°or a Variable

The above compromise and approximation may cause substantial discrepancy for concrete failure under high compressive strength, but the tension failure surface obtained this way is low and more realistic to the actual behaviour of concrete, as shown in Fig.4.6.

Apart from the above described problem in using the Mohr-Coulomb, the other shortcoming is that the fracture behaviour of concrete is not reflected, the tensile stress not being released after the yielding has taken place in the material.

This Mohr-Coulomb criteria is supported in LUSAS, and will be used for the analysis of the RC waffle slabs tested in this study.

4.3.3 CONCRETE FAILURE CRITERIA CONSIDERING FRACTURE

Concrete can be modelled as a brittle fracture material under relatively low confining pressures. Cracking is assumed to be an important aspect of the behaviour of concrete under such a stress status. The representation of cracking and of post cracking behaviour dominates the modelling. Cracking is assumed to occur when the stress reaches a certain value or the fracture energy has built up to a certain level. Various failure surfaces have been proposed for concrete. Once a crack has been detected its orientation is stored, and the material is considered as anisotropic. Subsequent cracking at the same point is assumed to be orthogonal to this direction.

The crack is usually modelled as smeared crack, in the sense that it does not track individual 'macro' cracks. Instead, constitutive calculations are performed independently at each integration point of the finite element. The presence of cracks enters into the calculations by the way in which the cracks affect the stress and material stiffness associated with the integration point of the finite element model.

The post-failure behaviour for the direct straining across cracks is modelled with the Tension Stiffening feature, the retaining shear stress on the crack surface is modelled by the shear retention. In reinforced concrete this generally means giving the post failure stress as a function of the strain across the crack.

Apart from tension failure, the concrete may also fail under stresses of dominantly compression. This types of failure is caused by relative sliding between adjacent parts of concrete. This type of failure may be modelled by the type of *CRACK II* [1] using fracture mechanics, or may be modelled by using the traditional plastic theory. In this study, the latter one is used and the criteria is the Mohr-Coulomb criteria.

4.3.3.1 Modelling of Tension Failure and Post-Crack Behaviour

Cracking Detection

The equation governing the crack detection is simplified as Eq. 4.42 in this study,

$$F = \sigma_i - f_t' = 0 \qquad i=1,2,3 \qquad (4.42)$$

where,

σ_i the principal stress at a point,

f_t' the fracture strength of concrete.

The fracture strength f_t' is a material factor, which varies in the uniaxial and biaxial stress status and in this study it is considered as constant being the uniaxial fracture strength. The uniaxial fracture strength may be determined from experiments and is taken as

$$f_t' = 0.6 f_t \qquad (4.43)$$

where, f_t is the tensile strength obtained from split test on concrete cylinders

In this study, the simple fracture criteria is used: the maximum tensile strength. Once a principal stress σ_1 reaches the maximum tensile strength of concrete, the crack will occur perpendicular to the direction of the tensile stress.

After the crack has appeared, the stress normal to the crack surface is partially released and the cracked concrete can still support the stresses with a modified material characteristic. These are explained in the following section.

Post-Crack Behaviour Modelling

Before the occurrence of the crack, the material is modelled as isotropic elastic, and the matrix of elastic modulus is given in Eq.4.44.

$$[D]=\frac{E}{(1+\nu)(1-2\nu)}\begin{bmatrix} 1-\nu & \nu & \nu & 0 & 0 & 0 \\ \nu & 1-\nu & \nu & 0 & 0 & 0 \\ \nu & \nu & 1-\nu & 0 & 0 & 0 \\ 0 & 0 & 0 & 1-2\nu/2 & 0 & 0 \\ 0 & 0 & 0 & 0 & 1-2\nu/2 & 0 \\ 0 & 0 & 0 & 0 & 0 & 1-2\nu/2 \end{bmatrix} \tag{4.44}$$

Once a crack has formed, it is generally assumed that tensile stresses can not be supported across the crack and the stiffness of the material is reduced to a negligible value in this direction. However, material parallel to the crack is still capable of carrying stress according to the uniaxial or biaxial conditions prevailing parallel to the crack. On increased loading, further cracks are allowed to occur perpendicular to the original crack when the limiting condition Eq.4.42 is exceeded in this direction.

After the first principal stress has reached the fracture strength, the orientation of the first crack is determined and the local co-ordinate system X'Y'Z', based on the crack orientation and the corresponding principal stress directions as shown in Fig.4.7, is recorded as T.

$$T=\begin{bmatrix} l_{11} & l_{12} & l_{13} \\ l_{21} & l_{22} & l_{23} \\ l_{31} & l_{32} & l_{33} \end{bmatrix} \tag{4.45}$$

where, l_{ij} is the direction cosine of the local axes in the global co-ordinate system.

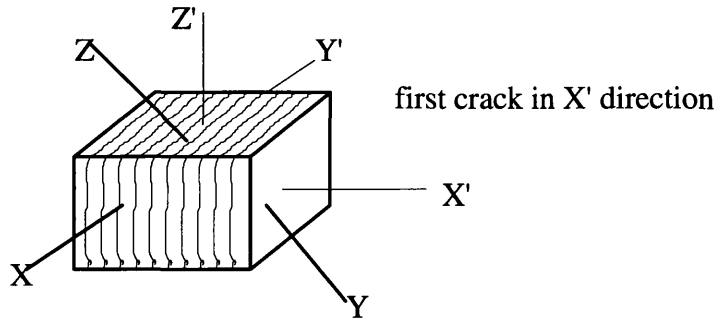

Fig.4.7 Local co-ordinate system in the cracked concrete point

The elastic modulus matrix of the cracked concrete is dependent on the crack numbers in the material and is expressed in the local co-ordinate system by Eq.4.46a, b, c & d for cracks with number 1, 2, 3 respectively.

After the first cracks have appeared, the modulus matrix is

$$[D_c']_1 = \frac{E}{(1+\upsilon)(1-2\upsilon)} \begin{bmatrix} 0 & 0 & 0 & 0 & 0 & 0 \\ 0 & 1-\upsilon & \nu & 0 & 0 & 0 \\ 0 & \upsilon & 1-\upsilon & 0 & 0 & 0 \\ 0 & 0 & 0 & \beta_x \dfrac{1-2\upsilon}{2} & 0 & 0 \\ 0 & 0 & 0 & 0 & \dfrac{1-2\upsilon}{2} & 0 \\ 0 & 0 & 0 & 0 & 0 & \beta_x \dfrac{1-2\upsilon}{2} \end{bmatrix} \tag{4.46a}$$

If the second cracks are along the y direction then after the crack the modulus matrix is,

$$[D_c']_2 = \frac{E}{(1+\upsilon)(1-2\upsilon)}\begin{bmatrix} 0 & 0 & 0 & 0 & 0 & 0 \\ 0 & 0 & 0 & 0 & 0 & 0 \\ 0 & 0 & 1-\upsilon & 0 & 0 & 0 \\ 0 & 0 & 0 & \frac{(\beta_x+\beta_y)}{2}\frac{1-2\upsilon}{2} & 0 & 0 \\ 0 & 0 & 0 & 0 & \beta_y\frac{1-2\upsilon}{2} & 0 \\ 0 & 0 & 0 & 0 & 0 & \beta_x\frac{1-2\upsilon}{2} \end{bmatrix}$$

(4.46b)

If the second cracks are along the z direction then after the crack the modulus matrix is,

$$[D_c']_2 = \frac{E}{(1+\upsilon)(1-2\upsilon)}\begin{bmatrix} 0 & 0 & 0 & 0 & 0 & 0 \\ 0 & 1-\upsilon & 0 & 0 & 0 & 0 \\ 0 & 0 & 0 & 0 & 0 & 0 \\ 0 & 0 & 0 & \beta_x\frac{1-2\upsilon}{2} & 0 & 0 \\ 0 & 0 & 0 & 0 & \beta_z\frac{1-2\upsilon}{2} & 0 \\ 0 & 0 & 0 & 0 & 0 & \frac{(\beta_z+\beta_x)}{2}\frac{1-2\upsilon}{2} \end{bmatrix}$$

(4.46c)

After the third cracks has appeared, the modulus matrix is

$$[D_c']_3 = \frac{E}{(1+\upsilon)(1-2\upsilon)} \begin{bmatrix} 0 & 0 & 0 & 0 & 0 & 0 \\ 0 & 0 & 0 & 0 & 0 & 0 \\ 0 & 0 & 0 & 0 & 0 & 0 \\ 0 & 0 & 0 & \frac{(\beta_x+\beta_y)}{2}\frac{1-2\upsilon}{2} & 0 & 0 \\ 0 & 0 & 0 & 0 & \frac{(\beta_y+\beta_z)}{2}\frac{1-2\upsilon}{2} & 0 \\ 0 & 0 & 0 & 0 & 0 & \frac{(\beta_z+\beta_x)}{2}\frac{1-2\upsilon}{2} \end{bmatrix}$$

(4.46d)

In the above equations, the modulus of elasticity of concrete is reduced to zero in the direction normal to the crack. Further, a reduction factor β is applied to the shear modulus on the cracked plane to account for the aggregate interlocking — shear retention. The value of β is in the range of 0.0~1.0, depending on the plastic strain in the direction perpendicular to the crack surface (i.e., a measurement of the crack width). The determination of the value of β is shown in Fig.4.8,

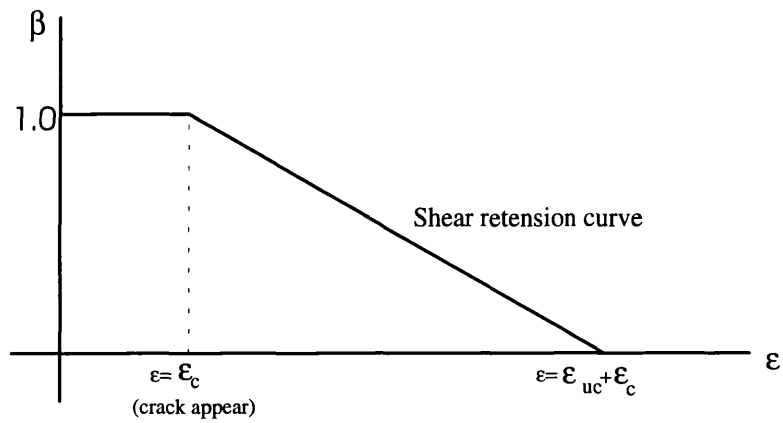

Fig.4.8 Shear retention model

It is assumed that β is equal 1.0 just after the crack of the concrete, then it is linearly reduced to zero once the strain reachs the value of $\varepsilon = \varepsilon_c + \varepsilon_{uc}$. ε_{uc} is the ultimate plastic strain at which the shear retention is assumed to disappear. β is calculated by the Eq.4.47.

$$\beta_i = \frac{\varepsilon_i - \varepsilon_c}{\varepsilon_{uc}} \qquad i=1, 2, 3 \qquad (4.47)$$

Due to the interaction between concrete and reinforcement, the stress normal to the crack direction is not lost instantly, instead a gradual process takes place. Such a tension-stiffening character can be taken into account by employing a tension stress-strain curve shown in Fig.4.9.

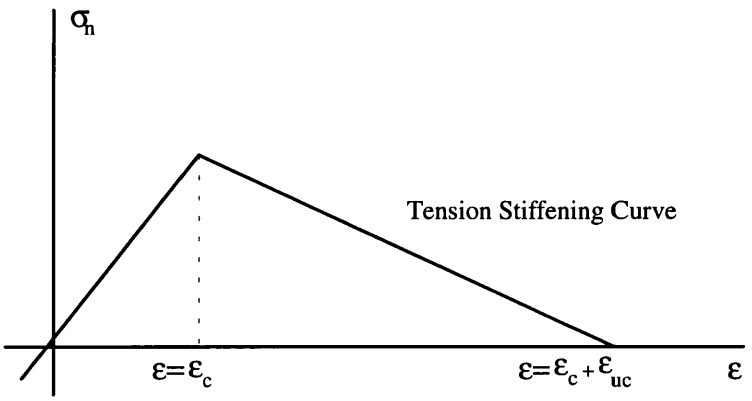

Fig.4.9 Tension stiffening model

The remaining stress normal to the crack surface is

$$\sigma_i = \frac{\varepsilon_i - \varepsilon_c}{\varepsilon_{uc}} f_t' \qquad i=1,2,3 \qquad (4.48)$$

4.3.3.2 Modelling of Shear Failure and Post-Yield Behaviour

Under a relatively high confining pressure, the concrete material may fail due to the difference in the principal stresses. The Mohr-Coulomb criteria is used to model this type of failure. The Mohr-Coulomb criteria was described in section 4.3.2. Here the post-yield behaviour of the material is briefly described.

Once the material reaches yield, the plastic strain will be introduced. A strain increment in the elastic-plastic stage can be decomposed into two parts as shown in Eq.4.49.

$$d\varepsilon = d\varepsilon^e + d\varepsilon^p \qquad (4.49)$$

where the superscript e denotes the elastic strain, and p for the plastic strain.

The plastic strain is determined normally based on the associate flow assumption, so

$$d\varepsilon^p = d\lambda \frac{\partial F}{\partial \sigma} \qquad (4.50)$$

where,

F the governing equation of the failure criteria, e.g., Mohr-Coulomb's;

$d\lambda$ the proportionality constant termed as plastic multiplier.

The stress strain relationship in the elastic-plastic stage is

$$d\sigma = D_{ep} d\varepsilon \qquad (4.51)$$

where D_{ep} is the elastic plastic stiffness modulus and a function of the non-linear status.

In the above equations, $d\lambda$ and D_{ep} can be expressed explicitly in terms of the deviator of the gradient of the governing equation of the strength criteria and the elastic modulus matrix.

4.4 NUMERICAL IMPLEMENTATION OF THE USER-BUILT MATERIAL MODEL

In the last section, two material constitutive relations of concrete have been described, one is the Mohr-Coulomn criteria and the other is the concrete model considering the fracture feature. The finite element package LUSAS supports the Mohr-Coulomb criteria for 3D analysis, but does not supports the latter one for 3D analysis.

To consider the fracture features of the concrete for the finite element analysis of the RC waffle slabs tested in this study, programming work is needed as there is no other available software. In later versions of LUSAS, the software is gradually developed toward an open system in the sense that the user can integrate his/her modules into the software package. A diagram shown in Fig.4.10 illustrates the logic flow chart of the system and how the user's module is integrated into the LUSAS package.

4.4.1 LOGICAL FLOW CHARTS OF THE ANALYSIS PROCEDURES

In Fig.4.10, it is seen that two main modules governing the stiffness matrix and the residual force are the user supplied. Actually these two modules together with the solution modules are the core parts in non-linear finite element analysis package, the other modules are somewhat more standardised.

In this study, the above two modules and other supporting subroutines were built based on the material model described in section 4.3.3. The logic flow charts of the two modules are shown in Fig.4.11 and 4.12.

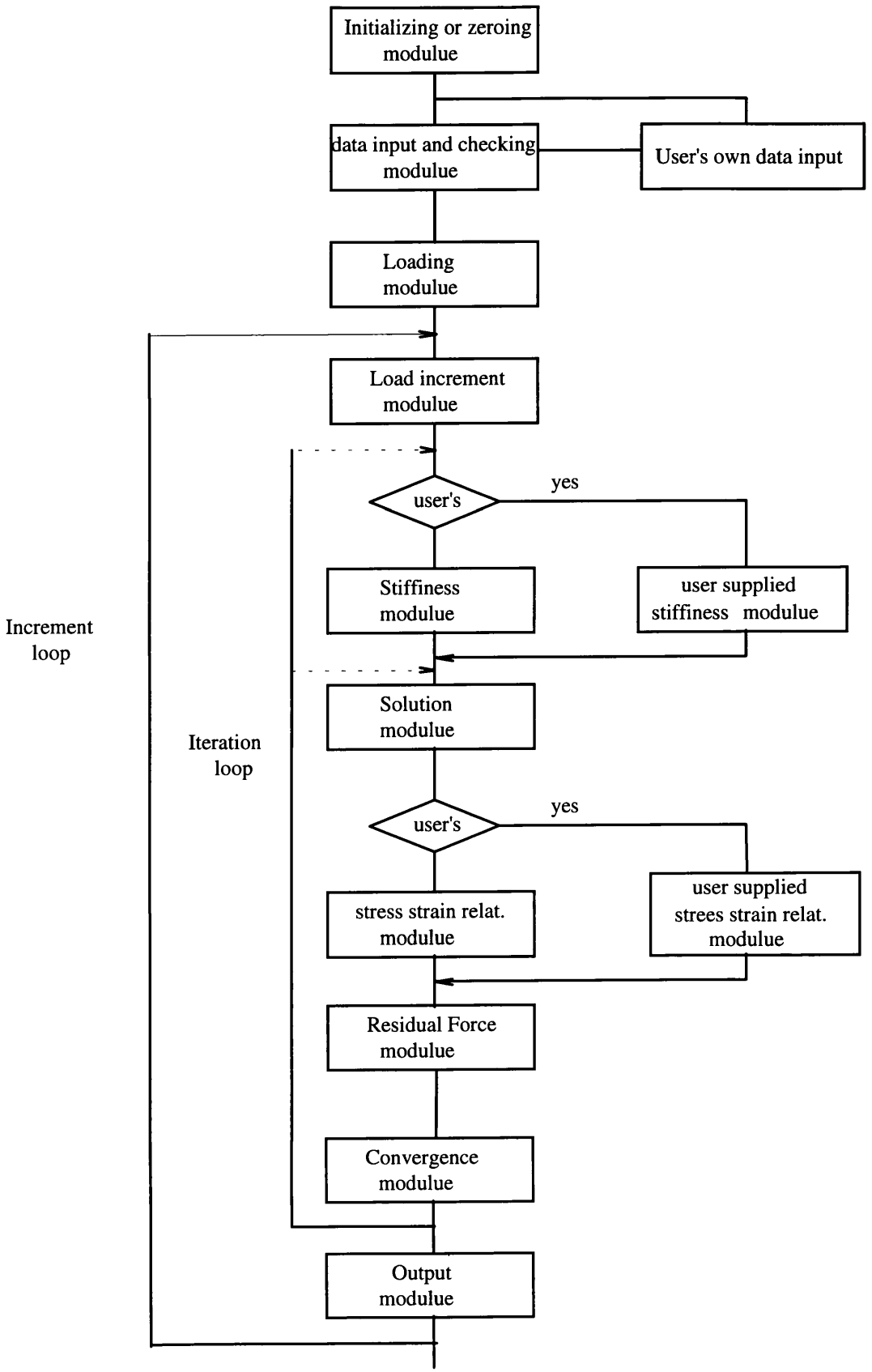

Fig. 4.10 Logic flow chart of the Lusas

Purpose: calculate the stiffiness matrix for the
jth iteration of the ith load increment.

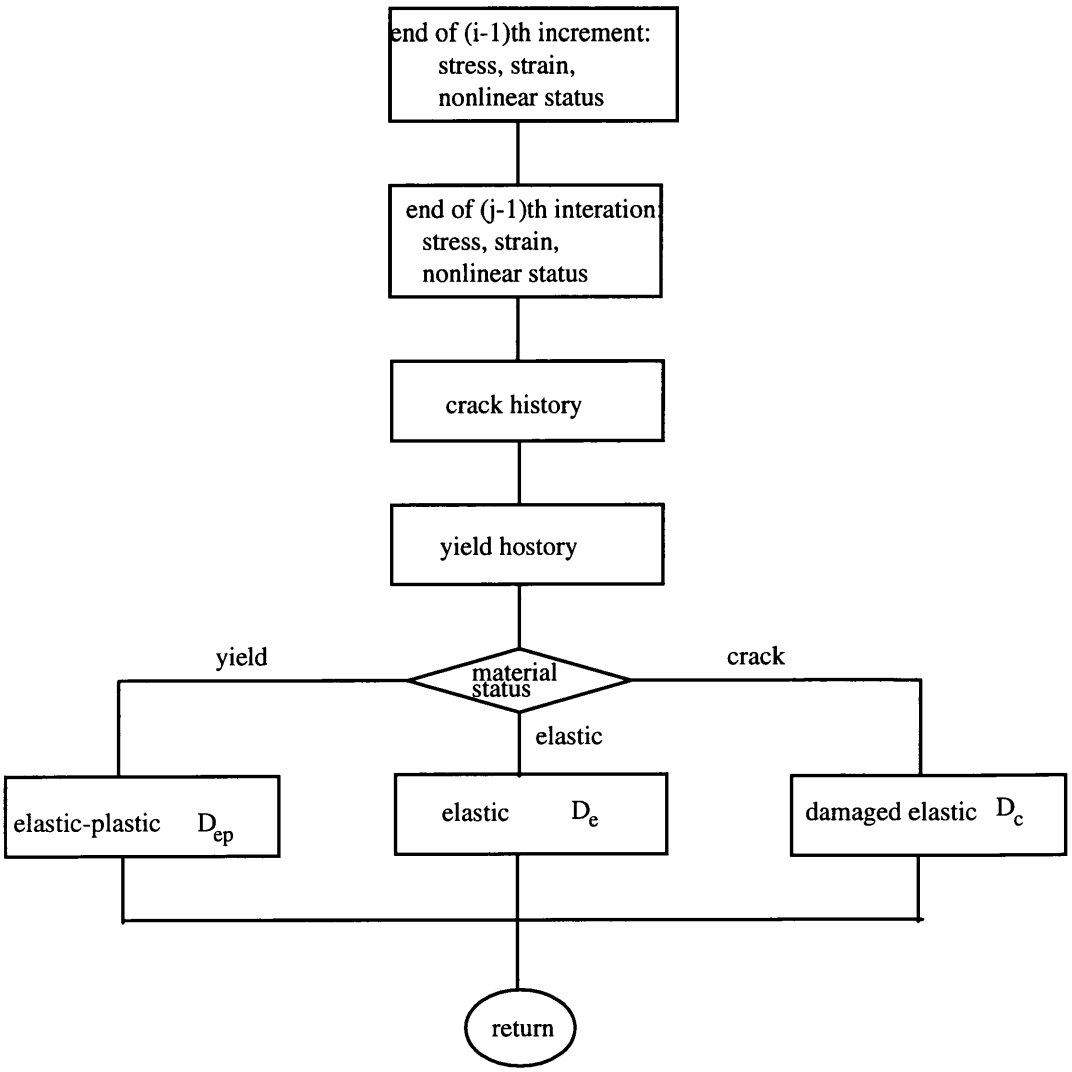

Fig. 4.11 Flow chart of calculating the stiffness matrix

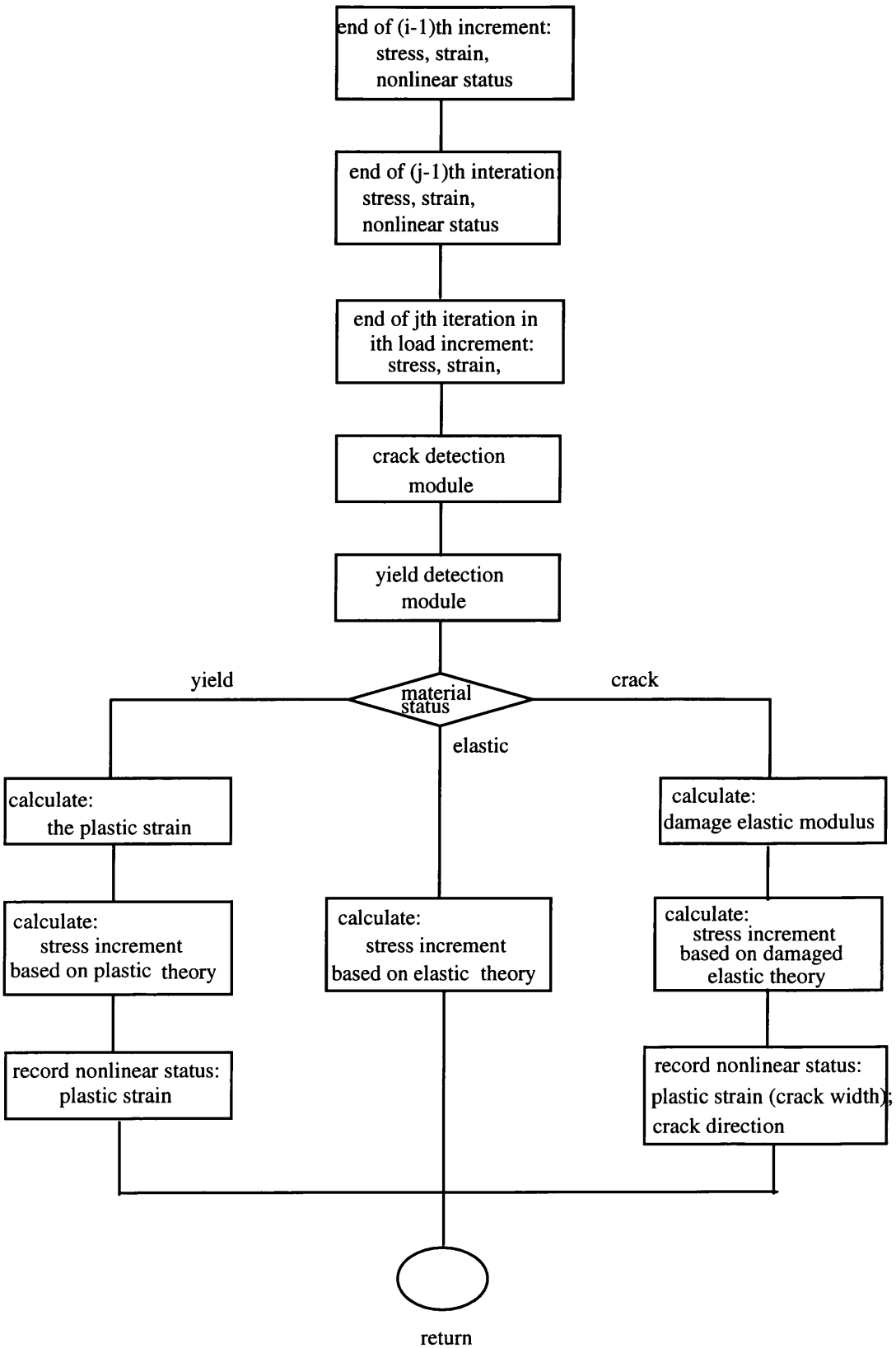

Fig. 4.12 Flow chart for calculating the stress from strain and nonlinear status

The implementation of the stress strain relations of the elastic-plastic stage and the damaged elasticity is the process to calculate the stress based on the current strain and the history of the stress, strain, and non-linear status.

For the elastic-plastic constitutive relations, the first thing to do is to check if it is freshly yielded or already yielded in the last iteration. If it is freshly yielded, the strain increment is divided into two segments, as shown in Fig.4.13. The first is the part from the result of last iteration to the stress level which just reaches yield surface, the second part is the remaining strain developed beyond the yield surface. The second segment of the strain is the combination of the plastic strain and the elastic strain; the exact proportion between them and the exact location of the corresponding stress status on the yield surface have to be determined based on the associated flow assumption, and this is done by an explicit process: dividing the second part further into several sub-increments, and the plastic strain and the stress increase in each of the sub-increment are calculated, as shown in Fig.4.13. If the material has yielded before the current iteration, the process to find the plastic strain and the location of the corresponding stress on the failure surface is similar to that of the second segment mentioned above.

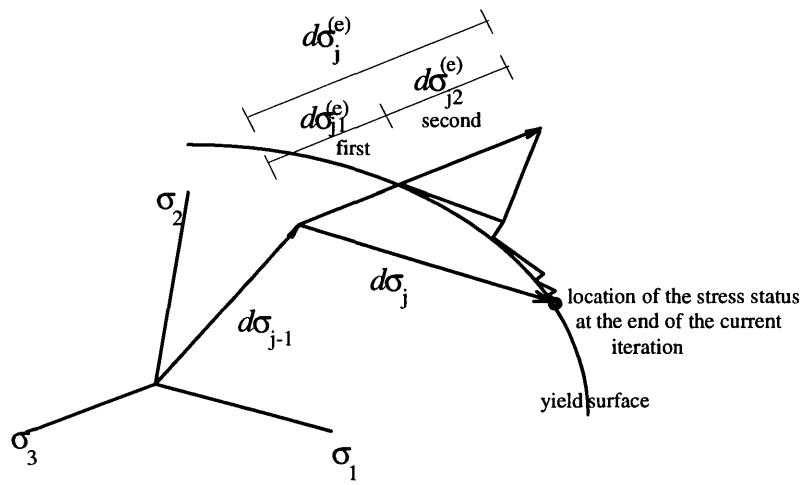

Fig. 4.13 Determine the location of the stress status at the end of the current iteration

If the concrete is under dominantly tension stress status, the cracks in the concrete develops; first, second and third cracks may appear subject to the development of the applied load. In Fig.4.14, a complete process from the elastic stage to the appearance of the third crack is schematically illustrated. First the elastic stage, then the first crack

appears and the stiffness is modified and plastic strain normal to the crack orientation is calculated; the corresponding principal axes at the time the first crack appears is recorded and maintained as the local co-ordinate system. After the stress in the local y or z direction has reached the fracture strength, second crack appears; plastic strain in the crack directions is then calculated and the stiffness matrix is modified; the stress in the remaining uncracked direction is monitored and once it reaches the fracture strength, third crack occurs; again, modify the stiffness matrix and calculate the plastic strain in all three crack directions.

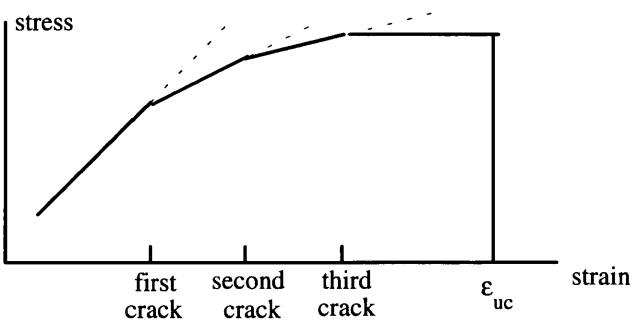

Fig. 4.14 Change of stress in the cracked concrete

The above is the complete process, while, during each of the iterations, there might be only part of the above process involved.

During each interval from the beginning of the iteration to the next appearance of the crack, this interval is further divided into several sub-intervals for the calculation of the plastic strain and the modified stiffness matrix. The reason for the sub-division is that the modified matrix is a function of the plastic strain (crack width), a few sub-division can improve the accuracy.

4.4.2 DESCRIPTION OF USER SUPPLIED SUBROUTINES

The above processes were coded into FORTRAN programs and integrated with the existing LUSAS modules. The user supplied modules were made up of 37 subroutines of about 2400 lines of source codes. The function of each subroutine is explained below.

USRSTR

calculate the stress and non-linear state variables of the current iteration based on the current strain, results of previous iteration and previous load increment.

CHKYLD

using the Mohr-Coulomb criteria to check if the current stress status has reached the yield surface or not. An elastic stress increment is assumed for the strain increment of current iteration, calculate the effective stress (Mohr-Coulomb's) and the equivalent strength limit, and then compare them.

USRDLAMD

calculate the plastic multiplier $d\lambda$ based on the results of the plastic strain and the non-linear status variable of last iteration or last sub-increment.

USRYLD

control the process of the calculation of plastic strain and the stress increment.

YLDRECOV

restore the stress state to the yield surface for the segment which is beyond the yield surface.

USRVECT

calculate the vector of the gradient of the plastic potential (the Mohr-Coulomb criteria is used here based on the associated flow assumption).

USRDELAS

calculate the elastic modulus matrix.

USRDPLAS

calculate the elastic-plastic modulus matrix.

USRLINST

calculate the elastic stress increment based on the strain increment.

USRINVAR

calculate the invariants of stress and invariants of stress deviator.

USREFSTR

calculate the effective stress for the Mohr-Coulomb criteria.

CHKCRK

check if the concrete has any crack or previously has cracked.

DAMGELST

calculate the stress of cracked concrete from the given strain.

USRCRK

control the process of the crack detection, crack orientation, plastic strain and stress increment.

NSEQU

determine which direction the next crack will occur based on the crack history and the current stress status.

STRSJP

calculate the change stress after the appearance of the crack.

STRNP

calculate the plastic strain increment in the cracked concrete for the current iteration.

TSTNP

calculate the total plastic strain increment in the cracked concrete for the current iteration.

CRKNO

determine the crack number existing in the cracked concrete.

NEWBLTA

calculate the value of β --- shear retention factor.

D12D

transformation of the elastic modulus from the local co-ordinate system to the global co-ordinate system.

D2D1

transformation of the elastic modulus from the global co-ordinate system to the local co-ordinate system.

SS12SS

transformation of stress vector (not tensor) from the local co-ordinate system to the global co-ordinate system.

SS2SS1

transformation of stress vector (not tensor) from the global co-ordinate system to the local co-ordinate system.

SN2SN1

transformation of engineering strain vector (not tensor) from the global co-ordinate system to the local co-ordinate system.

SN12SN

transformation of the engineering strain vector (not tensor) from the local co-ordinate system to the global co-ordinate system.

TSTRESS1

transformation matrix transforming stress in global co-ordinate system into the local system

TSTRESS

transformation matrix transforming stress in local co-ordinate system into the global system

TSTRAIN1

transformation matrix transforming engineering strain in global co-ordinate system into the local system

TSTRAIN

transformation matrix transforming the engineering strain in local co-ordinate system into the global system

USIGMA1

calculate the principal stresses.

UDIRECT

calculate the principal axes.

XYZ2CC

transformation matrix transforming the directional vector matrix into the direction cosine matrix.

CC2XYZ

transformation matrix transforming the directional cosine matrix into the direction vector matrix.

DDD

calculate the elastic modulus of the cracked concrete.

FIND_R

divide the strain (stress) increment into two segment, first part is the elastic part starting from the end of last iteration to the failure surface; the second segment is the one beyond the failure surface. If it is the cracked type, the first segment is from the end of last iteration to the stress just before the crack, and second segment is the one beyond the crack.

USRKDM

the process to find which elastic modulus matrix should be used for the next iteration, either the elastic one, elastic-plastic one or damaged elastic one.

In order to verify the correctness of each of the above subroutines, a sets of hand calculations were carried out using a single element and various material status were simulated; the computer analysis results were checked against the hand calculation results. After the integration of the user supplied modules to the LUSAS package, two separate analyses were carried out for a 2D beam under bending, one analysis was carried out using the original LUSAS, the other one was using the user supplied material model. The results of the two analyses were very close to each other.

4.5 FINITE ELEMENT MODEL OF THE RC WAFFLE SLABS AND ANALYTICAL CONSIDERATION

4.5.1 ANALYSIS MODEL OF THE RC WAFFLE SLABS

In the tests, the waffle slabs were loaded at the centre of the slabs and supported (tied) at eight points uniformly distributed near the four edges of the slabs. Due to the symmetry, 1/8 of the slab is selected for the analysis, as shown in Fig.4.15, where one supporting point is supplied, and 1/8 of the loading pad is applied. The supporting condition of the slab is

line L_{45}: $u_y = 0$ in local co-ordinate system;
line l_0: $u_y = 0$ in global co-ordinate system;
support point R: $u_z = 0$ in global co-ordinate system.

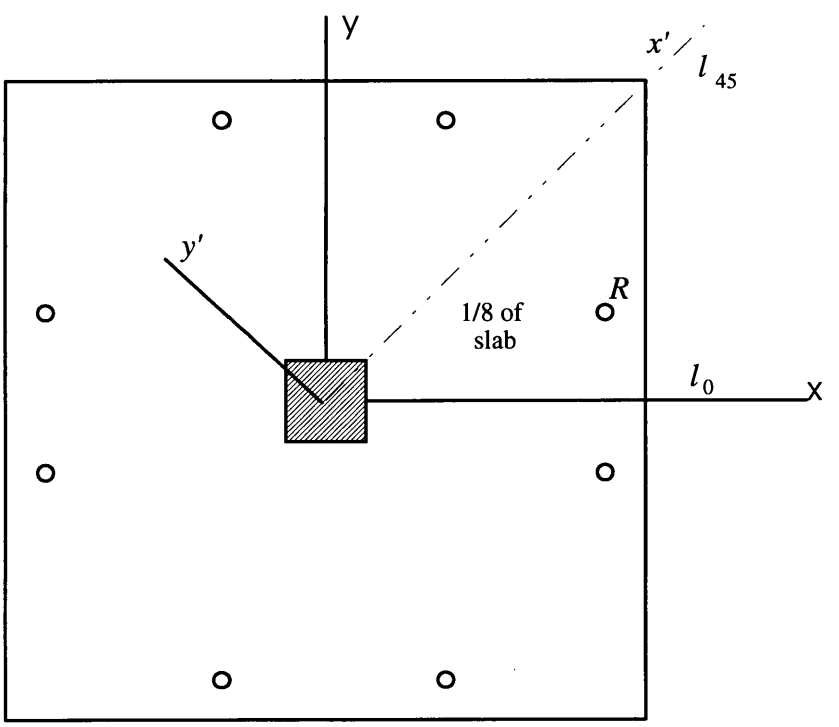

Fig.4.15 Location of the 1/8 of the slab for analysis

The element mesh of the 1/8 slab is shown in Fig.4.16, four layer of elements in z direction and 9 columns or rows of element in both x and y directions.

The concrete is modelled by 20-node cube elements HX20 and 15-nodes prismatic element PN15. Both the concrete fracture model and the Mohr-Coulomb model are

employed to simulate the fracture and plastic hardening characteristics of concrete. The steel inside the slabs have been modelled by space membrane element SMI4 and TSM3 with the Possion ratio μ=0; material model is the elastic-plastic model using the Von Mises criteria.

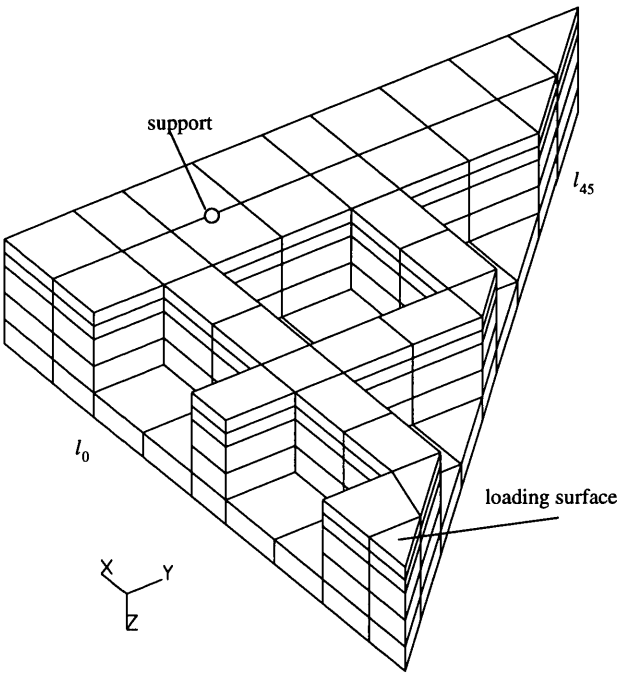

Fig 4.16 FEA Model — 1/8 of the Slab

The applied load is simulated by a uniformly distributed surface load in the position of the loading pad. The analysis is carried out by an incremental analysis with the load gradually built up.

Material parameter input is listed below.

Mohr-Coulomb Criteria (used for concrete),

Material Properties Non-linear 63
E, ν, C_o, φ_o, C_c, C_φ, L

where,

E	elastic modulus of concrete;
ν	Possio ratio;
C_o	cohesion factor of concrete;
φ_o	internal friction angle of concrete;
C_c	hardening rate of the cohesion factor of concrete
C_φ	hardening rate of the internal friction angle of concrete
L	the limit the plastic strain to which the hardening is valid.

Von Mises Criteria (used for reinforcements),

Material Properties Non-linear 62
$E,\ \nu,\ f_y,\ C_i,\ L_i$

where

E elastic modulus of concrete;
ν Possio ratio;
C_i hardening rate of the yield strength against the plastic strain;
L_i limit of the plastic strain to which the hardening is valid.

User Supplied Material Model (the crack model for concrete),

Material Properties Non-linear User *lptuser nprz nstat*
$E,\ \nu,\ C_o,\ \varphi_o,\ L,\ f_t',\ C_c,\ C_\varphi, \varepsilon_{uc}$

where

lptuser user defined material model number;
nprz number of user defined material parameter;
nstat number of non-linear state variables defined by the user;
E elastic modulus of concrete;
ν Possio ratio;
C_o cohesion factor of concrete;
φ_o internal friction angle of concrete;
C_c hardening rate of the cohesion factor of concrete;
C_φ hardening rate of the internal friction angle of concrete;
L the limit the plastic strain to which the hardening is valid.
f_t' uniaxial fracture strength of concrete;
ε_{uc} limit of the plastic strain to which the tension stiffening and shear retention no longer exist.

4.5.2 CONVERGENCE CONSIDERATION AND JUDGEMENT OF STRUCTURE FAILURE

The analysis employs the incremental method, the loading being gradually increased step by step with varied step length. In each step, iteration takes place until the residual force is reduced to the acceptable minimum or the number of the prescribed iteration being completed.

In the non-linear analysis, the maximum load is itself an unknown parameter and need to be determined. In the numerical analysis, the maximum load is one of the following

three loads: the final loading level before the analysis terminates; the load at which the structure's displacement is too large; or a mechanism has formed in the structure with the stiffness matrix becoming singularity. For the first type, the analysis is terminated, the reason for the termination might be due to either the structure is no longer stable or something is wrong so the iteration can not converge. Then an analyst has to use his/her experience to judge whether the maximum load has been reached or there are problems to be solved. For the second type of load, it depends on the problem under consideration, e.g., for slab under bending, the analysis may still carry on, but a large displacement may indicate that the structure has reached the ultimate load. As to the problem of punching, the displacement of the slab is usually quite small when the punching takes place, so it is more than likely that the analysis will terminate. As mentioned before, extra care has to be taken to check if the termination is a natural one or a fake one. The proper termination will be the one in which the cracks or the plastic zone will form a failure mechanism.

4.6 CONCLUSION

- The application of non-linear finite element analysis on punching of reinforced slabs is considerably more difficult compared to that on bending of slabs; the material model and the relevant parameters are more sensitive, and the final failure load need to be judged carefully.

- Two material models are employed for the analysis of RC waffle slabs, one is the Mohr-Coulomb criteria and the other is the concrete model considering the fracture feature of concrete. The merits and shortcomings of the two models were discussed.

- LUSAS supports the Mohr-Coulomb criteria in 3D analysis, while, the concrete fracture model is not supported in 3D analysis. The analysis of RC waffle slabs requires the 3D model and the fracture feature considered.

- The self written modules using the concrete fracture model was developed, which consists of 37 subroutines of about 2400 lines of source code. The user supplied modules can be integrated with original LUSAS.

- In the current analysis of the RC waffle slabs, 1/8 of the slab is taken for the analysis model.

In Chapter 6, the slabs tested in this study will be analysed using the FEA described above along with other methods of analysis.

CHAPTER 5

EXPERIMENTAL PROGRAMME AND RESULTS

5.1 EXPERIMENTAL PROGRAMME

To investigate the punching shear capacity of R.C. waffle slabs under concentrated load, a total of twelve square model slabs, with a scale of 1/3, overall depth of 150mm and side dimension of 1.65m, were tested to failure. Each slab was subjected to a concentrated load in the middle of the slab and supported by 8 points symmetrically located around the slab. The programme of the work was divided into four groups modelling punching failure in different location of the slab, different local configuration of the slabs and the effectiveness of the shear links. They are listed below in Table 5.1. Slabs No.1~12 are shown in Figure 5.2(a)~(l).

Table 5.1 R.C. Waffle Model Slabs Schedule

Slab No.	Punching Location	Slab Local Config.	Local Solid	Flexural Reinforcement	Link	Remarks
1	Middle of Slab	#	No	2T12 in each rib, T12 in middle of deck	No	No shear Reinforcement
2		+				
3	Slab-Column Connection	#	No	3T12 in each rib		
4		+				
5		#	Yes			
6		+				
7	Middle of Slab	#	No	2T12 in each rib, T12 in middle of deck	R6@90	Similar slabs as above but having shear links
8		+				
9	Slab-Column Connection	#	No	3T12 in each rib	R6@90	
10		+				
11		#	Yes		R4@90	
12		+				

Note:

# denotes the type of configuration shown in Fig.5.1a, the ribs are positioned around the loading area.

+ denotes the type of configuration shown in Fig.5.1b, the ribs are positioned just underneath the loading area.

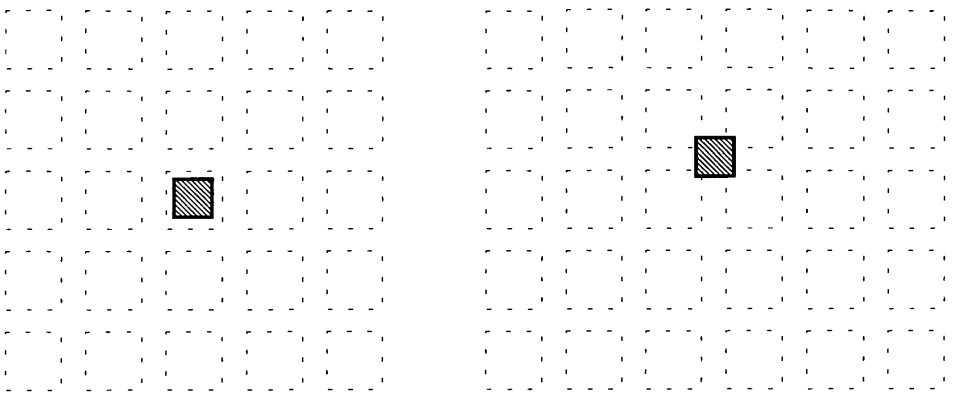

a) '#' type of Configuration b) '+' type of Configuration

Fig.5.1 Configuration of the Waffle Slabs

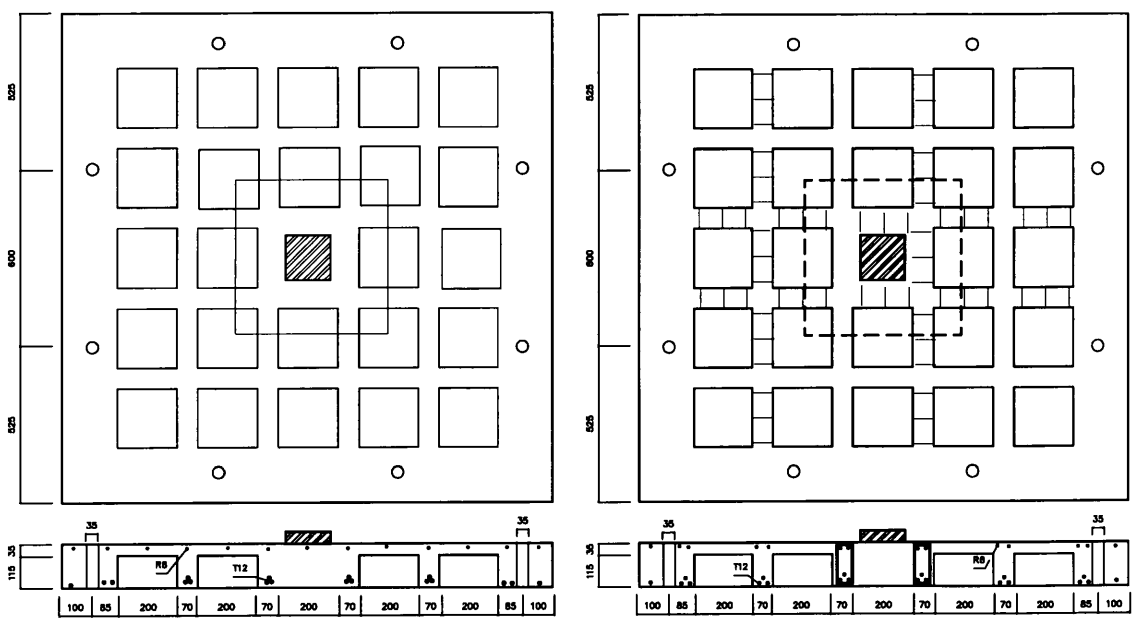

(a) Slab No. 1 (g) Slab No. 7

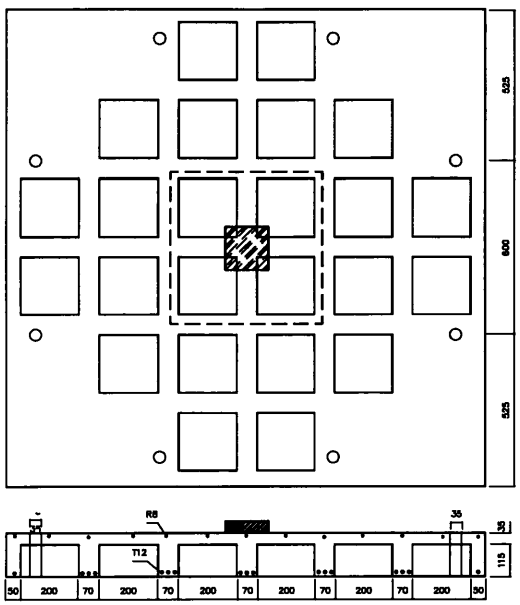

(b) Slab No. 2

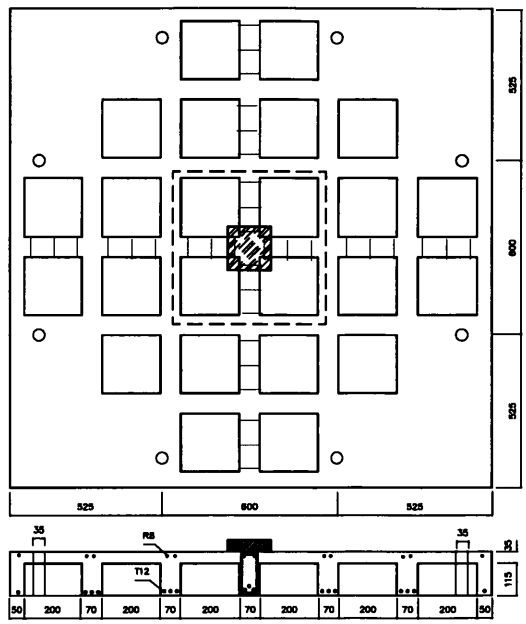

(h) Slab No. 8

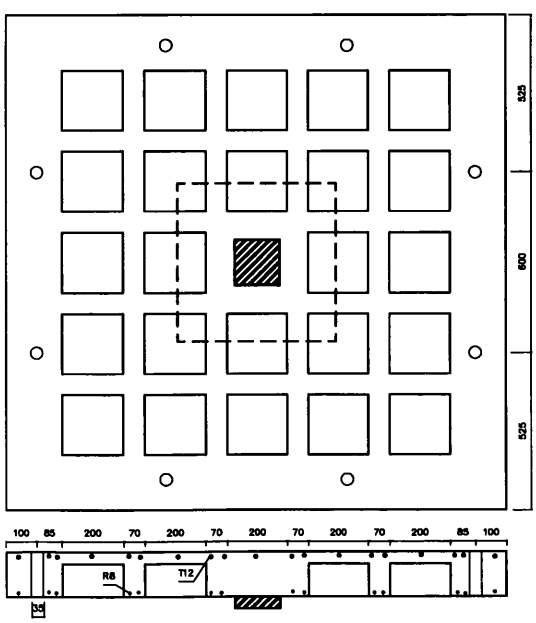

(c) Slab No. 3

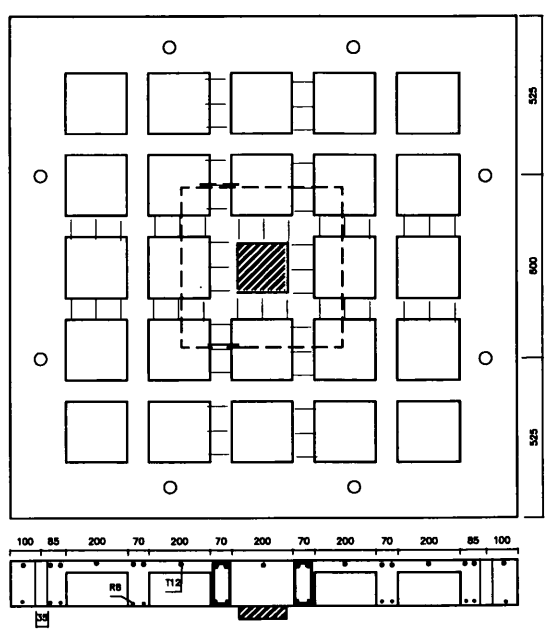

(i) Slab No. 9

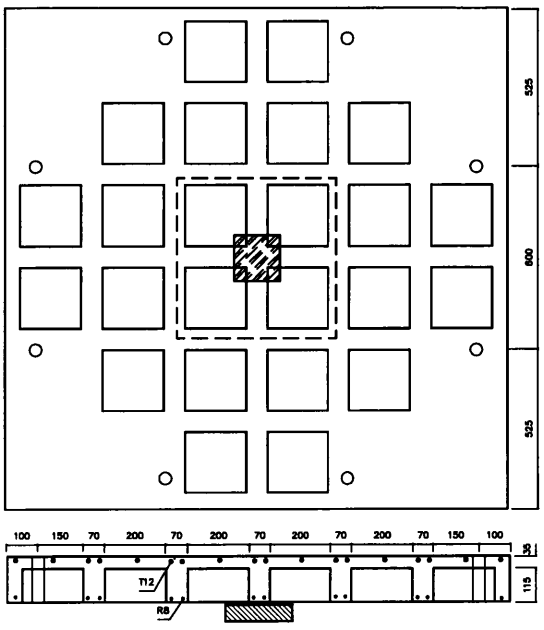

(d) Slab No. 4

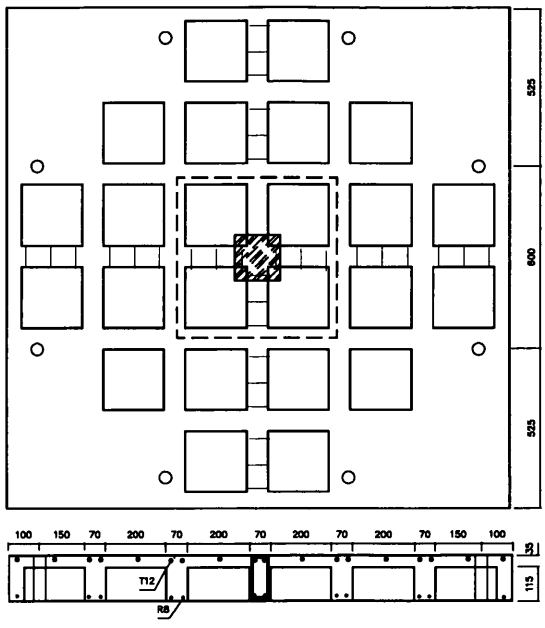

(j) Slab No. 10

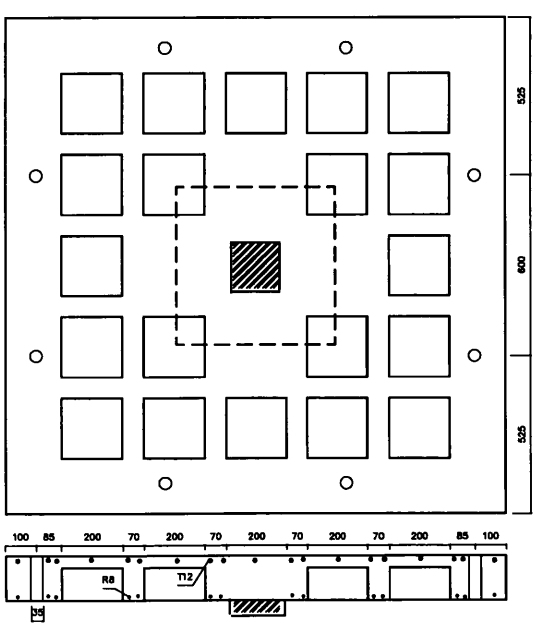

(e) Slab No. 5

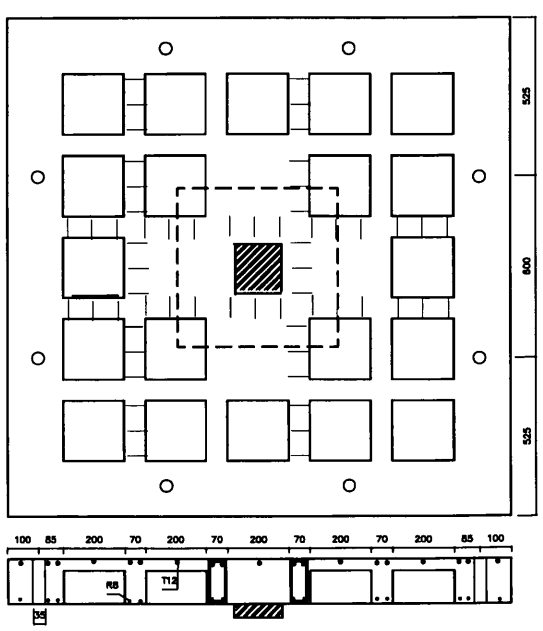

(k) Slab No. 11

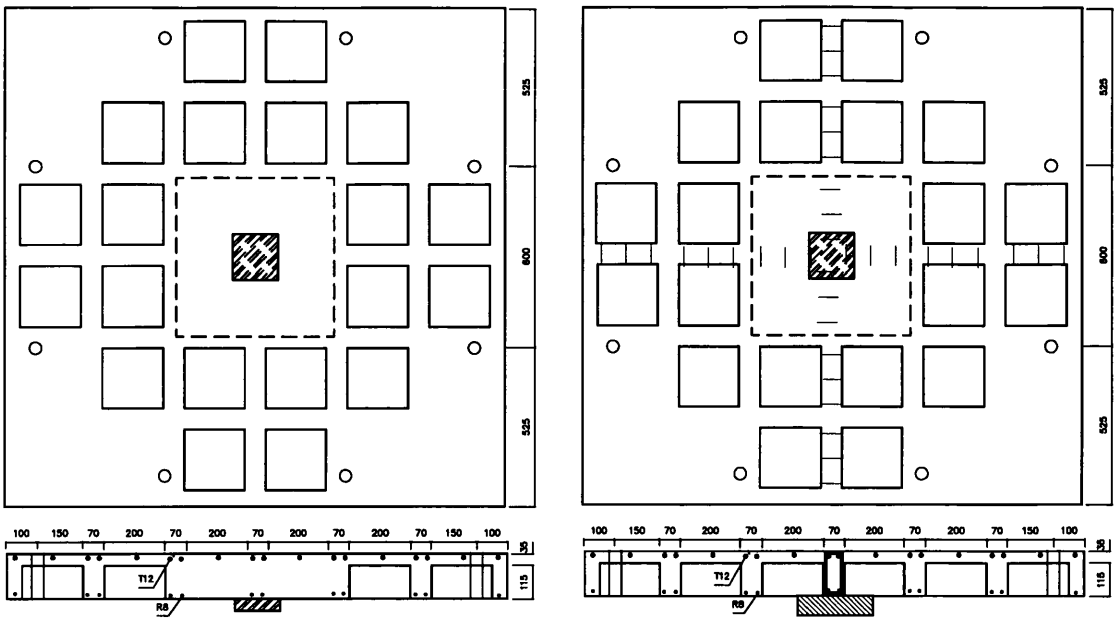

(f) Slab No. 6 (l) Slab No. 12

Fig.5.2 Drawings of the Model RC Waffle Slabs

5.1.1 DESCRIPTION OF MODELS

As mentioned earlier, the model slabs are of 1/3 scale which was chosen considering the scale effect on concrete structures and the availability of the testing facilities. All the twelve model slabs were of the same depth 150mm and side dimension 1.65m. The recesses in the slabs were of the same size 200×200×115mm^3, the position of them varied for the different groups of slabs.

The twelve model slabs were divided into four groups to consider the following influences

- **Punching location:** two locations were considered, one was in the middle of a slab panel with the load pointing downward, slabs No. 1, 2, 7 and 8 are the models to simulate this case. The other location was in the vicinity of the slab/column connection area with the concentrated load supplied by the column and pointing upward; slabs No. 4 to 6 and 9 to 12 represented this case. During the test, the

concentrated load was always applied upward for both the cases; in the latter case the slabs were turned upside down.

- **Local Configuration:** around the loading pad, two typical configuration of ribs and recesses are considered, one with the loading pad being in the position of a recess, as shown in Figure 5.1.a and referred as '#' type of configuration, the other with the loading pad at the intersection of two ribs, as shown in Figure 5.1.b and referred to as '+' type of configuration.

- **Local Solid Area:** In the vicinity of slab-column connection, some recesses were filled with concrete to form the local solid area increasing the shear capacity, slabs No. 5, 6, 12 and 12 represented these cases.

- **Shear Links:** shear links inside the ribs are used to enhance the shear capacity. Slabs No. 7 to 12 are reinforced with shear links.

5.1.1.1 Model Scale and Dimension

The selection of the model scale for this investigation was influenced by a number of factors such as space limitation and the availability of equipment for testing and loading. The major aspect which required great care was to ensure that the model scale chosen would not produce misleading results due to the scale or size effects. This is of great importance in R.C. structures on which the size factor does affect the behaviour of concrete. The dimensions of the prototype slab was chosen from a survey on existing waffle slabs[42]. The dimensions of the prototype and model slabs are listed below

	Prototype	**Model**
Depth	H=450mm	h=150mm
Span	L=10.5m	l=3.5m
Rib-spacing	A=810mm	a=270mm
Width of rib	B=210mm	b=70mm
Top slab depth	T=105mm	t=35mm
Column Dimension	C=450mm	c=150mm

Once the scale of the model was selected, the length of the model slab for the punching shear test is decided by the following consideration:

In the test for punching shear the area surrounded by the contra flexural line is normally considered. The contra-flexural position in a solid slab is about 0.21L from the centre of the column. In a waffle slab, the position of this point can be taken to be the same if the influence in flexure from the solid area in the vicinity of the column is neglected. The span of the model slab for the punching shear test should have been $2\times0.21\times3.5=1.47m$; however, considering the layout of the recesses, the span was actually taken as 1.45m. On the contra-flexural line, the bending moment is zero, while the shear force exists. The edges of the slabs tested are considered as simply supported having had eight symmetrically distributed supporting points, 2 on each side of the slab, see Fig.5.3.

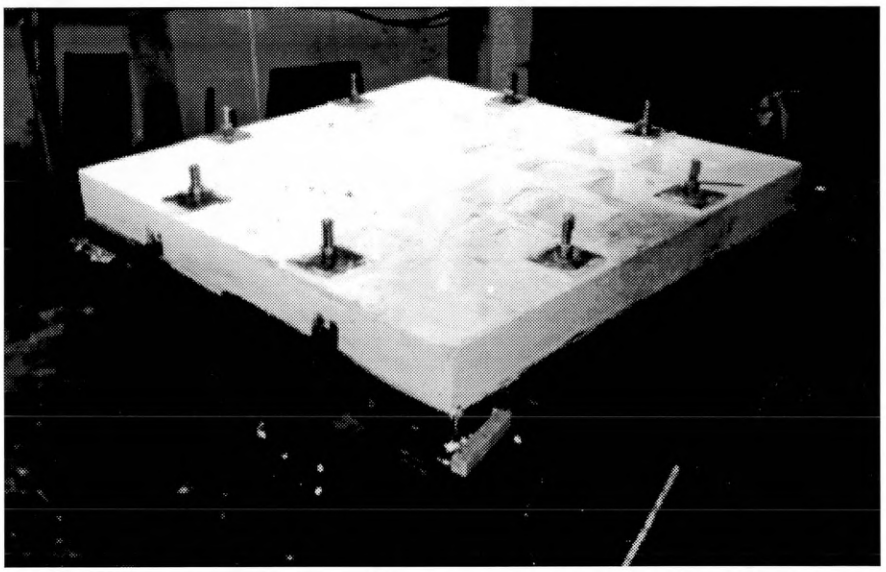

eight threaded bars tightening the slab to the test rig

Fig. 5.3 Support of the Slab on the Test Rig

5.1.2.2 Materials

Concrete for the specimens was normal weight and made with the Ordinary Portland cement. In view of the model scale aggregates with the maximum size of 10mm and a local zone 2 sand were used. The results of the sieve analysis of the gravel and sand are shown in Fig. 5.4 and 5.5. A target strength of 45N/mm^2 was adopted for slabs No. 1~6, 30N/mm^2 for slabs No. 7~12.

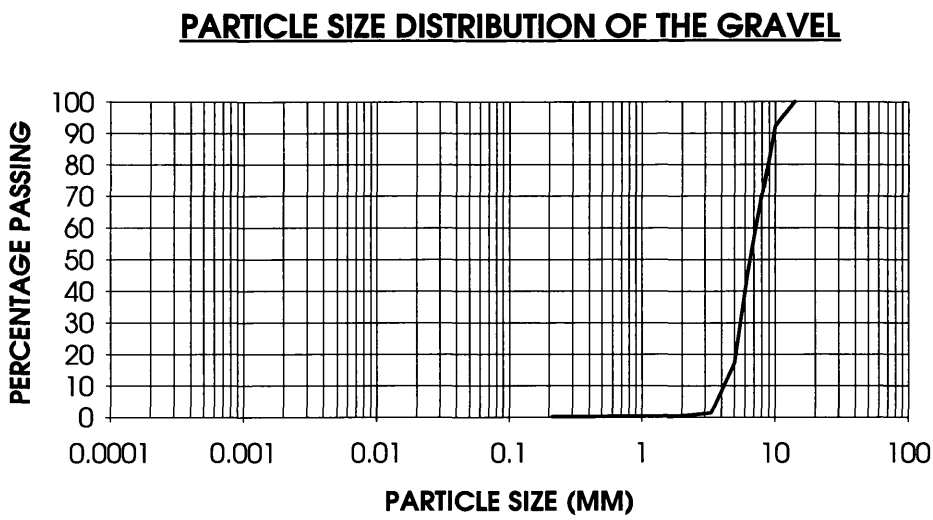

Figure 5.4 Sieve Analysis of the Gravel

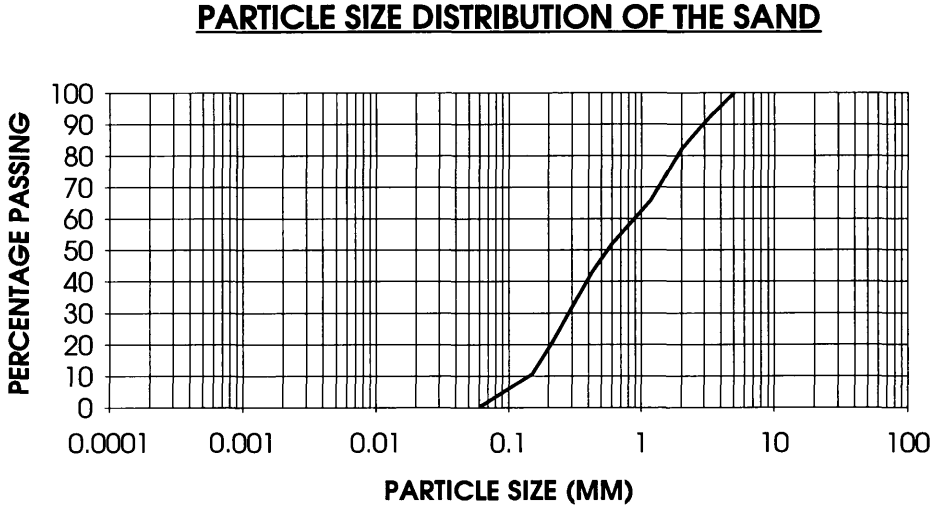

Figure 5.5 Sieve Analysis of the Sand

5.1.2.3 Reinforcement Cages

Four types of reinforcement are used, 12.0mm diameter high yield bars were used for the flexural reinforcement, 8.00mm diameter mild bars for the second reinforcement, 6.00 and 4.0 mm diameter mild steel bars were used for the stirrups inside ribs. Sufficient flexural reinforcements were provided to ensure failure by punching shear. The maximum amount of flexural reinforcement required was found by estimating the punching capacity of slab No. 11, which was the strongest among all the model slabs. In order to make the results comparable, the same amount of flexural steel was provided in all slabs with the configuration of the reinforcement slightly different due to the

variation of the configuration of the ribs in the slabs. The distribution reinforcement was provided to ensure the handling of slabs during transportation and turning over. The sections of slabs 7~12 were shown in Fig.5.2. The details of the cross-sections of a portion of the rib are shown in Fig.5.6.

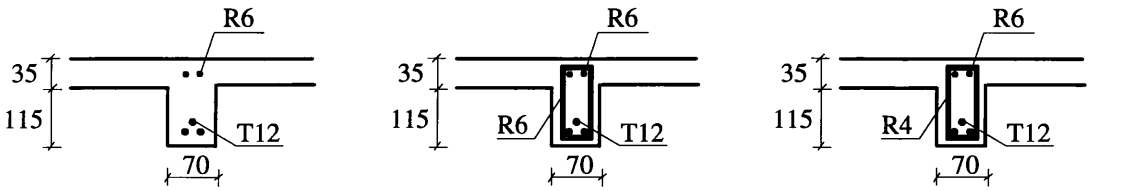

(a) rib of slab 1~6 (b) rib of slab 7~10 (c) rib of slab 11~12

Fig 5.6 Typical Cross-Section of the Ribs of the Waffle Slabs

The fabrication of the reinforcement cages was carried out by supporting the reinforcement on a timber frame with slots, which would allow fixing of the reinforcement in the required position, and then the reinforcements were tied together by steel wires to form the cage, see Fig. 5.8.

5.1.2 FABRICATION OF MODEL SLABS

5.1.2.1 Slab Forms

The slabs were constructed using polystyrene blocks which proved to be effective and easy to use method of forming the recesses, Fig.5.7. The polystyrene blocks were trimmed to size with ±1mm tolerance, by an electrical hot wire cutting machine which produced a good finished surface. These blocks were wrapped with very thin polythene film and then were fixed into the position on the base plate of the mould by heavy duty 20mm wide double sided tape. This type of fixing was chosen to prevent the floating of the polystyrene blocks during the vibration in casting and avoid any cement paste seeping underneath the polystyrene blocks. The variation of the configuration of the slabs was achieved by varying the positioning of the polystyrene blocks. Eight steel tubes of 35mmϕ and 300mm length, sealed at one end and wrapped by polythene film were bolted to the base of mould to provide holes in the slabs for supporting; they were extracted from the slabs 12 hours after the casting of the concrete. Fig. 5.7 and 5.8 show the slab forms.

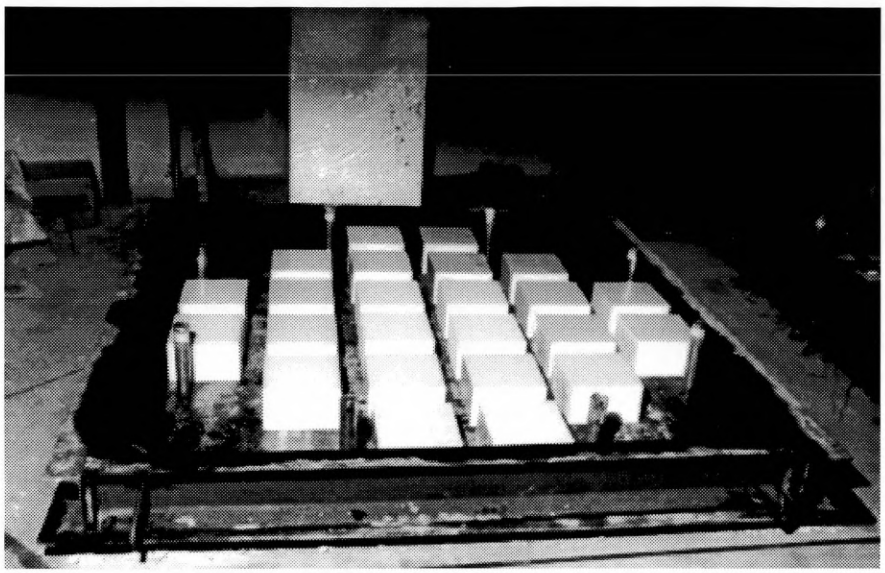

Fig.5.7 Fixing of polystyrene blocks onto the slab form

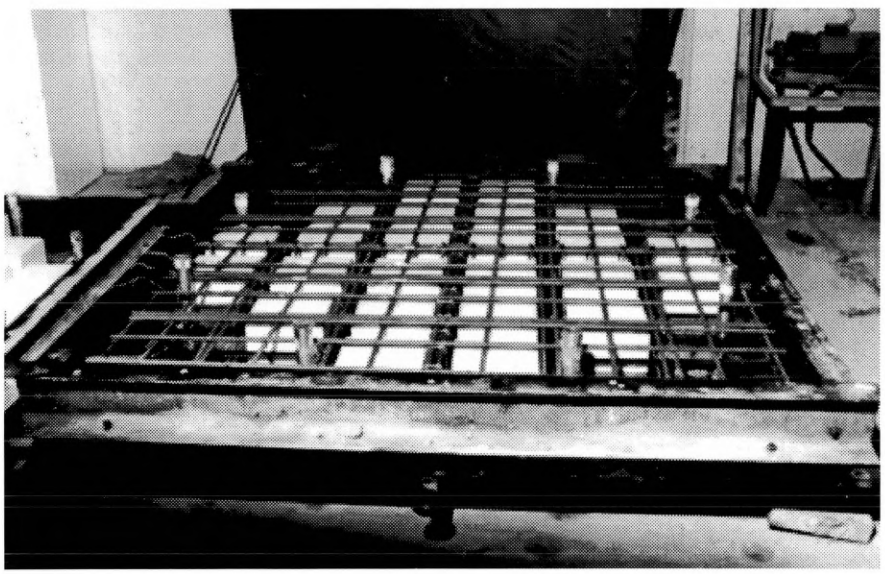

Fig.5.8 Positioning of polystyrene blocks and reinforcement cage into the slab form

5.1.2.2 Casting

Each model slab had a volume of concrete of about $0.35m^3$ and the concrete mixer had a capacity of about $0.1m^3$, therefore three and half batches of concrete were mixed to cast each slab. Three cubes and one cylinder were prepared for each batch to determine the compressive and tensile strength of the concrete respectively. The fresh concrete was carefully placed into ribs and kept on the same level all over the slab. The concrete was

compacted by a poker vibrator. The slabs, control cubes and cylinders were covered by wet hessian sacks and plastic sheeting after casting was completed. The moulds were stripped off after 24 hours, and the slabs and samples were covered again by the sacks which were kept wet for 14 days.

5.1.3 LOADING SYSTEM

The test rig consisted of an upper frame and four supporting legs, all fabricated from universal channels. The upper frame was welded to the top of the supporting legs to transfer the tensile force. The legs were then bolted through to the prestressed concrete floor of 1m depth. The bolts were fabricated from 35mmϕ mild steel bar. The test rig is illustrated in Fig.5.9b & c.

The loading system adopted in this study was such that the jack applied the concentrated load upward (simulating the applied load at the middle of the slab or the column reaction); the slab was balanced on eight threaded bars of 24mmϕ symmetrically distributed around the edge of the slabs. The threaded bars were bolted to the steel frame, which in turn was bolted to the strong concrete floor.

The loading screw jacks, 30 Tons and 50 Tons capacity, were located on the floor underneath the slab and in line with the centre of the slab. These jacks were manually operated by an extend lever. The load from the jack was spread to the slab by a loading pad which was made of two pieces of steel plates, 150mm square and 20mm in thickness. The load cell was located between the jack's face plate and the loading plate. The load cell had a cap which could rotate so that the load was always normal to the surface of slab even when it was tilted. Fig.5.9a shows the loading system.

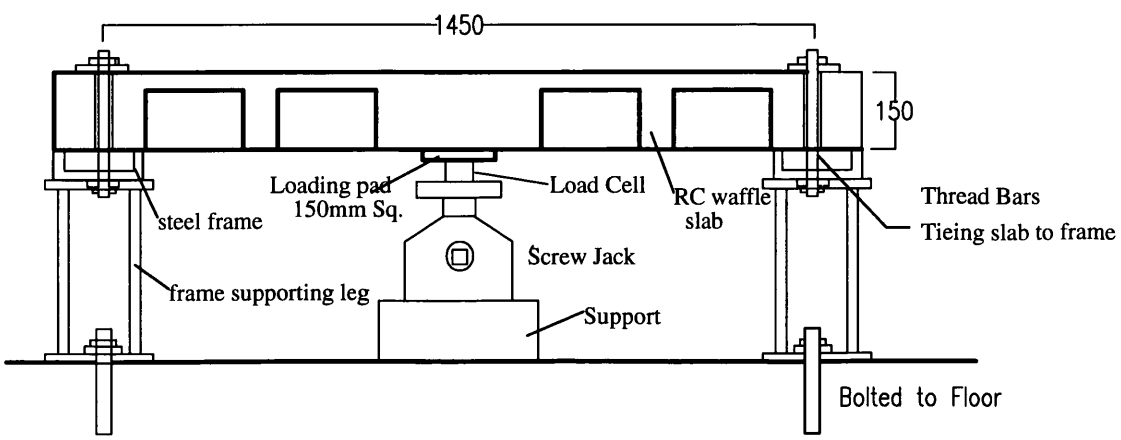

Fig. 5.9a Set-up of the loading rig

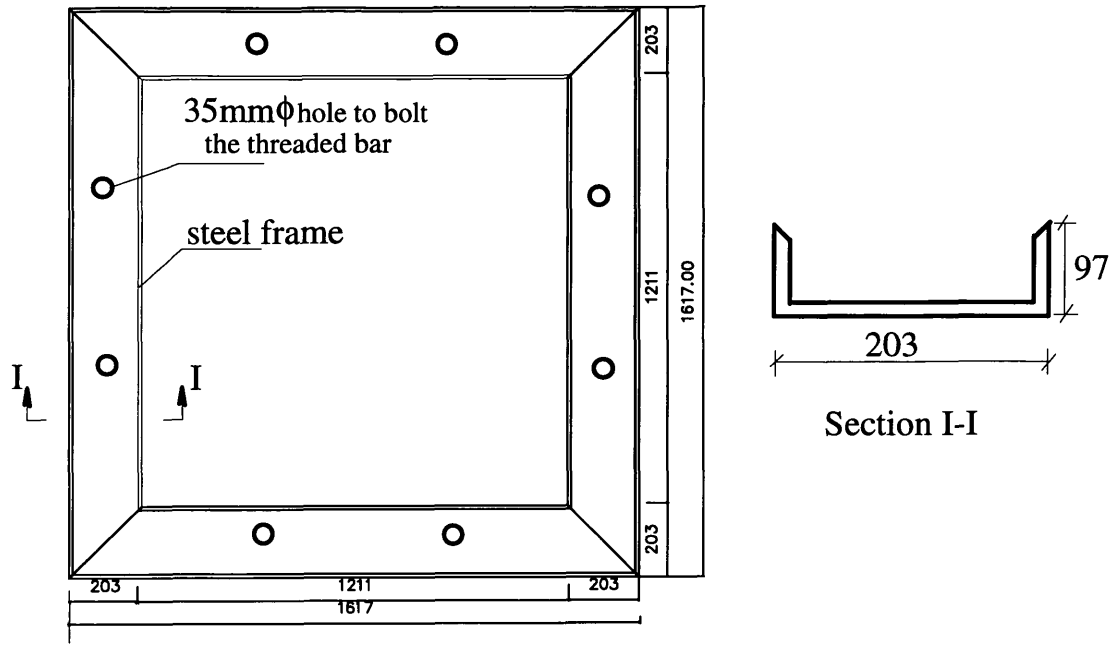

Fig. 5.9b Plane View of the Test Rig

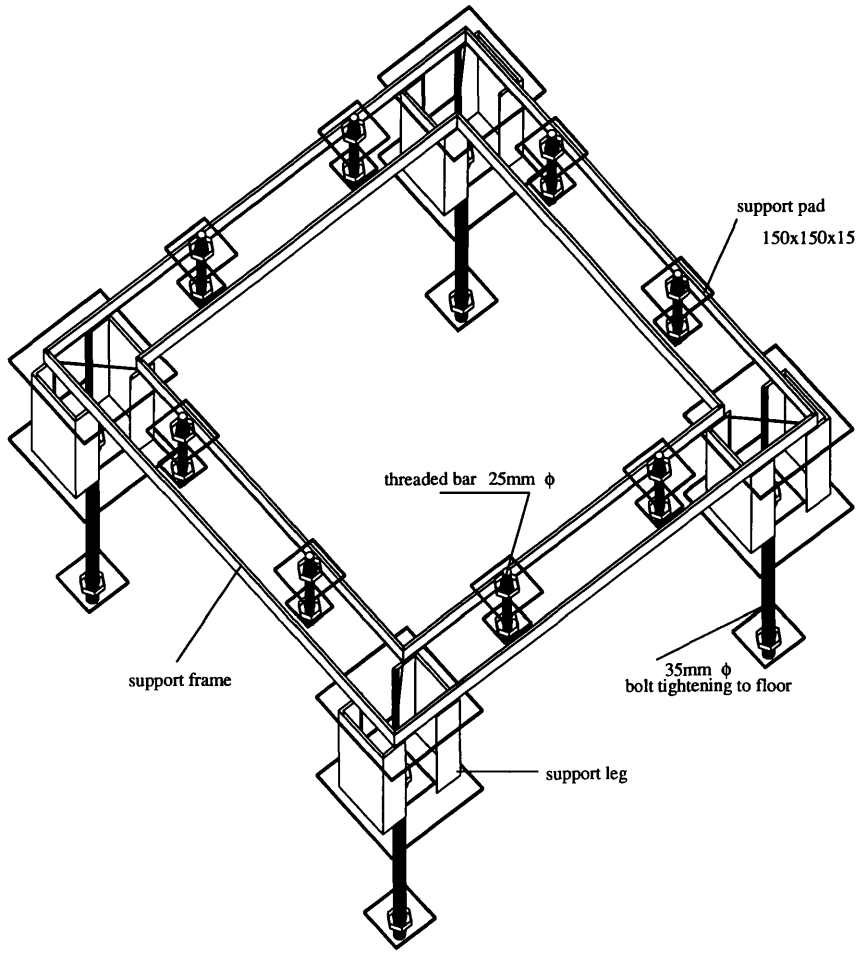

Figure 5.9c Test rig in 3D view

5.1.4 INSTRUMENTATION

The parameters of main concern in the test were the load, deflection, strain in the steel and the crack propagation. All these parameters were recorded for each load increment and upto and including the final collapse load. The instrumentation used is listed bellow:

Load Cell

The load cell used was the Maywood C4000 which has a capacity of 500 KN. The load cell was driven by 10 volts of excitation voltage which was supplied by a stabilised power supplier. The output parameter of the load cell was a voltage which was converted into the load by the load/voltage factor. The load cell was calibrated against an Avery-Dennison compression machine.

Transducers

LVDTs were used to measure the deflection of the slabs under loading. Five LVDTs, supported on a firm stand on the floor, were arranged in a line to measure the deflected profile of the centre section, as shown in Fig.5.13. The transducers were calibrated in advance against the standard samples and the calibration factors were recorded to convert the voltages into deflections.

Strain Gauges

Eight to twelve strain gauges were used to measure the strains in the reinforcements. The strain gauges were the type of FLK-6-11 manufactured by Tokyo Sokki Kenkyujo Co. Ltd. The strain gauges were attached to the reinforcements using the Cyanoacrylate adhesive, and then they were protected with two layers of waterproof coatings, i.e. M-coat A and D before the casting of concrete.

Datalogger

A Solartronic Datalogger was used to monitor and record the load, deflection and strain reading. The datalogger was connected to a PC which showed all the parameters on the screen at all stage of loading.

Fig.5.10 illustrates the logic connection of all the instrumentation used during the test. The load was monitored on the screen and the load increment was achieved by instructing the jack operator supplying load to achieve the nearest possible value as required.

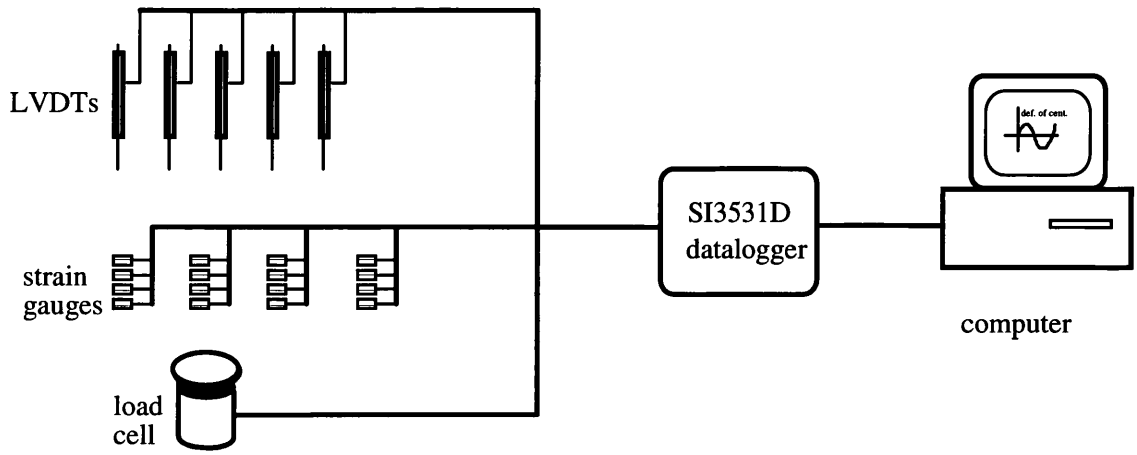

Fig.5.10 Logic Connection of the Instrumentation

5.1.5 TEST PROCEDURE

Each slab was cast and cured on the laboratory floor for 28 days before putting it on test. Slabs 3~6 and 9~12 had to be turned over by using the overhead crane in the laboratory and then placed on the testing rig. Other slabs were directly put onto the testing rig. In order to view the crack propagation clearly, the slabs were painted by a coat of thin white emulsion.

The slabs were tied to the frame by eight threaded bars. When the threaded bars were tightened up attention was give to make them not too tight to avoid restriction to the rotation of the edge of the slab. This was achieved by using a torque wrench which was set to the minimum torque and the threaded bars were tensioned symmetrically. During the test, it was noticed that a clear gap between the supporting channel and the edge of the slab existed, which verified the support condition as simply supported.

Once the instruments were set up, the loading was initially applied in increments of 10KN; once the required load level was reached the load, deflection and strain were recorded; the slab was examined for cracks on the top of the slab and on the ribs, and the cracks observed were marked. In the later stage of the loading, the load increment was reduced in order to get as accurate as possible the punching failure load. After the failure had occurred the load had a sharp reduction, but it still could sustain some load; a gradually reloading process was adopted to examine the post-failure behaviour. Such

test cycle including the pause to make the various reading took three to five hours. Care was always taken to ensure steady loading.

5.2 EXPERIMENTAL RESULTS

5.2.1 PROPERTIES OF MATERIALS

5.2.1.1 Concrete

The compressive and split cylinder strengths of each batch of concrete were obtained, the strength of each slab was taken as the average of the strengths of the batches. Table 5.2 lists the strengths of each batch of concrete, Table 5.3 lists the average compressive strength of each slab.

It is seen from the tables that slabs No. 1 to 6 have an average compressive strength 53.9N/mm^2, tensile strength 3.79N/mm^2 and the ratio of tensile/compressive is 0.071. Slabs 7 to 12 have an average compressive strength 35.4N/mm^2, tensile strength 2.92N/mm^2, the ratio of tensile/compressive is 0.083. Generally the actual compressive strength was higher than the target strength mainly because of the variation of the water content in the sand and gravel which were stored in containers with the material getting higher water content at the lower level. Because of the large amount of material used in casting each slab, it was unrealistic to dry all the material in the oven. Although care had been taken to adjust the water in the mixing, it was still difficult to get the exact prescribed amount.

Table 5.2 Strength of Concrete of Individual Batches

	Batch	Cube 1 (N/mm^2)	Cube 2 (N/mm^2)	Cube3 (N/mm^2)	Split Test (N/mm^2)
Slab 1	1	50.5	49.5	42	3.42
	2	49	46	42	3.66
	3	47	55	48.5	3.9
	4	64	60	49	3.44
Slab 2	1	63	60	52.5	3.73
	2	73.5	71	60	4.5
	3	70.5	71	60.5	4.07
	4	71	56	61	3.76
Slab 3	1	60.5	63.5	58.5	3.71
	2	53.5	52.5	47	3.93
	3	50.5	55.5	48.5	3.27
	4	53.5	55	52	3.65

Slab 4	1	54	50	52.5	3.71
	2	49.5	48.5	51	3.82
	3	46	48	44	3.88
	4	49.5	52.5	53.5	4.2
Slab 5	1	49	47.5	47.5	3.44
	2	64	65.5	61	3.76
	3	59.5	61.5	51	4.35
	4	56.5	66.5	52.5	4.71
Slab 6	1	49	49	49.2	3.73
	2	51.7	54.5	53	3.73
	3	43.5	43	43	3.42
	4	48.3	38	51	3.69
Slab 7	1	37.7	35.8	35.3	2.97
	2	35.6	36.6	34	2.8
	3	37.4	38.5	38	2.89
	4	36	31.2	38	2.5
Slab 8	1	36	31.2	38	2.5
	2	43.5	42	42.7	3.35
	3	27.3	32.7	37	3.14
	4	41	40	40.2	2.89
Slab 9	1	35	37.5	35.8	2.76
	2	33.5	35	31	2.8
	3	37.5	36.5	35	3.01
	4	39.2	43	40	3.18
Slab 10	1	38	36.6	39	3.18
	2	33.5	32	32	2.33
	3	32.5	33	30	2.93
	4	40.5	41	38.5	2.76
Slab 11	1	39.2	43	40	3.18
	2	32	31.5	31.5	2.65
	3	40	44	50	3.4
	4	36.5	40	35.5	2.48
Slab 12	1	40.5	41	38.5	2.76
	2	42	40.3	42.5	3.14
	3	44.3	41	43	3.61
	4	41.2	33.8	39.5	2.61

Table 5.3 Average Concrete Strength of Slabs

Slab No.	Compressive Strength	Tensile Strength	Ten./Comp. Ratio
	(N/mm2)	(N/mm2)	
1	50.2	3.61	0.072
2	64.7	4.02	0.062
3	54.3	3.64	0.067
4	49.6	3.86	0.078
5	56.6	3.97	0.07
6	48	3.64	0.076

7	31.2	2.93	0.094
8	31.2	2.93	0.094
9	37.1	2.9	0.078
10	37.8	2.94	0.078
11	37.1	2.9	0.078
12	37.8	2.94	0.078
Average	44.6	3.36	0.075

5.2.1.2 Reinforcements

Four types of steel were used in the experiments, they were high yield bars T12, mild steel R8 and R6, and wire R4. The mechanical properties of the reinforcements were determined according to the standard EN 100002 Part1[68]. Three samples were taken for each type of the reinforcement. The mechanical properties such as yield strength, percentage elongation, percentage of elongation after fracture etc. are listed in Table 5.4 obtained from the average of the test samples, where the strength have been converted into the values for nominal cross-section area.

Table 5.4 Properties of Reinforced Bars

Nominal Diameter (mm)	Diameter (mm)	Steel Type	Yield Strength (N/mm^2)	Tensile strength	Modules of Elasticity (KN/mm^2)	Percentage of Elongation (%)
12	11.58	deformed	423.0	552.0	227.0	30.1
8	7.80	undeformed	327.0	460.0	206.0	19.3
6	5.93	undeformed	350.0	468.0	204.0	28.3
4	3.72	undeformed	245.0	297.0	181.0	23.3

5.2.2 RESULTS OF R.C. WAFFLE SLAB TESTS

During the tests, a large amount of data were obtained from the series of tests which included the deflections, and strains of the reinforcement for every load increment. Table 5.5 provides a summary of the principal information on the ultimate load carrying capacity for the entire programme of testing.

Table 5.5 Summary of Principal Test Results at Failure Load

Slab No.	Failure Pattern	Failure Load (KN)	Centre Def. (mm)	Def./Depth (%)
1	Punch	187.0	4.0	2.67
2	Punch	165.0	3.1	2.07
3	Punch	172.5	4.6	3.07
4	Punch	198.9	5.2	3.47
5	Punch	332.5	7.0	4.67
6	Punch	283.0	5.0	3.33
7	Punch	271.0	9.5	6.33
8	Punch	202.5	6.4	4.27
9	Punch	272.0	8.3	5.53
10	Punch	227.5	9.0	6.00
11	Punch	362.5	10.8	7.20
12	Punch	272.5	6.3	4.20

5.2.2.1 Experimental Observation

As mentioned earlier, during the test, the load was gradually applied to the slab. The flexural cracks appeared on the tension side of the slab at quite an early stage and developed as the load was increased. But during the later stage of the loading, not many new flexural cracks further developed. Although the reinforcements had some local yielding no flexural yield lines were formed and none of the slabs experienced the distinctive yield stage as experienced in the flexural tests of slabs. Diagonal cracks were noticed before the final failure of the slabs; in some slabs, these cracks were developed quite early. Some of the cracks started from the tension side of the slabs and gradually extended toward the compression side, while, some cracks started right from the middle of the ribs and propagated toward both sides of the slab. It was also interesting to note that the initial diagonal cracks did not necessarily coincide with the final major diagonal cracks, and in many cases the initial diagonal cracks were actually the secondary instead.

During the late stage of loading, it was also noticed that the slabs experienced creep and it was difficult to hold the load. The creep lasted only a couple of minutes and then the slab was going to fail.

The final failure of the slabs was relatively sudden accompanied by an explosion. The major diagonal cracks was formed in an instant, and once the slab was punched through, the load dropped abruptly; the slab still could carry some load due to the resistance of reinforcements, the remaining load was about half of the peak load.

5.2.2.2 Failure Modes

During the tests all the slabs failed by punching, which was characterised by its suddenness and the sound of mild explosion. A volume of concrete, in the shape of an over-turned pyramid around the loading pad was punched away from the slab, resulting in a recess on the loading side of the slab. The perimeter at the bottom of the pyramid (inner perimeter) mostly coincided with the perimeter of the loading pad; the exception was slabs No. 5 & 11 which had the inner perimeter located at the arm of the local solid area. Fig. 5.11(a) to 5.11(l) show the failure pattern of the slabs. On the opposite surface of the loading side the original flat surface of the slab became slightly curved and the tips of the crack (i.e., the intersection of diagonal cracks with the opposite side of the slab) formed the outer perimeter of the over-turned pyramid, which was basically circular and shared the centre with the loading pad. The outer perimeter of the pyramid lay either inside the slab or reached the edge of slab.

Table 5.6 lists the dimensions of the inner and outer perimeters (on the loading surface of the slab and its opposite side respectively) of the pyramid which was punched away. The dimension of the outer perimeter of the pyramid was measured from the crack tips on the surface of the slab; another set of this parameter was also measured, which was measured from the level of the flexural reinforcements, i.e., at the level of the effective depth instead of the total depth, the values are listed inside the bracket in Table 5.6. The inner perimeter of the punching pyramid coincided with the perimeter of the loading pad except slabs No.5 & 11.

The major cracks cut across the ribs in both the orthogonal direction and also though the local solid areas if available; apart from the major cracks, there were also many secondary diagonal cracks on the ribs. The major diagonal cracks split the ribs into two parts and these major diagonal cracks in different ribs usually met each other and formed a curved spatial surface, which was the surface of the pyramid. The crack-surface inside a rib was usually skewed to the longitudinal axis of the rib, which indicated the effect of the torsion on the ribs. In slabs No.2, 4, 8 and 10 which had no local solid area, the major cracks had extended to a far distance away from the loading

pad and the crack orientation varied more smoothly; the cracks became almost horizontal once they reached the level of the flexural reinforcements. In other slabs with local solid area, the cracks also had extended to a far distance quite away from the loading pad but with the cracks changing orientation abruptly; the cracks were flat inside the solid area and changed to a steep orientation once they reached the ribs; again, the cracks orientation changed to almost horizontal once they reached the level of the flexural reinforcements. In almost all of the slabs, the cracks on the part of the rib near to the loading pad or the local solid area were steep; the inclination of this part of the crack was measured and represented by an angle α in relative to the vertical plan; the angles are listed in Table 5.6. In Table 5.6, the average inclination of the diagonal crack is also listed by employing the parameter $\overline{\alpha}$ which is defined by

$$\tan\overline{\alpha} = \frac{(d_1 - d)}{2h}.$$

Table 5.6 Dimension of the Punched Away Pyramid

Slab No.	outer perimeter d_1 (mm)	inner perimeter d (mm)	crack angle α (°)	$\tan\overline{\alpha} = \frac{(d_1 - d)}{2h}$
1	740 (640)	150	30~50	1.97 (1.63)
2	760 (580)	150	45~60	2.03 (1.43)
3	800 (620)	150	40~50	2.17 (1.57)
4	850 (590)	150	40~70	2.33 (1.47)
5	1100 (1000)	340	45~70	2.53 (2.20)
6	900 (810)	150	40~50	2.50 (2.20)
7	1250 (540)	150	40~70	3.67 1.30)
8	900 (500)	150	35~50	2.50 (1.17)
9	1000 (540)	150	40~55	2.83 (1.30)
10	640 (500)	150	40~60	1.63 (1.17)
11	1100 (900)	340	45~55	2.53 (1.87)
12	1060 (810)	150	45~70	3.03 (2.20)

Note: values inside brackets were obtained by measuring the crack dimension at the level of the effective depth.

Fig. 5.11 (a) Crack pattern after punching failure — slab No.1

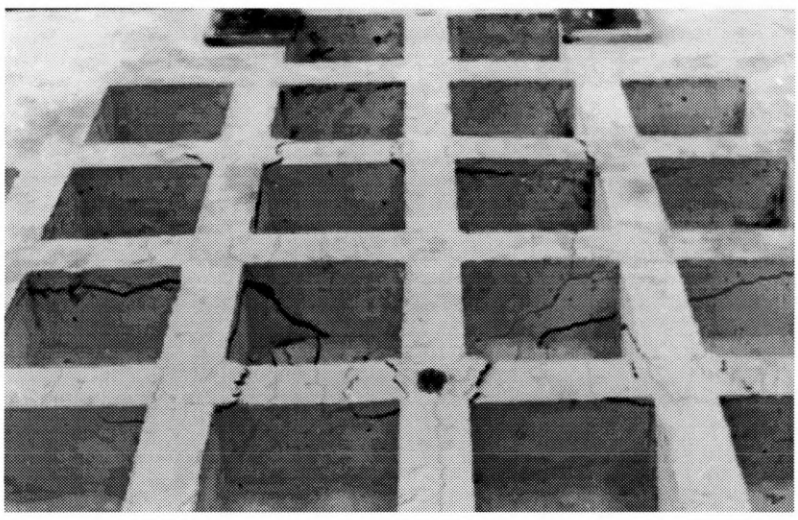

Fig. 5.11 (b) Crack pattern after punching failure — slab No.2

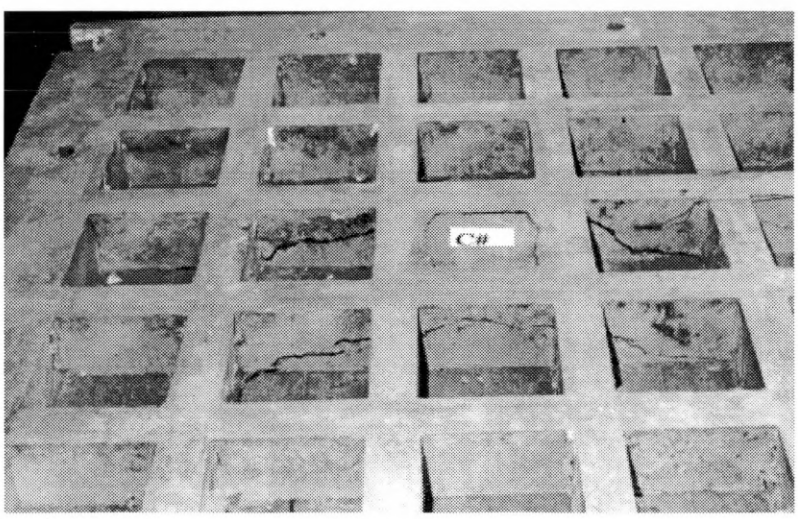

Fig. 5.11 (c) Crack pattern after punching failure — slab No. 3

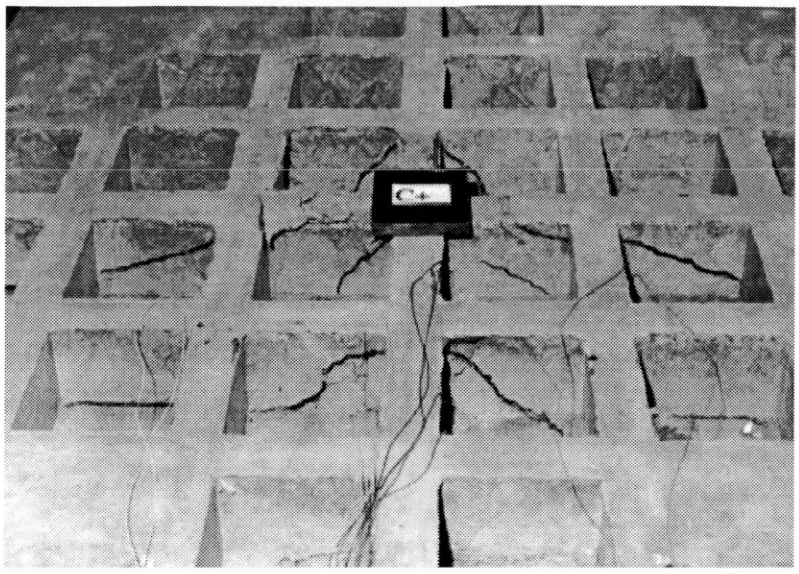

Fig. 5.11 (d) Crack pattern after punching failure — slab No. 4

Fig. 5.11 (e) Crack pattern after punching failure — slab No. 5

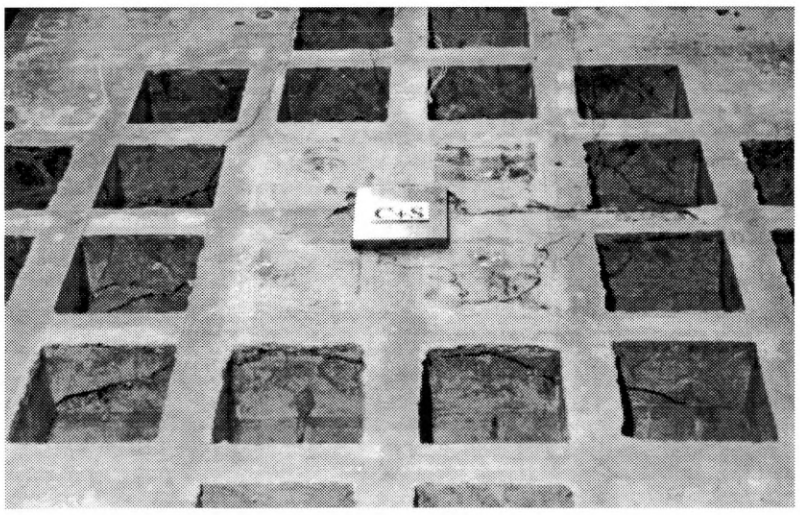

Fig. 5.11 (f) Crack pattern after punching failure — slab No. 6

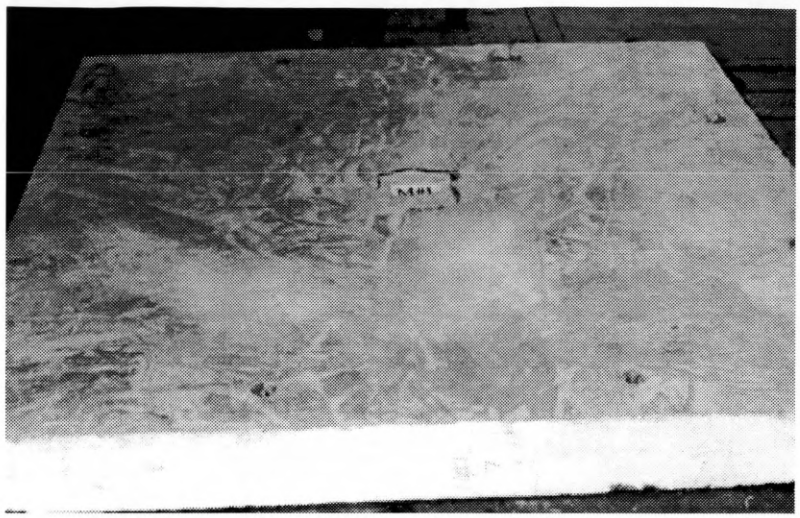

Fig. 5.11 (g) Crack pattern after punching failure — slab No. 7

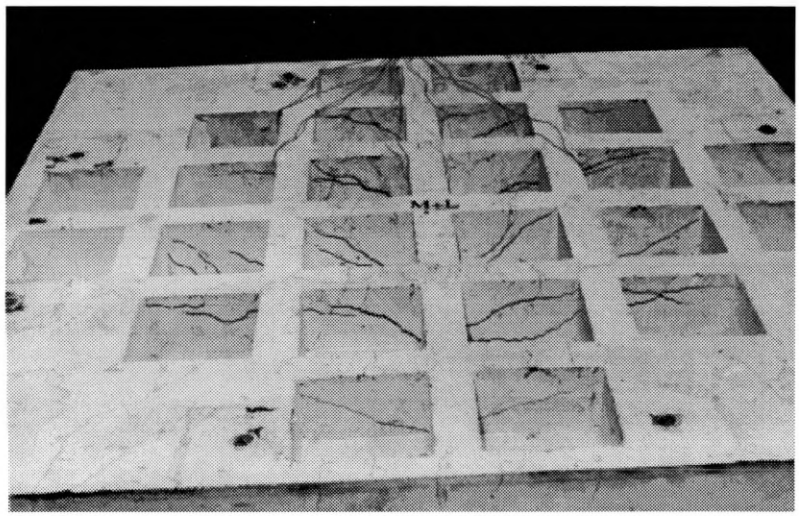

Fig. 5.11 (h) Crack pattern after punching failure — slab No. 8

Fig. 5.11 (i) Crack pattern after punching failure — slab No. 9

Fig. 5.11 (j) Crack pattern after punching failure — slab No. 10

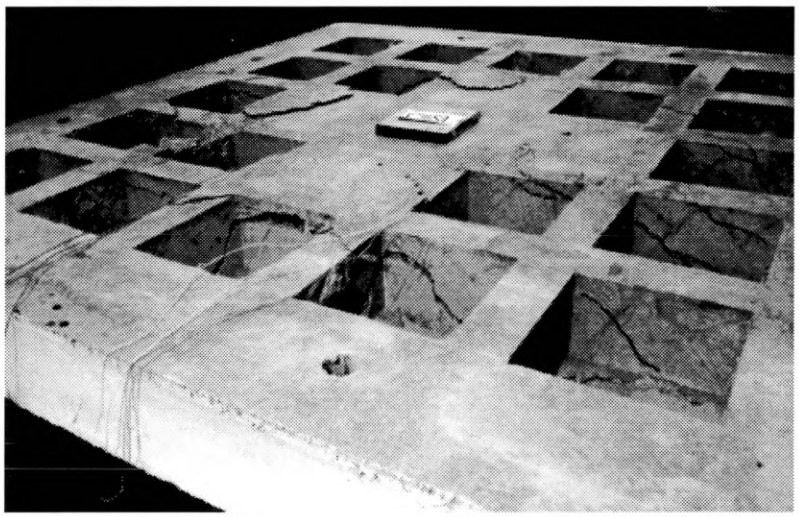

Fig. 5.11 (k) Crack pattern after punching failure — slab No. 11

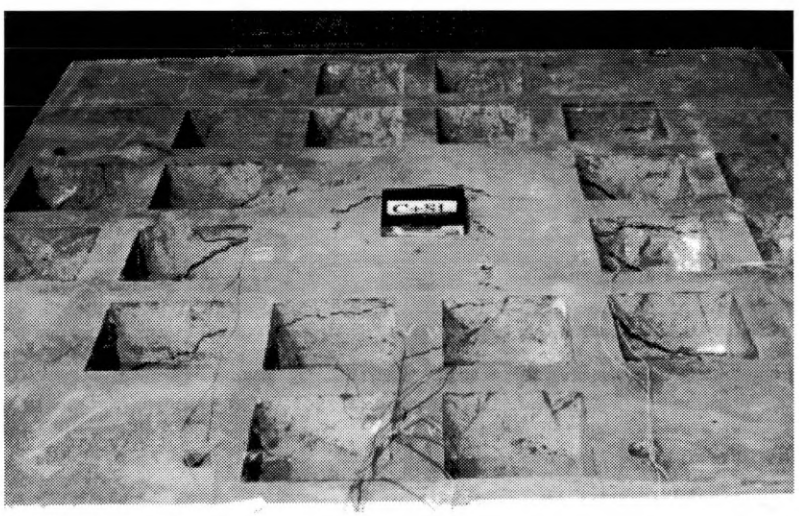

Fig. 5.11 (l) Crack pattern after punching failure — slab No. 12

5.2.2.3 Failure Loads and Diagonal Crack Loads

The failure load, the load at which the first diagonally crack was observed and the corresponding central deflections of the slabs, are listed in Table 5.7. From the table it is seen that the load reached about half of the ultimate failure load then the diagonal cracks were observed.

Table 5.7 Load at the appearance of first diagonal crack

Slab No.	Final Failure Load (KN)	Centre Def. at Failure Load (mm)	Diagonal Cracking Load (KN)	Centre Def. at diag. crack (mm)	crack-load to failure load	crack-def. to failure def.
	(1)	(2)	(3)	(4)	(3)/(1)	(4)/(2)
1	187.0	4.0	107	1.33	0.57	0.33
2	165.0	3.1	100	1.33	0.61	0.43
3	172.5	4.6	93	1.06	0.54	0.23
4	198.9	5.2	130	2.82	0.65	0.54
5	332.5	7.0	240	4.00	0.72	0.57
6	283.0	5.0	180	2.14	0.64	0.43
7	271.0	9.5	150	1.17	0.55	0.12
8	202.5	6.4	120	2.02	0.59	0.32
9	272.0	8.3	200	5.88	0.74	0.71
10	227.5	9.0	130	3.09	0.57	0.34
11	362.5	10.8	220	4.95	0.61	0.46
12	272.5	6.3	190	3.04	0.70	0.48

In the design of the test programme, as mentioned before, the intention was to compare the difference in the load capacity of slabs due to the variation of the configuration, influence of the local solid area on the punching load, loading position and location, loading directions, and the change of load capacity by the use of stirrups. In the following, these issues will be discussed.

1. **Influence of loading direction on the punching load**

   Slabs 1 and 3 have same type of configuration but the actual loading directions are opposite. On slab No. 1 the load was supplied on the slab face close to the

deck, this was to simulate the punching shear in the middle of a slab panel; slab No. 3 was loaded on the slab face with recesses simulating the punching shear in the vicinity of the slab-column connection area. These two slabs make a comparable pair. Among all the other slabs, slab 2 and 4 make a comparable pair, so does slab 7 with slab 9, and slab 8 with slab 10. Table 5.8 lists the ratio of the punching load between each pair of slabs.

Table 5.8 Load ratio between slabs with opposite loading direction

	slab3/slab1	slab4/slab2	slab9/slab7	slab10/slab8
load ratio	0.95	1.21	1.00	1.12

From the above table, it is seen that the load ratio between each pair of slab is quite close to 1.0, this means that the load capacity is not affected by the loading direction.

2. Influence of the configuration type on the load capacity

The difference between slab No. 1 and 2 is the configuration type, slab 1 has the '#' type and slab 2 has the '+' type, these two slabs make a comparable pair. Similarly, slab 3 with slab 4, slab 7 with slab 8, and slab 9 with slab 10 make the comparable pairs as far as the configuration type is concerned. The load ratio between them are listed in table 5.9.

Table 5.9 Load ratio between slabs with '#' and '+' type of configurations

	slab2/slab1	slab4/slab3	slab8/slab7	slab10/slab9
load ratio	0.88	1.15	0.75	0.84

From the above table, it is seen that, except the pair of slab 3 with slab 4, loads of slab with '+' type of configuration are smaller than those with the '#' type of configuration; the maximum difference is 25%. Keeping in mind that there is a local solid area near the loading pad for slabs of the '#' type configuration, as shown in Fig. 5.2a, the local solid area has increased the load capacity for this type of slabs. If the local solid area is removed (the punching failure in the deck itself is assumed not to occur as our interest here is to see the punching across a larger area, not on the local failure inside a recess) the load capacity of slabs with

'#' configuration will be reduced, therefore the difference between these two types of slabs should be much smaller.

The above two types of slab configuration was actually to simulate the two extreme cases when the loading pad (or the concentrated load) changes locations on the slab, this is shown in Fig.5.12. A rectangular area ABCD covering four recesses, see Fig.5.12, is the most representative area in the sense that any loading position on the slab can be represented by a position inside this area. Inside area ABCD, it is seen that the loading positions marked by '+' and '#' are the two limit cases, and any other loading position, e.g., position *N*, should get a punching load between these two extreme cases' results. As mentioned before from the analysis of the test results, the punching load associated with the two extreme cases have no big differences, therefore the conclusion can be drawn that the punching load is rather insensitive to the loading position on the waffle slabs provided that the loading pad is big enough to avoid local failure inside the deck.

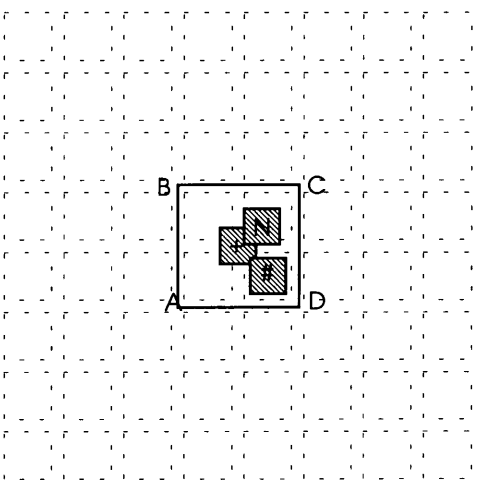

Fig.5.12 Possible load position on a waffle slab

3. Influence of the Local Solid Area

In slabs No. 5 & 6 and slabs No. 11 & 12, large local solid areas were provided to enhance the punching shear capacity. Slabs 11 & 12 were supplied with R4 stirrups and slabs No. 7~10 were supplied with R6 stirrups, so difference in stirrups would involve other factors; here they are still compared with slabs No.7~10 as slabs No.11 & 12 were provided with less steel.

Table 5.10 Load ratio between slabs with and without local solid area

	slab5/slab1	slab5/slab3	*slab6*/*slab2*	slab6/slab4	slab11/slab7	slab11/slab9	slab12/slab8	slab12/slab10
load ratio	1.78	1.93	1.72	1.42	1.34	1.33	1.34	1.20

From the above table it is seen that the local solid area is very effective in increasing the punching capacity. In slabs without stirrups, the increase is about 42~93%; in slabs with stirrups, the increase is about 20~34%, which is less than previous one because slabs No.7~9 have more stirrups than slab No. 11 & 12.

4. Load increase by stirrups

The load ratio between slabs with and without stirrups are listed in Table 5.11.

Table 5.11 Load ratio between slabs with and without Stirrups

	slab7/slab1	slab8/slab2	slab9/slab3	slab10/slab4	slab11/slab5	slab12/slab6
load ratio	1.45	1.23	1.58	1.14	1.09	0.96

From the table, it is seen that the maximum load increment is 58%. The load increase in slabs 11 and 12 is small due to the small amount of steel provided.

5.2.2.4 Deflection of Slabs

Five transducers (LVDT) were used to record the deflection along the centre profile of the slabs. The location of the LVDT on the slabs are shown in Fig.5.13a & b.

As the slabs deflected under the upward loading of the jack, only relative displacement of traducer readings against the supporting points were of interest, traducers 1 and 5 were actually measuring the movement of the support. Fig.5.14(a)~(l) show the load-deflection curves of the central three transducers.

Table 5.12 lists the deflections at the ultimate failure load. It is seen that the deflection of the slabs are very small, the maximum deflection, occurred in slab No. 11, among these slabs is only 10.8mm being equivalent to 7.2% of the slab depth. For slabs with stirrups, the deflection is almost doubled compared with slabs with out stirrups.

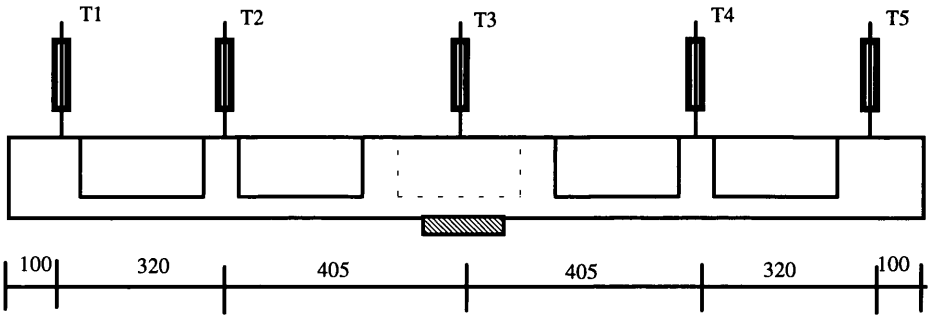

Fig. 5.13a Position of the transducers (LVDT) on slabs No. 1, 3, 5, 7, 9, 11

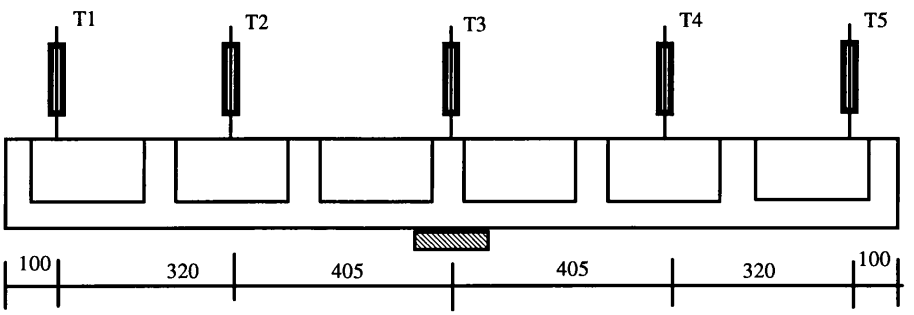

Fig. 5.13b Position of the transducers (LVDT) on slabs No. 2, 4, 6, 8, 10, 12

Table 5.12 Central deflection of slab at ultimate load

Slab No.	Failure Load (KN)	Centre Def. (mm)	Def./Depth (%)
1	187.0	4.0	2.67
2	165.0	3.1	2.07
3	172.5	4.6	3.07
4	198.9	5.2	3.47
5	332.5	7.0	4.67
6	283.0	5.0	3.33
7	271.0	9.5	6.33
8	202.5	6.4	4.27
9	272.0	8.3	5.53
10	227.5	9.0	6.00
11	362.5	10.8	7.20
12	272.5	6.3	4.20

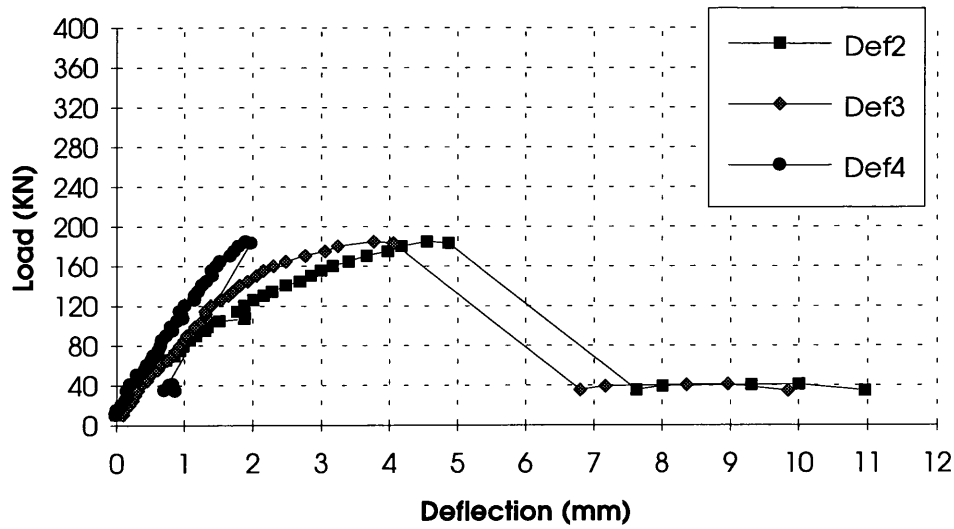

Figure 5.14(a) Load-Deflection Curves of Slab No. 1

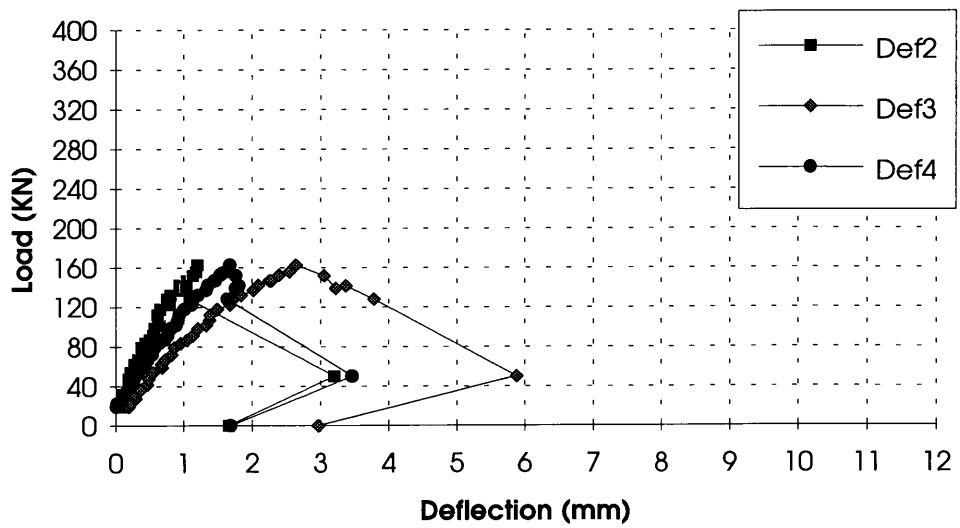

Figure 5.14(b) Load-Deflection Curves of Slab No. 2

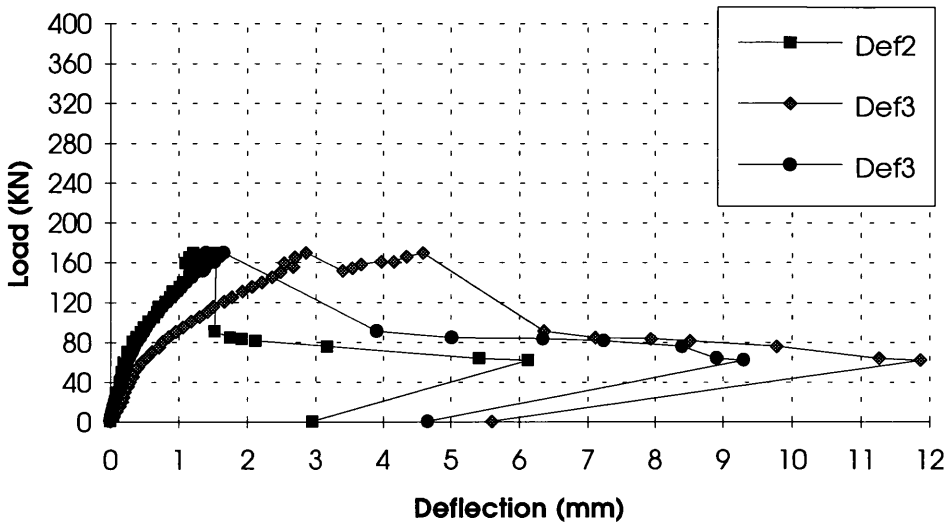

Figure 5.14(c) Load-Deflection Curves of Slab No. 3

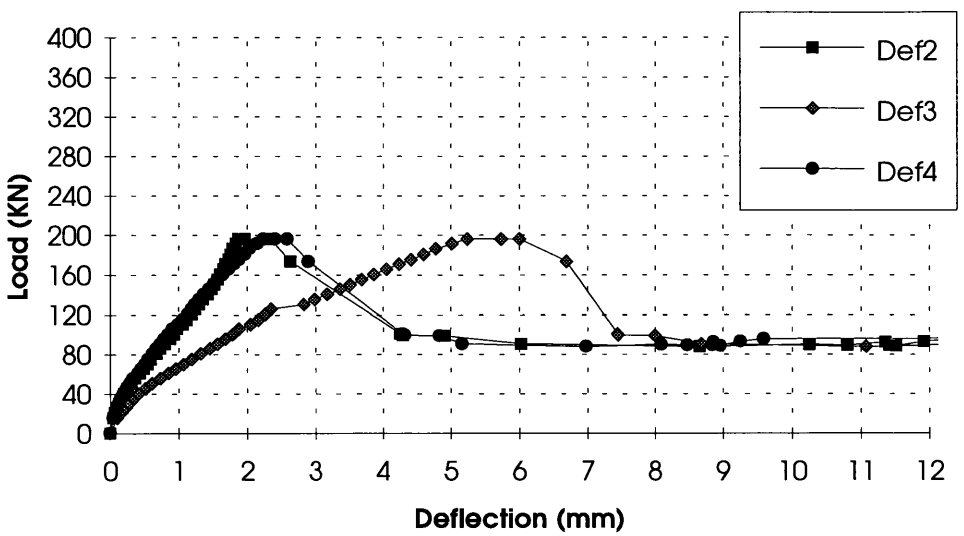

Figure 5.14(d) Load-Deflection Curves of Slab No. 4

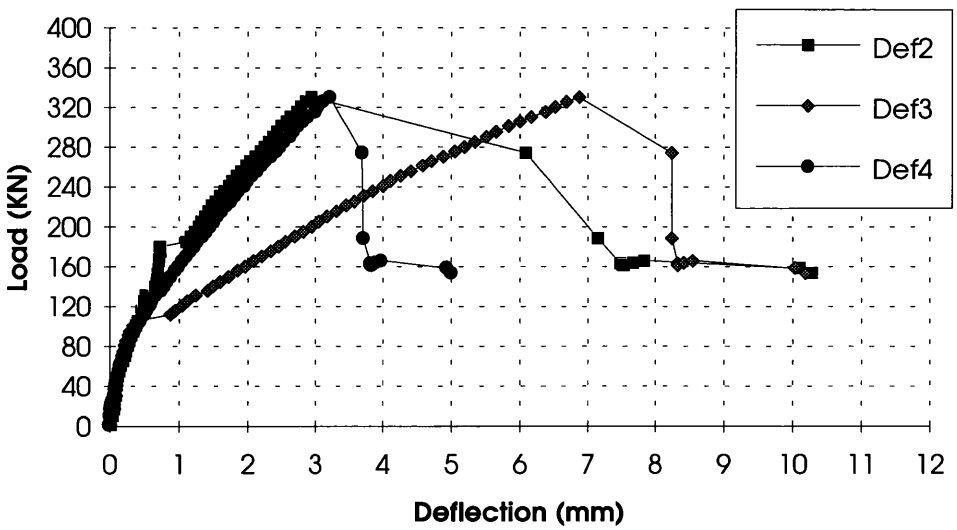

Figure 5.14(e) Load-Deflection Curves of Slab No. 5

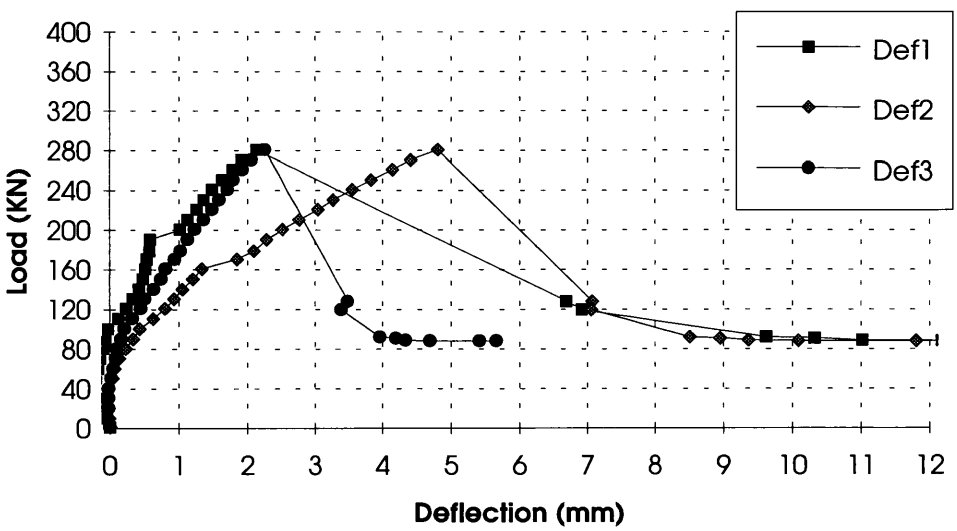

Figure 5.14(f) Load-Deflection Curves of Slab No. 6

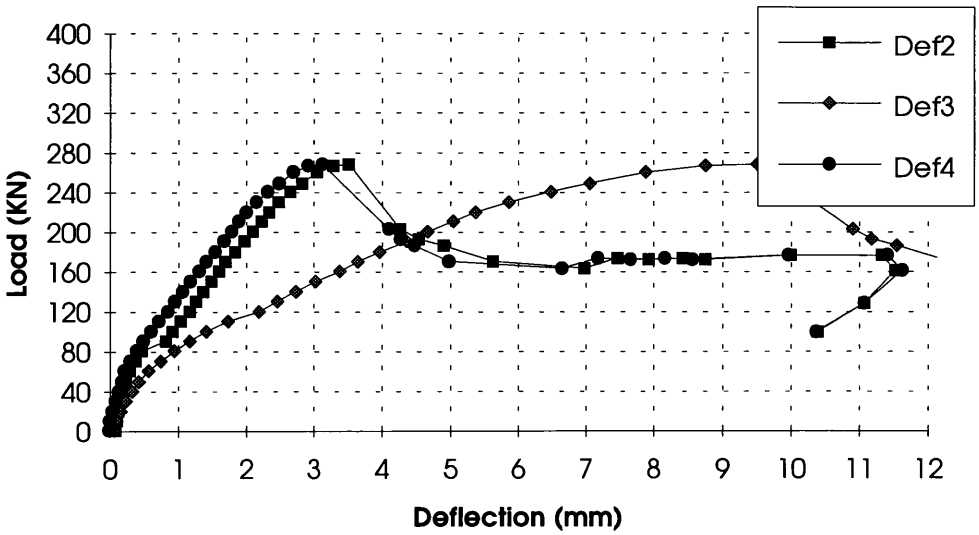

Figure 5.14(g) Load-Deflection Curves of Slab No. 7

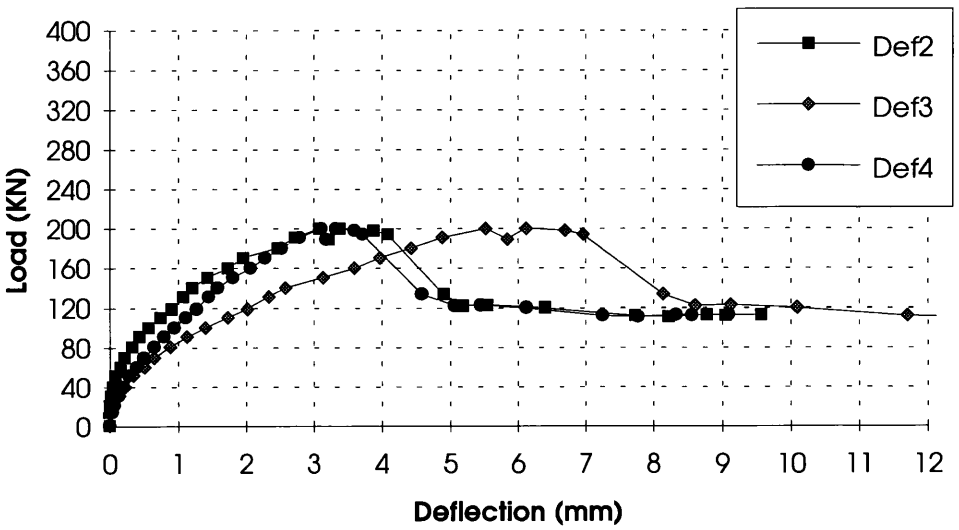

Figure 5.14(h) Load-Deflection Curves of Slab No. 8

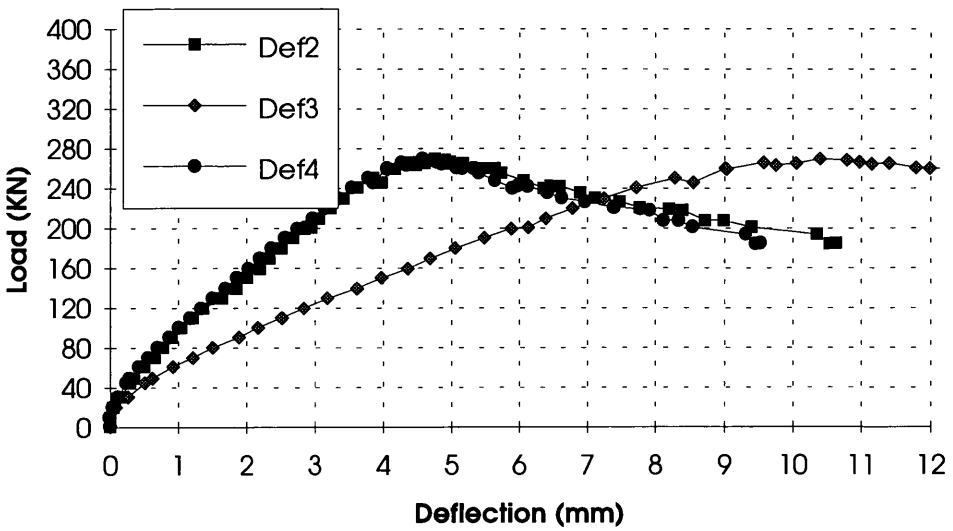

Figure 5.14(i) Load-Deflection Curves of Slab No. 9

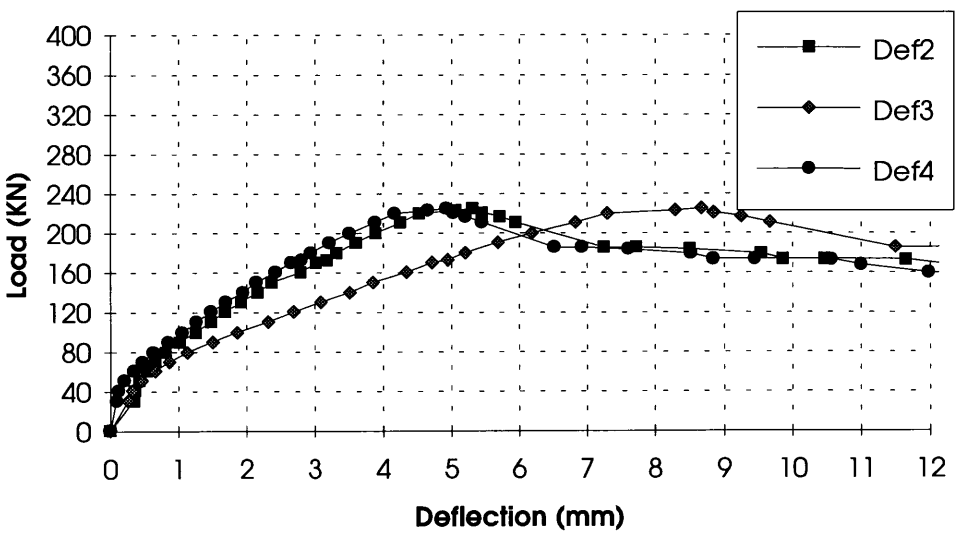

Figure 5.14(j) Load-Deflection Curves of Slab No. 10

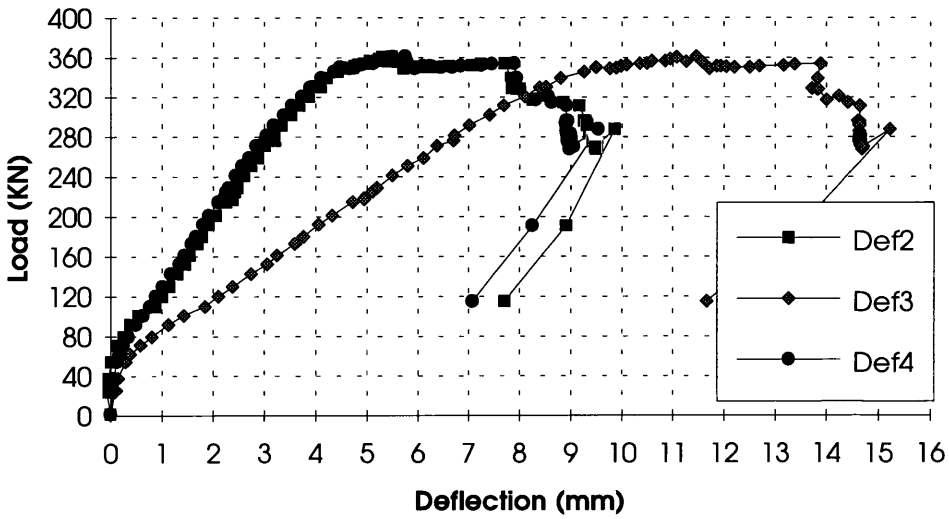

Figure 5.14(k) Load-Deflection Curves of Slab No. 11

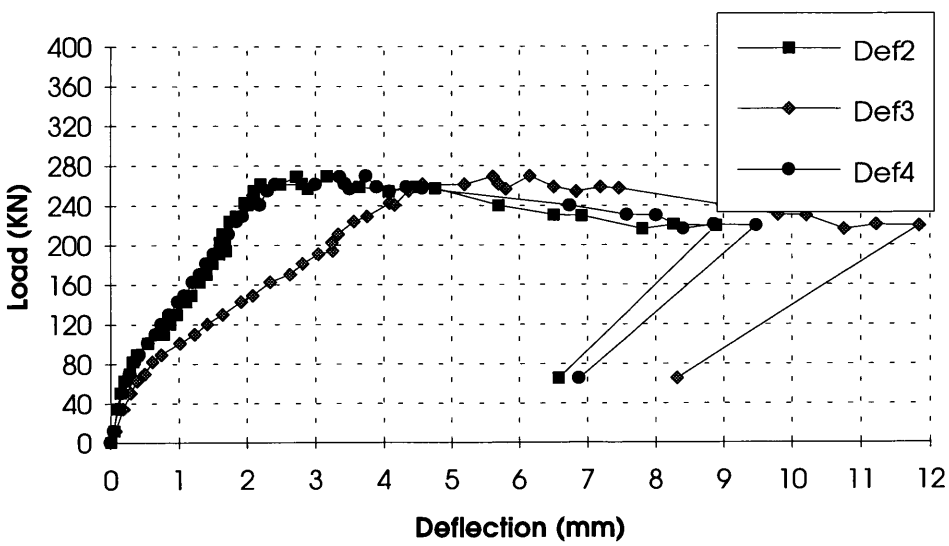

Figure 5.14(l) Load-Deflection Curves of Slab No. 12

5.3 CONCLUSIONS

In this chapter, the design of the test programme was described and followed by the presentation of the test results and discussion.

Twelve waffle slabs (1/3 scale model) with various configuration and steel reinforcement were tested to failure under concentrated load; the load capacity, failure pattern, deflection etc. were recorded.

The conclusion can be summarised as below.

1. Like the punching shear failure inside solid slabs, the failure inside waffle slabs were also sudden accompanied by a drop of the load; slabs underwent very small deflections before the failure took place, the largest deflection among slabs with stirrups was 7.2% of the slab depth and the largest among slabs without stirrups was only 4.7% of the slab depth;

2. The punching failure pattern in waffle slabs was different from that of a solid slab in the sense that the cracks changed orientation abruptly; on the ribs, the cracks consisted of two segments, the one near the load pad was steep, and the second segment was almost horizontal; in slabs with solid area, the cracks cut through the solid area and were flat inside the solid area. The steep inclination of the crack near the loading pad or the local solid area indicated a smaller effective punching dimension in waffle slabs.

3. The loading position and the loading direction did not make a significant change in the shear capacity. The existence of large solid area increased the load capacity substantially, the shear links also did the work but not as effective as local solid area.

4. The punching load were dissipated to an enlarged area instead confining to the local area near the loading pad; the ribs both parallel and perpendicular to the edge of the slab participated in the shear resistance.

CHAPTER 6

THEORETICAL ANALYSIS EMPLOYED AND RESULTS

6.1 INTRODUCTION

Concrete exhibits brittle fracture characteristic under tension and non-linear and plastic characteristics under compression. Before the appearance of cracks, concrete can be considered as a uniform material with isotropic response, while, after cracks have developed, concrete exhibits anisotropic behaviour.

The methods of analysis applied to concrete structures have coincided with the understanding and development of the theories of fracture and plasticity, and also depended on the type of structure under consideration. Each method has its advantages and short comings.

Limit analysis applied at the ultimate state can provide two types of solution, one is the Upper Bound Solution (UBS) which gives an ultimate failure load; the other is the Lower Bound Solution (LBS) which gives a safe limit load. These solutions are simple to apply, good to predict the ultimate load, but can not give the deflection at failure.

Finite Element Analysis (FEA) on the other hand can provide a total solution, failure load can deflection. While the FEA is versatile in terms of application to structures with isotropic materials, its application to reinforced concrete is frangible with many difficulties mainly caused by the lack of precise modelling of the material, its fracture, crushing and yielding criteria under a 3-D stress condition.

In engineering practice, engineers are in favour of simplified methods, which are clear in concept and easy to handle. In the codes of practice of many countries these simplified methods are mainly based on the method of rational analysis, the main design factors being determined by using experimental data. Although the simplified methods do not have comprehensive theoretical understanding, they are by no means inferior. For some complicated problems these methods yield better results than some advanced analytical methods.

In this chapter, the Upper Bound Analysis, FEA and simplified methods are employed for the analysis and the results are compared with those obtained using provisions of BS8110 for RC waffle slabs. The objective is to ascertain whether the provisions of

BS8110 can fairly predict the shear load capacity of RC waffle slabs, and if not, then to develop an alternative method.

6.2 UPPER BOUND ANALYSIS

In chapter 3, the analysis model and the yield criteria employed for concrete were described and the formulae for the ultimate load were derived. These formulae are suitable for slabs with recesses distributed thoroughly, but the slabs in this programme have some local solid area and therefore the formulae have to be modified.

6.2.1 ANALYSIS FORMULA FOR SLABS WITH LOCAL SOLID AREA

1. RC waffle slabs with the deck in the compression side — deck-top case

In a waffle slab with local solid area, the dimensions of the solid area are shown in Fig.6.1. S is the distance from the centre of the loading pad to the edge of the central solid area, shown by the shaded area; B is the distance from the centre to the edge of the arm of the solid area; $\overline{h}$ is the depth of the deck; h_s the distance from the top of the slab to the intersection between the edge of the central area of the local solid area and the failure surface; h_b is the distance from the top of the slab to the intersection between the edge of the arm of the solid area and the failure surface.

Similarly, following the procedures in chapter 3, the loading corresponding to a failure surface can be expressed as

$$P = 4 f_t' \left[\begin{array}{l} \int_0^{\overline{h}} \left(d + \frac{\pi}{2} t \right) \left(t' + \frac{K}{t'} \right) dz - \rho_{xy} \int_{\overline{h}}^{h} \left(d + \frac{\pi}{2} t \right) \left(t' + \frac{K}{t'} \right) dz \\ + \rho_{xy} \int_{\overline{h}}^{h_s} \left(d + \frac{\pi}{2} t \right) \left(t' + \frac{K}{t'} \right) dz + \rho_{xy} \int_{h_s}^{h_b} b \left(t' + \frac{K}{t'} \right) dz \end{array} \right] \quad (6.1)$$

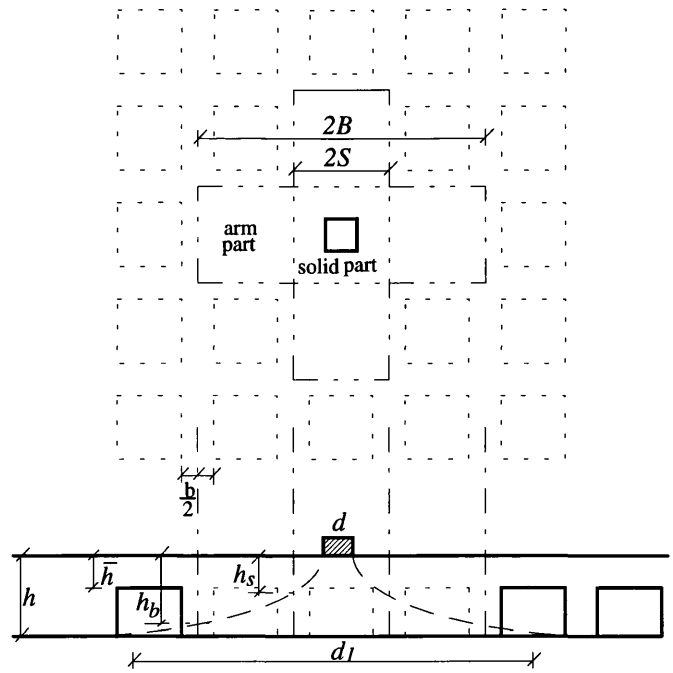

Fig.6.1 RC waffle slabs with local solid area

In Eq.6.1 the third term on the right hand side represents the contribution by the central part of the solid area; the forth term represents the contribution of the arm of the local solid area.

Using the variation of calculus, solution to Eq.6.1 is obtained as

$$P = 4f_t'\left\{\begin{aligned}&\left[\frac{d^2}{\pi}\left(\left(\frac{\pi}{4}\frac{d_1-d}{d}+1\right)^2-1\right)+\frac{\pi kh^2}{2\ln\left(\frac{\pi}{4}\frac{d_1-d}{d}+1\right)}\right]-\rho_{xy}\left[\frac{d^2}{\pi}\left(\left(\frac{\pi}{4}\frac{d_1-d}{d}+1\right)^2-\left(\frac{\pi}{4}\frac{d_1-d}{d}+1\right)^{\frac{2\bar{h}}{h}}\right)+\frac{\pi kh(h-\bar{h})}{2\ln\left(\frac{\pi}{4}\frac{d_1-d}{d}+1\right)}\right]\\&+\rho_{xy}\left[\frac{d^2}{\pi}\left(\left(\frac{\pi}{4}\frac{d_1-d}{d}+1\right)^{\frac{2h_s}{h}}-\left(\frac{\pi}{4}\frac{d_1-d}{d}+1\right)^{\frac{2\bar{h}}{h}}\right)+\frac{\pi kh(h_s-\bar{h})}{2\ln\left(\frac{\pi}{4}\frac{d_1-d}{d}+1\right)}\right]\\&+\rho_{xy}\left[\frac{2db}{\pi}\left(\left(\frac{\pi}{4}\frac{d_1-d}{d}+1\right)^{\frac{h_b}{h}}-\left(\frac{\pi}{4}\frac{d_1-d}{d}+1\right)^{\frac{h_s}{h}}\right)-\frac{\pi kh^2b}{2d\ln^2\left(\frac{\pi}{4}\frac{d_1-d}{d}+1\right)}\left(\left(\frac{\pi}{4}\frac{d_1-d}{d}+1\right)^{-\frac{h_b}{h}}-\left(\frac{\pi}{4}\frac{d_1-d}{d}+1\right)^{-\frac{h_s}{h}}\right)\right]\end{aligned}\right\} \tag{6.2}$$

The above formula will give variation of load P for different values of punching diameter d_1, the minimum one being the expected punching failure load.

2. RC waffle slabs with the deck on the tension side — deck-bottom case

When the deck is on the tension side of the slab, the geometric parameters are illustrated in Fig.6.2.

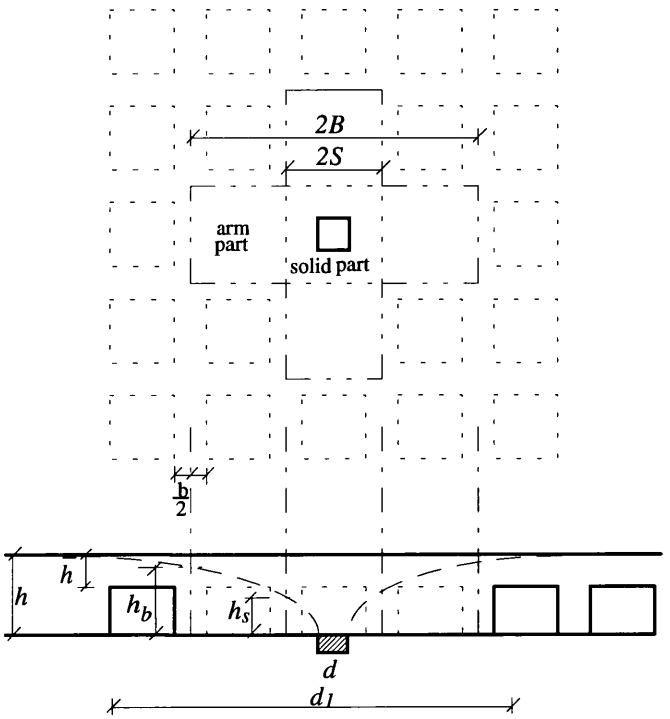

Fig.6.2 RC waffle slab with the deck on the tension side

Then as before, the equation for the punching load is

$$P = 4 f_t' \left[\begin{array}{l} \int_0^{h} \left(d + \frac{\pi}{2} t \right) \left(t' + \frac{K}{t'} \right) dz - \rho_{xy} \int_0^{h-\bar{h}} \left(d + \frac{\pi}{2} t \right) \left(t' + \frac{K}{t'} \right) dz \\ + \rho_{xy} \int_0^{h_s} \left(d + \frac{\pi}{2} t \right) \left(t' + \frac{K}{t'} \right) dz + \rho_{xy} \int_{h_s}^{h_b} b \left(t' + \frac{K}{t'} \right) dz \end{array} \right] \quad (6.3)$$

The solution to Eq.6.3 is

$$P = 4f_t' \left\{ \begin{aligned} &\left[\frac{d^2}{\pi}\left(\left(\frac{\pi}{4}\frac{d_1-d}{d}+1\right)^2-1\right)+\frac{\pi k h^2}{2\ln\left(\frac{\pi}{4}\frac{d_1-d}{d}+1\right)} \right]-\rho_{xy}\left[\frac{d^2}{\pi}\left(\left(\frac{\pi}{4}\frac{d_1-d}{d}+1\right)^2-1\right)+\frac{\pi k h^2}{2\ln\left(\frac{\pi}{4}\frac{d_1-d}{d}+1\right)} \right] \\ &+\rho_{xy}\left[\frac{d^2}{\pi}\left(\left(\frac{\pi}{4}\frac{d_1-d}{d}+1\right)^{\frac{2(h-\bar{h})}{h}}-1\right)+\frac{\pi k h(h-\bar{h})}{2\ln\left(\frac{\pi}{4}\frac{d_1-d}{d}+1\right)} \right] \\ &+\rho_{xy}\left[\frac{2db}{\pi}\left(\left(\frac{\pi}{4}\frac{d_1-d}{d}+1\right)^{\frac{h_b}{h}}-\left(\frac{\pi}{4}\frac{d_1-d}{d}+1\right)^{\frac{h_b}{h}}\right)-\frac{\pi k h^2 b}{2d\ln^2\left(\frac{\pi}{4}\frac{d_1-d}{d}+1\right)}\left(\left(\frac{\pi}{4}\frac{d_1-d}{d}+1\right)^{-\frac{h_b}{h}}-\left(\frac{\pi}{4}\frac{d_1-d}{d}+1\right)^{-\frac{h_b}{h}}\right) \right] \end{aligned} \right\} \tag{6.4}$$

6.2.2 ANALYTICAL PROCEDURE FOR UPPER BOUND METHOD

In the upper bound analysis it is necessary to find the lowest solution to the problem. For a solid slab or a waffle slab without local solid area, an explicit solution can be found; but if there are local solid area in the slab, the explicit solution is not straight forward, the lowest solution having to be found by using computer.

By using computer, a series of punching diameters, d_{1i}, are assumed, then their corresponding punching load, P_i, are compared, from which the lowest value is obtained as P and d_1, as shown in Fig.6.3.

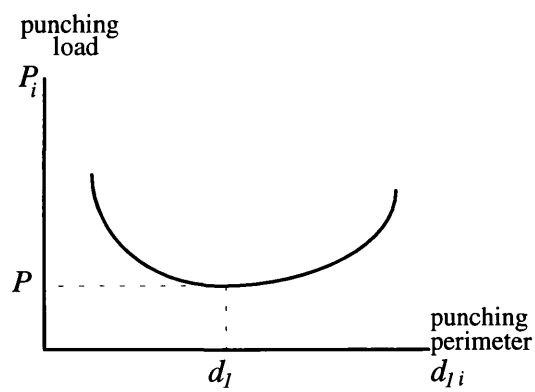

Fig. 6.3 Variation of Punching Load vs. Punching Diameter

The procedures to find the solution are illustrated below:

(i) assume an initial punching diameter, d_{1i}

(ii) compute the values of the parameter C_1 for the equation governing the failure surface,

$$x = \frac{d}{2} + \frac{2d}{\pi}\left(e^{c_1 z} - 1\right) \tag{6.5}$$

$$C_1 = \frac{1}{h}\ln\left(\frac{\pi}{4}\frac{d_{1i} - d}{d} + 1\right) \tag{6.6}$$

(iii) compute the values of h_s, h_b by Eq.(6.5) & (6.6),

(iv) using Eq.6.2 & 6.4 to obtain the load P_i,

(v) ascertain if the minimum P has been achieved; if not increase the punching diameter and go to step 1; once the minimum P has been obtained then stop the cycle.

A computer program, UPBOUND.FOR, in FORTRAN, was written to implement the above analysis.

6.2.3 GEOMETRIC & MATERIAL PARAMETERS OF THE MODEL SLABS

In the analysis, the input parameters included the geometric parameters which define the dimensions of the slab, the recesses, the solid area etc.; the material parameters are the strength of concrete, effective strength, etc. In this section, the parameters for all the twelve model slabs tested are listed and explained.

1. Geometric Parameters of the Model Slabs

(i) Void Ratio of the slab

As defined in Chapter 3, the void ratio is used to measure the plane area ratio between the recesses and the solid part. For the model slabs tested in this study, the width of the rib is 70mm, and the centre to centre distance between the ribs is 270mm, as shown in Fig.6.4.

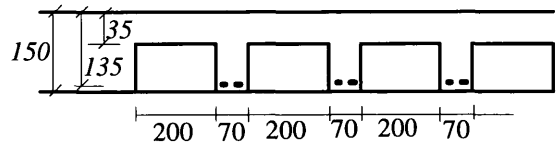

Fig.6.4 Dimensions of the RC waffle slabs

Then using Eq.3.42 and 3.43, we have

$$\rho_x = \rho_y = \frac{200}{270} = 0.7407$$

$$\rho_{xy} = \rho_x \cdot \rho_y = 0.5487$$

(ii) Depth of Slab

As shown in Fig.6.4,

the depth of the slab h=150mm

the depth of the deck $\overline{h} = 35\text{mm}$

effective depth $h_d = 135mm$

(iii) Dimensions of Local Solid Area

The local solid area can be considered as consisting of two parts, as shown in Fig.6.5, the central solid part shown by the shaded area, and the solid arm shown by the dotted area.

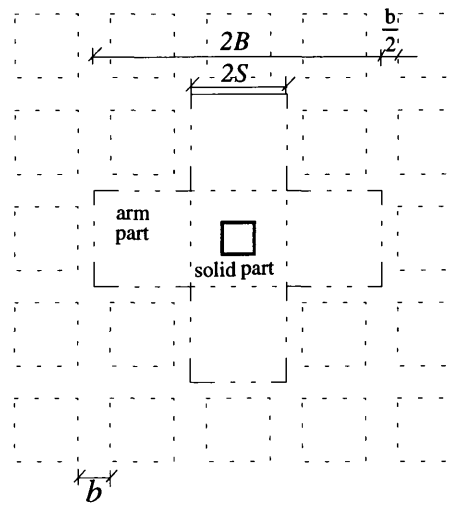

Fig. 6.5 Local Solid Area inside the Waffle Slabs

In Fig.6.5, it is seen that the boundaries surrounding the central part or the arm of the local solid area lie on the centre line of the ribs instead of the edge; this is because half of the ribs has already been included in the waffle slab part when calculating the void ratio of the waffle slab. Therefore, it has to be noted that the dimensions of the central part or the arm of the solid area should be half ribs toward the central of the loading pad.

As shown in Fig.6.5, S is the dimension of the central part of the solid slab, B is dimension of the arm of the local solid area. For all the twelve model slabs tested in this study, as shown in Fig.5.2(a)~(l), the dimensions of the local solid area are listed below.

Table 6.1 Dimensions of Local Solid Area

Slab	1	2	3	4	5	6	7	8	9	10	11	12
S	270	0	270	0	270	540	270	0	270	0	270	540
B	0	0	0	0	910	540	0	0	0	0	910	540

2. Material Parameters of the Model Slabs

In the upper bound analysis, as described in chapter 3, the effective (plastic) strength of concrete are used for the analysis; these are:

f_t' effective tensile strength of concrete,
f_c' effective compressive strength.

The effective strengths are the results of the assumption of perfect plasticity, and these can not be determined by experiments on test cubes or cylinders. These two parameters are a function of the compressive and tensile strength from sample tests, and are also influenced by the structural types under consideration.

The effective compressive and tensile strength can be further expressed as

$$f_c' = \upsilon_c f_c \qquad (6.7)$$

$$f_t' = f_c'/m \qquad (6.8)$$

where υ_c is the effective factor, f_c is the compressive strength of concrete cylinder, and m is the ratio between the effective compressive and tensile strength.

In order to use Eq.6.7 & 6.8, the results from cubes have to be converted into those of cylinders by[35] using

$$f_c = 0.85 f_{cu} \qquad (6.9)$$

From reference [46], a range of υ_c and m were suggested as

$$\upsilon_c = \frac{F_k}{\sqrt{f_c}} \qquad (f_c \text{ in } N/mm^2) \qquad (6.10a)$$

$$F_k = 2 \sim 5 \qquad (6.10b)$$

$$m = 50 \sim 400 \qquad (6.11)$$

where F_k is a parameter, which is equivalent to υ_c. The exact value of the above parameters have to be determined by the experiments on the particular type of structure. Once these two parameters have been determined, they can be used in practice for the analysis on that type of structure. In the current study on the punching shear on RC waffle slabs, efforts have been made to determine these two parameters, and this will be described in section 6.2.5.

The experimental material parameters for the twelve model slabs are listed in Table 6.2

Table 6.2 Concrete Strength of the Model Slabs

	1	2	3	4	5	6	7	8	9	10	11	12
$f_{cu}(N/mm^2)$	50.2	64.7	54.3	49.6	56.6	48.0	31.2	31.2	37.1	37.8	37.1	37.8
$f_c(N/mm^2)$	42.7	55.0	46.2	42.2	48.1	40.8	26.5	26.5	31.5	32.1	31.5	32.1
$f_t(N/mm^2)$	3.61	4.02	3.64	3.86	3.97	3.64	2.93	2.93	2.90	2.94	2.90	2.91
f_c/f_t	11.83	13.68	12.69	10.93	12.12	11.21	9.04	9.04	10.86	10.92	10.86	10.03

6.2.4 CONSIDERATION OF SHEAR LINK

In slabs 7~12, stirrups are used to increase the punching shear capacity of slabs. The stirrups are located inside the ribs evenly distributed, the details of the links are shown in Fig.5.2 (g)~(l).

In chapter 3, the formulae were derived for slabs with stirrups uniformly distributed all over the slabs; for slabs with stirrups only inside the ribs, the formula have to be modified.

Slabs No.7, 9 & 11 have the same pattern of stirrups; slabs No.8, 10, and 12 have a different pattern, and the corresponding formulae are derived below.

The steel ratio of the stirrups is defined below based on the steel content inside ribs,

$$\rho_{sv} = \frac{A_{sv}}{b \cdot l_{sv}} \qquad (6.12)$$

where, A_{sv} the area of the stirrups (including both of the branches of the link),

b width of the rib,

l_{sv} the distance between stirrups inside the rib.

In slabs No.7, 9, and 11, there are 4 ribs reinforced with stirrups. It has to be noted that not all of the stirrups inside the rib participate in the shear resistance, only the part of ribs which intersects with the failure surface does, as shown in Fig6.6

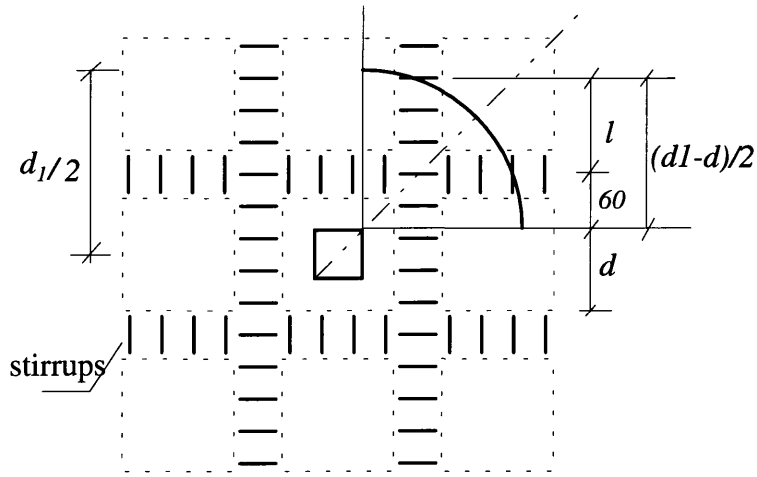

Fig.6.6 Length of the rib part which intersects with the failure surface

The length of the rib inside which the steel participates in the shear resistance, is calculated as:

$$l = \sqrt{\left(\frac{d_1}{2} - 75 - 60\right)^2 - 60^2} \qquad (6.13)$$

then, the shear resistance of the stirrups is

$$P_{sv} = 8 \cdot \rho_{sv} \cdot l \cdot b \cdot F_{sv} \cdot f_{sv} \qquad (6.14)$$

where,

F_{sv} the factor to reduce the strength of the stirrups due the ineffective anchorage of stirrups inside the slabs. This factor will be determined in section 6.2.5.

For slabs No.8, 10 and 12, 4, four ribs are reinforced with stirrups, as shown in Fig.6.7. The shear resistance is

$$P_{sv} = 4 \cdot \rho_{sv} \cdot \left(\frac{d_1}{2} - \frac{d}{2}\right) \cdot b \cdot F_{sv} \cdot f_{sv} \qquad (6.15)$$

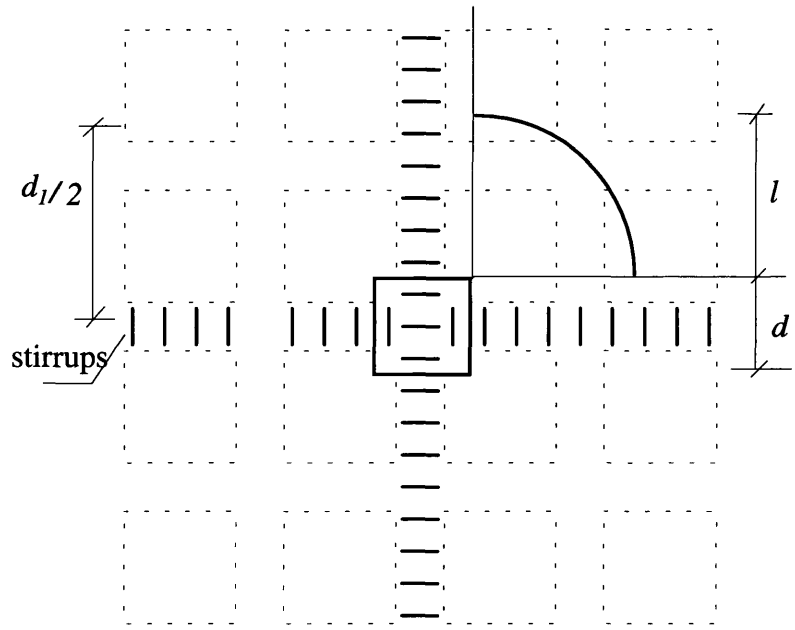

Fig.6.7 Length of the rib part which intersects with the failure surface

The total punching shear capacity consists of the resistance of the concrete and the stirrups, and therefore

$$P = P_c + P_{sv} \tag{6.16}$$

where,

P_c the resistance of the concrete, which can be calculated by Eq.6.2 or 6.4;

P_{sv} the resistance of the stirrups, calculated by Eq.6.14 or 6.15.

Slabs No.7 to 10 are reinforced with R6 stirrups of two legs, and slabs No.11 & 12 with R4 of two legs. The ratio of shear reinforcement, ρ_{sv}, for the twelve model slabs tested in this study are listed in Table 6.3

Table 6.3 Content of Stirrups for the Model RC Waffle Slabs

	1	2	3	4	5	6	7	8	9	10	11	12
ρ_{sv}(%)	0	0	0	0	0	0	0.898	0.898	0.898	0.898	0.399	0.399

The strength of the stirrups are

R6: $f_y = 250 N/mm^2$

R4: $f_y = 245 N/mm^2$

6.2.5 DETERMINATION OF A FEW ANALYSIS PARAMETERS

In chapter 3, we have derived the formulae for punching in RC waffle slabs, in sections 6.2.3 and 6.2.4 of this chapter, the formulae were further modified to consider the effect of the local solid area and the distribution of stirrups in the slabs. As mentioned in section 6.2.3, the application of upper bound analysis to RC structures is based on the assumption that the material is perfectly plastic, some parameters used in the formulae have to be determined by experiments to reduce the errors caused by the approximation of the material characteristics. These material parameters include the m and F_k (see Eq.6.8 & 6.10). In section 6.2.4, we introduced the strength reduction factor of the stirrups, F_{sv}, which was employed to reflected the poor anchorage of the stirrups inside slabs; this factor also having to be determined by test results. In the upper bound analysis, either the total depth or the effective depth might be used, it is up to the tests results to ascertain which one fits better.

In this section, we will try to determined these parameters using the trial and error method. A series of the parameters is assumed, and the analysis results are compared with test results to see what values the parameters should take.

First the strength reduction factor is determined; then the choice of the slab depth; followed by determination of parameters m and F_k. The formulae used are Eqs.6.2, 6.4, 6.14, 6.15, 6.16, and the geometric and material parameters of the model slabs were listed in Tables 6.1, 6.2, and 6.3.

The analysis were conducted by using the self-written program UPBOUND.FOR.

6.2.5.1 Choice between Total Depth and Effective Depth of Slab

In this section, we'll determine which depth should be used for the calculation of upper bound analysis. We do two separate analysis using either the total depth or the effective depth, then compare them with the test results. The factor F_k is taken as 2.0, and the factor F_{sv} taken as 0.5. The validation of using values for these two parameters will be explained in later sections. The parameter $\boldsymbol{m}$ is taken as 50 and 100.

1 Using Total Depth for Calculation

In this part, it is assumed that the concrete over the whole depth of the slab provides the shear resistance.

Table 6.4 Upper-Bound Analysis Results of Punching Load Using Total Depth

		slab1	slab2	slab3	slab4	slab5	slab6	slab7	slab8	slab9	slab10	slab11	slab12
m=50	P_c	217.4	227.0	294.0	219.9	370.8	353.2	205.9	169.9	268.3	199.9	312.1	316.4
	P_{sv}	0.0	0.0	0.0	0.0	0.0	0.0	70.3	58.3	74.0	54.9	52.7	42.6
	P	217.4	227.0	294.0	219.9	370.8	353.2	276.2	228.2	342.3	254.8	364.8	359.0
m=100	P_c	187.7	203.2	255.8	197.3	325.0	301.4	196.7	161.2	250.2	185.9	283.4	286.2
	P_{sv}	0.0	0.0	0.0	0.0	0.0	0.0	81.2	66.8	88.8	64.8	69.4	53.7
	P	187.7	203.2	255.8	197.3	325.0	301.4	277.9	228.0	339.0	250.6	352.8	339.8

2 Using the Effective Depth for Calculation

Using the effective depth, we have assumed that the shear resistance of the concrete cover can be neglected. The effective depth of the model slabs is $135mm$. The punching loads of the model slabs by calculation are listed in table 6.5.

Table 6.5 Upper-Bound Analysis Results of Punching Load Using Effective Depth

		slab1	slab2	slab3	slab4	slab5	slab6	slab7	slab8	slab9	slab10	slab11	slab12
m=50	P_c	188.3	198.5	235.5	171.5	312.4	302.6	181.3	149.6	220.6	157.9	265.0	271.3
	P_{sv}	0.0	0.0	0.0	0.0	0.0	0.0	59.2	53.1	62.6	49.4	46.1	39.0
	P	188.3	198.5	235.5	171.5	312.4	302.6	240.5	202.7	283.2	207.2	311.1	310.3
m=100	P_c	161.4	176.7	203.1	153.2	270.4	244.6	172.8	141.6	206.3	147.5	239.5	223.8
	P_{sv}	0.0	0.0	0.0	0.0	0.0	0.0	69.0	60.8	74.9	57.4	61.0	61.2
	P	161.4	176.7	203.1	153.2	270.4	244.6	241.8	202.4	281.2	204.9	300.4	285.0

3 Comparison of Results Using Total Depth and Effective Depth

In Table 6.6, the ratio between the calculated loads based on a series of assumed parameters and the test results are listed for all the twelve model slabs. Table 6.7 lists the statistical results of the load ratio for slabs without stirrups, slabs with stirrups, and the average of these two groups of slabs.

Table 6.6 Ratio of Calculated Load to Test Load (Total and Effective Depth)

	m	slab 1	slab 2	slab 3	slab 4	slab 5	slab 6	slab 7	slab 8	slab 9	slab 10	slab 11	slab 12
Total Depth	50	1.16	1.38	1.70	1.11	1.12	1.25	205.9	1.02	1.13	1.26	1.12	1.01
	100	1.00	1.23	1.48	0.99	0.98	1.06	70.3	1.03	1.13	1.25	1.10	0.97
Eff. Depth	50	1.01	1.20	1.37	0.86	0.94	1.07	0.89	1.00	1.04	0.91	0.86	1.14
	100	0.86	1.07	1.18	0.77	0.81	0.86	0.89	1.00	1.03	0.90	0.83	1.05

Table 6.7 Average of the Ratio of Calculated Load to Test Load

	m	Slab 1~6		Slab 7~12		Slab 1~12	
		$\overline{R}$	$\delta/\overline{R}$	$\overline{R}$	$\delta/\overline{R}$	$\overline{R}$	$\delta/\overline{R}$
Total Depth	50	1.29	16.25%	1.14	10.03%	1.21	15.09%
	100	1.13	16.11%	1.12	9.14%	1.12	13.12%
Eff. Depth	**50**	**1.07**	**15.62%**	**0.97**	**10.04%**	**1.02**	**14.30%**
	100	0.93	15.83%	0.95	8.50%	0.94	12.68%

From Table 6.7, it is seen that, when using the effective depth and taking $m=50$, the best fit is obtained; the average of the load ratios is 1.07 for slabs without stirrups, 0.97 for slabs with stirrups, and 1.02 for the whole slabs. Therefore, the effective depth should be used in the upper bound analysis. This also coincides with the experimental observations: the diagonal cracks inside the concrete cover did not appear until further displacement took place after the ultimate load had passed.

From now on all the analysis will be based on the effective depth.

6.2.5.2 Strength Reduction Factor for the Stirrups

As mentioned before in chapter 3, the yield strength of stirrups should be reduced due to the poor anchorage of stirrups inside slabs. This factor is not considered in this study by a theoretical approach (although it is possible) but will be determined by experiments. In order to find what value should the strength reduction factor be, a series of assumed values, F_{vs} =*0.3, 0.5* and *0.7* are used for the analysis.

In this part of the analysis, the other factors are taken as F_k=2, *m=50, 100, 200*, and 400. The reason for adopting F_k=2 is that it fits the experimental data better, which will be verified in section 5.2.5.3.

The punching loads of the analysis for slabs No. 7~12 are listed in Table 6.8, and the ratios of the calculated load vs. test loads are listed in Table 6.9. The average ratio and its standard derivation are also listed in Table 6.9.

Table 6.8 Upper Bound Analysis Results of Punching Load in Slabs with Shear Reinforcements (Strength Reduction)

F_{sv}	m	slab7	slab8	slab9	slab10	slab11	slab12
0.3	50	213.0	180.0	254.8	186.4	290.9	294.3
	100	209.5	175.8	246.9	180.2	273.3	259.6
	200	209.2	174.0	243.6	176.4	261.8	235.6
	400	210.4	173.7	243.1	174.6	255.2	220.6
0.5	50	240.5	202.7	283.2	207.2	311.1	310.3
	100	241.8	202.4	281.2	204.9	300.4	285.0
	200	244.8	203.5	282.4	204.4	294.9	265.5
	400	248.2	205.3	285.0	205.1	292.9	254.7
0.7	50	261.4	222.8	305.6	226.0	328.0	325.5
	100	265.9	225.1	307.8	226.5	322.7	312.2
	200	271.2	228.1	312.0	228.2	321.2	292.6
	400	276.1	231.2	316.5	230.4	322.2	284.5

Table 6.9 Ratio of Calculated Load Against Test Load (strength reduction)

F_{sv}	m	slab 7	slab 8	slab 9	slab 10	slab 11	slab 12	Aver. $\overline{R}$	Devia δ	$\delta/\overline{R}$ (%)
0.3	50	0.79	0.89	0.94	0.82	0.80	1.08	0.89	0.10	11.45
	100	0.77	0.87	0.91	0.79	0.75	0.95	0.84	0.07	8.71
	200	0.77	0.86	0.90	0.78	0.72	0.86	0.81	0.06	7.59
	400	0.78	0.86	0.89	0.77	0.70	0.81	0.80	0.06	7.73
0.5	50	**0.89**	**1.00**	**1.04**	**0.91**	**0.86**	**1.14**	**0.97**	**0.10**	**10.04**
	100	0.89	1.00	1.03	0.90	0.83	1.05	0.95	0.08	8.50
	200	0.90	1.00	1.04	0.90	0.81	0.97	0.94	0.08	8.04
	400	0.92	1.01	1.05	0.90	0.81	0.93	0.94	0.08	8.32
0.7	50	0.96	1.10	1.12	0.99	0.90	1.19	1.05	0.10	9.58
	100	0.98	1.11	1.13	1.00	0.89	1.15	1.04	0.09	8.97
	200	1.00	1.13	1.15	1.00	0.89	1.07	1.04	0.09	8.48
	400	1.02	1.14	1.16	1.01	0.89	1.04	1.04	0.09	8.69

From Table 6.8, it is seen that, when F_{sv} increases from 0.3 to 0.5 and further to 0.7, the load increases about 10% respectively. When taking $F_{sv} = 0.5$ and m=*50*, the average of the ratio between calculated load to test is 0.97, which is the best fit among all the analysed cases. This means it is reasonable to adopt $F_{sv} = 0.5$ for the calculation of the waffle slabs tested in this study.

6.2.5.3 Determination of Factor F_k

In the upper bound analysis, we assumed the material is perfectly plastic and used the plastic concrete strength, $f_c' = \upsilon_c f_c$. The plastic factor υ_c can be expressed as

$$\upsilon_c = F_k / \sqrt{f_c},$$

or there is $$f_c' = F_k \sqrt{f_c}.$$

The determination of υ_c is equivalent to determining the factor F_k. This factor depends on characteristics of concrete and also on the type of structures. It is difficult to determine this parameter by theoretical analysis, and has to be done by experiments. Here we try to find the value of this parameter for RC waffle slabs. We will assume a series of values for this parameter, do the calculation, and then compare the calculation results with the tests.

Based on the values for some other type of structures[1], the following values are assumed

$$F_k = 2;3;4.$$

From the previous study, we have already known that it is reasonable to use the effective depth for the analysis. The factor F_{sv} should be taken as 0.5 for the model waffle slabs. Another parameter m is still waiting to be determined so we used a wide range of values.

$$m=50,\ 100,\ 200,\ 400.$$

The calculated punching loads of the twelve slabs, using different values for the parameters, are listed in Tables 6.10a, b, & c. The ratios between calculation loads and tests are listed in Table 6.11.

Table 6.10a Upper Bound Analysis Results of Punching Load — $F_k = 2$

		slab1	**slab2**	**slab3**	**slab4**	**slab5**	**slab6**	**slab7**	**slab8**	**slab9**	**slab10**	**slab11**	**slab12**
m=50	P_c	188.3	198.5	235.5	171.5	312.4	302.6	181.3	149.6	220.6	157.9	265.0	271.3
	P_{sv}	0.0	0.0	0.0	0.0	0.0	0.0	59.2	53.1	62.6	49.4	46.1	39.0
	P	188.3	198.5	235.5	171.5	312.4	302.6	240.5	202.7	283.2	207.2	311.1	310.3
m=100	P_c	161.4	176.7	203.1	153.2	270.4	244.6	172.8	141.6	206.3	147.5	239.5	223.8
	P_{sv}	0.0	0.0	0.0	0.0	0.0	0.0	69.0	60.8	74.9	57.4	61.0	61.2
	P	161.4	176.7	203.1	153.2	270.4	244.6	241.8	202.4	281.2	204.9	300.4	285.0
m=200	P_c	139.6	157.5	176.6	136.6	231.8	206.0	169.2	136.9	198.9	140.4	221.6	194.6
	P_{sv}	0.0	0.0	0.0	0.0	0.0	0.0	75.6	66.6	83.5	64.0	73.3	70.9
	P	139.6	157.5	176.6	136.6	231.8	206.0	244.8	203.5	282.4	204.4	294.9	265.5
m=400	P_c	124.0	140.7	154.6	122.1	197.0	176.4	168.3	134.7	195.5	136.4	210.9	175.5
	P_{sv}	0.0	0.0	0.0	0.0	0.0	0.0	79.9	70.6	89.4	68.7	82.1	79.2
	P	124.0	140.7	154.6	122.1	197.0	176.4	248.2	205.3	285.0	205.1	292.9	254.7

Table 6.10b Upper Bound Analysis Results of Punching Load —$F_k = 3$

		slab1	slab2	slab3	slab4	slab5	slab6	slab7	slab8	slab9	slab10	slab11	slab12
m=50	P_c	282.5	297.8	353.3	257.3	468.6	453.8	251.3	216.4	313.5	231.0	388.6	404.8
	P_{sv}	0.0	0.0	0.0	0.0	0.0	0.0	75.9	59.6	76.6	54.1	53.3	40.7
	P	282.5	297.8	353.3	257.3	468.6	453.8	327.2	276.0	390.1	285.1	441.8	445.5
m=100	P_c	242.0	265.0	304.7	229.7	405.7	366.9	234.0	200.5	285.9	212.0	344.9	330.7
	P_{sv}	0.0	0.0	0.0	0.0	0.0	0.0	89.4	70.4	94.0	64.9	72.5	65.2
	P	242.0	265.0	304.7	229.7	405.7	366.9	323.5	270.9	379.9	276.9	417.4	395.9
m=200	P_c	209.4	236.2	264.8	205.0	347.7	309.1	224.8	190.0	269.0	197.7	312.2	283.5
	P_{sv}	0.0	0.0	0.0	0.0	0.0	0.0	99.3	79.1	107.4	74.5	89.6	77.7
	P	209.4	236.2	264.8	205.0	347.7	309.1	324.1	269.0	376.4	272.2	401.8	361.2
m=400	P_c	186.0	211.1	231.9	183.1	295.5	264.6	220.8	183.8	260.1	188.2	290.1	250.7
	P_{sv}	0.0	0.0	0.0	0.0	0.0	0.0	105.8	85.5	116.5	82.0	103.4	89.4
	P	186.0	211.1	231.9	183.1	295.5	264.6	326.5	269.3	376.6	270.3	393.4	340.0

Table 6.10c Upper Bound Analysis Results of Punching Load —$F_k = 4$

		slab1	slab2	slab3	slab4	slab5	slab6	slab7	slab8	slab9	slab10	slab11	slab12
m=50	P_c	376.6	397.0	471.1	343.1	624.8	605.1	322.5	283.8	407.3	304.7	513.3	538.5
	P_{sv}	0.0	0.0	0.0	0.0	0.0	0.0	86.8	63.7	85.8	56.9	57.4	41.8
	P	376.6	397.0	471.1	343.1	624.8	605.1	409.3	347.4	493.1	361.6	570.7	580.3
m=100	P_c	322.7	353.4	406.3	306.3	540.9	489.2	294.6	259.9	366.1	276.9	451.6	438.1
	P_{sv}	0.0	0.0	0.0	0.0	0.0	0.0	104.5	76.9	107.1	69.8	79.5	67.6
	P	322.7	353.4	406.3	306.3	540.9	489.2	399.1	336.7	473.1	346.7	531.2	505.7
m=200	P_c	279.2	314.9	353.1	273.3	463.6	412.1	278.3	242.6	338.8	255.0	403.4	373.3
	P_{sv}	0.0	0.0	0.0	0.0	0.0	0.0	117.8	88.3	124.5	81.9	100.7	81.8
	P	279.2	314.9	353.1	273.3	463.6	412.1	396.1	330.9	463.4	336.9	504.1	455.0
m=400	P_c	247.9	281.5	309.2	244.2	394.0	352.8	270.1	231.6	322.6	239.5	368.9	326.6
	P_{sv}	0.0	0.0	0.0	0.0	0.0	0.0	126.8	97.1	137.4	91.9	118.8	95.9
	P	247.9	281.5	309.2	244.2	394.0	352.8	396.8	328.7	460.0	331.4	487.7	422.5

Table 6.11a Ratios between Calculated Load and Test (slabs without stirrups)

Factor	*m*	Slab 1	Slab 2	Slab 3	Slab 4	Slab 5	Slab 6
$F_k = 2$	50	1.01	1.20	1.37	0.86	0.94	1.07
	100	0.86	1.07	1.18	0.77	0.81	0.86
	200	0.75	0.95	1.02	0.69	0.70	0.73
	400	0.66	0.85	0.90	0.61	0.59	0.62
$F_k = 3$	50	1.51	1.80	2.05	1.29	1.41	1.60
	100	1.29	1.61	1.77	1.16	1.22	1.30
	200	1.12	1.43	1.54	1.03	1.05	1.09
	400	0.99	1.28	1.34	0.92	0.89	0.94
$F_k = 4$	50	2.01	2.41	2.73	1.72	1.88	2.14
	100	1.73	2.14	2.36	1.54	1.63	1.73
	200	1.49	1.91	2.05	1.37	1.39	1.46
	400	1.33	1.71	1.79	1.23	1.18	1.25

Table 6.11b Ratios between Calculated Load and Test (slabs with stirrups)

Factor	*m*	Slab 7	Slab 8	Slab 9	Slab 10	Slab 11	Slab 12
$F_k = 2$	50	0.89	1.00	1.04	0.91	0.86	1.14
	100	0.89	1.00	1.03	0.90	0.83	1.05
	200	0.90	1.00	1.04	0.90	0.81	0.97
	400	0.92	1.01	1.05	0.90	0.81	0.93
$F_k = 3$	50	1.21	1.36	1.43	1.25	1.22	1.64
	100	1.19	1.34	1.40	1.22	1.15	1.45
	200	1.20	1.33	1.38	1.20	1.11	1.33
	400	1.20	1.33	1.38	1.19	1.09	1.25
$F_k = 4$	50	1.51	1.72	1.81	1.59	1.57	2.13
	100	1.47	1.66	1.74	1.52	1.47	1.86
	200	1.46	1.63	1.70	1.48	1.39	1.67
	400	1.46	1.62	1.69	1.46	1.35	1.55

Table 6.12 Average of the Load Ratio

Factor	*m*	slab 1~6		slab 7~12		slab 1~12	
		$\overline{R}$	$\delta/\overline{R}$	$\overline{R}$	$\delta/\overline{R}$	$\overline{R}$	$\delta/\overline{R}$
	50	**1.07**	**15.62%**	**0.97**	**10.04%**	**1.02**	**14.30%**
	100	0.93	15.83%	0.95	8.50%	0.94	12.68%
$F_k = 2$	200	0.81	16.40%	0.94	8.04%	0.87	14.49%
	400	0.71	17.11%	0.94	8.32%	0.82	18.68%
	50	1.61	15.62%	1.35	11.11%	1.48	16.51%
	100	1.39	15.83%	1.29	8.60%	1.34	13.50%
$F_k = 3$	200	1.21	16.41%	1.26	7.65%	1.23	12.79%
	400	1.06	17.11%	1.24	7.85%	1.15	14.87%
	50	2.15	15.62%	1.72	12.06%	1.94	18.15%
	100	1.85	15.83%	1.62	8.97%	1.74	14.92%
$F_k = 4$	200	1.61	16.41%	1.56	7.55%	1.58	13.03%
	400	1.41	17.11%	1.52	7.52%	1.47	13.41%

Table 6.12 lists the average load ratios and its standard deviation for slabs without stirrups, slabs with stirrups and the whole samples. From Table 6.12, it is seen that the results using the $F_k = 3$ or 4 give too large a punching load compared with the test results. Among the lot of analytical results, the best fit is obtained when taking $F_k = 2$ and *m=50*, which give a load ratio very close to 1.0.

From these analysis, we can conclude that the factor F_k should be taken as 2.0.

6.2.5.4 Determination of the Factor *m*

Factor *m* is the ratio between the plastic compressive strength and the tensile strength, i.e.,

$$m = f_c' / f_t'.$$

We already know that the plastic strength is a concept borrowed from plastic theory, which is just an approximation for the reinforced concrete. The plastic strengths depend on the material characteristics of concrete and also on the structural type. They have to be determined by experiment instead of theory. In the previous section, we have already known how to calculate the plastic compressive strength, here we'll study how to obtain the plastic tensile strength, or what a value for the parameter *m*.

In the following, we will try to find the value of m by a gradual approach: first a coarse value is sought, and then gradually refine this value.

In the analysis, we'll make use of the results of previous study, taking $F_k = 2$, $F_{sv} = 0.5$, and using the effective depth.

1. Preliminary Determination of *m*

In section 6.2.5.3, we tried a series of values for m when we tried to determine the value of F_k. Tables 6.10, 6.11 & 6.12 listed respectively the calculated punching loads, ratios between calculated load and test, and the statistic data. As described in section 6.2.5.3, the best fit between calculation and test was obtained when taking m=50, $F_k = 2$.

So it seems that the parameter m should be taken as 50. This value is smaller than what Nelson[46] has suggested, this is because the yield criteria employed here is a parabolic curve instead of the straight lines of Mohr-Coulomb criteria employed by Nelson. Furthermore, the structural member here is the waffle slabs instead of solid slabs.

Although taking *m=50* can get reasonable good results for the punching load, we will try to refine this parameter. Bearing in mind that m is the ratio between plastic compressive strength and plastic tensile strength, it might not be a constant. We can guess that this parameter might be related to the test results in concrete specimens: the uniaxial compressive strength of concrete cylinder and the tensile strength by split test on concrete cylinder. The latter one is available from the tests and the former one can be converted from the tests on concrete cubes. We will try the following formula for calculating the parameter m. Next section is dedicated to evaluate this formula.

$$m = \left(f_c / f_t\right)^2 / 2.78 \qquad (6.17)$$

2. Taking *m* as a variable

Here, we use Eq.6.17 to calculate m instead of taking the constant *m=50*. Similar to the analysis conducted before, we will calculate the punching load for all the twelve slabs.

Using $F_k = 2$, Eq.6.7, 6.8, 6.10 and 6.17, there are

$$f_c' = \upsilon_c f_c = \frac{2}{\sqrt{f_c}} f_c = 2\sqrt{f_c} \qquad (6.18)$$

$$f_t' = \frac{f_c'}{m} = 5.56\left(\frac{f_t}{f_c}\right)^2 \sqrt{f_c} \qquad (6.19)$$

By using Eq. 6.17~6.19, the factor *m*, plastic strength f_c' and f_t' for all the model slabs are calculated and listed in Table 6.13, and then use them for the upper bound analysis. Table 6.14 lists the punching loads and the punching angles of the calculation results, and Table 6.15 for the ratios between calculation and tests, Table 6.16 the statistical data.

Table 6.13 Material Parameters of the RC waffle slabs Using Eq. 6.17

		slab 1	slab 2	slab 3	slab 4	slab 5	slab 6	slab 7	slab 8	slab 9	slab 10	slab 11	slab 12
f_{cu}	(N/mm^2)	50.2	64.7	54.3	49.6	56.6	48.0	31.2	31.2	37.1	37.8	37.1	37.8
f_c	(N/mm^2)	42.7	55.0	46.2	42.2	48.1	40.8	26.5	26.5	31.5	32.1	31.5	32.1
f_c'	(N/mm^2)	13.1	14.8	13.6	13.0	13.9	12.8	10.3	10.3	11.2	11.3	11.2	11.3
f_t	(N/mm^2)	3.6	4.0	3.6	3.9	4.0	3.6	2.9	2.9	2.9	2.9	2.9	2.9
f_c/f_t		11.8	13.7	12.7	10.9	12.1	11.2	9.1	9.1	10.9	10.9	10.9	10.9
m		50.3	67.3	57.8	42.9	52.8	45.2	29.5	29.5	42.5	43.0	42.5	43.0

Table 6.14 UP-Bound Analysis Results of Punching Load using Eq.6.17

	slab1	slab2	slab3	slab4	slab5	slab6	slab7	slab8	slab9	slab10	slab11	slab12
P_c	188.1	188.8	228.2	175.8	308.9	307.7	192.4	158.1	225.1	160.8	272.1	277.8
P_{sv}	0.0	0.0	0.0	0.0	0.0	0.0	49.7	46.4	59.2	47.3	42.3	36.9
P	188.1	188.8	228.2	175.8	308.9	307.7	242.1	204.4	284.3	208.1	314.4	314.7

Table 6.15 Ratios of Calculated Load to Tests (*m* by Eq.6.17)

	slab1	slab2	slab3	slab4	slab5	slab6	slab7	slab8	slab9	slab10	slab11	slab12
P_c/P_{test}	1.01	1.14	1.32	0.88	0.93	1.09	0.71	0.78	0.83	0.71	0.75	1.02
P_{sv}/P_{test}	0.00	0.00	0.00	0.00	0.00	0.00	0.18	0.23	0.22	0.21	0.12	0.14
P/P_{test}	**1.01**	**1.14**	**1.32**	**0.88**	**0.93**	**1.09**	**0.89**	**1.01**	**1.05**	**0.91**	**0.87**	**1.15**

Table 6.16 Average of the Ratio of Analysis to Test (m by Eq.6.17)

	Slab 1~6	Slab 7~8	Slab 1~12
$\overline{R}$	**1.06**	**0.98**	**1.02**
$\delta/\overline{R}$	13.75%	10.21%	12.89%

From Table 6.16, it is seen that an average ratio of 1.06, 0.98 and 1.02 are obtained respectively for slabs without stirrups, with stirrups and the whole samples. This is slightly improved than those using a constant value of *m=50.*

By comparing the ***m*** factor listed in Table 6.14 with the cube strength of concrete f_{cu}, it is interesting to find out that m is almost equal to f_{cu} for all the twelve slabs, so the following equation might exist

$$m = f_{cu} \qquad (f_{cu} \text{ in the unit of } N/mm^2) \quad (6.20)$$

In the following, we will examine this equation.

3. Taking $m = f_{cu}$

Using $F_k = 2$, Eq.6.7, 6.8, 6.10 and 6.20, there are

$$f_c' = 2\sqrt{f_c} \qquad (6.21)$$

$$f_t' = \frac{2\sqrt{f_c}}{f_{cu}} \qquad (6.22)$$

where f_c is the compressive strength of concrete cylinder and f_{cu} is the compressive strength of concrete cube.

In the following, we will do the punching analysis by using Eq.6.20~6.21. Table 6.17 lists the value of *m*. Table 6.18 lists the results of the analysis; Table 6.19 lists the ratio between the calculated load and the tests.

Table 6.17 Material Parameters using $m = f_{cu}$

		slab 1	slab 2	slab 3	slab 4	slab 5	slab 6	slab 7	slab 8	slab 9	slab 10	slab 11	slab 12
f_{cu}	(N/mm^2)	50.2	64.7	54.3	49.6	56.6	48.0	31.2	31.2	37.1	37.8	37.1	37.8
f_c	(N/mm^2)	42.7	55	46.2	42.2	48.1	40.8	26.5	26.5	31.5	32.1	31.5	32.1
f_t	(N/mm^2)	3.6	4.0	3.6	3.9	4.0	3.6	2.9	2.9	2.9	2.9	2.9	2.9
f_c'	(N/mm^2)	13.1	14.8	13.6	13	13.9	12.8	10.3	10.3	11.2	11.3	11.2	11.3
f_t'	(N/mm^2)	0.26	0.23	0.25	0.26	0.25	0.27	0.33	0.33	0.30	0.30	0.30	0.30
m		50.2	64.7	54.3	49.6	56.6	48.0	31.2	31.2	37.1	37.8	37.1	37.8

Table 6.18 UP-Bound Analysis Results of Punching Load using $m = f_{cu}$

	slab1	slab2	slab3	slab4	slab5	slab6	slab7	slab8	slab9	slab10	slab11	slab12
P_c	188.2	190.1	231.3	171.8	304.5	304.6	218.3	152.5	200.6	168.0	266.0	283.3
P_{sv}	0.0	0.0	0.0	0.0	0.0	0.0	49.7	42.3	57.2	50.9	42.3	35.2
P	188.2	190.1	231.3	171.8	304.5	304.6	268.0	194.8	257.8	218.9	308.3	318.5

Table 6.19 Ratios between Calculated Load and Test Load using $m = f_{cu}$

	slab1	slab2	slab3	slab4	slab5	slab6	slab7	slab8	slab9	slab10	slab11	slab12
P_c/P_{test}	1.01	1.15	1.34	0.86	0.92	1.08	0.81	0.75	0.74	0.74	0.73	1.04
P_{sv}/P_{test}	0.00	0.00	0.00	0.00	0.00	0.00	0.18	0.21	0.21	0.22	0.12	0.13
P/P_{test}	1.01	1.15	1.34	0.86	0.92	1.08	0.99	0.96	0.95	0.96	0.85	1.17

Table 6.20 Average of Load Ratio between Analysis to Test using $m = f_{cu}$

	Slab 1~6	Slab 7~8	Slab 1~12
$\overline{R}$	1.06	0.98	1.02
$\delta/\overline{R}$	14.92%	9.70%	13.36%

It is seen from Table 6.20 that the average ratio is quite close to 1.0, i.e., the calculated results are very close to the test results.

From the above analysis, we can finally concluded that the parameter m can be taken as the values of concrete cube strength.

6.2.6 RESULTS OF THE UPPER BOUND ANALYSIS

In using the upper bound analysis, several parameters have to be determined by experimental results, which has been done in section 6.2.5. We have established the values for these parameters, and they are listed below for a quick reference.

$$F_k = 2;$$
$$F_{sv} = 0.5;$$
$$m = f_{cu} \qquad (f_{cu} \text{ in the unit of } N/mm^2);$$

Using the above equations there are:

plastic (effective) compressive strength: $f_c' = 2\sqrt{f_c}$;

plastic (effective) tensile strength: $f_t' = \dfrac{2\sqrt{f_c}}{f_{cu}}$;

Using the above parameters, the analysis was done for all the twelve waffle slabs, which was carried in section 6.2.5.4, the results are listed below. Table 6.21 lists the material parameters; Table 6.22 lists the punching load, the punching angle, the resistance of concrete and the resistance of the stirrups.

Table 6.21 Material Parameters of the Waffle Slabs

		slab 1	slab 2	slab 3	slab 4	slab 5	slab 6	slab 7	slab 8	slab 9	slab 10	slab 11	slab 12
f_{cu}	(N/mm^2)	50.2	64.7	54.3	49.6	56.6	48.0	31.2	31.2	37.1	37.8	37.1	37.8
f_c	(N/mm^2)	42.7	55	46.2	42.2	48.1	40.8	26.5	26.5	31.5	32.1	31.5	32.1
f_t	(N/mm^2)	3.6	4.0	3.6	3.9	4.0	3.6	2.9	2.9	2.9	2.9	2.9	2.9
f_c'	(N/mm^2)	13.1	14.8	13.6	13	13.9	12.8	10.3	10.3	11.2	11.3	11.2	11.3
f_t'	(N/mm^2)	0.26	0.23	0.25	0.26	0.25	0.27	0.33	0.33	0.30	0.30	0.30	0.30
m		50.2	64.7	54.3	49.6	56.6	48.0	31.2	31.2	37.1	37.8	37.1	37.8

Note: f_{cu} compressive strength of concrete cube;
f_c compressive strength of concrete cylinder;
f_t tensile strength by split test;
f_c' plastic compressive strength of concrete;
f_t' plastic tensile strength of concrete;
m ratio between plastic compressive strength and tensile strength.

Table 6.22 UP-Bound Analysis Results of the Waffle Slabs

	slab1	**slab2**	**slab3**	**slab4**	**slab5**	**slab6**	**slab7**	**slab8**	**slab9**	**slab10**	**slab11**	**slab12**
$\tan\overline{\alpha}$	2.23	2.15	2.04	1.6	2.03	1.72	1.12	1	1.2	1.2	1.34	1.37
P_c	188.2	190.1	231.3	171.8	304.5	304.6	218.3	152.5	200.6	168.0	266.0	283.3
P_{sv}	0.0	0.0	0.0	0.0	0.0	0.0	49.7	42.3	57.2	50.9	42.3	35.2
P	188.2	190.1	231.3	171.8	304.5	304.6	268.0	194.8	257.8	218.9	308.3	318.5
P_{test}	187.0	165.0	172.5	198.9	332.5	283.0	271.0	202.5	272.0	227.5	362.5	272.5

note:

$\tan\overline{\alpha}$ punching angle measuring the punching perimeter;
P_c shear resistance of the concrete;
P_{sv} shear resistance of the stirrups;
P calculated punching load;
P_{test} test result of punching load.

6.3 RESULTS OF ANALYSIS USING BS8110

In chapter 2, we have mentioned that BS8110 provides an analysis method for the punching load of RC waffle slabs, which neglects the resistance of the deck and considers only the shear resistance of ribs. The analysis formulae are similar to those of solid slabs. Here the analysis method will be described and then applied to all the twelve waffle slabs tested in this study.

6.3.1 DESCRIPTION OF THE ANALYSIS METHOD

6.3.1.1 Punching in Waffle Slabs without Shear Reinforcement

In BS8110, the analysis method for punching in waffle slab uses similar concept as that of a solid slab. A nominal (critical) punching perimeter is assumed; the ribs intersected with the nominal perimeter are assumed to provide the shear resistance, the deck's contribution being neglected.

The nominal punching perimeter is $1.5d$ away from the loading perimeter as shown in Fig.6.8. No matter what shape the loading area is, the outer perimeter is simplified as rectangular with a side dimension of $C+3d$. When counting the number of ribs intersected with the nominal perimeter, if the perimeter lies on the ribs (shown by dotted line in Fig.6.9), count the ribs on the inner side of the perimeter.

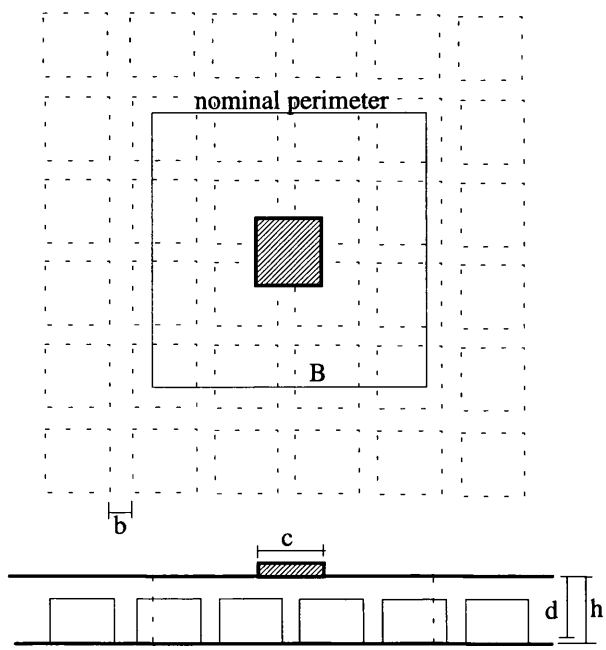

Fig 6.8 Nominal Punching Perimeter

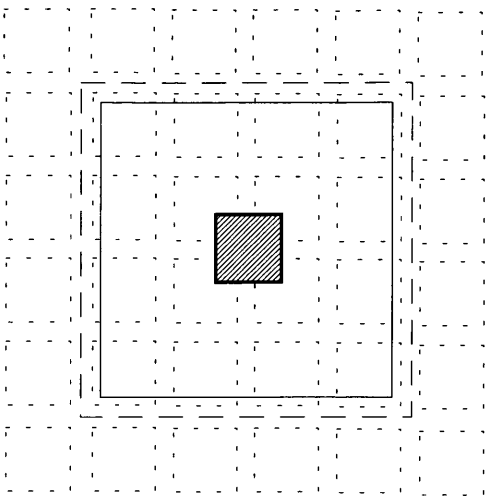

Fig 6.9 Intersection of Ribs with Nominal Punching Perimeter

The shear strength of the ribs is the nominal shear strength, which is governed by Eq.6.23 with the safety factor γ_m=1.2. The side length of the control perimeter, *B*, is calculated by Eq.6.24. The section area of the ribs intersected with the nominal perimeter is given be Eq.6.25. The punching capacity is given by Eq.6.26.

$$\upsilon_c = \frac{0.79}{\gamma_m}\sqrt[3]{100\rho}\sqrt[3]{f_{cu}/25}\sqrt[4]{400/d} \tag{6.23}$$

$$B=C+3d \tag{6.24}$$

$$S_{rib} = N \cdot A_{rib} = N \cdot b \cdot d \tag{6.25}$$

$$P=P_c=S_{rib} \cdot \upsilon_c \tag{6.26}$$

$$\nu_{max}= P/(U_o d) \tag{6.27}$$

$$U_o=4Cd \tag{6.28}$$

where,

υ_c is the nominal shear strength;

γ_m is the safety factor of the material;

ρ is the flexural steel ratio inside the rib;

f_{cu} is the cube strength of concrete;

d is the effective depth of the slab;

B is the side length of the control perimeter;

C is the side length of loading pad or column;

S_{rib} is the total area of the ribs intersected with the nominal perimeter;

A_{rib} section of each rib;

N number of ribs intersected with the nominal perimeter;

P is the punching capacity of the slab;

P_c is the part of the punching capacity provided by concrete, flexural steel;

ν_{max} is the maximum design shear stress at the loading perimeter;

U_c is the length of the perimeter of the loading pad.

The flexural steel ratio ρ and cube strength of concrete f_{cu} should not exceed 3% and $40N/mm^2$ respectively. The effective depth of slab, *d,* should not be less than $125mm$. The maximum design shear stress at the column face or the loading perimeter should not exceed$0.8\sqrt{f_{cu}}$ or $5N/mm^2$, whichever is the lesser.

6.3.1.2 Punching in Waffle Slabs with Shear Reinforcement

If the actual shear stress exceeds the nominal shear strength v_c, shear reinforcement may be provided in slabs over 200mm deep to increase the shear resistance. The stirrups inside waffle slabs are positioned inside the ribs. The calculation of the resistance of the stirrups may be carried out in two ways: one uses the formula for solid slabs; the other uses formula for beams. These two methods are explained below.

1. Method BS-ONE — using formula of flat solid slabs

In this method, the stirrups lying inside the failure zone (between perimeter of the loading pad and the nominal perimeter) is counted, then assume all the stirrups participating in the shear resistance. Eq.6.29 is used to calculate the resistance of the stirrups, Eq.3.80 for the total punching load..

$$P_{sv} = \frac{1}{\gamma_{sv}} f_{sv} S_{sv} = \frac{1}{\gamma_{sv}} f_{sv} \sum^{n} a_{sv} \tag{6.29}$$

$$P = P_c + P_{sv} \tag{6.30}$$

where,

γ_{sv} is the partial safety factor for links, 1.15;
f_{sv} is the characteristic strength of steel;
n number of legs of stirrups inside failure zone;
a_{sv} the section area of a leg of a stirrup;
S_{sv} section area of all legs of stirrups inside failure zone;
P_c resistance of concrete, by Eq.6.26

2. Method BS-TWO — using formulae for beams

Here the ribs are treated as beams. The shear resistance provided by the links is calculated by Eq.6.32.

$$\upsilon_{sv} = \frac{1}{\gamma_{sv}} \frac{f_{sv} A_{sv}}{b \cdot l_{sv}} \qquad (6.31)$$

$$P_{sv} = S_{rib} \cdot \upsilon_{sv} \qquad (6.32)$$

$$P = P_c + P_{sv} \qquad (6.33)$$

where,

υ_{sv}	is the nominal shear strength provided by the links;
γ_{sv}	safety factor for material;
f_{sv}	yield strength of stirrups;
A_{sv}	the section area of a stirrup including all its legs;
l_{sv}	horizontal spacing between stirrups.

6.3.2 CALCULATION RESULTS USING BS-ONE: TREATING STIRRUPS AS INSIDE SOLID SLAB

In this section, we will do the analysis for the twelve model slabs by treating stirrups as those inside solid slabs. The equations used are Eq.6.26, 6.29, and 6.30.

BS8110 has put some limit on the steel ratio, strength of concrete and the depth of the slab. In order to compare with the test result, two sets of calculation have been done, one strictly follows the provisions of BS8110, the second with the limit on those parameters removed. In all the analysis, the safety factor γ_m and γ_{sv} are taken as 1.0. The detailed analysis are described in Appendix A, and the results are summarised below.

Table 6.23 Punching Load Using BS-ONE

	d (mm)	B (mm)	N	S_{rib} (mm^2)	f_{cu} (N/mm^2)	ρ $(\%)$	υ_c (N/mm^2)	P_c (KN)	n	S_{sv} (mm^2)	f_{sv} (N/mm^2)	P_{sv} (KN)	P (KN)
Slab 1	125	525	8	70000	40.0 (50.2)	3.0 (3.88)	1.78 (2.10)	124.8 (146.7)	0	0	0	0	124.8 (146.7)
Slab 2	125	525	4	35000	40.0 (64.7)	3.0 (3.88)	1.78 (2.28)	62.4 (79.7)	0	0	0	0	62.4 (79.7)
Slab 3	125	525	8	70000	40.0 (54.3)	2.58 (2.58)	1.7 (1.88)	118.7 (131.4)	0	0	0	0	118.7 (131.4)
Slab 4	125	525	4	35000	40.0 (49.6)	2.58 (2.58)	1.7 (1.82)	59.5 (63.8)	0	0	0	0	59.5 (63.8)
Slab 5	125	525	LS	170000	40.0 (56.2)	1.33 (1.33)	1.36 (1.53)	231.1 (259.4)	0	0	0	0	231.1 (259.4)
Slab 6	125	610	12	105000	40.0 (48.0)	2.58 (2.58)	1.70 (1.80)	178.5 (189.3)	0	0	0	0	178.5 (189.3)
Slab 7	125	525	8	70000	31.2	3.0 (3.88)	1.64 (1.79)	114.8 (125.2)	28	791.7	250	197.9	312.7 (323.1)
Slab 8	125	525	4	35000	31.2 (31.2)	3.0 (3.88)	1.64 (1.79)	57.4 (62.6)	16	452.4	250	113.1	170.5 (175.7)
Slab 9	125	525	8	70000	37.1 (37.1)	2.58 (2.58)	1.65 (1.65)	115.5 (115.5)	28	791.7	250	197.9	313.4 (313.4)
Slab 10	125	525	4	35000	37.8 (37.8)	2.58 (2.58)	1.68 (1.68)	58.7 (58.7)	16	452.4	250	113.1	171.8 (171.8)
Slab 11	125	525	LS	170000	37.1 (37.1)	1.33 (1.33)	1.33 (1.33)	225.4 (225.4)	28	351.9	340	119.6	345.0 (345.0)
Slab 12	125	610	12	105000	37.8 (37.8)	2.58 (2.58)	1.68 (1.68)	176.0 (176.0)	16	201.1	340	68.3	244.3 (244.3)

*Note: values inside the bracket are results with the limitation stripped off on a few factors.
LS: local solid.

6.3.3 RESULTS USING BS-TWO-- TREATING STIRRUPS AS INSIDE BEAMS

In this part, the analysis were carried out following BS8110 and treating the stirrups inside ribs as that of inside beams. The equations used are Eq.6.26, 6.32 and 6.33. Two

sets of analysis were carried out: one follows BS8110 strictly; the other with the limitation striped off on the flexural steel ratio ρ, cube strength of concrete, f_{cu}, effective depth of slab, d. The safety factors are taken as 1.0. The horizontal distance between the stirrups inside a rib, $l_{sv} = 90mm$. The detailed analysis are described in Appendix A, and the results listed below.

Table 6.24 Punching Load Using BS-TWO

	d (mm)	B (mm)	N	S_{rib} (mm^2)	f_{cu} (N/mm^2)	ρ (%)	υ_c (N/mm^2)	P_c (KN)	A_{sv} (mm^2)	f_{sv} (N/mm^2)	υ_{sv} (N/mm^2)	P_{sv} (KN)	P (KN)
Slab 1	125	525	8	7000	40.0 (50.2)	3.0 (3.88)	1.78 (2.10)	124.8 (146.7)	0	0		0	124.8 (146.7)
Slab 2	125	525	4	3500	40.0 (64.7)	3.0 (3.88)	1.78 (2.28)	62.4 (79.7)	0	0		0	62.4 (79.7)
Slab 3	125	525	8	70000	40.0 (54.3)	2.58 (2.58)	1.7 (1.88)	118.7 (131.4)	0	0		0	118.7 (131.4)
Slab 4	125	525	4	3500	40.0 (49.6)	2.58 (2.58)	1.7 (1.82)	59.5 (63.8)	0	0		0	59.5 (63.8)
Slab 5	125	525	LS	170000	40.0 (56.2)	1.33 (1.33)	1.36 (1.53)	231.1 (259.4)	0	0		0	233.1 (259.4)
Slab 6	125	610	12	105000	40.0 (48.0)	2.58 (2.58)	1.70 (1.80)	178.5 (189.3)	0	0		0	178.5 189.3
Slab 7	125	525	8	70000	31.2	3.0 (3.88)	1.64 (1.79)	114.8 (125.2)	56.5	250	2.24	156.8	271.6 (282.0)
Slab 8	125	525	4	35000	31.2 (31.2)	3.0 (3.88)	1.64 (1.79)	57.4 (62.6)	56.5	250	2.24	78.4	135.8 (141.0)
Slab 9	125	525	8	70000	37.1 (37.1)	2.58 (2.58)	1.65 (1.65)	115.5 (115.5)	56.5	250	2.24	156.8	272.3 (272.3)
Slab 10	125	525	4	35000	37.8 (37.8)	2.58 (2.58)	1.68 (1.68)	58.7 (58.7)	56.5	250	2.24	78.4	137.1 (137.1)
Slab 11	125	525	LS	170000	37.1 (37.1)	1.33 (1.33)	1.33 (1.33)	225.4 (225.4)	25.1	340	0.56	95.2	320.6 (320.6)
Slab 12	125	610	12	105000	37.8 (37.8)	2.58 (2.58)	1.68 (1.68)	176.0 (176.0)	25.1	340	1.36	47.6	223.6 (223.6)

*Note: values inside the bracket are results with the limitation stripped off on a few factors.

LS: local solid area.

6.4 RESULTS OF FINITE ELEMENT ANALYSIS

Non-linear finite element analysis has been used for the analysis of the model slabs. The material model used included the Mohr-Columb criteria and the fracture model. The software used were the LUSAS finite element package and a software written by the author which is based on LUSAS but with the material modules replaced, as described in chapter 4.

Due to the symmetry of the slabs, 1/8 of the slab is used for the analysis, as mentioned in chapter 4. The plan view of the model in Fig.6.11 where the reference lines are also shown. Lines A-A and I-I refer to the centre lines of the slab in X and Y directions respectively.

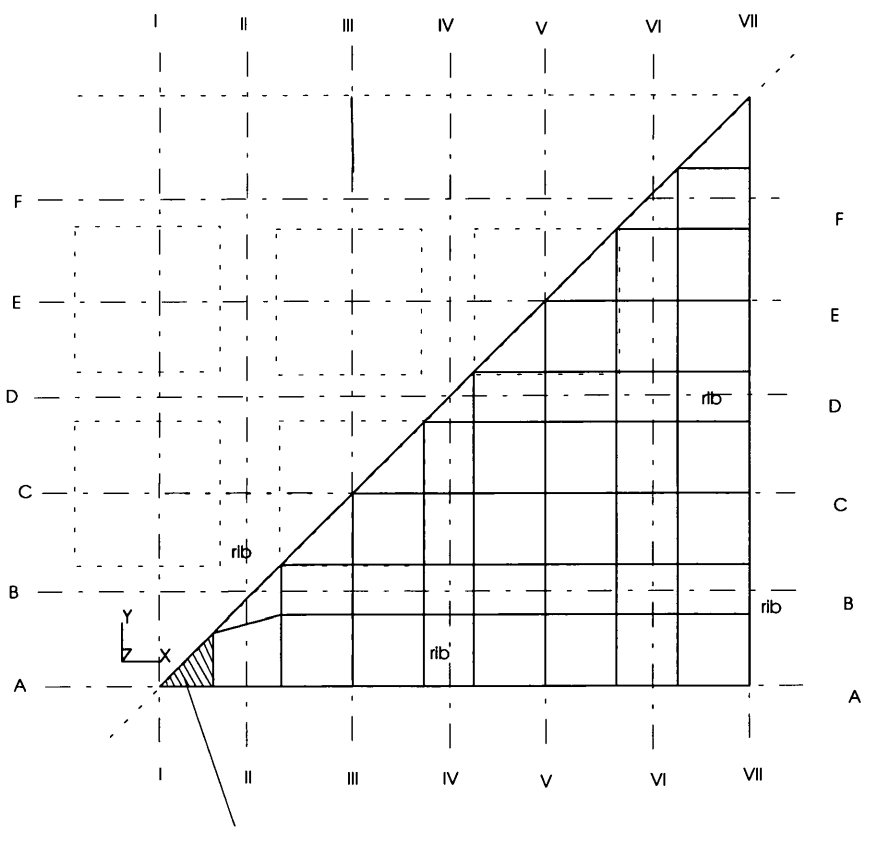

(solid line: mesh; dotted line: slab geometry)

Fig. 6.11 Plane View of the FEA Model

Due to the very long computation time required for the analysis, only slabs No.1, 3 and 5 were analysed using both the original LUSAS and user-modified LUSAS. In the following sections, results of both the analysis methods are presented.

6.4.1 ANALYSIS USING MOHR-COLOMB CRITERIA

As discussed in chapter 4, LUSAS provides a few material models for the non-linear finite element analysis[69], these includes the models of Von Mises, Tresca, Mohr-Coulomb, Druck-Prager etc. A concrete model is also provided, but unfortunately it can only be applied to 2-D or axisymmetrical problems. Among all the material models LUSAS can support, the Mohr-Coulomb is the one which is the closest to simulate the yield behaviour of concrete.

The values of φ and C of the slabs tested in this study are calculated and listed in Table 6.25; the elastic modulus of the slabs are calculated according to BS8110[12] and are also listed in the table. The LUSAS analysis results of slabs No.1, 3 and 5 are described below which include the central deflection of the slabs, the propagation of yield zones in the slabs, and the shear stress distribution along the sections of the slabs.

Table 6.25 Material Parameters of the Slabs

	f_{cu} (N/mm^2)	f_c (N/mm^2)	f_t (N/mm^2)	C (N/mm^2)	φ (°)	**E** (KN/mm^2)
Slab1	50.20	42.67	3.61	6.21	57.56	30.0
Slab3	54.30	46.16	3.64	6.48	58.63	30.9
Slab5	56.60	48.11	3.97	6.91	57.95	31.3

6.4.1.1 Displacements of the waffle slabs

The deformed shapes of slabs No.1 and 3 are shown in Fig.6.12a & b, where slab No.1 has a downward deflection and slab No.3 has an upward deflection due to the direction of the applied load. Table 6.26 lists the analysis results of the history of the load increment level and the corresponding deflection at the centre of the slab. Fig.6.13a, b, and c show the displacement history of the loading process at the central point of the slabs No.1, 3 and 5 respectively, where the test results and analysis results from crack-model (described later in section 6.4.2) are also plotted.

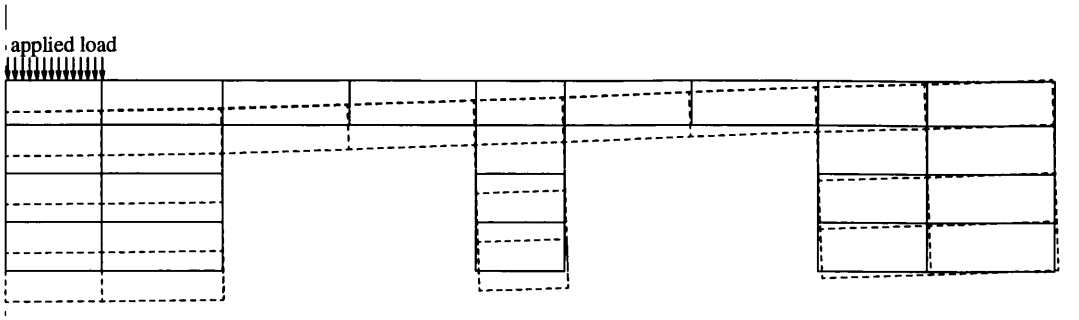

dotted line: deformed shape

Fig.12a Deformation of the Central Section of Slab1

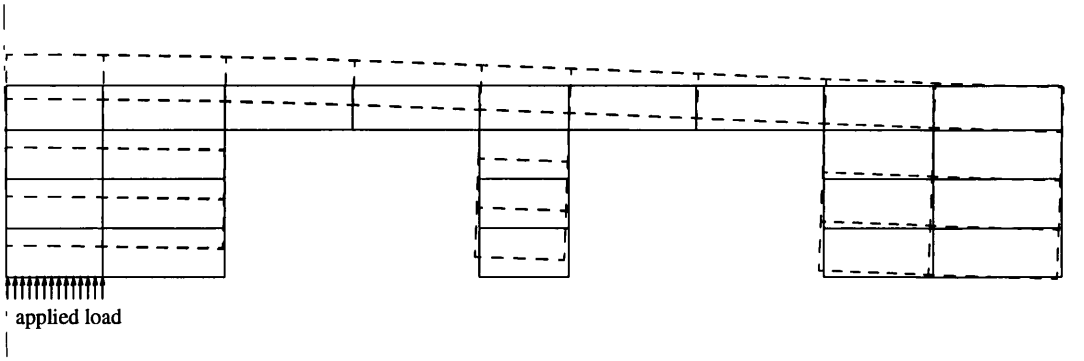

dotted line: deformed shape

Fig.6.12b Deformation of the Central Section of Slab3

Table 6.26 Lusas Analysis Results of the Load Increment Level and the Corresponding Deflection at the Centre of Slabs

Load Increment Step	Slab 1		Slab 3		Slab 5	
	Load Level	Central Def.	Load Level	Central Def.	Load Level	Central Def.
	(KN)	*(mm)*	*(KN)*	*(mm)*	*(KN)*	*(mm)*
0	0.00	0.00	0.00	0.00	0.00	0.00
1	11.25	0.10	11.25	0.12	11.25	0.10
2	33.75	0.31	33.75	0.35	33.75	0.30
3	56.25	0.53	56.25	0.54	56.25	0.50
4	78.75	0.74	78.75	0.73	78.75	0.70
5	100.11	1.01	89.66	0.86	100.71	0.92
6	121.76	1.28	100.41	0.97	122.09	1.14
7	143.46	1.59	110.38	1.10	136.10	1.31
8	158.19	1.80	120.11	1.21	157.41	1.56
9	180.20	2.15	129.32	1.34	178.47	1.86
10	201.43	2.48	138.21	1.46	192.52	2.06
11	223.53	2.86	146.79	1.58	213.65	2.40
12	245.54	3.23	155.03	1.70	226.85	2.61
13	267.48	3.64	163.04	1.82	237.07	2.79
14	289.31	4.05	170.83	1.94	247.84	2.97

15			178.48	2.06	262.45	3.24
16			185.93	2.18	271.88	3.41
17			200.78	2.43	285.90	3.66
18			209.90	2.58	300.42	3.92
19			219.56	2.75	310.55	4.12
20			228.52	2.91	322.97	4.35
21			237.79	3.07	344.30	4.76
22			246.90	3.23	363.16	5.12
23			255.90	3.39	384.46	5.54
24			264.86	3.56	405.77	5.95
25			282.96	3.72		

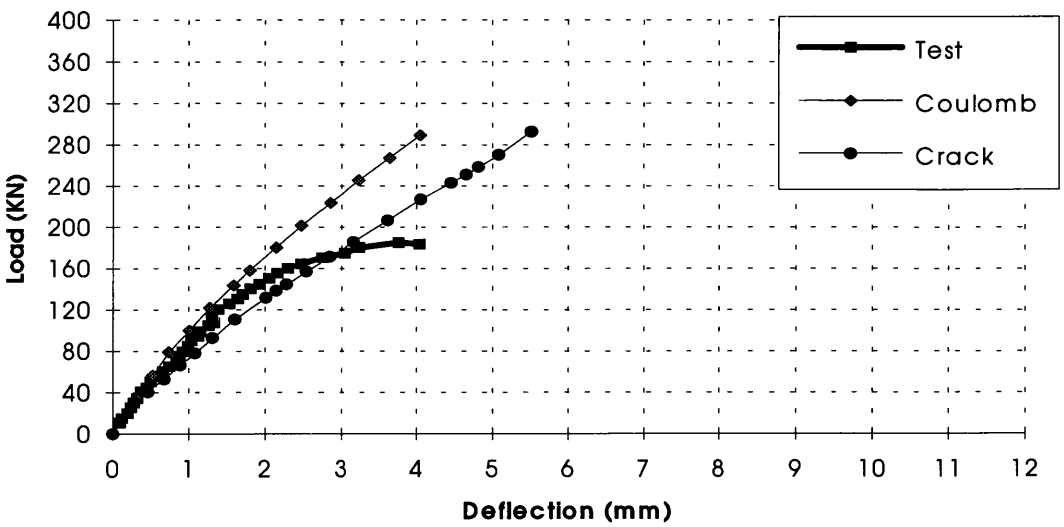

Fig. 6.13a Central Deflection of Analysis and Test Results —Slab No.1

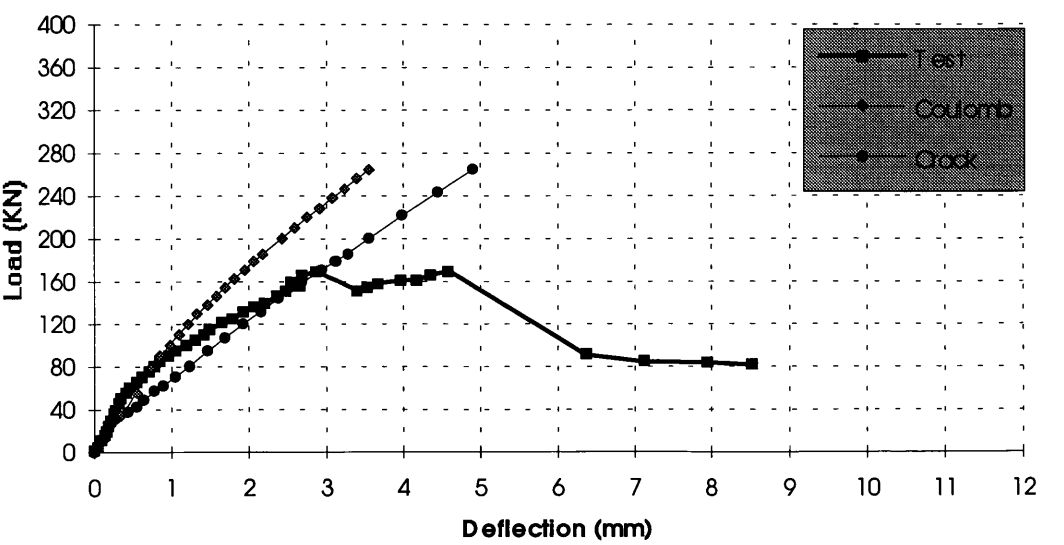

Fig. 6.13b Central Deflection of Analysis and Test Results —Slab No.3

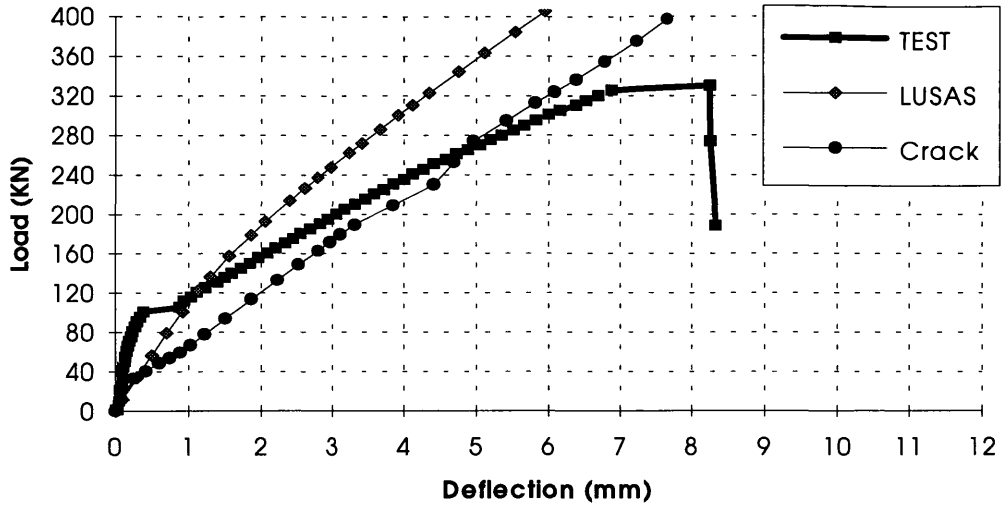

Fig. 6.13c Central Deflection of Analysis and Test Results —Slab No.5

The deflections at the centre of the slab corresponding to the ultimate test load are listed in Table 6.27.

Table 6.27 Central Deflections at the Ultimate Failure Load of Test

	LUSAS (mm)	TEST (mm)
Slab 1	2.26	4.0
Slab 3	1.97	4.6
Slab 5	4.53	7.0

It is obvious that the deflections obtained by LUSAS calculation are much smaller than those from tests, this is due to the use of Mohr-coulomb criteria which does not consider the energy dissipation in the development of cracks, the tension stress being remained at the yield surface.

6.4.1.2 Propagation of the Yield Zone in the Slabs

In this section, we will show the LUSAS analysis results about the gradual material yielding (failure) inside the slab during the progress of load increase. The purpose is to shown where the material yielding takes place. Two sections are taken to show the yield zone, section A-A is taken through a centre line of the slab and section B-B is taken through a rib; the exact location of the sections are shown in Fig.6.11.

Fig.6.14a & b show the plots for sections A-A and B-B of slab No.1. Fig.6.15a & b are for slab No.3.

From Fig.6.14a & b, it is seen that the yield zone is in the form of a 'pyramid'; the upper inner perimeter of the yield 'pyramid' is inside the local solid area, gradually approaching the perimeter of the loading pad as load increases; the lower outer perimeter of the yield 'pyramid' gradually extends towards the edge of the slab but there seems to be no further development after a certain load is exceeded (load increment 10 in slab1); the height of the yield 'pyramid' increases with the increment of the applied load. From Fig.6.14a & b, it is also seen that the region near the edge of the local solid area and its adjacent region on the ribs have the yielding developed earlier than other regions. The lower outer perimeter of the yield 'pyramid' extends about 500mm away from the centre of the slab. As the deck is on the compression side of the slab, the deck is the last area to get yield.

Slab No.3 is loaded in a direction opposite to that of Slab No.1. It can been seen that similar yield 'pyramid' exists but with the orientation upside down, see Fig.6.15a & b. The yielding appears quite early over most part of the deck, evidenced as the early tension cracks on the surface of the slab. The yield 'pyramid' of slab No.3 is much flatter compared with that of slab No.1, the outer perimeter being about 640mm away from the centre of the slab.

Please Refer to Fig.6.11 for the location of the sections.

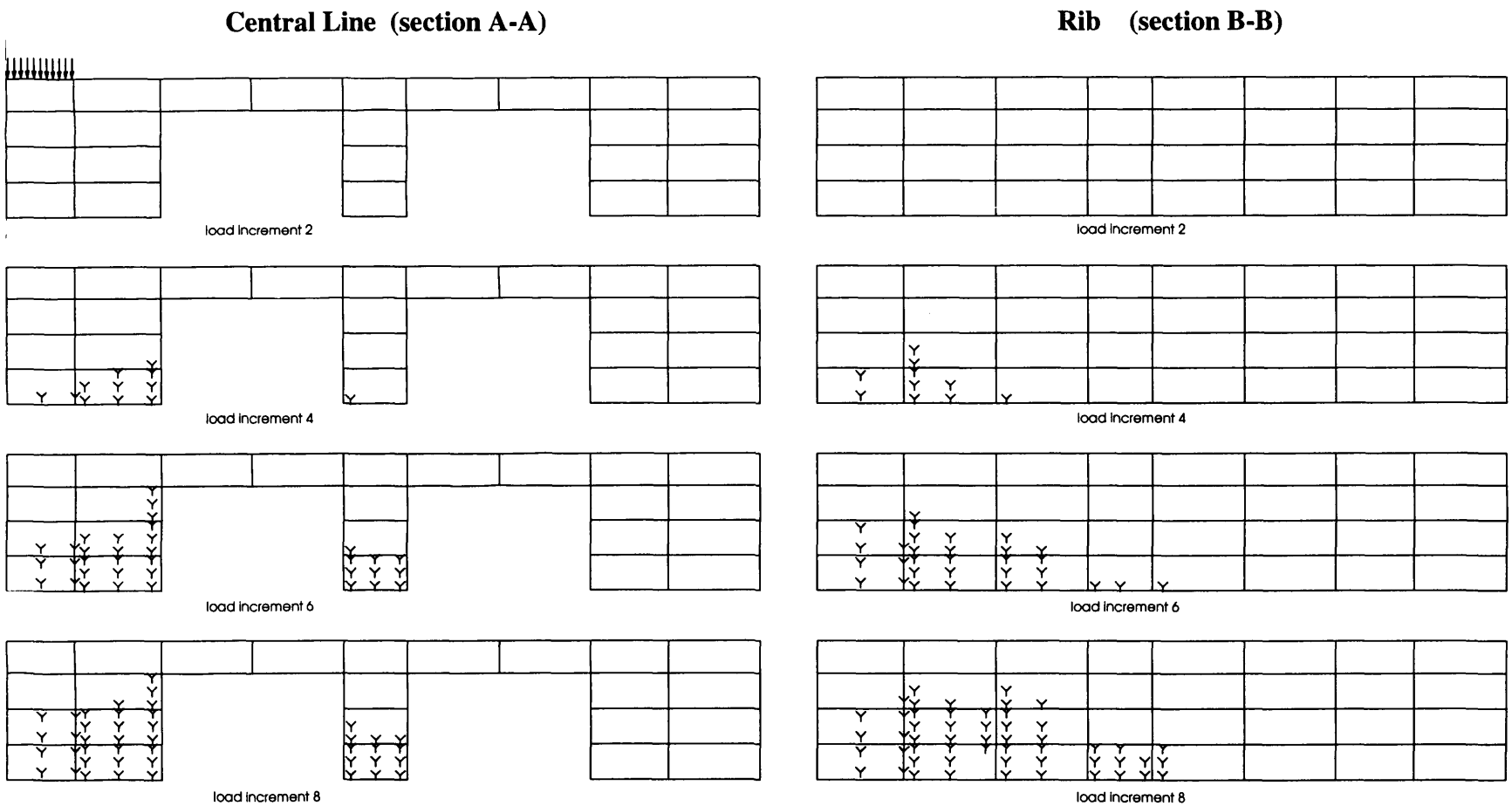

Fig.6.14a Propagation of Yield Zone (Slab 1)

Please Refer to Fig.6.11 for the location of the sections.

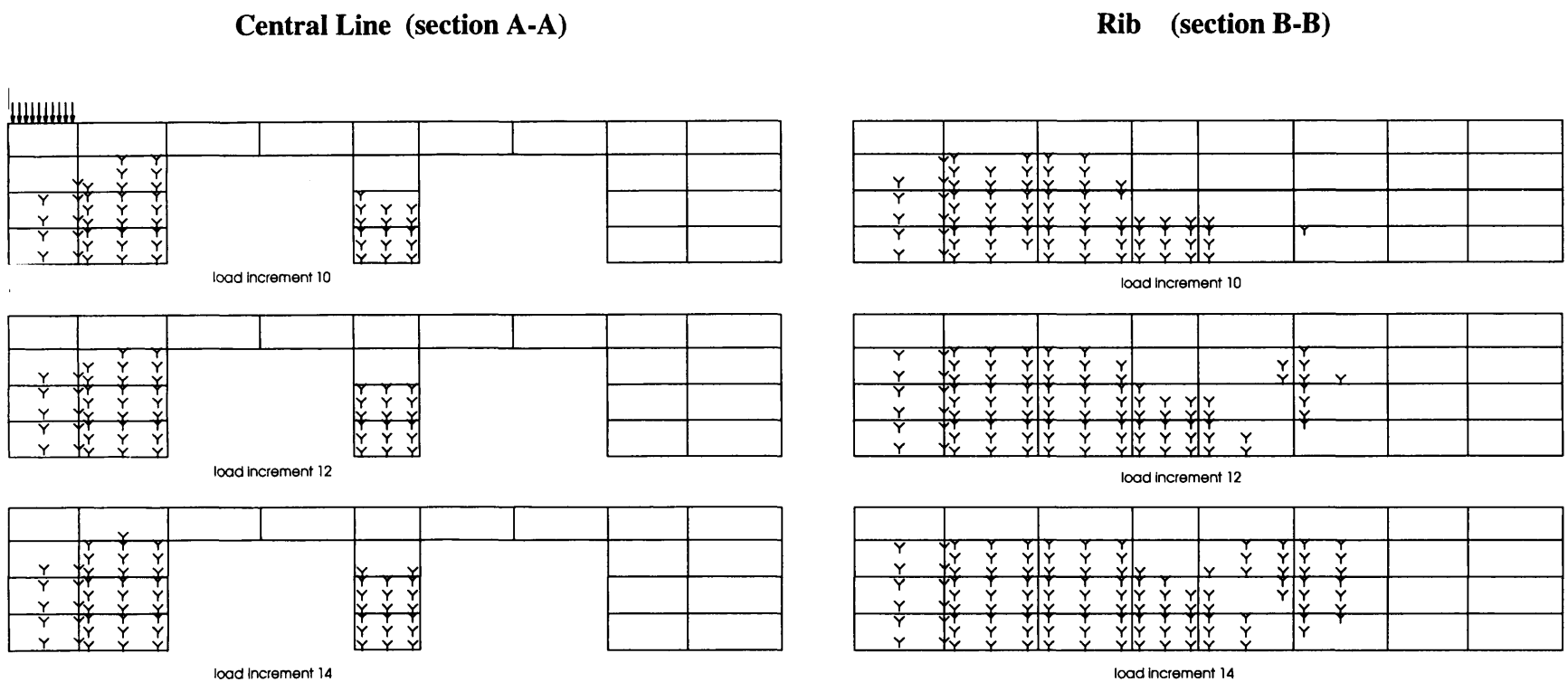

Fig.6.14b Propagation of Yield Zone (Slab 1)

Please Refer to Fig.6.11 for the location of the sections.

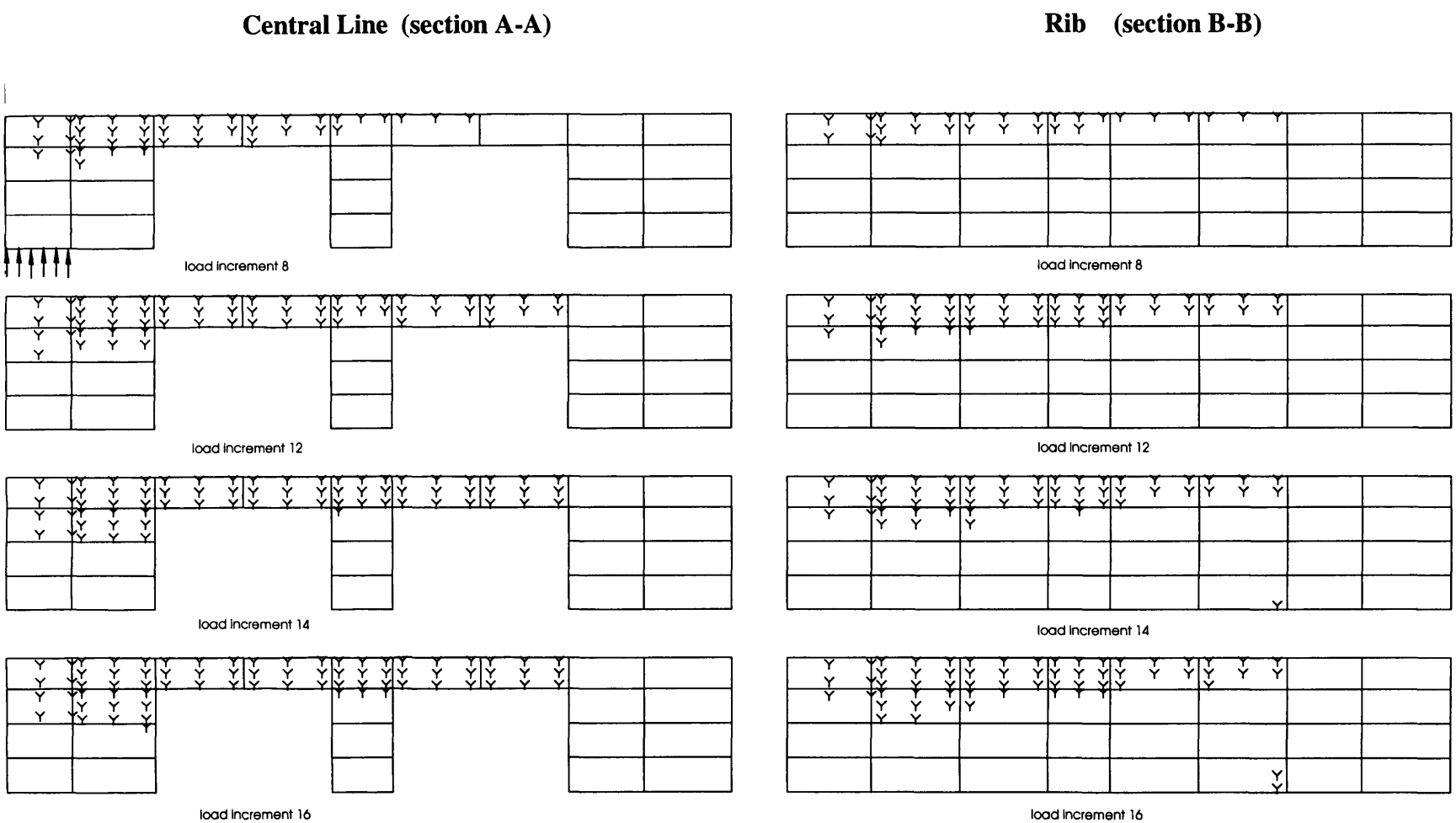

Fig.6.15a Propagation of Yield Zone (Slab 3)

Please Refer to Fig.6.11 for the location of the sections.

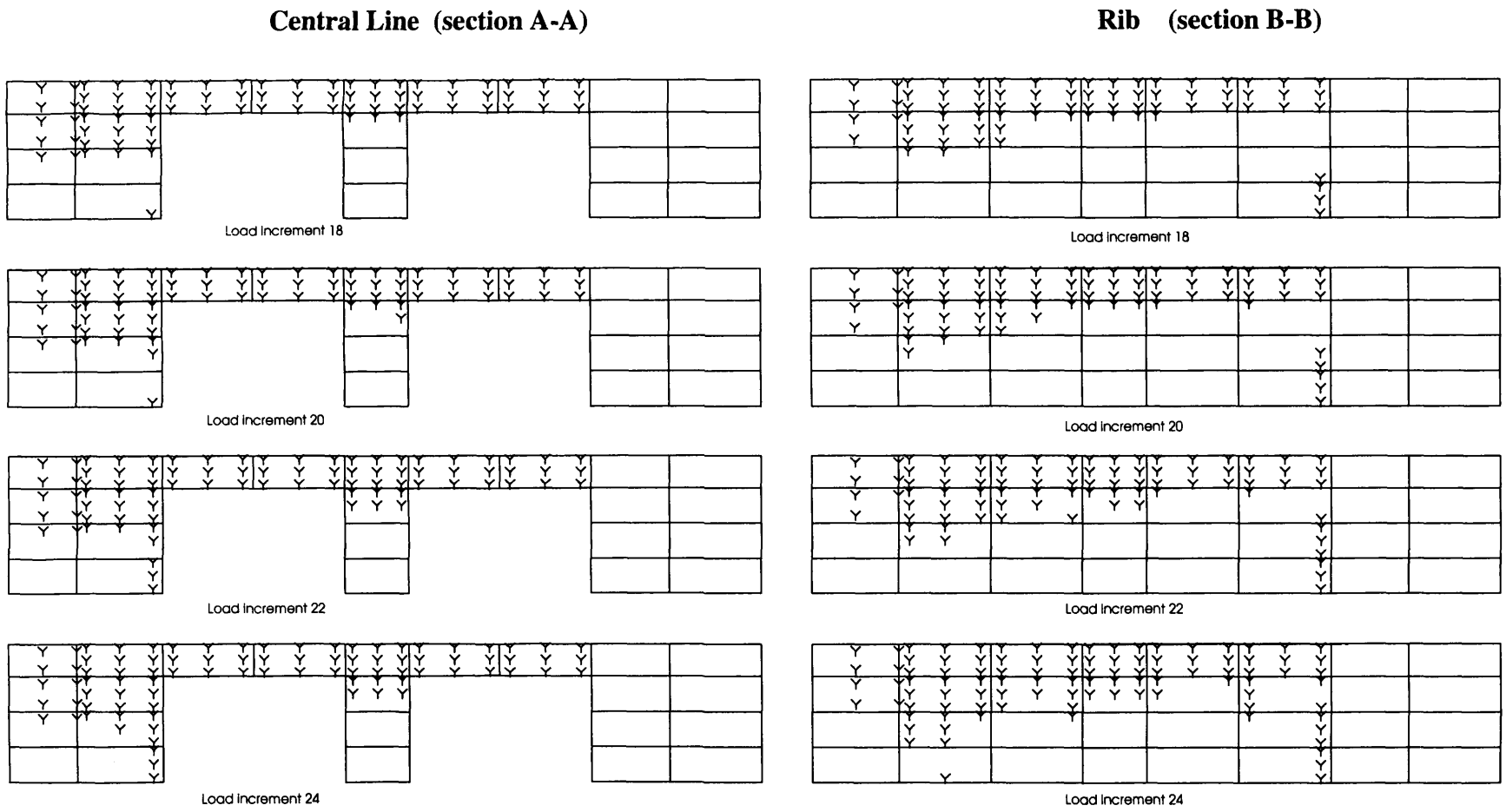

Fig.6.15b Propagation of Yield Zone (Slab 3)

6.4.1.3 Stress Distribution and Redistribution

In this section the results of the stress of the analysis are presented by means of stress contours along various sections. The stresses of interest are the shear stress τ_{xz} and normal stressσ_z(in global axes) which are related to the shear resistance. After some examination of the above two stresses, it was found that σ_z is only prominent in the region under or very near to the loading pad; in other areas it was very small and therefore this stress is not plotted. The stress τ_{xz} is the main component (for this 1/8 part of the slab) which is related to the punching load. Six sections are selected to show the shear stress distribution on them, as shown in Fig.6.16. Section 1-1 is just adjacent to the edge of the loading pad; section 2-2 cuts through the first rib along the Y direction, section 3-3 is adjacent to the first rib in the Y direction but cuts through the deck; section 4-4 cuts through the middle of recesses in Y direction; section 5-5 is adjacent left to the second rib in Y direction; section 6.6 is adjacent right to the second rib in Y direction.

In slab No.1 the applied load is downward, therefore τ_{xz} of the positive value resists the punching load as shown in Fig.6.16; in slab No.3 the applied load is upward therefore τ_{xz} of negative value resists the punching load.

The stress contour of τ_{xz} in slabs No.1, 3 & 5 are shown in Fig.6.17, 6.18, and 6.19 respectively. In each of the figure, a few loading increment step's results are plotted in order to show the relative change of the stress contour along the history of loading.

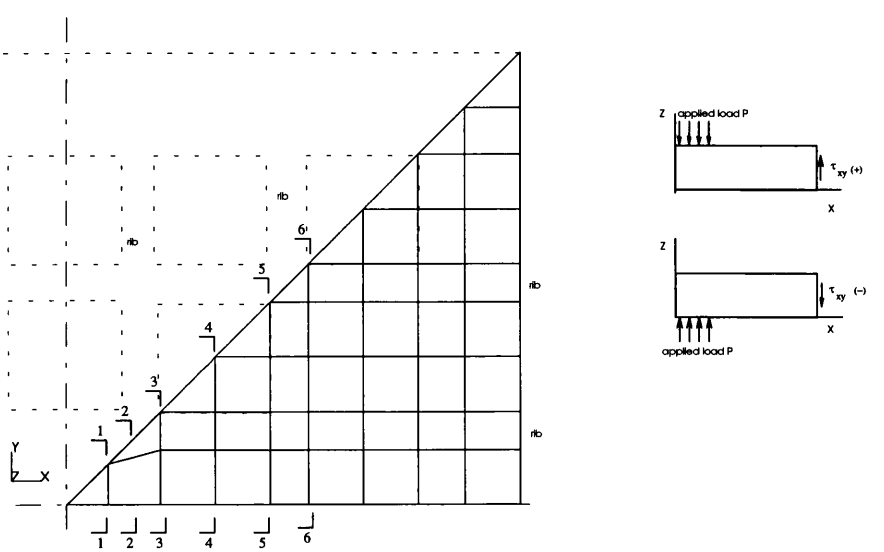

Fig.6.16 Position of Section cut to Show Shear Stress Distribution

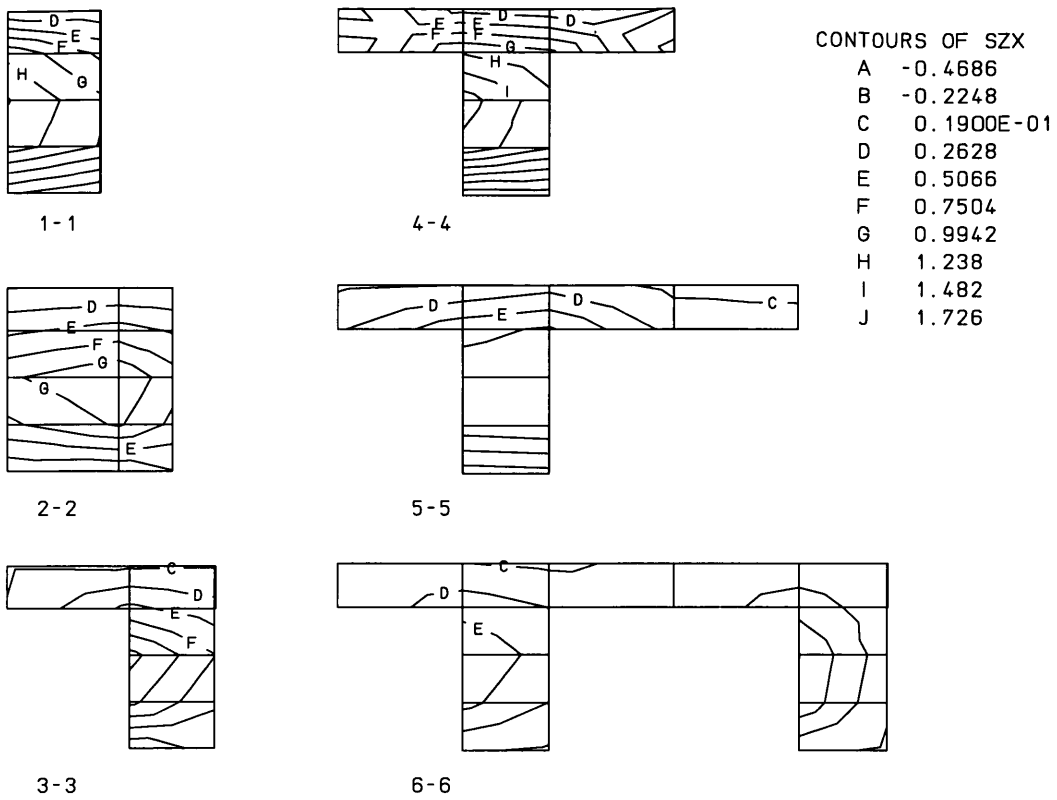

Load Increment 4 of slab No.1

Fig.6.17a Contours of Shear Stress τ_{xz}

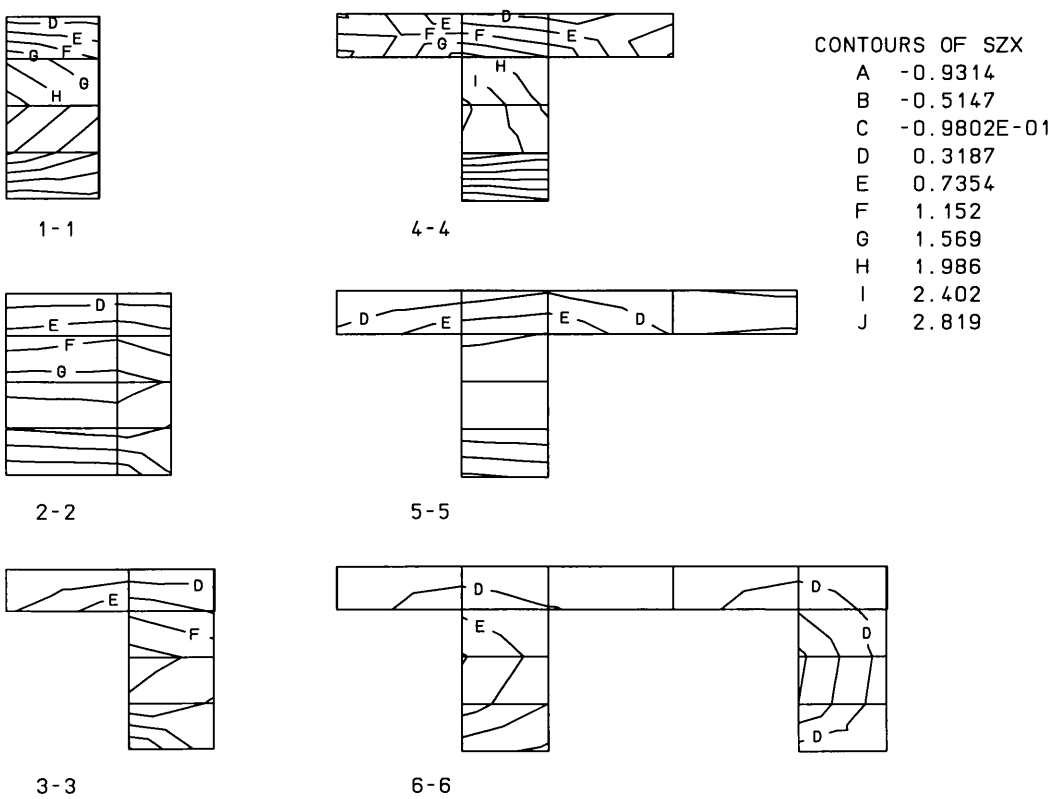

Load Increment 6 of slab No.1

Fig.6.17b Contours of Shear Stress τ_{xz}

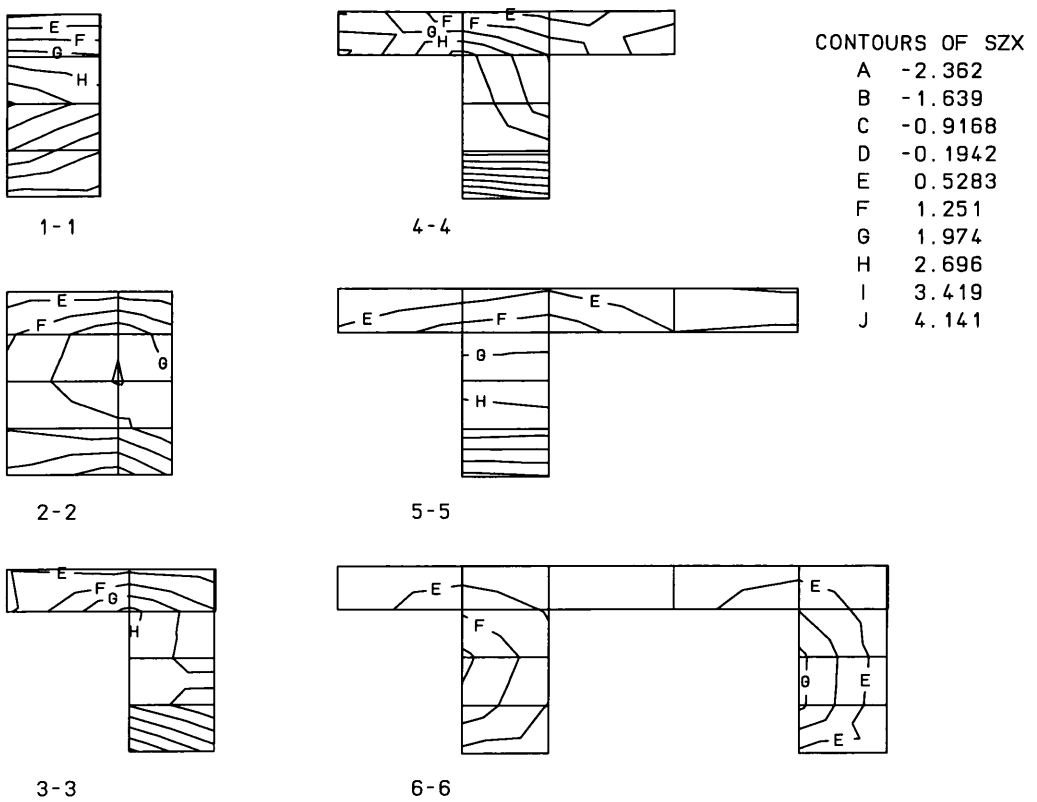

Load Increment 10 of slab No.1

Fig.6.17c Contours of Shear Stress τ_{xz}

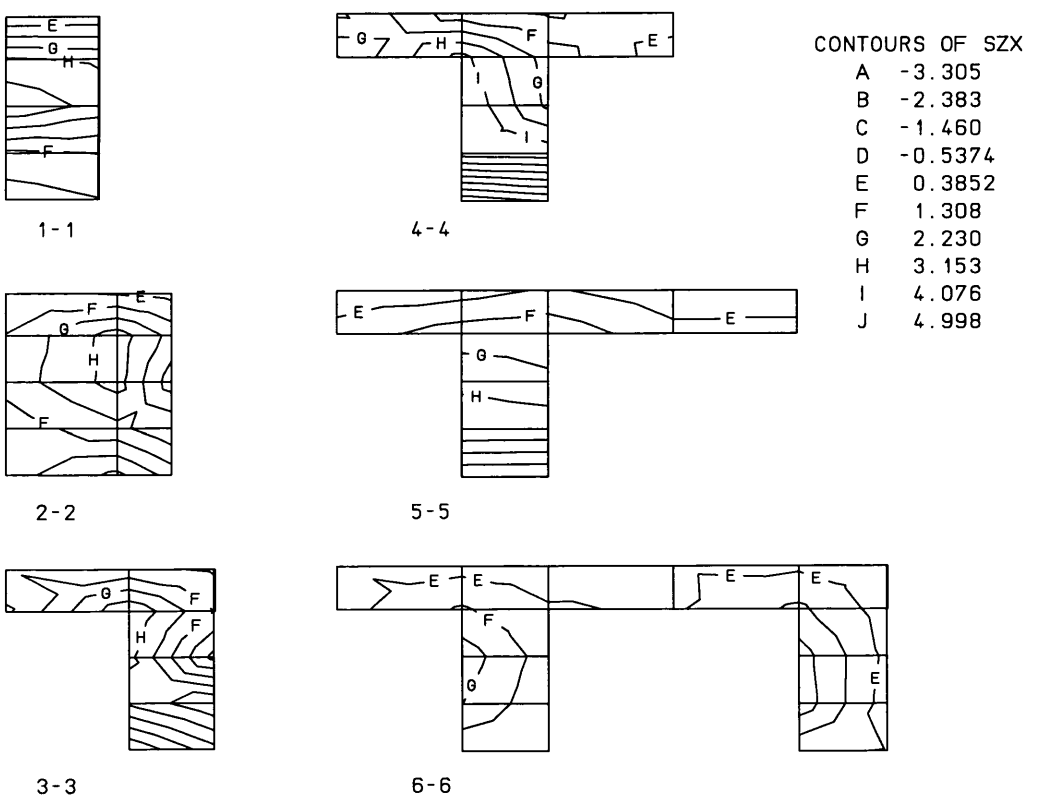

Load Increment 12 of slab No.1

Fig.6.17d Contours of Shear Stress τ_{xz}

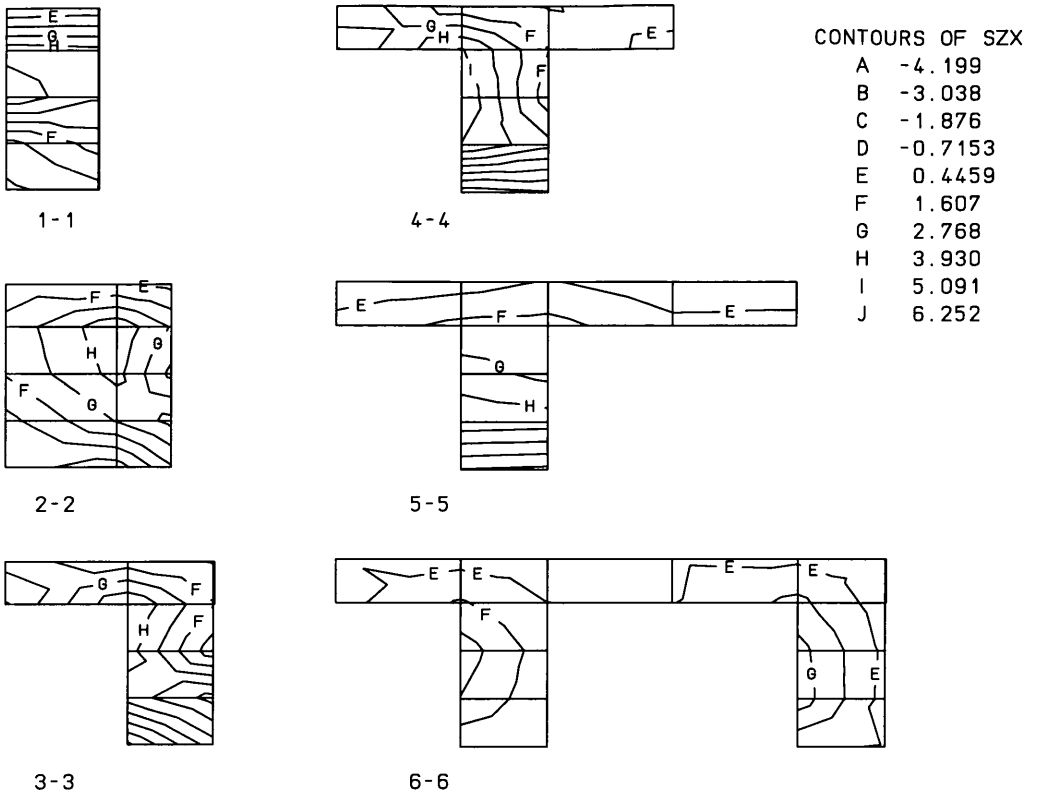

Load Increment 14 of slab No.1

Fig.6.17e Contours of Shear Stress τ_{xz}

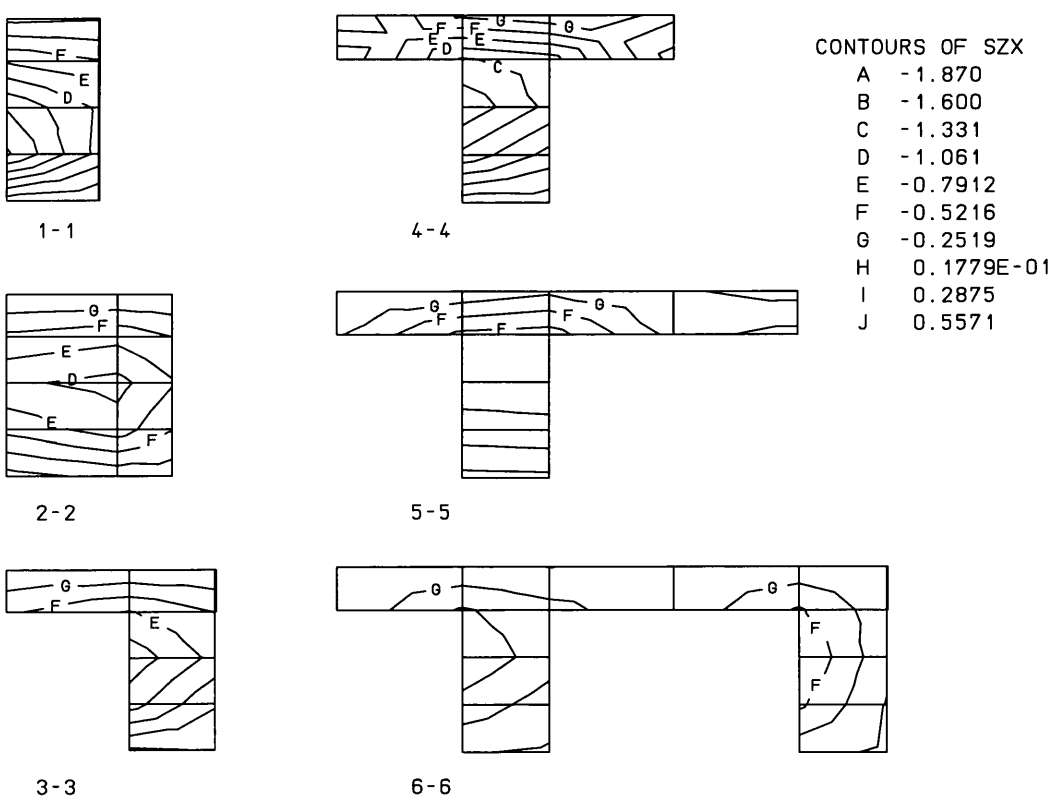

Load Increment 4 of slab No.3

Fig.6.18a Contours of Shear Stress τ_{xz}

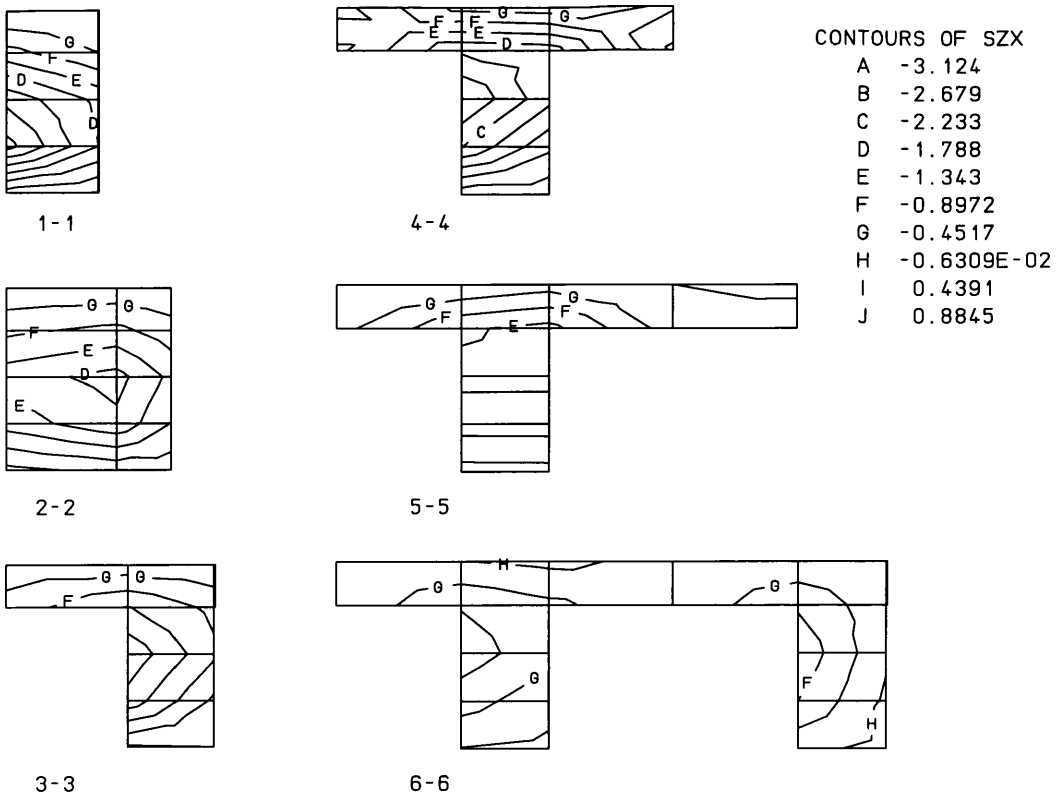

Load Increment 8 of slab No.3

Fig.6.18b Contours of Shear Stress τ_{xz}

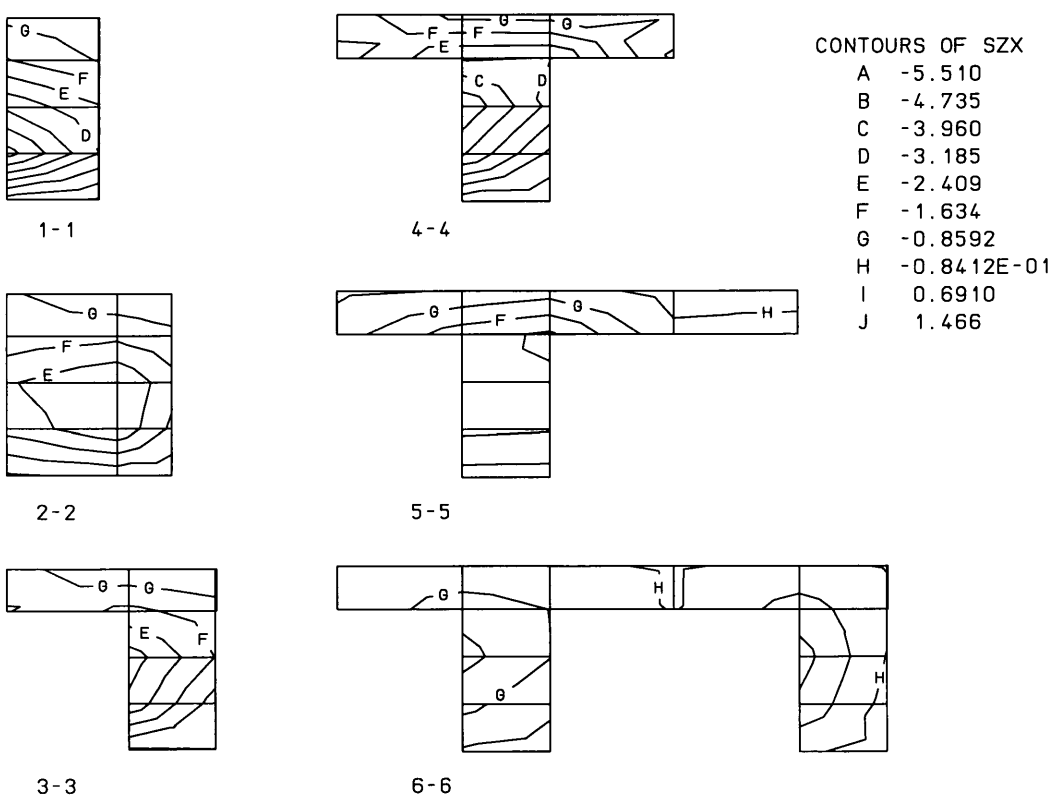

Load Increment 16 of slab No.3

Fig.6.18c Contours of Shear Stress τ_{xz}

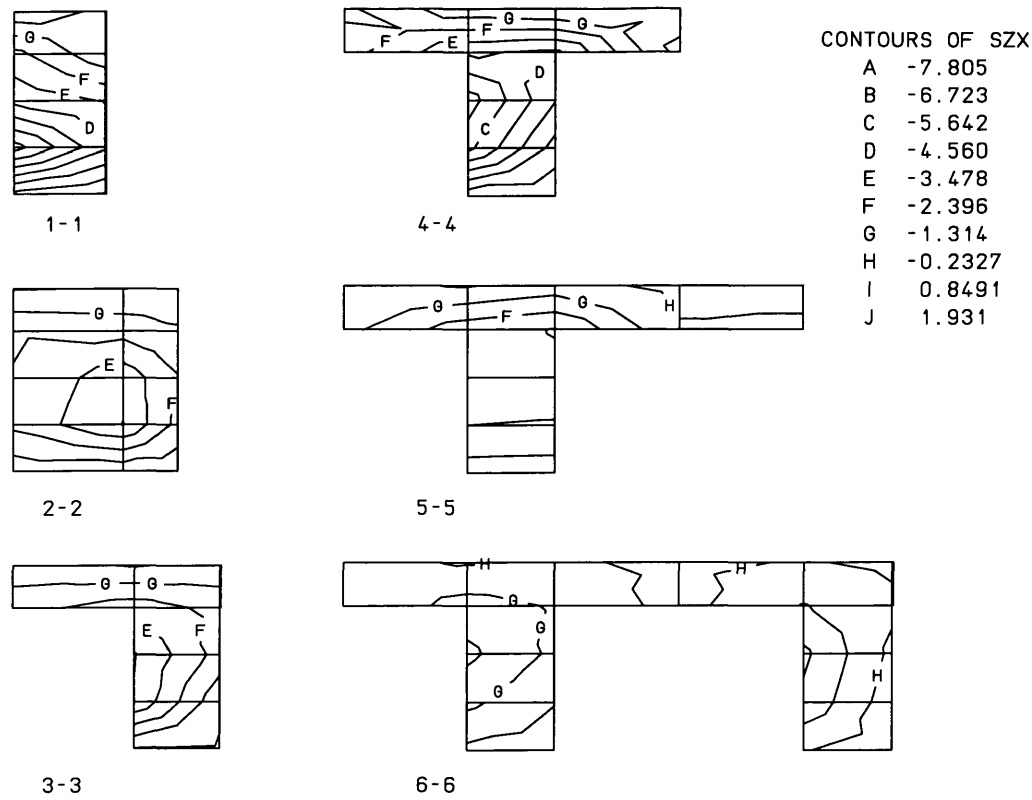

Load Increment 22 of slab No.3

Fig.6.18d Contours of Shear Stress τ_{xz}

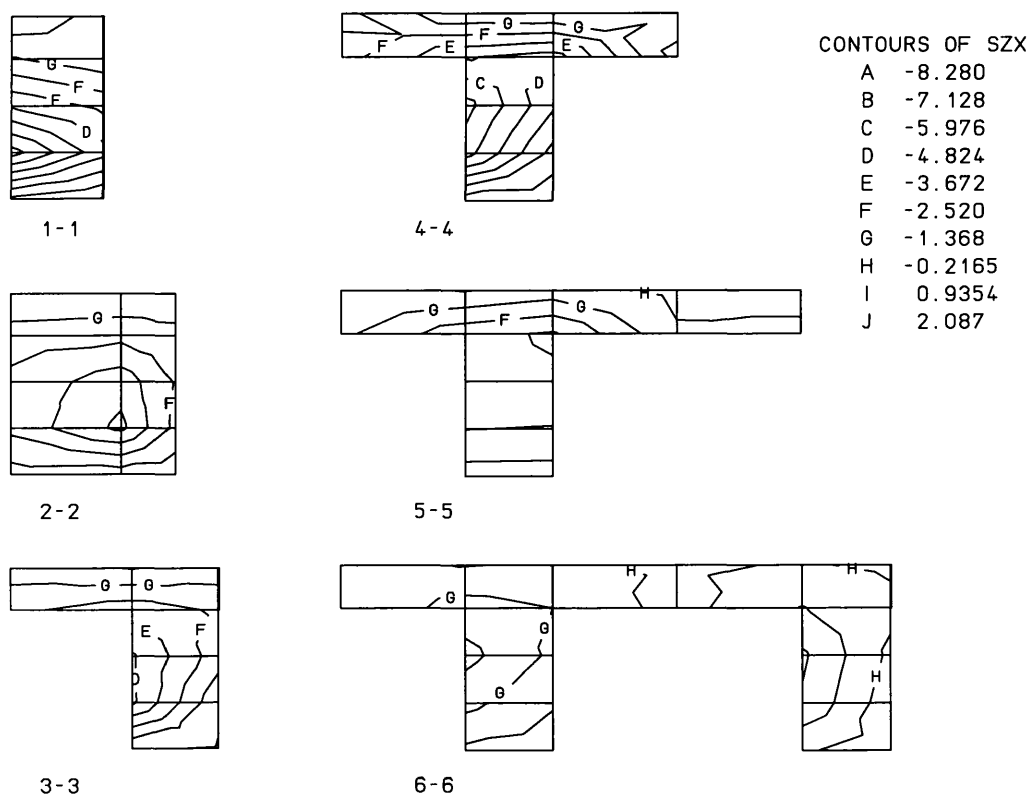

Load Increment 24 of slab No.3

Fig.6.18e Contours of Shear Stress τ_{xz}

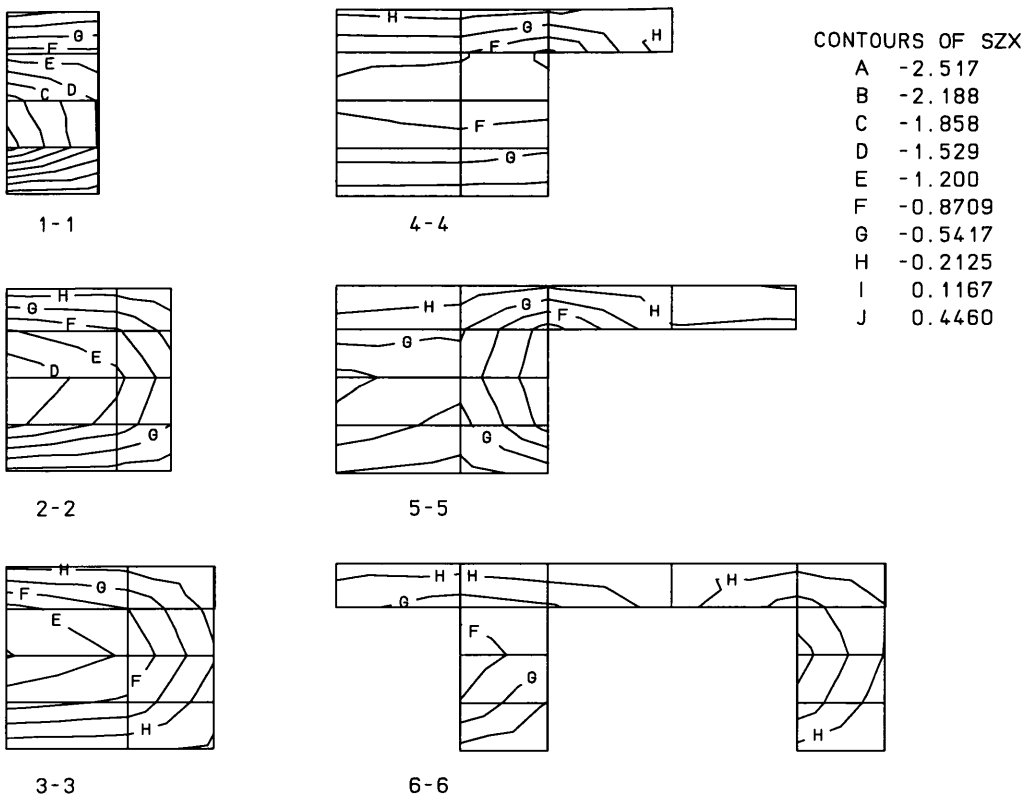

Load Increment 6 of slab No.5

Fig.6.19a Contours of Shear Stress τ_{xz}

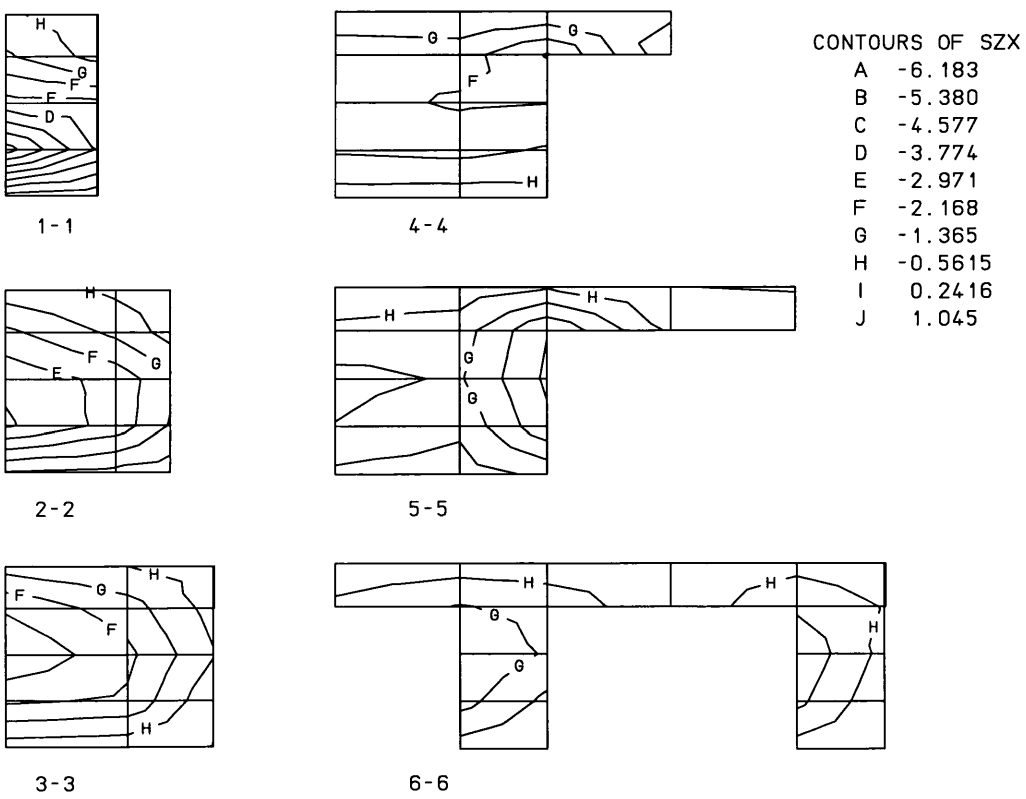

Load Increment 12 of slab No.5

Fig.6.19b Contours of Shear Stress τ_{xz}

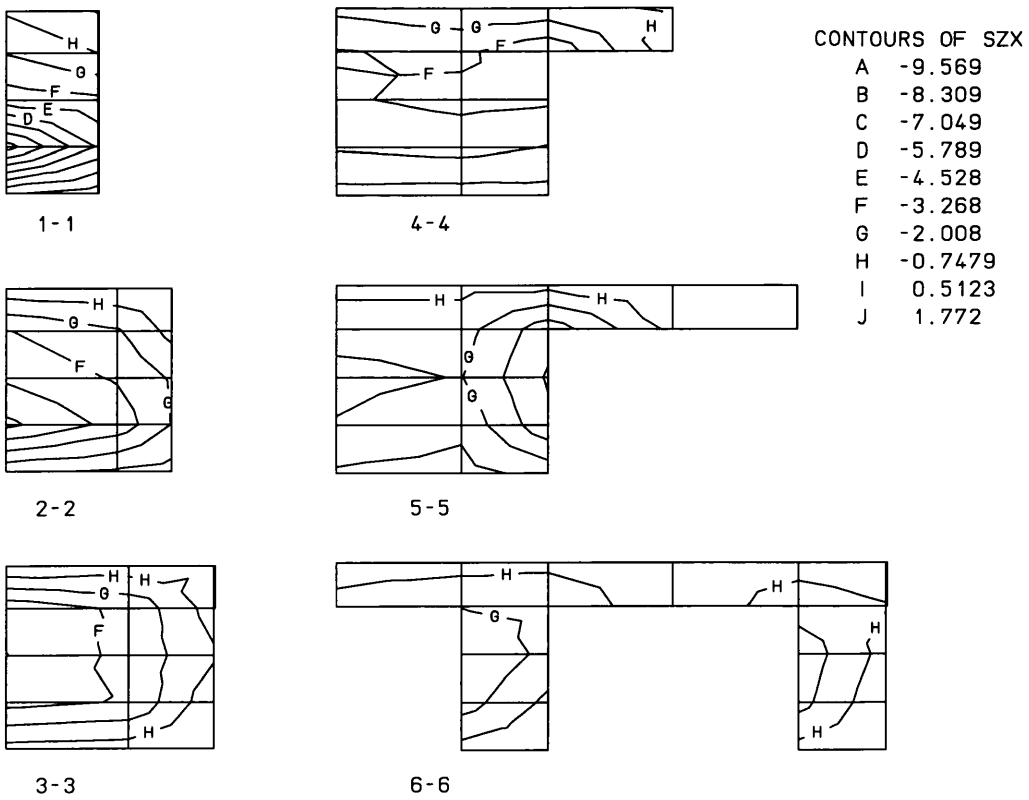

Load Increment 20 of slab No.5

Fig.6.19c Contours of Shear Stress τ_{xz}

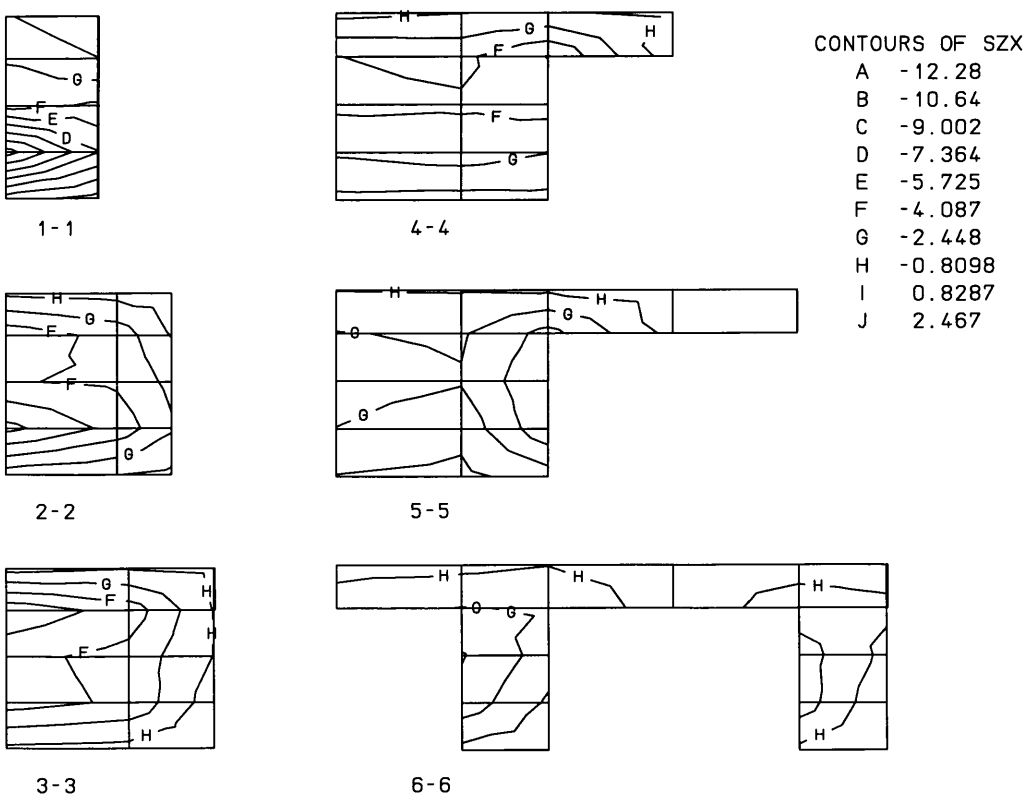

Load Increment 24 of slab No.5

Fig.6.19d Contours of Shear Stress τ_{xz}

From the contours of the shear stress, it is seen that the ribs have the largest shear stress and the more they are nearer to the loading pad, their stresses are higher. Although the deck is not as active as the ribs in resisting the load, they do participate in the resistance, especially for those near to the loading area. Tables 6.28 and 6.29 list the proportion of the total shear forces acting on the deck to the applied load at several sections with a distance x from the centre of the slab.

Table 6.28 Resistance of decks --Slab1 (Mohr-Coulom Model)

Load Level	x=220 *mm*	x=320 *mm*	x=590 *mm*	x=690 *mm*
load4	0.15	0.18	0.15	0.17
load6	0.18	0.19	0.16	0.17
load8	0.20	0.21	0.16	0.18
load12	0.21	0.21	0.17	0.18
load14	0.23	0.21	0.18	0.18

Table 6.29 Resistance of decks --Slab3 (Mohr-Coulom Model)

Load Level	x=220 *mm*	x=320 *mm*	x=590 *mm*	x=690 *mm*
Load4	0.12	0.16	0.12	0.15
load8	0.15	0.18	0.17	0.19
load16	0.17	0.18	0.17	0.18
load22	0.19	0.19	0.16	0.17
load24	0.19	0.19	0.16	0.16

From Tables 6.28 and 6.29, it is seen that the decks resist about 18~23% of the total shear forces in slab No.1, about 16~19% for slab No.3. As slab No.5 has a large local solid area, the deck's contribution is not significant and therefore not listed.

6.4.2 ANALYSIS RESULTS USING CONCRETE FRACTURE MODEL

The model of the slabs is the same as that of the previous analysis, shown in Fig.6.11, 1/8 of the slab is taken for the analysis. Here the concrete's fracture behaviour is considered by using the smeared crack modelling. Concrete will crack once the principle stress exceeds the tensile strength of the concrete. The cracks are in orthogonal directions in the local axes and might oriente in one, two, or three directions depending on how many principle stresses will exceed the strength limit. Once the cracks have occurred, the stresses perpendicular to the crack orientation are released but stresses along other directions are not affected. Under further loading, normal tensile stress can not be built up in the direction perpendicular to the crack orientation, but shear stress in the crack orientation can build up by employing the concept of shear retention. The concrete is considered at ultimate failure once cracks have occurred in all the three directions. The failure of concrete by shear is modelled by employing the Mohr-Coulomb criteria. Crushing in concrete is not modelled in this study. The reinforcement inside the slab are modelled as elastic-plastic material, the Von-Misses criteria being employed as the yield criteria.

The analysis are carried out in self-written program in combination with LUSAS, as described in chapter 4. The geometric data input of the model is the same as that of analysis using LUSAS, the material data input included the parameters defining the fracture characteristics and shear failure of concrete.

The material parameters of concrete used in the analysis are listed in Table 6.30.

Table 6.30 Material Parameters of the Slabs - Concrete

	Test Result		Analysis Parameters of Concrete Material					
	f_{cu} (N/mm^2)	f_t (N/mm^2)	f_c (N/mm^2)	f_t' (N/mm^2)	C_{37} (N/mm^2)	φ (°)	ε_{uc}	E_c (KN/mm^2)
Slab1	50.20	3.61	42.67	2.16	10.64	37	0.5E-3	30.0
Slab3	54.30	3.64	46.16	2.18	11.51	37	0.5E-3	30.9
Slab5	56.60	3.97	48.11	2.38	11.99	37	0.5E-3	31.3

Note:

f_t' tensile strength of concrete, taken as 60% of the splitting test result f_t;

C_{37} cohesion factor for Mohr-Column criteria, calculated using Eq.6.38 and taking φ as 37°;

φ the friction angle of concrete, taken as 37°;

ε_{uc} the maximum tensile strain the concrete can be extended after crack, beyond this value the shear retention does not maintain. The value in the table is about 5 time the tension strain at which the crack occurs.

The design yield strength of flexural reinforcement is $460 N/mm^2$, the elastic modulus is taken as $200 KN/mm^2$.

6.4.2.1 Results of Displacements

The results of the displacements at the centre of the slabs, using the crack model, were plotted in Fig.6.14a, b, and c for slabs No.1, 3 & 5 respectively. The load-deflection history of the analysis using the crack model is listed in Table 6.31. The calculated deflections in corresponding to the ultimate test load are listed in Table 6.32.

From Fig.6.14a, b & c, and Table 6.32, it is seen that the central deflection using the crack model is still less than the test result, but significantly improved compared with the results using Mohr-Coulomb model.

In the analysis, after the ultimate test load has been reached, the applied load can still increase and the slab is still stable. This is not consistent with the experimental observation, and may be due to the modelling of the cracking criteria and the post crack behaviour of the concrete.

Table 6.31 Crack Model Analysis Results of the Load Increment Level and the Corresponding Deflection at the Centre of Slabs

Load Increment Step	Slab 1		Slab 3		Slab 5	
	Load Level	Central Def.	Load Level	Central Def.	Load Level	Central Def.
	(KN)	*(mm)*	*(KN)*	*(mm)*	*(KN)*	*(mm)*
0	0.00	0.00	0.00	0.00	0.00	0.00
1	11.25	0.11	11.25	0.10	11.25	0.09
2	29.25	0.28	30.60	0.28	33.19	0.26
3	40.48	0.47	37.45	0.44	40.38	0.42
4	52.83	0.68	42.18	0.55	48.32	0.60
5	66.17	0.89	48.42	0.64	53.57	0.74
6	78.10	1.09	56.81	0.77	59.01	0.89
7	92.34	1.31	62.88	0.90	66.70	1.03
8	110.98	1.61	70.19	1.05	77.65	1.22

9	131.47	2.01	80.82	1.23	93.60	1.51
10	138.38	2.15	94.86	1.47	113.39	1.87
11	144.38	2.28	106.89	1.69	132.83	2.23
12	156.83	2.55	119.50	1.92	148.57	2.52
13	170.93	2.85	132.21	2.16	162.63	2.80
14	185.45	3.16	143.90	2.38	171.46	2.97
15	206.58	3.62	158.92	2.68	179.20	3.12
16	227.01	4.06	170.44	2.92	189.43	3.31
17	242.85	4.46	179.27	3.11	209.07	3.84
18	251.02	4.66	186.27	3.27	229.88	4.41
19	258.23	4.83	200.10	3.55	252.38	4.69
20	269.87	5.09	221.40	3.99	274.19	4.96
21	292.37	5.51	242.91	4.44	294.74	5.42
22			264.24	4.89	312.77	5.82
23			285.57	5.29	323.83	6.08
24					336.58	6.39
25					354.58	6.78
26					374.93	7.23
27					397.22	7.65

Table 6.32 Crack Model Analysis Result of the Central Deflection at the Ultimate Failure Load of Test

	Crack model *(mm)*	TEST (mm)
Slab 1	3.2	4.0
Slab 3	3.1	4.6
Slab 5	6.4	7.0

6.4.2.2 Crack Propagation in the Slabs

The propagation of the cracks in the slab No.1 and Slab No.3 is shown in Fig.6.20 & 6.21, where the cracks are shown in the sections cut along the central line and the first rib in x direction (lines A-A and B-B in Fig.6.12). Several load increment steps in the analysis are shown for each slab.

In Figs.6.20 and 6.21, the cracking status are shown at the Gauss points with different marks: a dot sign symbolise one crack at the point, a cross sign 'x' for two cracks and a tip sign '∨' for three cracks.

In Fig.6.20 (slab No.1), it is seen that the first type of crack appears quite early. At load increment 4, most of the part on the tension side of the slab has got cracks. These are mainly the vertical tension cracks and have no significantly influence on the stability of the slab. At load increment 6 (about 40% of the test ultimate load), the crack zones have reached 3/4 deep of the slab depth, and the second cracks have developed on the tension side near the loading pad. More and more second cracks appear when the load continuously increase. The zone of second cracks concentrated on the local solid part and on the rib at 370mm away from the centre of the slab. The load increments 18 and 20 are beyond the test load, but they are still plotted in order to look at the trend of the crack propagation. From the plots, we see that two band of second cracks have formed in the slab, one is near to the local solid area, the other is extended to the rib in line V-V. It appears these two bands are more close to the final crack pattern observed in the test.

In slab No.3, from Fig.6.21, it is seen that the first cracks distributed over most part of the slabs and the second crack zone forms a pattern similar to that of the test.

From the above, it appears the second cracks zone and the first crack zone near the loading pad forms the crack pattern similar to the test observation. The explanation is that the first crack in the slab is caused by the bending and torsion, they are not important for the shear analysis except those near the loading pad where the orientation of the first cracks coincides with the final failure pattern. In other area, the failure will not take place until the second cracks have formed a continuous zone,.

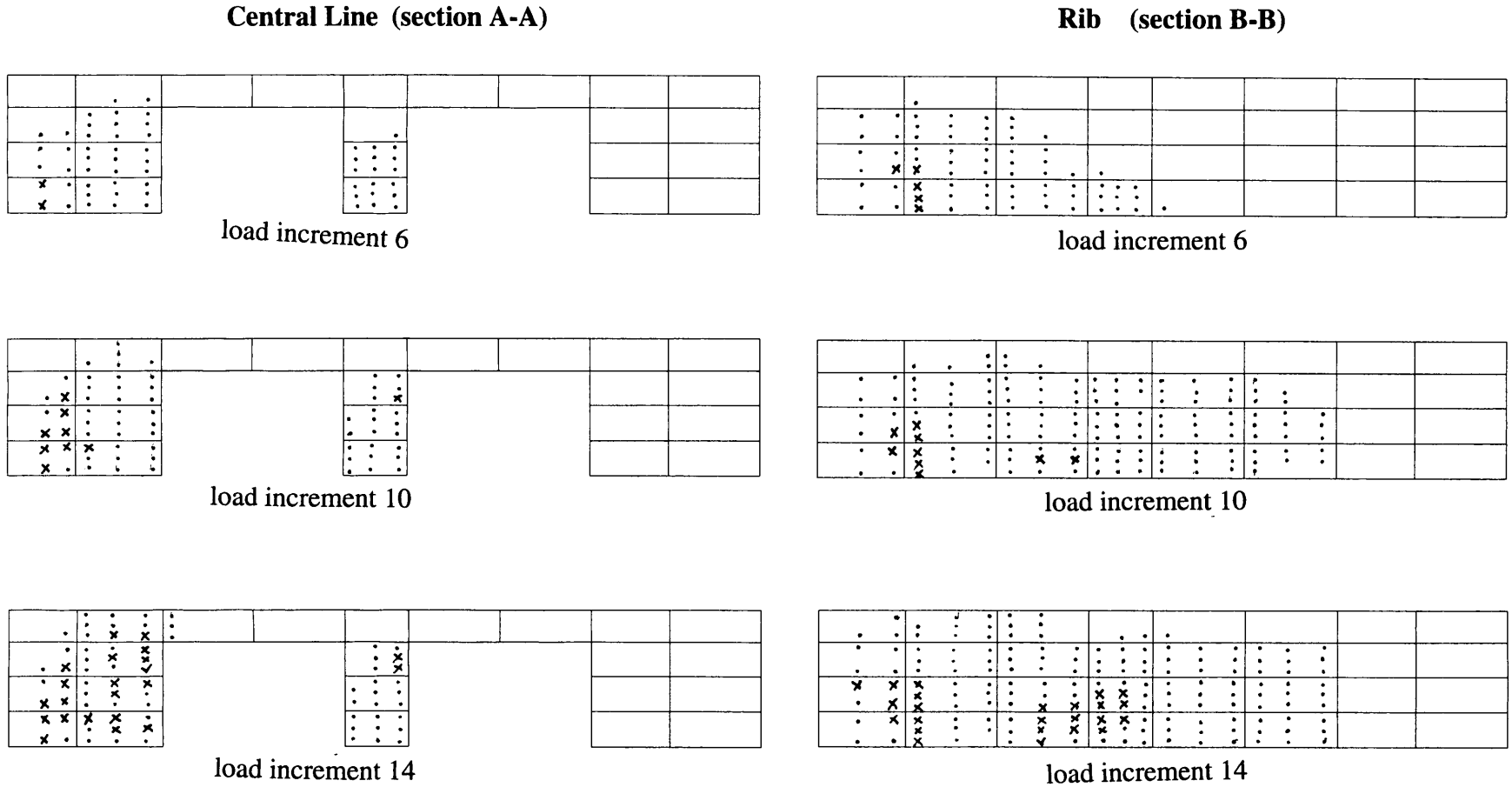

Fig.6.20 Propagation of Cracks on Slab No. 1

cont. to next page

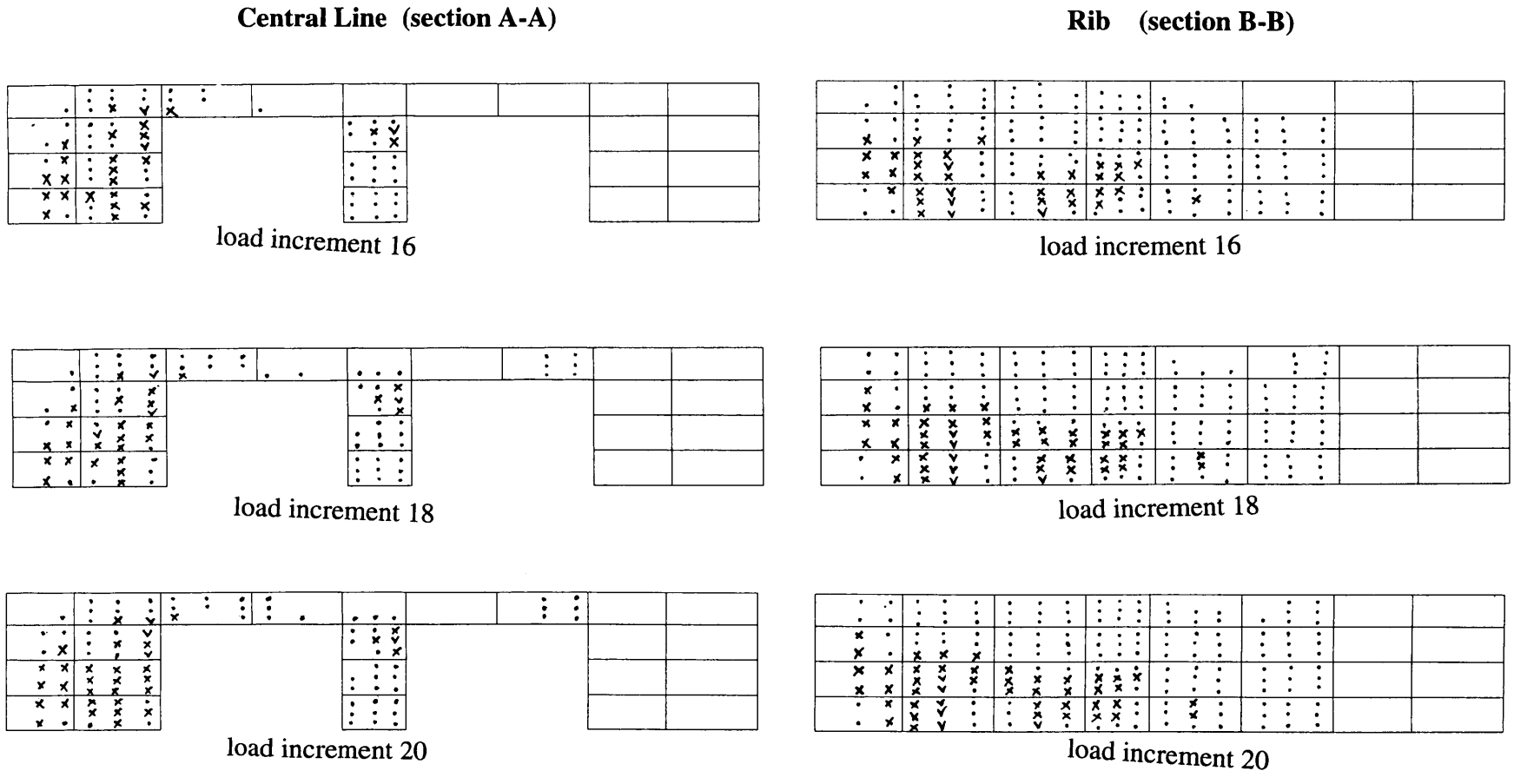

Fig.6.20 Propagation of Cracks on Slab No. 1

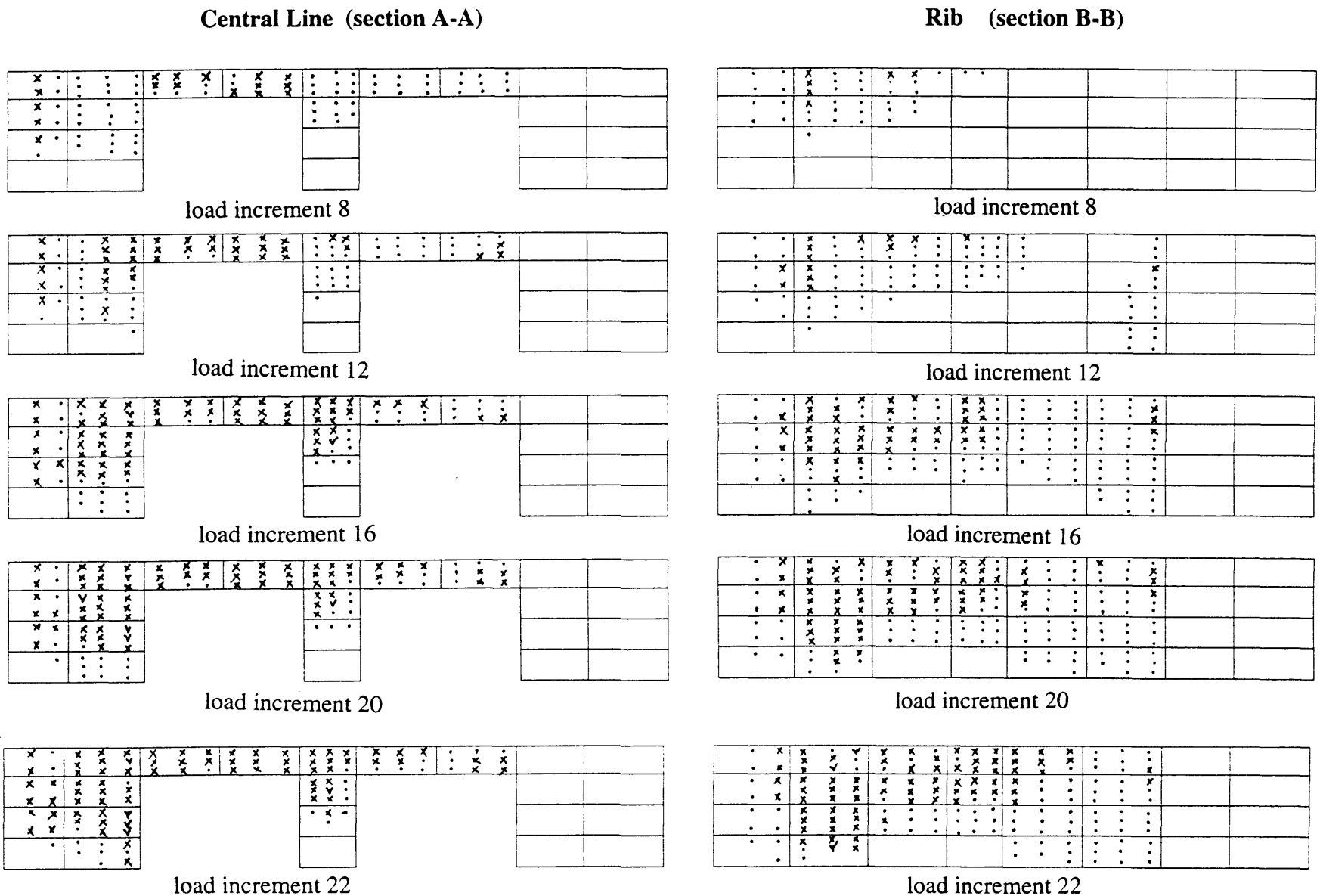

Fig.6.21 Propagation of Cracks on Slab No. 3

6.4.2.3 Stress Distribution and Redistribution

The shear stress τ_{xz} (shear stress in xz plan of global axes) on several cut-off sections are plotted for slabs No.1 and 5; the location of the sections were shown in Fig.6.16. Fig.6.22, 6.23 and 6.24 are for slab No.1, No.3 and No.5 respectively. In each of the figures, the crack patterns of several load increment levels are shown.

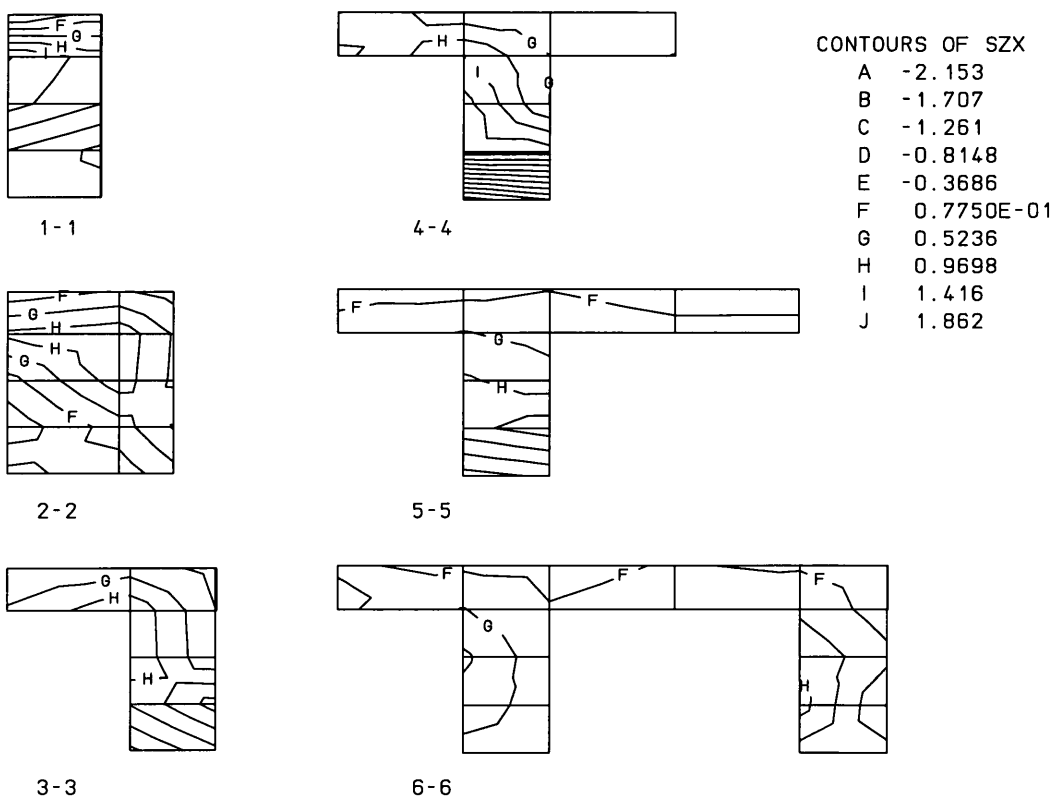

Load Increment 6 of slab No.1

Fig.6.22a Contours of Shear Stress τ_{xz}

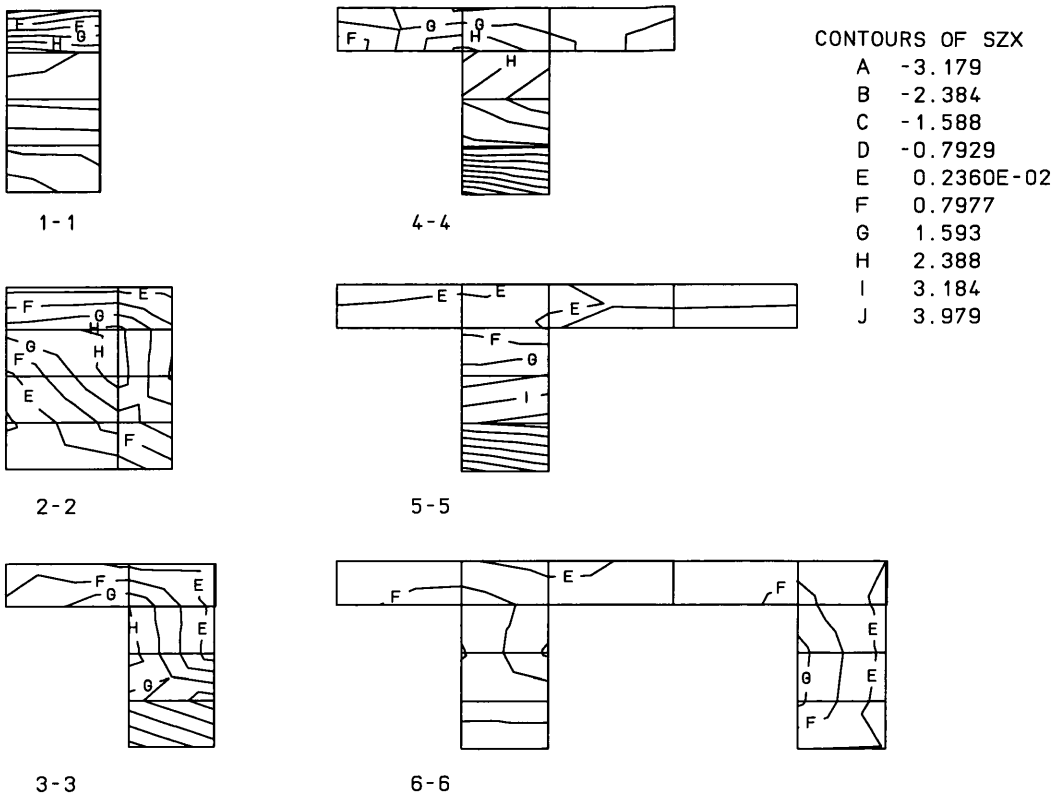

Load Increment 10 of slab No.1

Fig.6.22b Contours of Shear Stress τ_{xz}

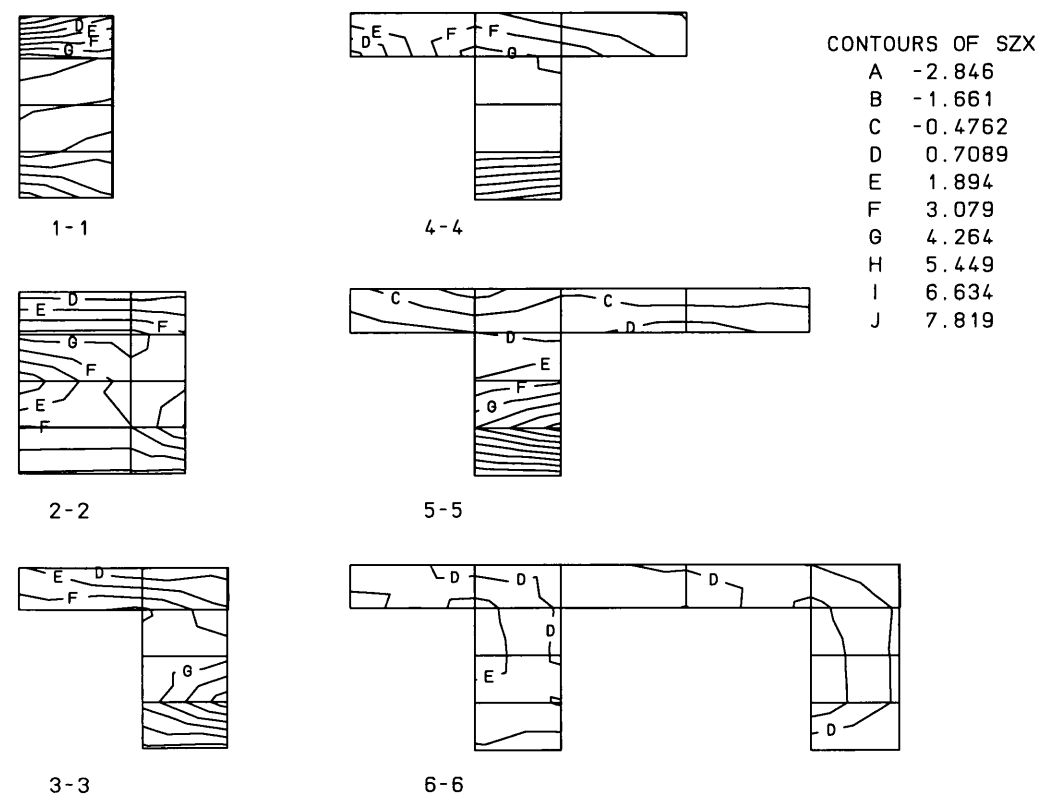

Load Increment 16 of slab No.1

Fig.6.22c Contours of Shear Stress τ_{xz}

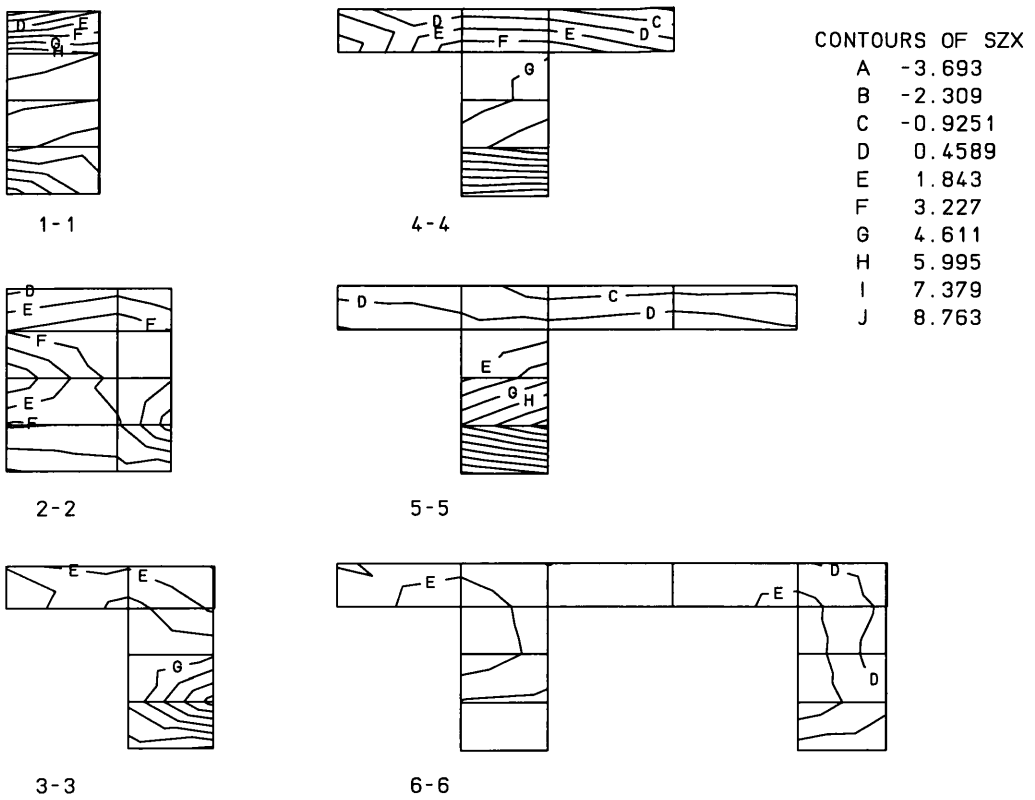

Load Increment 18 of slab No.1

Fig.6.22d Contours of Shear Stress τ_{xz}

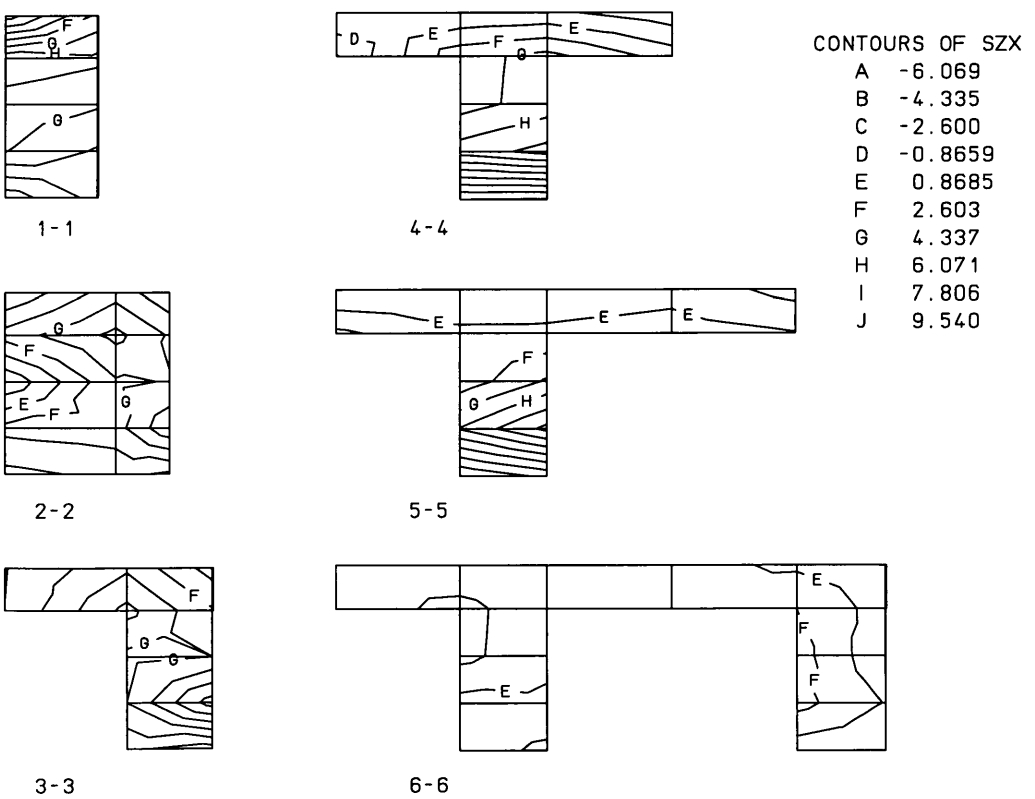

Load Increment 20 of slab No.1

Fig.6.22e Contours of Shear Stress τ_{xz}

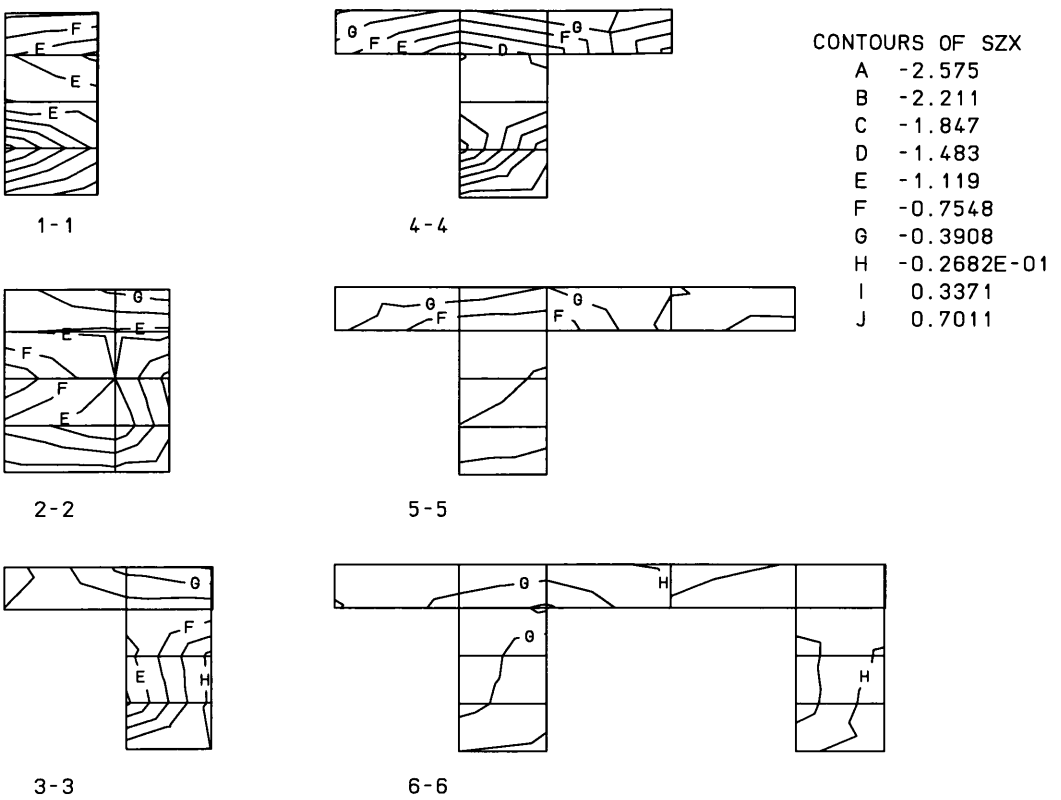

Load Increment 8 of slab No.3

Fig.6.23a Contours of Shear Stress τ_{xz}

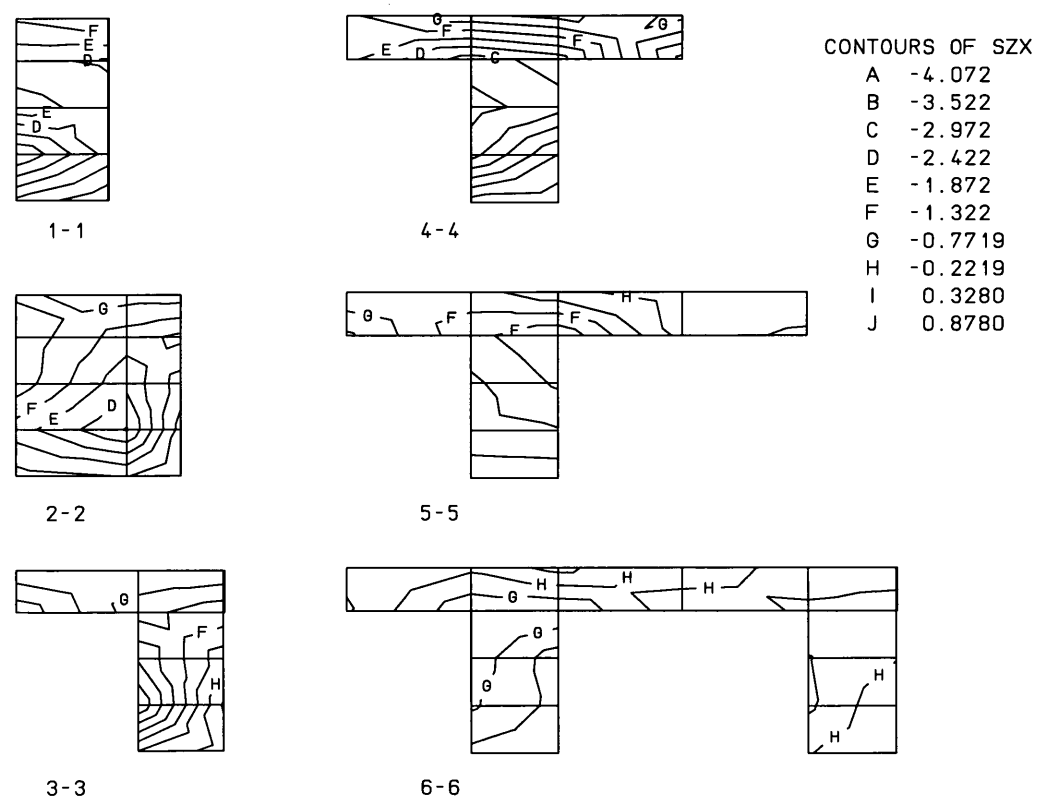

Load Increment 12 of slab No.3

Fig.6.23b Contours of Shear Stress τ_{xz}

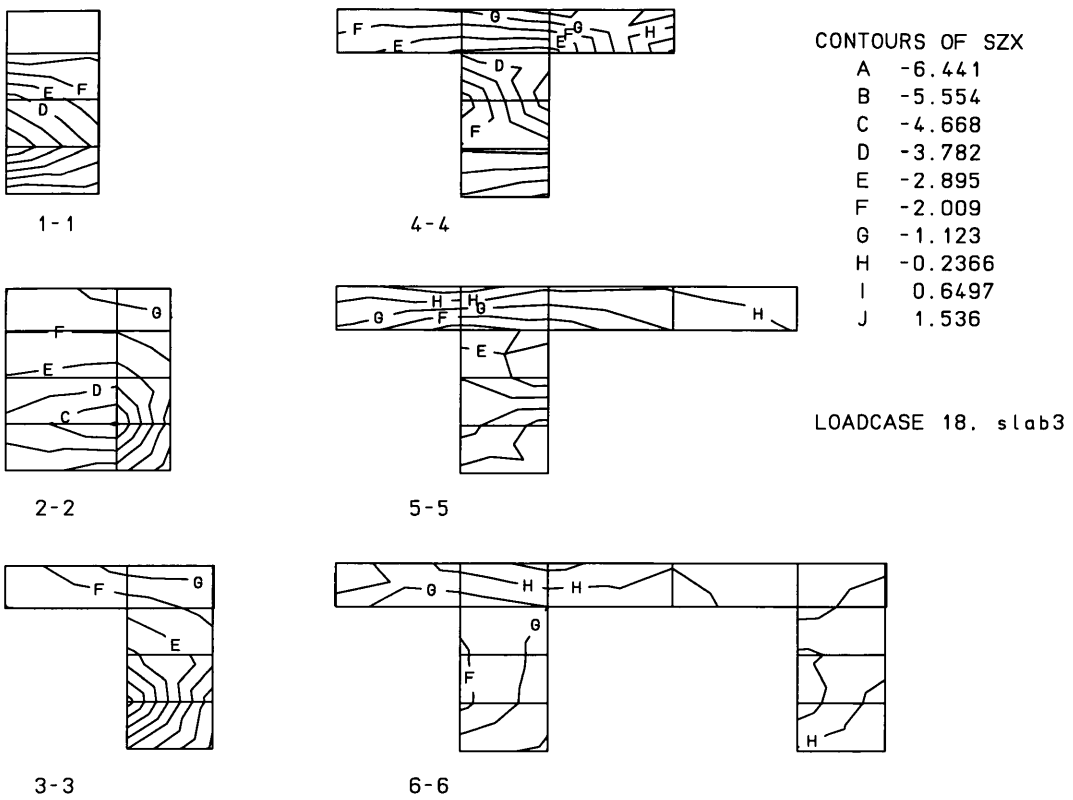

Load Increment 18 of slab No.3

Fig.6.23c Contours of Shear Stress τ_{xz}

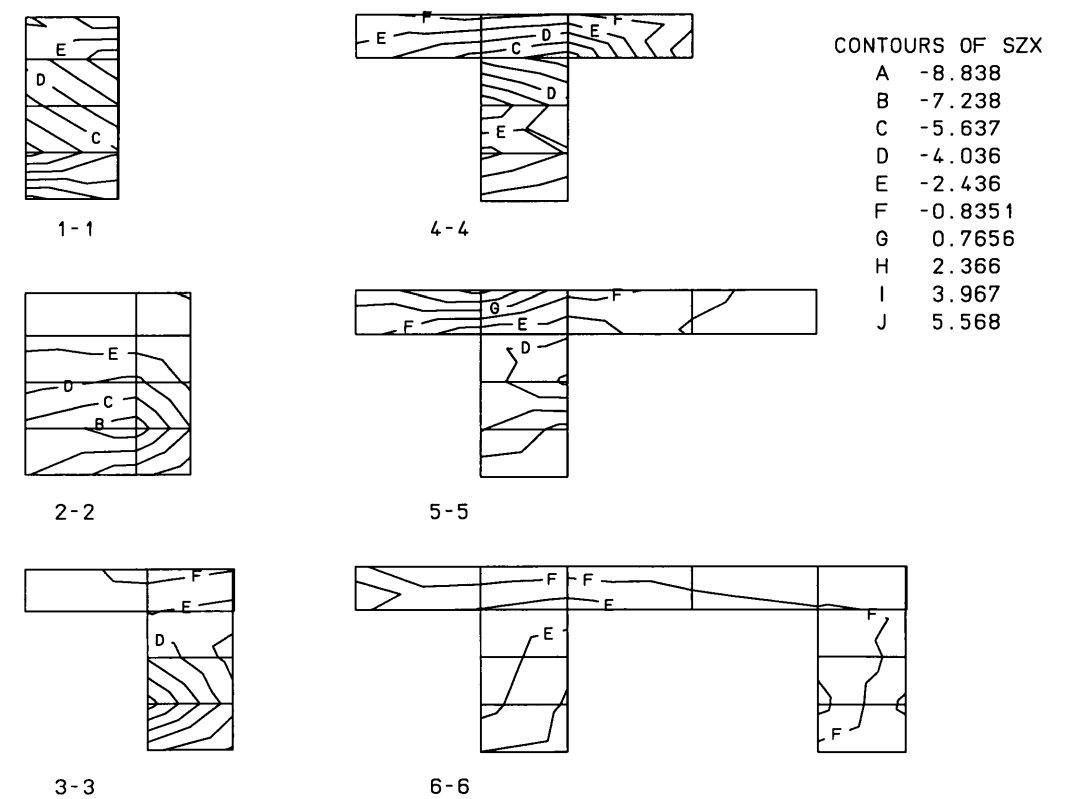

Load Increment 22 of slab No.3

Fig.6.23d Contours of Shear Stress τ_{xz}

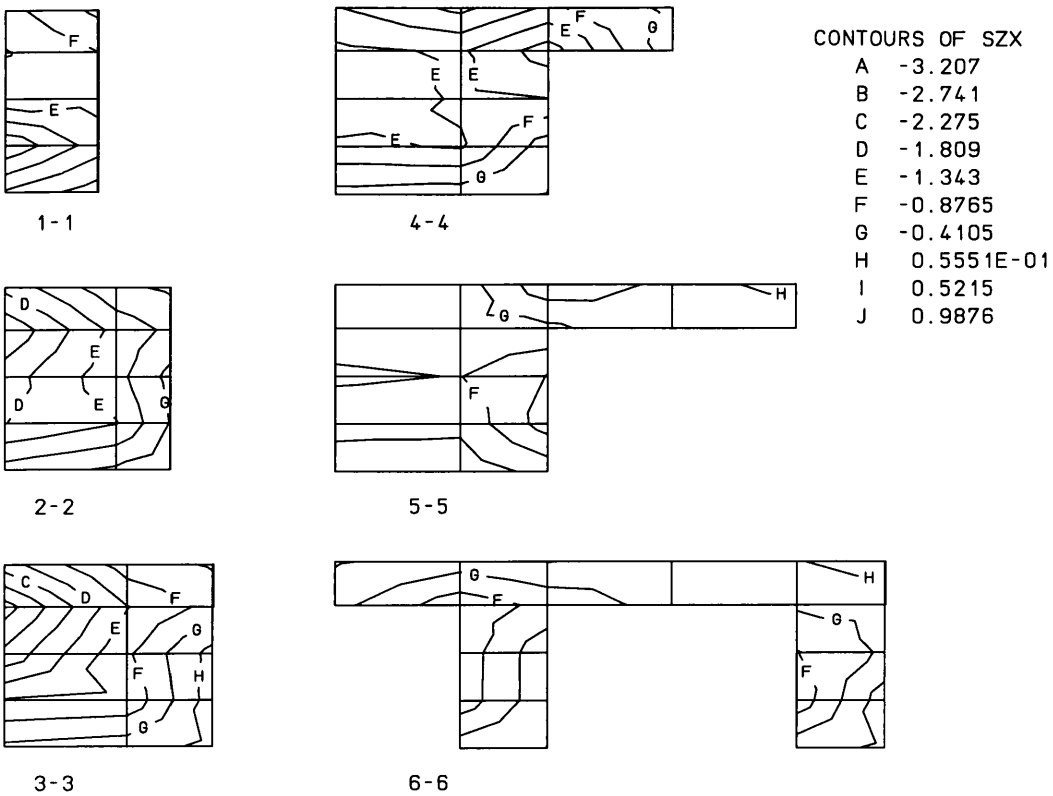

Load Increment 10 of slab No.5

Fig.6.24a Contours of Shear Stress τ_{xz}

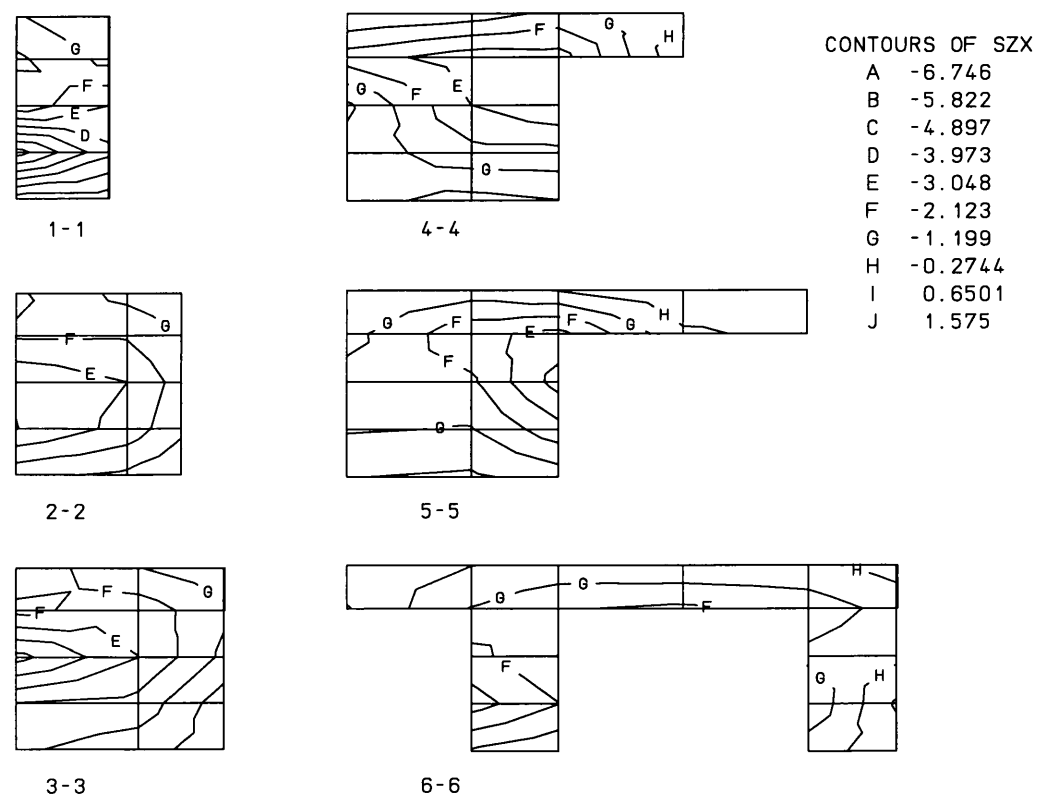

Load Increment 18 of slab No.5

Fig.6.24b Contours of Shear Stress τ_{xz}

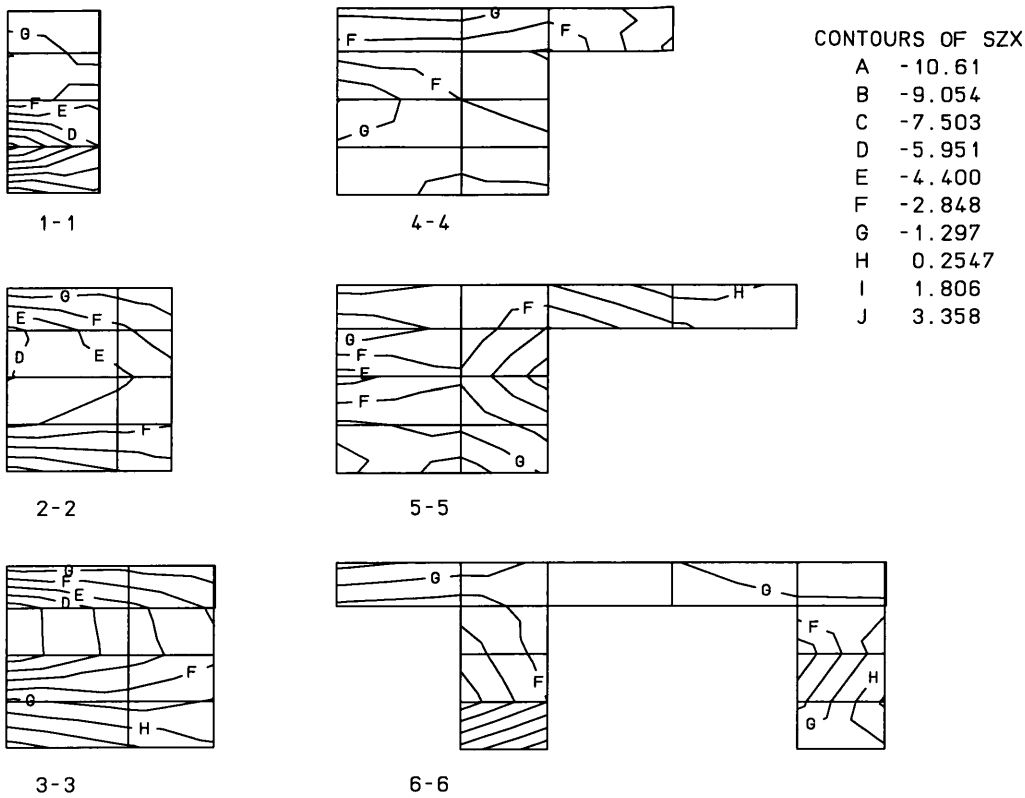

Load Increment 24 of slab No.5

Fig.6.24c Contours of Shear Stress τ_{xz}

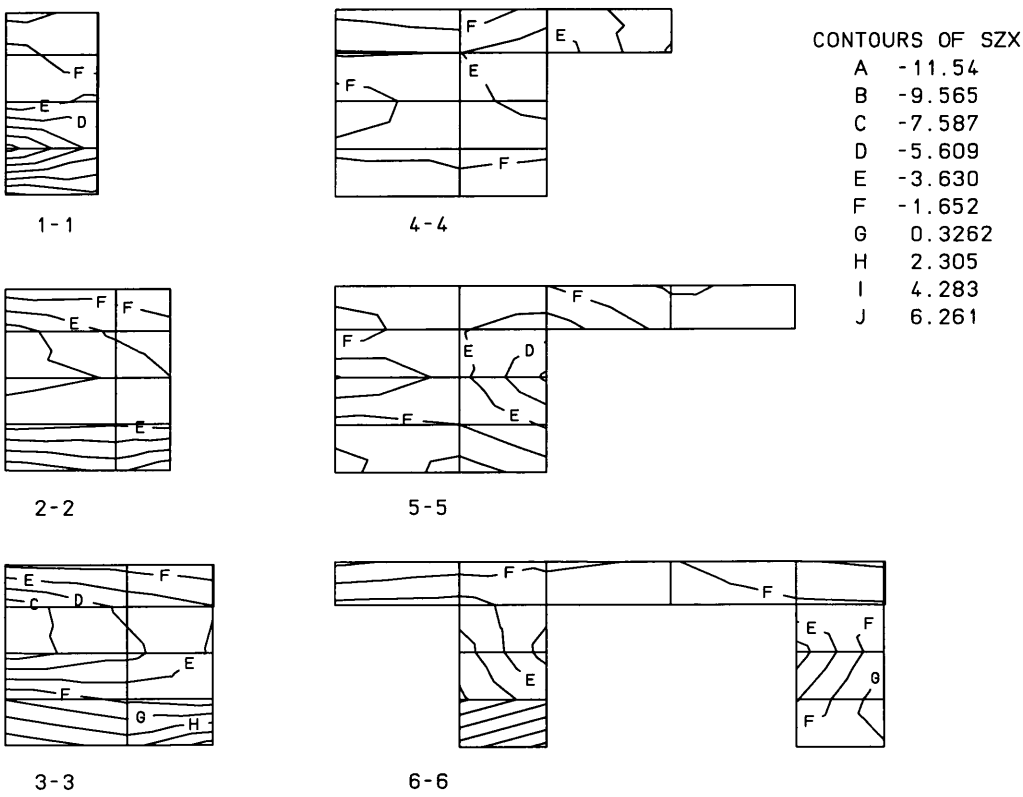

Load Increment 26 of slab No.5

Fig.6.24d Contours of Shear Stress τ_{xz}

From the stress contours it is seen that shear stress in the deck is still substantially compared with that of ribs. The total shear force along xz plan in the deck is calculated and its proportion in relative to the total applied load is listed in Tables 6.33 and 6.34 for slabs No.1 and 5.

Table 6.33 Ratio of Shear Resistance of Deck (slab1)
(Concrete Fracture Model)

Load Increment Level	x=220	x=320	x=590	x=690
load 6	0.27	0.21	0.20	0.19
load 10	0.32	0.19	0.15	0.17
load 16	0.33	0.23	0.18	0.17
load 18	0.32	0.19	0.14	0.13
load 20	0.30	0.19	0.12	0.12

Table 6.34 Ratio of Shear Resistance of Deck (slab3)
(Concrete Fracture Model)

	320	590	220	690
load 8	0.22	0.20	0.18	0.17
load12	0.22	0.21	0.16	0.16
load18	0.25	0.22	0.17	0.16
load22	0.25	0.17	0.12	0.14

From the above tables, it is seen that the rib's participation in shear resistance is quit a big proportion, at about 17~33% in load increment 16 for slab No.1, and 16~25% at load increment 18 for slab No.3. These tables also indicate that the deck near to the loading area takes more shear force than those far away; the proportion of the shear forces the decks take varies from the history of the loading; deck in slab No.1, which has the deck in the compression side takes more load than that of slab No.3, which has the deck in the tension side, this is probably due to the tension cracks in the deck of slab No.3.

6.5 ALTERNATIVE METHOD CALCULATING THE PUNCHING LOAD OF RC WAFFLE SLABS

In the above sections, the analysis was carried out by using upper bound analysis, following BS8110, and finite element analysis. In this section, the alternative methods, which were described in section 3.8 of chapter 3, will be applied to the twelve slabs. The detailed analysis are described in Appendix A, the main results are summarised in the following tables.

In every analysis, two sets of calculation are carried out: one without limits on the material and geometric parameters, and the other with the limit removed.

The symbols used in the tables are explained below.

B	dimension of the nominal punching perimeter;
S_{rib}	cross section area of the ribs intersected with the nominal perimeter;
S_{dk}	area of deck slab intersected with the nominal perimeter;
S	$=S_{rib}+S_{dk}$;
ρ	ratio of flexural steel;
f_{cu}	compressive strength of concrete cube;
υ_c	nominal shear strength of concrete;
υ_{sv}	is the nominal shear strength provided by the links;
P_c	shear resistance of concrete;
P_{sv}	shear resistance of stirrups;
f_{sv}	yield strength of stirrups;
a_{sv}	the section area of a leg of the stirrup;
n_1	coefficient for affine slab;
d_{aff}	depth of the affine solid slab.

6.5.1 METHOD ONE

The detailed analysis is described in appendix A, here the results are tabulated in Table 6.35.

Table 6.35 Punching Load Using Alternative Method One

	B (mm)	S_{rib} (mm^2)	S_{dk} (N/mm^2)	ρ $(\%)$	f_{cu} (N/mm^2)	υ_c (N/mm^2)	υ_{sv} (N/mm^2)	P_{rib} (KN)	P_{dk} (KN)	P (KN)
slab 1	525	70000	53900	2.15	40 (50.2)	1.60 (1.72)	0.0	111.7 (120.4)	86.0 (92.7)	197.7 (213.0)
slab 2	525	35000	63700	2.15	40 (64.7)	1.60 (1.87)	0.0	55.8 (65.5)	101.6 (119.1)	157.4 (184.6)
slab 3	525	70000	53900	2.15	40 (54.3)	1.60 (1.77)	0.0	111.7 (123.9)	86.0 (95.4)	197.7 (219.3)
slab 4	525	35000	63700	2.15	40.0 (49.6)	1.60 (1.71)	0.0	55.8 (59.8)	101.6 (108.9)	157.4 (168.7)
slab 5		170000	25900	1.16	40.0 (56.6)	1.30 (1.30)	0.0	220.4 (248.2)	33.6 (37.8)	254.0 (286.0)
slab 6	610	105000	56000	2.15	40.0 (48.0)	1.60 (1.70)	0.0	167.5 (178.5)	89.3 (95.2)	256.8 (273.7)
slab 7	525	70000	53900	2.15	31.2 (31.2)	1.47 (1.47)	2.24 (2.24)	259.6 (259.6)	79.1 (79.1)	338.7 (338.7)
slab 8	525	35000	63700	2.15	31.2 (31.2)	1.47 (1.47)	2.24 (2.24)	129.8 (129.8)	93.5 (93.5)	223.3 (223.3)
slab 9	525	70000	53900	2.15	37.1 (37.1)	1.65 (1.65)	2.24 (2.24)	266.0 (266.0)	83.9 (83.9)	349.9 (349.9)
slab 10	525	35000	63700	2.15	37.8 (37.8)	1.56 (1.56)	2.24 (2.24)	133.2 (133.2)	99.7 (99.7)	232.9 (232.9)
slab 11	525	170000	25900	1.16	37.1 (37.1)	1.27 (1.27)	0.56 (0.56)	309.4 (309.4)	32.8 (32.8)	342.2 (342.2)
slab 12	525	105000	56000	2.15	37.8 (37.8)	1.56 (1.56)	1.36 (1.36)	211.9 (211.9)	87.6 (87.6)	299.5 (299.5)

6.5.2 METHOD TWO

The detailed analysis is described in appendix A, here the results are tabulated in Table 6.36.

Table 6.36 Punching Load Using Alternative Method Two

	B (mm)	S_{rib} (mm^2)	S_{dk} (N/mm^2)	ρ $(\%)$	f_{cu} (N/mm^2)	υ_c (N/mm^2)	υ_{sv} (N/mm^2)	P_{rib} (KN)	P_{dk} (KN)	P (KN)
slab 1	525	70000	53900	1.01	40 (50.2)	1.24 (1.33)	0.0	86.5 (93.1)	66.6 (71.7)	153.1 (165.0)
slab 2	525	35000	63700	1.01	40 (64.7)	1.24 (1.45)	0.0	43.2 (50.8)	87.7 (92.4)	122.0 (143.2)
slab 3	525	70000	53900	1.01	40 (54.3)	1.24 (1.37)	0.0	86.5 (95.9)	66.6 (73.8)	153.1 (169.5)
slab 4	525	35000	63700	1.01	40.0 (49.6)	1.24 (1.33)	0.0	43.3 (46.6)	78.9 (84.7)	122.2 (131.3)
slab 5		170000	25900	0.86	40.0 (56.6)	1.18 (1.32)	0.0	199.8 (224.4)	30.4 (34.2)	230.2 (258.4)
slab 6	610	105000	56000	1.01	40.0 (48.0)	1.24 (1.32)	0.0	130.0 (138.6)	69.2 (73.9)	199.2 (211.7)
slab 7	525	70000	53900	1.01	31.2 (31.2)	1.14 (1.14)	2.24 (2.24)	236.6 (236.6)	61.4 (61.4)	298.0 (298.0)
slab 8	525	35000	63700	1.01	31.2 (31.2)	1.14 (1.14)	2.24 (2.24)	118.3 (118.3)	72.6 (72.6)	190.9 (190.9)
slab 9	525	70000	53900	1.01	37.1 (37.1)	1.21 (1.21)	2.24 (2.24)	241.3 (241.3)	65.0 (65.0)	306.3 (306.3)
slab 10	525	35000	63700	1.01	37.8 (37.8)	1.22 (1.22)	2.24 (2.24)	120.9 (120.9)	77.4 (77.4)	198.3 (198.3)
slab 11	525	170000	25900	0.86	37.1 (37.1)	1.18 (1.18)	0.56 (0.56)	295.0 (295.0)	30.4 (30.4)	325.0 (325.0)
slab 12	525	105000	56000	1.005	37.8 (37.8)	1.22 (1.22)	1.36 (1.36)	175.2 (175.2)	68.0 (68.0)	243.2 (243.2)

6.6.3 METHOD THREE

The detailed analysis is described in appendix A, here the results are tabulated in Table 6.37.

Table 6.37 Punching Load Using Alternative Method Three

	n_1	d_{aff} (mm)	B (mm)	S (mm^2)	ρ $(\%)$	f_{cu} (N/mm^2)	υ_c (N/mm^2)	P_c (KN)	n	f_{sv} (N/mm^2)	a_{sv} (mm^2)	P_{sv} (KN)	P (KN)
Slab 1	0.605	75.62	376.9	113993	2.38	40 (50.2)	1.65 (1.78)	188.1 (202.9)					188.1 (202.9)
Slab 2	0.605	75.62	376.9	113993	1.19	40 (64.7)	1.31 (1.54)	149.3 (175.3)					149.3 (175.3)
Slab 3	0.605	75.62	376.9	113993	1.98	40 (54.3)	1.55 (1.72)	176.9 (195.9)					176.9 (195.9)
Slab 4	0.605	75.62	376.9	113993	1.59	40.0 (49.6)	1.44 (1.55)	164.2 (176.6)					164.2 (176.6)
Slab 5	0.605	75.62	525	225944	1.33	40.0 (56.6)	1.36 (1.53)	307.3 (345.0)					307.3 (345.0)
Slab 6	0.605	75.62	610	184513	1.66	40.0 (48.0)	1.46 (1.55)	269.4 (286.4)					269.4 (286.4)
Slab 7	0.605	75.62	376.9	113993	2.38	31.2 (31.2)	1.52 (1.52)	173.1 (173.1)	16	250	28.27	113.1	286.2 (286.2)
Slab 8	0.605	75.62	376.9	113993	1.19	31.2 (31.2)	1.21 (1.21)	138.0 (138.0)	8	250	28.27	56.5	194.5 (194.5)
Slab 9	0.605	75.62	376.9	113993	1.98	37.1 (37.1)	1.51 (1.51)	172.5 (172.5)	16	250	28.27	113.1	285.6 (285.6)
Slab 10	0.605	75.62	376.9	113993	1.59	37.8 (37.8)	1.41 (1.41)	161.2 (161.2)	8	250	28.27	56.5	217.7 (217.7)
Slab 11	0.605	75.62	525.0	225944	1.33	37.1 (37.1)	1.33 (1.33)	299.5 (299.5)	16	340	12.56	68.4	367.9 (367.9)
Slab 12	0.605	75.62	610.0	184513	1.66	37.8 (37.8)	1.44 (1.44)	265.0 (265.0)	8	340	12.56	34.2	299.2 (299.2)

6.6 CONCLUSIONS

In this chapter, the calculations were carried out for all the twelve slabs tested in this study. The methods employed include Upper Bound Analysis, Finite Element Analysis, BS8110's provisions, and three alternative method proposed in secion 3.8 of chapter 3.

In the upper bound analysis, first the formulae derived in chapter 3 were further developed to reflect the existence of local solid area in the waffle slabs; second, several analysis parameters, relating to the plastic (effective) strength of concrete, the yield strength reduction for stirrups due to poor anchorage, and the choice between effective depth and total depth, were determined for the RC waffle slabs. After the determination of the analysis parameters, the results of upper bound analysis were obtained.

The BS8110's provisions for RC waffle slabs were applied to the model slabs; the analysis included two methods to calculate the shear resistance of the stirrups: one treating stirrups as that in solid slabs, the other treating stirrups as in beams.

The non-linear finite element analysis was applied to the waffle slabs No.1 3 & 5. In the analysis, two types of material models were employed in simulating the behaviour of concrete, one is the Mohr-Coulomb criteria and the other is the concrete fracture model. The deflections of the slabs, the propagation of the yield zone or cracks in the slabs, and the distribution of shear stress τ_{xy} on several sections of the slabs were described. The FEA analysis using both types of material models failed to predict the ultimate failure load of the slabs.

Finally the proposed alternative methods for calculating the punching loads of waffle slabs were applied to the slabs tested in this study.

The analysis results obtained in this chapter will be compared with the test results in chapter 7.

CHAPTER 7

COMPARISON BETWEEN THEORETICAL AND EXPERIMENTAL RESULTS

7.1 INTRODUCTION

In chapter 5, the results of twelve slabs tested in this study were listed; in Chapter 6, methods of non-linear finite element and upper bound analysis were applied to obtain the theoretical results. In chapter 6, the BS8110 method for calculating the punching shear capacity of waffle slabs was also used to test if it fairly predicted the punching load; further, a few alternative methods to calculate the punching load were also applied to the model slabs.

In this chapter, the results of various methods used are compared with the experimental results.

7.2 COMPARISON OF EXPERIMENTAL RESULTS WITH THOSE OBTAINED USING BS8110 METHOD

The results of the analysis of the 12 model slabs using the provisions of BS8110 were listed in Tables 6.23 to 6.24. In the following, the calculated results are compared with the experimental ones, the ratios of the calculated loads to test loads are tabulated in Tables 7.1 and 7.2. In Tables 7.1 and 7.2, method BS1 refers to BS8110 method, method BS2 refers also to BS8110 method but with the resistance of stirrups calculated by adopting the method for beams, as described in Chapter 6. The values inside brackets are those calculated with the limits removed on the parameters flexural steel ρ, cube strength of concrete f_{cu}, and the effective depth of the slab d. The discussion considers slabs with and without shear reinforcements.

7.2.1 SLABS WITHOUT SHEAR REINFORCEMENT

For the six slabs without stirrups, theoretical results are the same using these two methods BS1 and BS2, Table 7.1. It is seen from the table that the ratios, ranging from 0.3 to 0.7 and an average of 0.56, are significantly less then 1.0, i.e., the calculated

failure loads are much smaller than the experimental ones. Although the values inside the bracket are somewhat higher they are no significantly improvement. From these results, it appears that the actual punching capacity of these RC waffle slabs are much greater than what BS8110 suggests. It is apparent therefore that the code underestimates the shear capacity of RC waffle slabs; this is possibly due to neglecting the interaction between the orthogonal ribs and the resistance of the top deck of the slab.

Table 7.1 Ratio between Calculated Failure Loads and Tests (BS8110)
(Waffle Slabs Without Shear Links) Unit: KN

Group	Series No.	Configur ation	Methd BS1	Methd BS2
No-link	1	M#	0.67 (0.78)	0.67 (0.78)
	2	M+	0.38 (0.48)	0.38 (0.48)
	3	C#	0.69 (0.76)	0.69 (0.76)
	4	C+	0.30 (0.32)	0.30 (0.32)
	5	C#S	0.70 (0.78)	0.70 (0.78)
	6	C+S	0.63 (0.67)	0.63 (0.67)
Average			0.56 (0.63)	0.56 (0.63)

Table 7.2 Ratio between Calculated Failure Loads and Tests (BS8110)
(Waffle Slabs With Shear Links) Unit: KN

Group	Series No.	Configur ation	Methd BS1	Methd BS2
	7	M#L	1.15 (1.19)	1.00 (1.04)
	8	M+L	0.84 (0.87)	0.67 (0.70)
Link	9	C#L	1.15 (1.15)	1.00 (1.00)
	10	C+L	0.76 (0.76)	0.60 (0.60)
	11	C#SL	0.95 (0.95)	0.88 (0.88)
	12	C+SL	0.90 (0.90)	0.82 (0.82)
Average			096 (0.97)	0.83 (0.84)

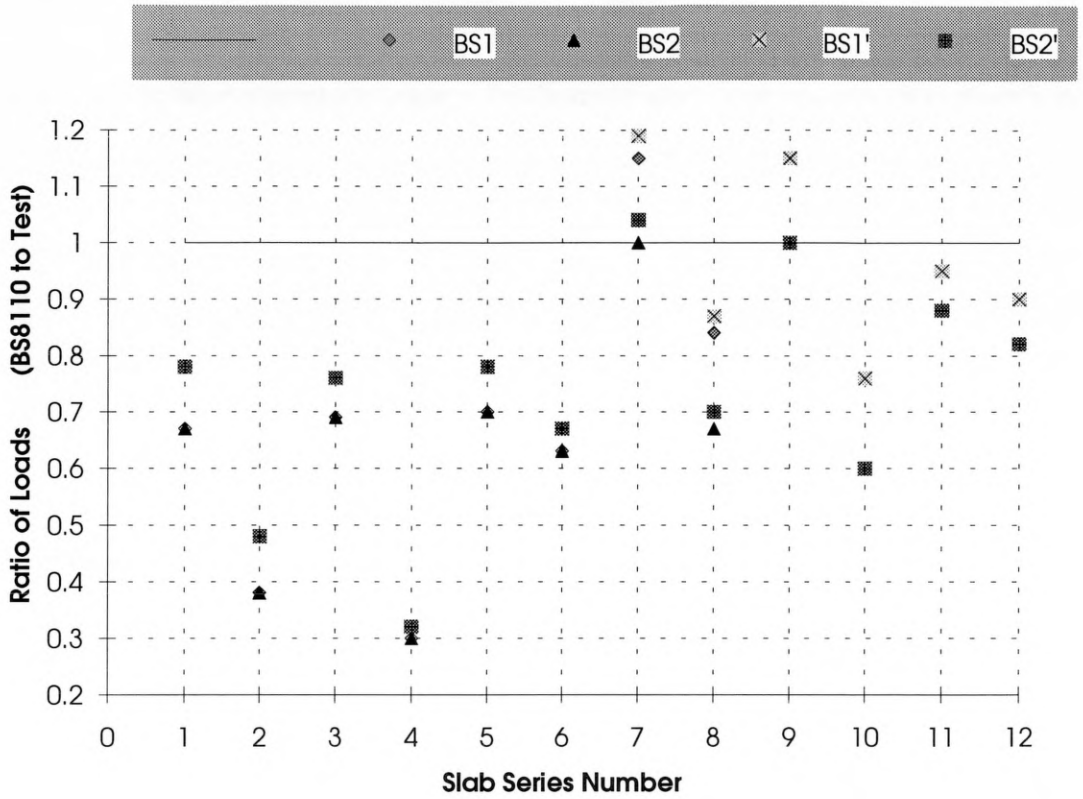

Fig.7.1 Plot of the Ratios of Calculated (BS8110) and Experimental Punching Failure Loads

In Fig.7.1 the ratios between the punching loads obtained using BS8110 and experiments are plotted. BS1' and BS2' refer to the methods one and two without the limitations on parameters.

From Table 7.1, it is seen that the theoretical results of slabs 2 and 4, with ratios of 0.38 and 0.3 respectively, are particularly small compared with the test results. This is due to the method employed in BS8110, which considers the shear resistance of the RC waffle slabs as the summation of the resistance of the ribs intersected with the nominal punching perimeter. Following such a method will inevitably induces the sudden jumps of the punching load, as shown in Fig.7.2, which illustrates the change of load against the punching perimeter. In Fig.7.2, there are four assumed nominal punching perimeters A, B, C & D, they intersect with 4, 12, 16 and 20 ribs respectively. When the punching perimeter increases from A to B, the punching load will increase three times. This also suggest a sudden decrease of the punching load when the punching perimeter decreases from B to A. This can hardly be true as the difference between the two perimeters is only a width of a rib; there should be some decrease of the load but not such an amount. When using BS8110, if the nominal perimeter happens to be in the position of

perimeter A, obviously the punching load will be significantly underestimated. In calculation of the model slabs, slabs No.2 and 4 happen to be like this.

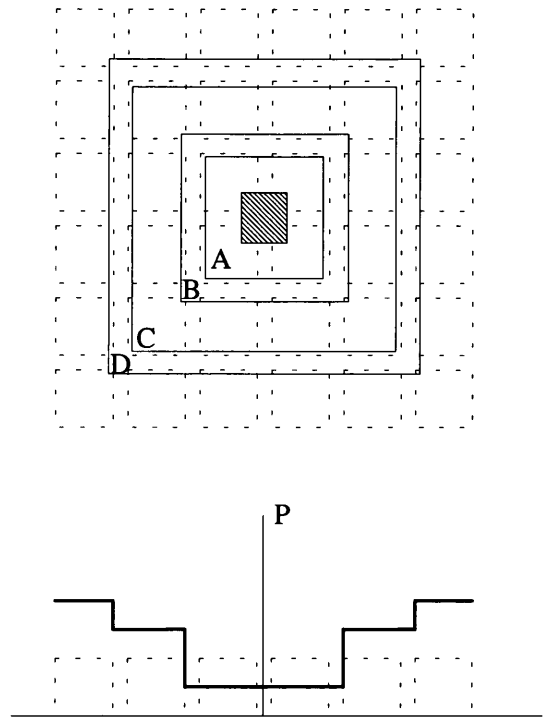

Fig.7.2 Variation of Punching Load against the Nominal Punching Perimeter

Slabs No 1 & 3 and No.2 & 4 have different configuration, but with identical loading pad, same depth and similar amount of flexural reinforcement. By using BS8110, these slabs will have the same dimension of nominal punching perimeter, but the punching perimeter of slabs No.1 & 3 intersect with 8 ribs, whereas slabs No. 2 & 4 intersects with only 4 ribs. Therefore, if the strength of concrete is the same the punching capacity of slabs No.1 & 3 will double those of slabs No.2 & 4. It should be noted that the tests results show that the punching load capacity of these four slabs are close to each other. This demonstrates that the punching load is not particularly sensitive to the position of the loading pad on the slabs (or the configuration of slabs), or the number of ribs intersecting the nominal punching perimeter; it appears that the punching load depends on the dimension of the loading pad, the punching perimeter, the depth of the slabs, similar to that of a solid slab. This is to say that the punching load capacity of RC waffle slabs is somewhat like that in a solid slab, the shear resistance gradually changing with the change of the punching perimeter.

From the above analysis, it can be concluded that it is not proper to calculate the punching load capacity of a RC waffle slab by using the number of ribs intersected by

the nominal pinching perimeter; it might be better to consider the waffle slab as a solid slab of uniform thickness which responds to the punching shear in a continuous manner.

7.2.2 SLABS WITH SHEAR REINFORCEMENT

As was noted the first group of slabs (No.1~6) have no stirrups and the second group (No.7~12) have stirrups. The comparative study is to find out how effective the stirrups are in carrying shear load and how the BS8110 method copes with slabs with stirrups. The two groups of slabs in the tests are not strictly comparable as their strength of concrete are not the same even though other parameters are identical. The concrete strength in the second group of slabs is smaller than those of the first. The stirrups do increase the load capacity, while, the drop in concrete strength will reduce the shear resistance. It is understood that the influence of the change of the concrete strength on the punching load can be estimated as BS8110's calculation formulae can accommodate the change of concrete strength. Therefore, we will still consider these two groups of slabs comparable.

The objective here is to compare the load increment that actually occurred in the tests between the two groups of slabs and that predicted by BS8110. Table 7.2 lists the ratios of the punching load between the calculation and test. Here the results of methods BS1 and BS2 are different, because the former uses the formulae for solid slabs to calculate the shear resistance of the stirrups, while, the latter uses the formulae for beams.

At first glance the values in Table 7.2 seem quite close to one, especially the results from method BS1, that is to say the calculated results are close to the test results. This however needs a close examination. As stated before, in a slab with shear reinforcements both the concrete section and the shear reinforcements contribute to the punching load capacity. In the last section it has been shown that the punching load capacity of RC waffle slabs without shear reinforcement is underestimated by BS8110 method. If the concrete's part is underestimated, and the reinforcements' part is overestimated, then the combination of the two parts may still give a close estimation but with a wrong proportion between the two constitutive parts. This appears to be the case for the RC waffle slabs with stirrups. In Table 7.3 and Fig.7.3, the ratios of the punching loads between each pair of slabs, reinforced/unreinforced, are listed and plotted, i.e., slab No. 7 against No.1, No.8 against No.2 and so on.

Table 7.3 Comparison of Punching Load of Slabs with & without Stirrups (BS8110)

Group	Configur ation	test	methd 1	methd 2
Slab7/Slab1	M#	1.45	2.51 (2.20)	2.18 (1.92)
Slab8/SLab2	M+	1.23	2.73 (2.20)	2.18 (1.77)
Slab9/Slab3	C#	1.58	2.64 (2.39)	2.29 (2.07)
Slab10/Slab4	C+	1.14	2.89 (2.69)	2.30 (2.15)
Slab11/Slab1	C#S	1.09	1.49 (1.33)	1.39 (1.24)
Slab12/Slab6	C+S	0.96	1.37 (1.29)	1.25 (1.18)
Avg.		1.24	2.27 (2.02)	1.93 (1.72)

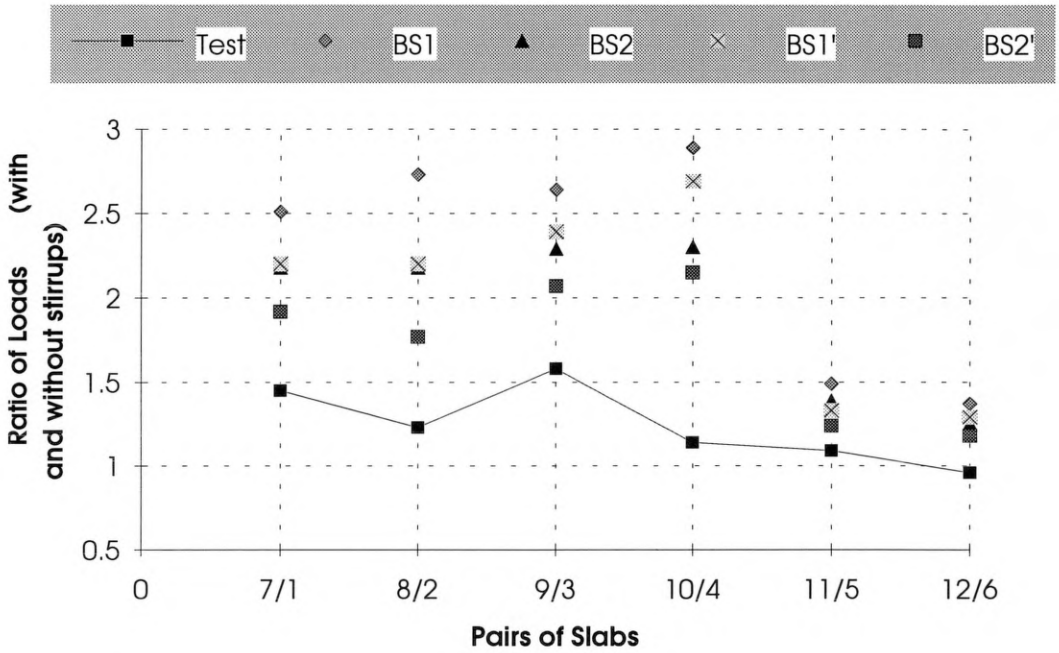

Fig.7.3 Ratio of Punching Load Between Slabs with and without Stirrups

From table 7.3, experimental results show that the ratios of slabs No.7~8 to No.1~4 are 1.45, 1.23, 1.58 and 1.14 respectively, i.e., the increase of the load are 45%, 23%, 58% and 14% respectively due to the stirrups. Using the BS8110 method, the corresponding ratios would be 2.51, 2.73, 2.64 and 2.89 respectively, i.e., an increase of 151%, 173%, 164% and 189% respectively, which are obviously too large. Experiments show that in slabs No.11 & 12 the load increment is small; this is because the volumes of stirrups are small in these two slabs and the strength of concrete is also lower compared with slabs No.5 & 6. Even so, the BS8110 still predicts an increase in load capacity of 49% and 37% respectively. From this analysis, it is seen that the stirrups effectiveness has been overestimated for RC waffle slabs using BS8110 methods.

In Table 7.4, the concrete's resistance and the stirrups' resistance calculated using BS8110 (expressed as fraction of the total resistance) are listed separately. From this table, it can be seen that, in slabs 7~10, the concrete resistance contributes less than 40% toward the total resistance, while, the stirrups contribute more than 60%.

Table 7.4 Shear Resistance of Concrete & Stirrups in Proportion to Calculated Load Using BS8110

Series No.	Configuration	Methd BS1		Methd BS2	
		P_c/P	P_{sv}/P	P_c/P	P_{sv}/P
7	M#L	0.37 (0.39)	0.63 (0.61)	0.42 (0.44)	0.58 (0.56)
8	M+L	0.34 (0.36)	0.66 (0.64)	0.42 (0.44)	0.58 (0.56)
9	C#L	0.37 (0.37)	0.63 (0.63)	0.42 (0.42)	0.58 (0.58)
10	C+L	0.34 (0.34)	0.66 (0.66)	0.43 (0.43)	0.57 (0.57)
11	C#SL	0.65 (0.65)	0.35 (0.35)	0.70 (0.70)	0.30 (0.30)
12	C+SL	0.72 (0.72)	0.28 (0.28)	0.79 (0.79)	0.21 (0.21)
Avg.		0.46 (0.47)	0.54 (0.53)	0.53 (0.54)	0.47 (0.46)

Similarly, for slabs without shear reinforcement, counting the numbers of ribs to calculate the shear resistance of an RC waffle slabs can cause gross errors. The punching loads for Slabs No.8 & 10 have smaller values compared with slabs No.7 & 9, as shown in Table 7.5, where the concrete resistance and stirrups resistance are shown as a fraction of the test load. Slabs No.8 and 10 have a ratio of 0.84 and 0.76 compared to the test results, while slabs No.7 & 9 have higher values of 1.15 and 1.15 respectively.

Table 7.5 Ratios of Concrete Shear Resistance to Test Load & Stirrups Shear Resistance to Test Load (BS8110)

Series No.	Configuration	Methd BS1			Methd BS2		
		P_c/P_t	P_{sv}/P_t	P/P_t	P_c/P_t	P_{sv}/P_t	P/P_t
7	M#L	0.42 (0.46)	0.73 (0.73)	1.15 (1.19)	0.42 (0.46)	0.58 (0.58)	1.00 (1.04)
8	M+L	0.28 (0.31)	0.56 (0.56)	0.84 (0.87)	0.28 (0.31)	0.39 (0.39)	0.67 (0.70)
9	C#L	0.42 (0.42)	0.73 (0.73)	1.15 (1.15)	0.42 (0.42)	0.58 (0.58)	1.00 (1.00)
10	C+L	0.26 (0.26)	0.50 (0.50)	0.76 (0.76)	0.26 (0.26)	0.34 (0.34)	0.60 (0.60)

11	C#SL	0.62 (0.62)	0.33 (0.33)	0.95 (0.95)	0.62 (0.62)	0.26 (0.26)	0.88 (0.88)
12	C+SL	0.65 (0.65)	0.25 (0.25)	0.90 (0.90)	0.65 (0.65)	0.17 (0.17)	0.82 (0.82)
		0.44 (0.45)	0.52 (0.52)	096 (0.97)	0.44 (0.45)	0.39 (0.39)	0.83 (0.84)

Both the methods employed in this section to calculate the shear resistance of the stirrups appear to over-estimate this, see Table 7.3. It is thought that some modifications are necessary to balance the contribution of stirrups.

7.2.3 EFFECTIVENESS OF THE SHEAR REINFORCEMENT

The use of stirrups in the ribs of the RC waffle slabs is to increase the shear or punching shear capacity of the slabs. This type of shear reinforcements has also been used inside beam and solid slabs with the same purpose. The effectiveness of this type of shear reinforcement is a matter of long standing debate. Previous studies [25] have suggested that due to the shallow depth of beams or slabs, the anchorage of the links inside the concrete is not sufficient to allow the links to develop their full capacity; there is slip between the concrete and the reinforcement bars. In this study, evidence from the tests have supported these findings. Furthermore, it has been found that apart from the insufficient anchorage of the stirrups, there are other reasons which prevent the stirrups from fully developing their capacity. In the following section, we will discussed the experimental results relating to the inefficiency of the stirrups in carrying the shear load in waffle slabs and the number of stirrups inside the ribs being accounted as resisting the punching shear.

From Table 7.3, the increases in punching load capacity by the use of stirrups are about 45%, 23%, 58% and 14% respectively for slabs No.7~10 in relation to Slabs 1~4. If we consider the decrease in the strength of concrete from slabs No.7~10 to slabs No.1~4, the increase should be a little bit higher than what Table 7.3 shows.

The maximum increase occurred is about 58% in slab No.3. The total punching load of slab No.3 is 172.5KN; therefore the increase of load by stirrups is about

$$0.58\% \times 172.5 = 100 KN$$

Using the nominal pouching perimeter suggested by BS8110, we have,

$$B = c + 3d = 150 + 3 \times 125 = 525 mm$$

Inside the zone between the perimeter of the loading pad and the nominal punching perimeter, there are 40 legs of the stirrups. If we consider the increment is evenly distributed to all the 40 legs, each of them has a share of

$$100/40 = 2.50KN$$

The diameter of the stirrups is 6mm, and the design yield strength is $250N/mm^2$, so the full capacity of a leg of the stirrups is

$$\frac{\pi 6^2}{4} \times 250 = 7.07(KN)$$

This suggests that only 35.0% $(2.50/7.07 \times 100)$ of the shear capacity is mobilised. Even the legs very close to the loading pad are neglected (as their anchorage length is very short if close to the loading pad), 28 legs should be considered and then each leg has a share of resistance of 3.57KN (100/28); this amounts to 50.5% $(3.57/7.07)$, i.e., only 50% of the potential strength has been put into use.

From the above analysis it is know that the stirrups inside the ribs are not very effective in resisting the punching shear. When using BS8110, a reduction in the strength of stirrups should be used, or the number of stirrups participating in the shear resistance should be reduced.

7.3 COMPARISON OF EXPERIMENTAL RESULTS WITH THE RESULTS USING UPPER BOUND METHOD

In chapter 6, the upper bond method was applied to the model slabs in the tests. The upper bound method has the advantage of relatively simple calculation, but at the same time, due to the simplification made to the material failure criteria and the structure failure pattern, the method itself is changed to a semi-empirical one. From the theoretical analysis, a few parameters has been extracted which are considered as the major factors influencing the results; but some of these parameters are difficult to be determined by theory and have to be obtained by experiments. In the punching shear problems, the parameters which need to be determined are

- m the ratio between the effective compressive strength and the effective tensile strength of concrete;
- F_k the factor for determining the effective compressive strength of concrete in the formula $f_c' = F_k\sqrt{f_c}$, as described in Chapter 3;

F_{sv} the factor to reduce the strength of stirrups due to inefficient anchorage, i.e., use $F_{sv} f_{sv}$ in the analysis instead of f_{sv}.

In order to determine these parameters, a trial-and-error method has been adopted and the results are then compared with the experimental results.

In Chapter 6, after a series of calculations and matching them with experimental data, it has been found that the above parameters have the following values:

$m = f_{cu}$ (f_{cu} in the unit of N/mm^2)
F_k=2.0
$F_{sv} = 0.5$

From calculations in chapter 6 using both the total depth and effective depth of slabs, it was found that results with effective depth gave a better fit with experimental data. Using the values given above and the effective depth of slabs, the upper bound analysis have been carried out and are compared with the experimental results.

Table 7.6 lists the inclination angle, the concrete resistance, the stirrups' resistance, and the total resistance or load capacity of the slabs. The ratios of the punching shear load of upper bound analysis to the test results are given in Table 7.7

Table 7.6 Upper Bound Analysis Results of Punching Load

	slab1	slab2	slab3	slab4	slab5	slab6	slab7	slab8	slab9	slab10	slab11	slab12
$\tan\overline{\alpha}$	2.23	2.15	2.04	1.60	2.03	1.72	1.12	1.00	1.20	1.20	1.34	1.37
P_c	188.2	190.1	231.3	171.8	304.5	304.6	218.3	152.5	200.6	168.0	266.0	283.3
P_{sv}	0.0	0.0	0.0	0.0	0.0	0.0	49.7	42.3	57.2	50.9	42.3	35.2
P	188.2	190.1	231.3	171.8	304.5	304.6	268.0	194.8	257.8	218.9	308.3	318.5
P_{test}	187.0	165.0	172.5	198.9	332.5	283.0	271.0	202.5	272.0	227.5	362.5	272.5

Table 7.7 Ratio of Punching Load Using Upper Bound Analysis to Test Results

	slab 1	slab 2	slab 3	slab 4	slab 5	slab 6	slab 7	slab 8	slab 9	slab 10	slab 11	slab 12
P_c/P_{test}	1.01	1.15	1.34	0.86	0.92	1.08	0.81	0.75	0.74	0.74	0.73	1.04
P_{sv}/P_{test}	0.00	0.00	0.00	0.00	0.00	0.00	0.18	0.21	0.21	0.22	0.12	0.13
P/P_{test}	1.01	1.15	1.34	0.86	0.92	1.08	0.99	0.96	0.95	0.96	0.85	1.17
$\frac{(P-P_{test})}{P_{test}}$	0.64%	15.2%	34.1%	13.6%	8.42%	7.63%	1.11%	3.80%	5.22%	3.78%	14.9%	16.9%

From Table 7.7 & Fig.7.4, it is seen that, apart from slabs No.3 and 12, the discrepancy between loads from calculation and tests is ≤15%.

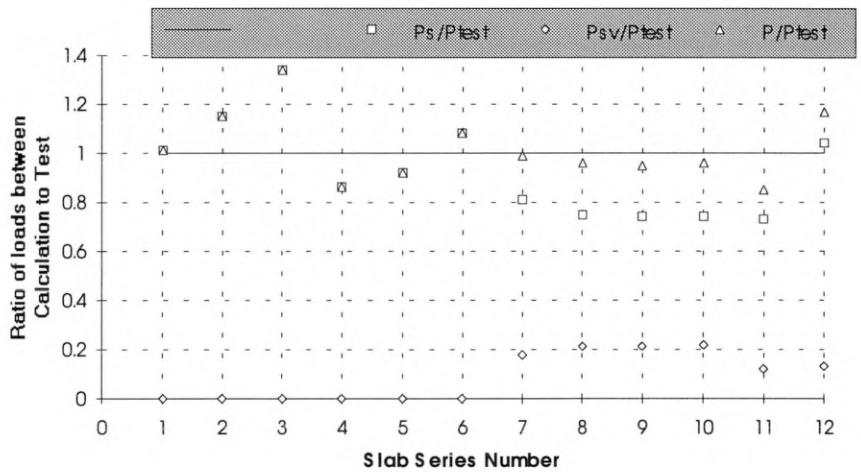

Fig.7.4 Ratio of loads between calculation and test

From Table 7.6, the punching angles of slabs with stirrups are in the range of $\tan\overline{\alpha} = 1.0 \sim 1.4$, while, for slabs without stirrups, $\tan\overline{\alpha} = 1.7 \sim 2.2$. This means that slabs with stirrups will have the punching perimeters reduced.

Table 7.8 lists in percent terms the resistance of concrete and stirrup in relation to the total punching resistance of the slabs. It is seen that the stirrups' contribution for slabs No. 7, 8, 9, 10 are about 20%, slabs No. 11 and 12 are 13.7% and 11% respectively.

Table 7.8 Ratios of Concrete's Shear Resistance and Stirrups' Resistance in Relation to the Punching Load Capacity—Upper Bound Analysis

	slab 1	slab 2	slab 3	slab 4	slab 5	slab 6	slab 7	slab 8	slab 9	slab 10	slab 11	slab 12
P_c/P (%)	100.0	100.0	100.0	100.0	100.0	100.0	81.5	78.3	77.8	76.7	86.3	88.9
P_{sv}/P (%)	0.0	0.0	0.0	0.0	0.0	0.0	18.5	21.7	22.2	23.3	13.7	11.1

If the recommendations of the BS8110 nominal punching perimeter are adopted, and assume that all the stirrups falling inside this perimeter will participate in the shear resistance, then it would be interesting to see how much of their strength can be put into use. In Table 7.9, the number of legs of the stirrups, N, which fall into the nominal perimeter is listed for slabs No.7~12; their total strength capabilities to resist shear, P'_{sv}, are calculated; the shear resistance of stirrups calculated by the upper bound analysis, P_{sv}, are listed in Table 7.6; then the ratio between P_{sv} and P'_{sv} measures the efficiency of the stirrups, and these are listed in Table 7.9.

Table 7.9 Ratio of Stirrups Resistance Calculated Using Upper Bound Analysis and BS8110

Symbols	Unit	Slab 7	Slab 8	Slab 9	Slab 10	Slab 11	Slab 12
N		42	24	42	24	42	24
d_{sv}	(mm)	6.0	6.0	6.0	6.0	4.0	4.0
A_{sv}	(mm^2)	1187.3	678.5	1187.3	678.5	527.8	301.6
f_y	(N/mm^2)	250	250	250	250	340	340
P'_{sv}	(KN)	296.8	169.6	296.8	169.6	179.4	102.5
P_{sv}	(KN)	49.7	42.3	57.2	50.9	42.3	35.2
P_{sv}/P'_{sv}	(%)	16.7	24.9	19.3	30.0	23.6	34.3

Note:

N number of stirrup legs falling inside the zone between the load pad perimeter and the nominal punching perimeter defined in BS8110;

d_{sv} diameter of one leg of the stirrups;

A_{sv} total areas of the stirrups inside the zone, $A_{sv} = N \cdot \pi d_{sv}^2 / 4$;

f_y yield strength of the stirrups;

P'_{sv} nominal shear resistance of the stirrups using BS8110, $P'_{sv} = f_y \cdot A_{sv}$;

P_{sv} the shear resistance of the stirrups calculated by upper bound analysis.

From Table 7.9, it can be seen that the efficiency of the stirrups in terms of development of strength is less than 35%.

7.4 COMPARISON OF FEA RESULTS WITH THE TEST RESULTS

In chapter 4, the application of non-linear finite element to RC waffle slabs was discussed, and two material models were discussed, i.e., the Mohr-Coulomb criteria and the concrete fracture model. In chapter 6, analysis employing both of the above criteria were carried out for Slabs No.1, 2 & 3. The software used were the LUSAS package and the self-developed modules in conjunction with the original LUSAS package. The results were listed and described in section 6.4 of chapter 6, where the central deflections of the slabs, the crack pattern or yield zone propagation in the slab were plotted, and the shear stress distribution on a few sections were drawn to show the redistribution of the shear stress along with the load increment. The calculation results are analysed in comparison with the test results below.

7.4.1 COMPARISON OF DEFLECTIONS OF FEA RESULTS WITH THE TEST RESULTS

In both of the two types of analysis, the calculation can not give the ultimate failure load, the loading progress can still carry on after the ultimate test loads have been exceeded. After examining the analysis results (see Fig.6.14), it was found that the centre deflection of the slabs obtained from both of the material models, the analysis results were smaller than those obtained from experiments, especially in the later stage of the loading. The calculated centre deflection corresponding to the ultimate test loads are listed in Table 7.10.

Table 7.10 Comparison of Calculated Deflection with the Test Results

	Mohr-Coulomb Model *(mm)*	**Concrete Crack Model** *(mm)*	**TEST** *(mm)*
Slab 1	2.26 (56.5%)	3.2 (80.0%)	4.0
Slab 3	1.97 (42.8%)	3.1 (67.4%)	4.6
Slab 5	4.53 (64.7)	6.4 (91.4)	7.0

Note: values inside brackets are the ratio between calculated results and the test results.

From Table 7.10, it is seen that results using Mohr-Coulomb criteria is substantially smaller that those of tests. Deflection employing Mohr-Coulomb criteria is about only half of the deflection of tests. The results employing the concrete crack model have substantial improvement compared with the Mohr-Coulomb's, but are still smaller than those of the tests, 67~91% of the test's deflection. In general, the deflections from calculation are systematically smaller than the test results, especially for slabs No. 1 & 3 which have no extended local solid area.

The small deflections indicate that either the actual stiffness of the slabs is not as large as the finite elements analysis used, or more energy has dissipated due to the cracks than actually the analysis simulates. The later explanation may be more true and can be explained below.

In using Mohr-Coulomb criteria, the plastic theory was employed in the analysis. In the plastic theory, once the material yields, plastic strain will be present and the plastic distortion of the element will involve the energy dissipation, but the tensile stress will not be released and a substantial tensile stress is still maintained. This may make the slabs more strong than what actually is. Another reason is that the tensile strength from split test is used to calculate the cohesion factor C and the internal frictional angle φ in order to consider both the tensile dominant yield and compression dominant yield. The tensile strength from split test is about 40% higher than that of the actually fracture strength of concrete, so the tension side of the Mohr-Coulomb failure surface is extended beyond the actual failure surface of concrete.

The results of the concrete fracture model are improved because the fracture feature and the fracture strength were used in this type of analysis. The fracture model employed is rather a simple one — the maximum tensile strength criteria. The shear retention and the tension stiffening were modelled as a straight line (see section 4.3.3), while, the actual strength may not be as much as these models predict. Another reason is that slabs No.1, 3 & 5 have no shear links, so the shear retention and tension stiffening actions should be less effective in these cases.

7.4.2 COMPARISON OF THE YIELD ZONE AND THE CRACK PATTERN OF FEA RESULTS WITH THE TEST RESULTS

The analysis employing the Mohr-Coulomb criteria output information on the yielding of the material; the analysis employing the concrete fracture model reported on the crack status at the gauss points of the element.

The yield zones in the slabs were shown in Fig.6.14 and 6.15 for slabs No.1 and 3. The yield zones in the slab formed a 'pyramid' with the top perimeter gradually approaching the loading perimeter and the lower outer perimeter lying inside the slab; the outer perimeter almost stopped further expanding during the later stage of the loading progress. The geometry of the 'pyramid' had similarity to the diagonal cracks developed in the slabs tested, but no major yield zone like the major cracks observed in test could be singled out from this analysis as no plastic strain output facility was available. By examining the analysis results, it was found that the area close to the loading pad was the last part to get yield, where the principal stress σ_1 was a tensile stress, σ_2 and σ_3 were compressive stresses of substantial values. In slab No.1, the distance from the centre of the loading pad to the out perimeter was about 500mm at load increment No.8 (P=180KN) and this distance had not much further increase from then on; the distance from the centre of the loading pad to the out perimeter of the failure surface obtained from test was about 370mm.

Fig.6.20 and 6.21 showed the crack status on the central section and a section along a rib for slab No.1 & 3 respectively. It was found that cracks of the type 'first-crack' (the crack in the x direction of the local co-ordinate system) appeared rather early during the load increment, and this type of crack had spread on most part of the slab. The appearance of the 'first-crack' seemed have no substantial affect on the process of load increment. Under further loading, cracks of the type 'second-crack' were gradually developing in the slab started from the area adjacent to the local solid area, and this coincided with the appearance of the diagonal cracks in the slab observed during test. During subsequent continuous loading, more and more of the 'second-crack' developed in the slab. Finally two continuous bands of 'second-crack' were formed; one band located at the junction between local solid area and the ribs; the other band was away from the local solid area. These two bands of 'second-crack' resembled the crack pattern observed in the test.

The crack pattern of slab No.3 obtained by calculation had similar character but with the two carck bands not as so obvious as those of slab No. 1, but carefully examination could reveal that the crack band still existed.

For slab No.1, the second crack zone was extended to about 490mm away from the centre of the slab; for slab No.3, it was about 540mm (test's is 400mm) away from the centre of the slab.

From the analysis of the above two slabs' results, it seems that, the first crack area near the loading pad and the second cracks at the middle and lower parts of the slab are likely to form the continuous crack zone.

7.4.3 DISTRIBUTION OF SHEAR STRESS τ_{xz} IN THE DECK AND THE RIBS

The shear stress τ_{xz} made up the major reaction force (for the 1/8 of the slab analysis model) to balanced the applied load P in the vertical direction; the vertical stress σ_z were examined and found to be minor. The distribution of shear stress τ_{xz} along several slab sections for slabs No.1, 3 and 5 were plotted in Fig.6.17~19 (Mohr-Coulomb model) and Fig.6.22~24 (Concrete Fracture model). The total forces along the deck sections and the rib sections were calculated and listed in Tables 6.28 to 6.29 (Mohr-Coulomb model) and Tables 6.33 & 6.34 (Concrete Fracture model).

From the results of Mohr-Coulomb model, the results showed that the deck's participation in the shear resistance was increasing along with the increase of the loading; the deck near to the loading pad was more effective than those away from the loading pad. For slabs No.1, the deck took about 18~23% of the total resistance in the later loading stage; for slabs No.3, deck took about 16~19% of the resistance in the later stage.

The analysis results from the concrete crack model supported the conclusion that the deck near the loading pad was more effective in shear resistance; but the shear resistance of the deck was not always increasing along with the increase of the loading; the shear resistance may drop slightly in the later stage of the loading.

For slab No.1, the deck took about 12~30% of the applied load in the late stage of loading; for slab No.3, the deck took about 12~25% of the load.

From the above analysis, the conclusion can be drawn that the deck does take some of load by providing shear resistance along the vertical sections of the waffle slabs, and the amount is in the range of 12~30%.

7.5 COMPARISON OF RESULTS USING ALTERNATIVE METHODS WITH THE TEST RESULTS

BS8110 has adopted a simplified method, which has the advantage of clear concept, easy understanding and implementation. While, from the comparison between the results of BS8110 and the tests in section 7.2, it has been found that there are significant discrepancies between them.

Based on the study using the upper bound method and FEA, here it is intended to develop some simplified methods which can be easily put into use without complicated calculations. In Chapter 3, three alternative methods were proposed, and the calculations using these alternative methods were conducted in chapter 6. Here those results are compared with the test results to verify their acceptability. Table 7.11 lists the results of calculations and tests.

Table 7.11 Comparison of Punching Load using Alternative Methods to Test Results

	Test	Alter 1	Alter 2	Alter 3
	(KN)	(KN)	(KN)	(KN)
Slab1	187.0	197.7 (213.0)	153.1 (165.0)	188.1 (202.9)
Slab2	165.0	157.4 (184.6)	122 (143.2)	149.3 (174.5)
Slab3	172.5	197.7 (219.3)	153.1 (169.5)	176.9 (195.9)
Slab4	198.9	157.4 (168.7)	122.2 (131.3)	164.2 (176.6)
Slab5	332.5	254 (286.0)	230.2 (258.4)	307.3 (345.0)
Slab6	283.0	256.8 (273.7)	199.2 (211.7)	269.4 (286.4)
Slab7	271.0	338.7 (338.7)	298 (298.0)	286.2 (286.2)

Slab8	202.5	223.3 (223.3)	190.9 (190.9)	194.5 (194.5)
Slab9	272.0	349.9 (349.9)	306.3 (306.3)	285.6 (285.6)
Slab10	227.5	232.9 (232.9)	198.3 (198.3)	217.7 (217.7)
Slab11	362.5	342.9 (342.2)	325 (325.0)	367.9 (367.9)
Slab12	272.5	299.5 (299.5)	243.2 (243.2)	299.2 (299.2)

Tables 7.12 and 7.13 lists the ratio of punching loads using alternative methods and the test results for slabs No1~6 and 7~12., the average and the standard derivation of the ratios are also listed.

Table 7.12 Ratio of Punching Load of Alternative Methods to Tests

	Alter 1	Alter 2	Alter 3
Slab1	1.06 (1.14)	0.82 (0.88)	1.01 (1.09)
Slab2	0.95 (1.12)	0.74 (0.87)	0.90 (1.06)
Slab3	1.15 (1.27)	0.89 (0.98)	1.03 (1.14)
Slab4	0.79 (0.85)	0.61 (0.66)	0.83 (0.89)
Slab5	0.76 (0.86)	0.69 (0.78)	0.92 (1.04)
Slab6	0.91 (0.97)	0.70 (0.75)	0.95 (1.01)

Table 7.13 Ratio of Punching Load of Alternative Methods to Tests

	Alter 1	Alter 2	Alter 3
Slab7	1.25 (1.25)	1.10 (1.10)	1.06 (1.06)
Slab8	1.10 (1.10)	0.94 (0.94)	0.96 (0.96)
Slab9	1.29 (1.29)	1.13 (1.13)	1.05 (1.05)
Slab10	1.02 (1.02)	0.87 (0.87)	0.96 (0.96)
Slab11	0.95 (0.94)	0.90 (0.90)	1.01 (1.01)
Slab12	1.10 (1.10)	0.89 (0.89)	1.10 (1.10)

Table 7.14 Statistical Results of the Alternative Methods

	Slab No. 1~6			Slab No. 7~12			Slab No. 1~12		
	Alt1	Alt2	Alt3	Alt1	Alt2	Alt3	Alt1	Alt2	Alt3
Average $\overline{R}$	0.94 (1.04)	0.74 (0.82)	0.94 (1.04)	1.12 (1.12)	0.97 (0.97)	1.02 (1.02)	1.03 (1.08)	0.86 (0.90)	0.98 (1.03)
stand dv δ	0.15 (0.17)	0.10 (0.11)	0.07 (0.09)	0.13 (0.13)	0.11 (0.11)	0.06 (0.06)	0.16 (0.14)	0.15 (0.13)	0.07 (0.07)
$\delta/\overline{R}$ (%)	16.1 (16.31)	13.5 (13.78)	7.8 (8.20)	11.7 (11.69)	11.7 (11.71)	5.6 (5.55)	15.2 (13.4)	17.4 (14.3)	7.4 (6.4)

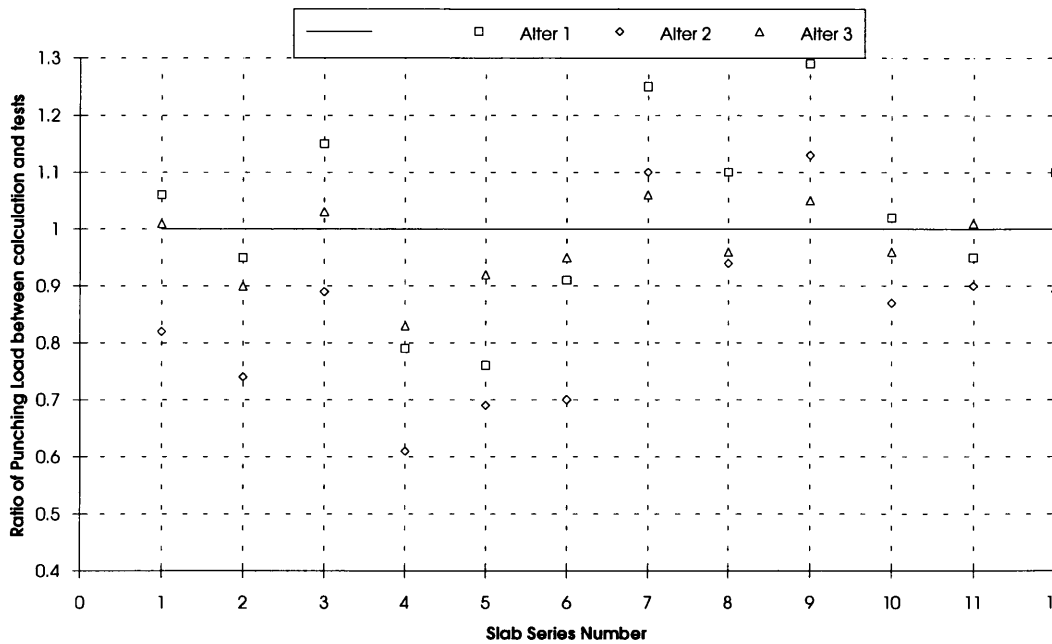

Fig 7.5 Comparison of Results of Alternative Methods with Test

From Fig.7.5, it is seen that the alternative method three has a better match with the experiment results; shown in Table 7.14, alternative method three has an average ratio of 0.94 for slabs No.1~6, 1.02 for slabs No.7~12, and 0.98 for all the slabs No.1~12. Therefore, method three is recommended for the simplified analysis of the punching load for RC waffle slabs.

7.7 CONCLUSIONS

In this chapter, first the experimental results were compared with the method proposed by BS8110; it has been found that BS8110 method under-estimates the shear resistance of concrete and over-estimates the shear resistance of the stirrups; BS8110's method of counting the number of ribs for the shear capacity is arbitrary.

By comparing the results of test with those of upper bound analysis, it has been found that the upper bound analysis can yield quite good results; it can consider the change of the punching perimeter when stirrups are provided.

The stirrups in RC waffle slabs are not very effective, less than 35% of the shear capacity of the stirrups were actually be mobilised for the slabs in this study.

The application of 3D non-linear finite element method to the RC waffle slabs employing both the Mohr-Coulomb criteria and the concrete crack model was partially success. FEA employing the concrete crack model gave a prediction of the deflection of the slab at about 67~91% of the test results, the Mohr-Coulomb model's gave about 50% of the actually deflection. Both the analysis methods failed to predict the ultimate load; the load increasing process could still carry on even after the applied load had exceeded the ultimate test load. The yield zone and the crack patter in the slab from the FEA analysis resembled the geometry of the failure surface of the test, but the exact dimension of the geometry was hard to measure, as no major crack could be singled out by the analysis. The distribution of the vertical shear stress along the vertical sections of the slab indicated that the deck of the waffle slabs provided about 12~30% of the shear resistance to the applied load. Compared to upper bound analysis, the method is good in predicting the deflection but difficult in predicting the exact load capacity.

Three alternative methods, which were simple and easy to handle, were proposed for calculating the punching loads in RC waffle slabs. Among the three methods, the third is based on the affine solid slabs, and by comparing with the test results it is found that this method is better than the other two alternative methods

Based on the comparative study in this chapter, either the upper bound method or the third alternative method is recommended to calculate the punching shear capacity of RC waffle slabs.

CHAPTER 8

CONCLUSIONS

The work carried out in this study was to get a better understanding of the punching shear behaviour of RC waffle slabs, and evaluate the method recommended by BS8110 in calculating the punching shear capacity of RC waffle slabs, and if appropriate to propose design formulae for predicting more accurately the punching shear capacity of the slabs.

8.1 CONCLUSIONS

The punching shear failure characteristics of waffle slabs were essentially similar to those of solid slabs; sudden and explosive type of brittle failure was experienced for all the slabs tested in this study; the deflection at the ultimate load was very small, the largest central deflection of the slabs with stirrups was 7.2% of the slab depth and that of the slabs without stirrups was only 4.7% of the slab depth. The final crack pattern in waffle slabs was different from that of solid slabs in the sense that cracks changed orientation abruptly, especially in the region at the junction between ribs and the local solid area; the cracks on the ribs also changed from a steep gradient to a flatter one once the cracks reached the level of the flexural reinforcements. The major cracks cut across the ribs in both the orthogonal directions. Together with the examination of the punching load capacity of tested slabs of various configuration, the following conclusions can be drawn from the experimental study:

(1) the effective dimension of the failure area of waffle slabs is smaller than those of solid slabs due to the abrupt change of the crack orientations;

(2) ribs parallel to the edges of the slab resist the punching load as well as ribs perpendicular to the edges of the slab;

(3) the punching load is dissipated to an area larger than the loading pad; the punching resistance is not sensitive to the variation of the local configuration of the ribs but depends on the concrete volume content in the slab;

(4) the loading direction (downward or upward) does not lead to a significant difference in the punching shear capacity;

(5) the presence of local solid area around the loading pad can effectively increase the punching capacity of the slab; the use of extended arm in the configuration of the local solid area is more favourable than a squared configuration;

(6) the shear reinforcement increases the shear load capacity but this increase is not as significant as that due to the local solid area.

By comparing the punching loads obtained by experiments with those obtained by calculation following the provisions of BS8110, the following conclusions can be drawn:

(1) the calculated results were substantially smaller than those of the test results for slabs without shear reinforcements, the average of the calculated load was only about 56% of the test load (see Table 7.1); this indicated that BS8110 under-estimated the punching shear capacity of the waffle slabs without shear reinforcements;

(2) the calculated results matched the test results well for slab provided with shear reinforcements, an average of 0.96 was obtained for the ratio between calculated load and tested load (see Table 7.2); but the proportion between the two parts of the shear resistance provided by the shear reinforcements and the concrete respectively was not reasonable in the sense that the shear resistance provided by the shear reinforcement was overestimated and that of concrete underestimated (see Table 7.4);

(3) the method employed by BS8110 in calculating the punching shear capacity of waffle slab could lead to the over-sensitivity to the local configuration of the ribs in the vicinity of the loading pad; calculated results of slab No. 2 & 4 were only 38% and 30% respectively of the tested load (see Table 7.1).

In this study, theoretical investigations were made for the purposes of studying the punching failure mechanism and predicting the ultimate failure load. The theoretical analysis methods employed included the upper bound analysis and non-linear finite element analysis. The preparation work involved with the theoretical study was as followings:

(1) the upper bound analysis: the derivation of the calculation formulae employing the modified Mohr-Coulomb criteria with parabolic failure surface; the calculation formulae were developed for solid slabs with rectangular loading pad and for waffle slabs with rectangular loading pad considering the shear

reinforcement and the presence of the local solid area; this work was described in chapters 3 and 6;

(2) finite element: programming for the user-supplied modules for LUSAS regarding the material failure criteria — the concrete cracking and yielding model; this work was described in chapter 4.

Using the upper bound and finite analysis the geometric parameters and the shear reinforcements affecting the punching shear capacity of waffle slabs were studied and then the methods were applied to the model slabs tested and compared with the test results. The conclusions drawn from this study are given below:

(1) both the upper bound analysis and the FEA analysis indicated that the deck of the waffle slab also participated in the resistance towards the punching shear; 20~30% contribution predicted by upper bound analysis (Table 3.4), 16~23% by FEA using Mohr-Coulomb (Table 6.28 & 6.29), 12~30% by FEA of fracture Model (Table 6.33 & 6.34);

(2) the shear reinforcement was able to increase the punching load capacity but the full strength of the stirrups can not be mobilised; apart from the reason that the anchorage of the stirrups was not sufficient in the slabs, the upper bound analysis revealed that the punching perimeter decreased with the increase of the content ratio of stirrups and resulted in not as many stirrups being mobilised as expected; the utilisation of the potential strength of the stirrups was found to be 17~34% for slabs tested in this study (see Table 7.9);

(3) the finite element analysis using the crack model could predict the deflection at the tested failure load with an accuracy of 67~91% (see Table 7.10); both the analysis using the material failure models of Mohr-Coulomb and the Concrete-Fracture failed to predict the ultimate punching load, the loading increase could still carry on even after the tested failure load had been reached; the reason for this is thought to be that the punching failure has the feature of brittle and sudden characteristics, and it requires a more advanced material model for the concrete and even the crack modelling;

(4) the calculated punching failure load using the upper bound analysis matched reasonably well with the experimental results; the ratio between the calculated load and the tested load varied from 0.85 to 1.34 with an average of 1.02 (Table 7.7).

Based on the experimental and theoretical study and also considering the merits of the method employed by the code of practice, alternative methods have been proposed to calculate the punching shear capacity of waffle slabs. After applying the three proposed alternative methods to the model slabs and comparing the analysis results with the test results, it was found that the alternative method three — using an affine solid slab, applying the concept of nominal punching perimeter and shear strength of BS8110 — predicted the punching failure load which matched very well with the test results for both slabs with and without stirrups; the average of the ratio between the predicted load and the test load was 0.94 for slabs without stirrups, and 1.02 for slabs with stirrups (see Table 7.14).

Based on this study, it is recommended that either the upper bound analysis or the alternative method 3 could be used with confidence for the assessment of the punching shear capacity of the RC waffle slabs.

8.2 PROPOSED FURTHER STUDY

The scope of this investigation has been necessarily limited and can only be considered as a step forward in the process of establishing general characteristics and criteria for the punching shear design of reinforced concrete waffle slabs subjected to concentrated loading conditions. Further investigations are suggested for a fuller understanding of this complex structural behaviour:

(1) Full scale experimental studies should be conducted fully to evaluate the methods proposed.

(2) All the model slabs in this study had the same size of recesses; it is necessary to conduct tests on a series of slabs with varied dimension of recesses.

(3) The upper bound analysis method involves the determination of a few parameters, more test data are needed fully to evaluate these parameters.

(4) From this study, it has been found that the potential strength of the stirrups is not fully mobilised; considering the difficulty in placing the stirrups in the ribs of the slabs during construction, other type of shear reinforcements should be considered and used. One possibility is to use the horizontal reinforcements for shear resistance by placing them at half depth of the ribs of the waffle slabs.

References

1. AMERICAN CONCRETE INSTITUTE, *Building code requirements for reinforced concrete*, Detroit, ACI 318-83 1983.

2. ASCE, *Finite element analysis of reinforced concrete - state-of-the-art report*, ASCE, 1982

3. Ajdukiewicz, A., and Starosolski, W., *Reinforced concrete slab-column structure*, Elsevier, 1990.

4. Ajdukiewicz A.B. etc., Experimental analysis of limit statues in six-panel waffle flat-plate structure, *ACI structural journal*, Nov.-Dec. 1986.

5. Alexander, S. D. B., and Simmonds, S. H., Tests of column-flat plate connections, *ACI Structural journal*, Vol. 89, No. 5, Sep. - Oct. 1992, pp 495-502.

6. Aokl Y., Strength and cracking in two-way slabs subjected to concentrated load, ASCE *SP30-5*, 1970.

7. Barr B, Hughes T, Khalifa S and Yacoub-Tokatly, A comparative study of the geometries used to investigate the fracture behaviour of material under mixed model loading", *Fracture of concrete and roack*, Proceed. of Intl. Conf. Elsevier science publisher Ltd, pp448-457.

8. Bazant, Z. P., and Cao, Z., Size effect in punching shear failure of slabs, *ACI Structural journal*, January-February 1987, pp 44-53.

9. Bazant, Z. P., Size effect in blunt fracture: concrete, rock, metal, *Journal of engineering mechanics*, ASCE, Vol. 110, No. 4, April 1984.

10. Bortolotti L. Punching shear design in the new Australian standard for concrete structure, *J. of Struct. Div.*, ASCE, Vol 87, No 2, March-April 1990.

11. Braestrup M.W. Dome Effect in RC slabs: Rigid-plastic Analysis, *Journal of Struct. Div.*, ASCE, vol 106, No ST6 June 1980.

12. BRITISH STANDARD INSTITUTION. *The Structural use of concrete*. London BS8110: 1985

13. BRITISH STANDARD INSTITUTION. *Code of practice for the Structural use of concrete*. London CP110: Part 1:1972

14. Broms, C. E., Punching of flat plates - a question of concrete properties in biaxial compression and size effect, *ACI Structural journal*, Vol. 87, No. 3, May - June 1990, pp 292-304.

15. Brotchie J.F. Membrane action in slabs, *ASCE SP 30-16*,1970.

16. CEB-FIP, *Model code for concrete structures*, Comite Euro-international du Beton, Paris, 1978.

17. Chana, P. S., and Desai, S. B., Membrane action, and design against punching shear, *The structural engineer*, Vol. 70, No. 19, 6 October 1992.

18. Chana, P. S., and Desai, S. B., Design of shear reinforcement against punching shear, *The structural engineer*, Vol. 70, No. 9, 5 may 1992.

19. Chen, W. F., *Plasticity in reinforced concrete*, McGraw-Hill, 1982.

20. Christiansen K.P. etc. The effect of membrane stress on the ultimate strength of the interior panel in a reinforced concrete slab, *The structure engineer*, Vol.4., No.8, Aug. 1963.

21. Corley, W. G., and Hawkins N. M., Shearhead reinforced for slab, *ACI journal*, October 1968, pp 811-824.

22. Csagoly P.F. etc, Advanced design method for concrete bridge deck slabs, Concrete Intn'l.: Design & Const. (US), Vol. 11, No. 5, May 1989, pp. 53-63.

23. Desayi P., and & Kulkarni A.B., Load-deflection behaviour of restrained R/C slabs, *Journal of Strut. Div.*, ASCE Vol 103, No ST2, Feb. 1977.

24. Desayi, P., Load-deflection behaviour of restrained R/C skew slabs, *Jour. of Strut. Div*, ASCE, Vol 107, No. St5, May 1981.

25. Dilger, W. H., and Ghali, A., Shear reinforcement for concrete slabs, Journal of the structural division, ASCE, Vol. 107, No. ST12, December 1981, pp2403-2420.

26. Elstner, R. C., and Hognestad, E., Shearing strength of reinforced concrete slabs, ACI Journal, Proceedings Vol. 53, No. 1, July 1956, PP 29-58.

27. Fenwick, R. C., and Dikson, A., Slabs subjected concentrated loading, *ACI Structural journal*, Vol. 86, No. 6, Nov.-Dec. 1989, pp 672-678.

28. Golley B.W. etc, Finite panel for static analysis of plates, *Jour. of Strut. Div., ASCE*, Vol. 114, No 10, Oct. 1988.

29. Gonzalez-Vidosa, F., Kotsovos, M. D., and Pavlovic, M. N., Symmetrical punching of reinforced concrete slabs: an analytical investigation based on nonlinear finite element modelling, *ACI Journal of structural engineering*, May-June 1988.

30. Helal, J. C., Ribbed slabs spanning in two directions, Constructional and engineering, April 1950.

31. Ho, S. L., *An investigation into the behaviour of hollow ribbed (waffle) rectangular reinforced concrete slabs at the ultimate state*, Ph.D thesis, Dundee Institute of Technology, Dundee, Scotland, 1989.

32. Hopkins D.C., Test on a reinforced concrete slab and beam floor designed with allowance for membrane action, *ASCE, SP 30-10*, 1970.

33. Hung, T.Y., Limit strength and serviceability factors in uniformly loaded, isotropically reinforced two-way slabs, *ASCE, SP 30-14*, 1970.

34. Jiang, D.H., and Shen, J.H., Strength of concrete slabs in punching shear, *Journal of Struct. Eng,* ASCE, Vol 112, No12, Dec. 1986

35. Kong & Evans, *Reinforced and prestressed concrete*, 3d edition, Van nostrand reinhold, UK, 1987

36. Kuang, J. S., and Morley, C. T., Punching shear behaviour of restrained reinforced concrete slabs, *ACI Structural journal*, Vol. 89, No. 1, Jan. - Feb. 1992, pp 13-19.

37. Kukreti, A.R., Analysis procedure for ribbed and grid plate system used for bridge decks, ACI *Journal of Strut. Engg.*, Vol 116, No2, Feb 1990.

38. Long, A. E., Cleland, D. J., and Kirk, D. W., Moment transfer and the ultimate capacity of slab column structures, *The structural engineer*, Vol 56A, No. 4, April 1978.

39. Lovrovich, J. S., and Mclean, D. I., Punching shear behaviour of slabs with varying span-depth ratios, *ACI Structural journal*, Vol. 87, No. 5, Sep.-Oct. 1990, pp 507-511.

40. Magura, D. D. and Corley, W. D.: *Test to Destruction of a Multipanel Waffle Slab - Full-scale Testing of New York World's Fair Structures*, The Rathskeller Structures, National Academy of Science, Washington, D. C., 1969.

41. Malvar, L. J., Punching shear failure of a reinforced concrete pier deck model, *ACI Structural journal*, Vol. 89, No. 5, Sep. - Oct. 1992, pp 569-576.

42. Matthew, P. W., and Bennett, D. F. H., Economic long-span concrete floors: a survey of 40 office buildings with long-span concrete floors, *Reinforced Concrete*, 1973.

43. Marzouk, H., and Hussein, A., Experimental investigation on the behaviour of high-strength concrete slabs, *ACI* structural *journal*, Vol. 88, No. 6, Nov.- Dec. 1991, pp 701-712.

44. Marshall, C. M. C., *An investigation into the behaviour at ultimate load of reinforced concrete multipanel slab-beam systems*, M.Phil thesis, The Hatfield Polytechnic, December, 1983.

45. Moe, J., Shearing strength of reinforced concrete slabs and footings under concentrated loads, Bulletin No. D47, Research and development laboratories, Portland Cement Association, Skokie, I11. 1961, 130 pp.

46. Nielsen, M. P., *Limit Analysis and concrete plasticity*, Prentice-Hall, New Jersey, 1984.

47. Owen, D. R. J., and Hinton, E., *Finite elements in plasticity: theory and practice*, Pineridge Press Ltd, 1980.

48. Park, R, and Gamble, W. L., *Reinforced concrete slabs*, John Wiley & Sons, 1980.

49. Park, R. Ultimate strength of Rectangular concrete slabs under short-term uniform loading with edges restrained against lateral movement, Paper No.6705, *Proc. ICE*, Vol 28, June 1964.

50. Regan, P. E., Symmetric punching of reinfocred concrete slabs, *Magazine of concrete research.* Vol. 38, No. 136, Sep. 1986, pp 115-128.

51. Regan, P. E., and Rezai-Jorbi, H., Shear resistance of one-way slabs under concentrated loads, *ACI Structural journal*, March - April 1988, pp 151-157.

52. Rangan, B. V., Punching shear design in the new Australian standard for concrete structures, *ACI Structural journal*, Vol. 87, No. 2, March-April 190, pp 140-144.

53. Reineck, K. H., Ultimate shear force of structural concrete members without transverse reinforcement derived from a mechanical model, *ACI* structural *journal*, Vol. 88, No. 5, Sep.- Oct. 1991, pp 592-602.

54. Reissm, M., and Sokal, J., Design of ribbed flat slabs, *The Structural engineer*, Vol. 50, No. 8, 1972.

55. Roll, F., Shear resistance of perforated reinforced concrete slabs, *ASCE SP 30-4*, 1970.

56. Sarkar, S., and Ho, S. L., The behaviour of hollow ribbed (waffle) rectangular reinforced concrete slabs; *Proceedings of 17th Conf. on Our World in Concrete & Structures*, August 1992, Singpore

57. Sarkar, S., Pei, S, Influence of boundary conditions on the membrane enhancement in reinforced concrete slabs, *Proceedings of RILEM Conf. on Failures of Concrete Structures*, Strbske Pleso, Slovakia, June 1993.

58. Sarkar, S., Pei, S, and Ho, S. L., Experimental study into the shear behaviour of hollow ribbed (waffle) rectangular reinforced concrete slabs; *Proceedings of 18th Conf. on Our World in Concrete & Structures*, August 1993, Singpore

59. Sabnis, G. M., and Gogate, A. B., Investigation of thick slab (pile cap) behaviour, *ACI* structural *journal*, January- February 1992, pp 35-39.

60. Tasta, Z. Z., and Levy, M., Two-way skewed ribbed slabs, *Proc. Instn. civil engineers*, Part 2, Vol. 59, December 1975.

61. Tebbet, I. E., Analysis and design of rib-stiffed plates and slabs, *Ph.D thesis*, university of Leeds.

62. Tong, P.Y.,, Compressive membrane enhancement in two-way bridge slabs, *ASCE, SP 30-12*, 1970.

63. Yamada, T., Nanni, A., and Endo, K.,. Punching shear resistance of flat slabs: Influence of reinforcement type and ratio. *ACI Structural journal*, Vol. 88, No. 4, Sep.-Oct 1992, pp 555-563.

64. Ueda, T., and Stitmannaithum, B., Shear strength of precast prestrengthed hollow slabs with concrete topping, *ACI Structural journal*, Vol. 88, No. 4, July-Aug. 1992, pp 402-410.

65. Yitzhaki, D., Punching strength of reinforced concrete slabs, *ACI Journal*, Vol.63, No.5, May 1966, pp527-540.

66. Zienkiewicz, O. C., and Taylor, R. L., *The finite element method*, 4ed, Volumn1: basic formulation and linear problems, McGraw-Hill, 1989.

67. Zienkiewicz, O. C., and Taylor, R. L., *The finite element method*, 4ed, Volumn2: solid and fluid mechanics, dynamics and non-linearity, McGraw-Hill, 1991.

68. EU10002, Part1.

69. Finite Element Analysis Limited, *The LUSAS user manual* (V 10), 1993

APPENDIX A

Calculation Sheets of calculating the punching capacity of model waffle slabs using the BS8110's method and the proposed Alternative Methods

1. Slab No. 1

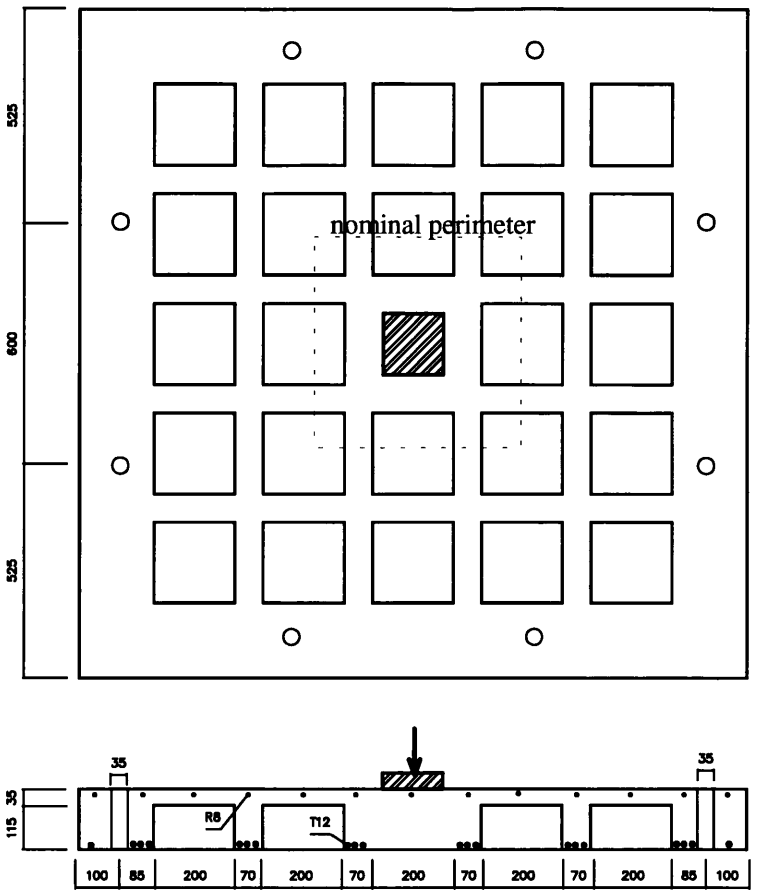

Layout of Slab No.1

f_{cu}:50.2 N/mm^2 ; load pad:150mm square; depth:150mm

BS8110

Method BS-One

The width of the nominal perimeter: B=150+3×125=525mm

Number of ribs intersected with the nominal perimeter: N=8

Effective depth of slab: 125mm; width of rib: 70mm

Total area of the ribs: S = 8 A_{rib} =70000mm^2

Flexural steel ratio: $\rho=A_s/(bd)=(3\times \pi \times 12^2/4)/(70\times 125)=3.88\%$

As the actual concrete strength and steel ratio exceed 40N/mm^2 and 3% respectively, they are taken as f_{cu}=40.0N/mm^2,ρ=3%

Nominal shear strength: $v_c = 0.79\sqrt[3]{3.0}\sqrt[3]{40/25}\sqrt[4]{400/125} = 1.782\,N/mm^2$

Punching Capacity: $P=Sv_c=124.8\,KN$

If not consider the limits on f_{cu} and ρ , there are

$v_c = 0.79\sqrt[3]{3.88}\sqrt[3]{50.21/25}\sqrt[4]{400/125} = 2.096\,N/mm^2$

$P=Sv_c=146.7\ KN$

Method BS-Two

As there are no stirrups, the results are the same as that of BS-one.

ALTERNATIVE METHODS

Method One

Total area of the ribs: $S_{rib}=8\,A_{rib}=8\times\ 70\times\ 125=70000\ mm^2$

Total area of deck: $S_{deck}=4\times\ ((525-2\times\ 70)\times\ 35)=53900mm^2$

Flexural steel ratio: $\rho\ =3\ (\pi\ 12^2/4)/(200\times\ 35+70\times\ 125)=339.3/15750=2.15\%$

Nominal shear strength: $v_c=0.79\sqrt[3]{2.15}\sqrt[3]{40/25}\sqrt[4]{400/125}=1.595\,N/mm^2$

Punching resistance of rib: $P_{rib}=S_{rib}v_c=70000\times\ 1.595=111.7\ KN$

Punching resistance of deck: $P_{deck}=S_{deck}v_c=53900\times\ 1.595=86.0\ KN$

Punching capacity of slab: $P=\ P_{rib}+P_{deck}=197.7\ KN$

If not considering limits on f_{cu} and ρ, then

$v_c=1.72N/mm^2$

$P=213KN$

Method Two

$S_{rib}=70000\ mm^2$

$S_{deck}=53900\ mm^2$

area of flexural steel: $A_s=3\ (\pi\ 12^2/4)=339.3\ mm^2$

ratio of flexural steel: $\rho\ =\dfrac{A_s}{d(a+b)}=\dfrac{339.3}{125\times(200+70)}=1.005\%$

nominal shear strength: $v_c=0.79\sqrt[3]{1.005}\sqrt[3]{40/25}\sqrt[4]{400/125}=1.236\,N/mm^2$

Punching resistance of rib: $P_{rib}=S_{rib}v_c=70000\times\ 1.236=86.5\ KN$

Punching resistance of deck: $P_{deck}=S_{deck}v_c=53900\times\ 1.236=66.6\ KN$

Punching capacity of slab: $P=\ P_{rib}+P_{deck}=153.1\ KN$

If not considering limits on f_{cu} and ρ, then

$v_c=1.33N/mm^2$

$P=165.1KN$

Method Three

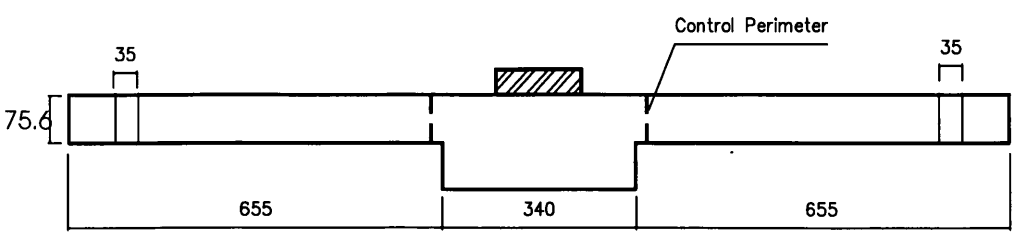

Section of the Affiine Slab

The coefficient: $n_1 = 1 - \frac{a^2(d-t)}{(a+b)^2 d} = 1 - \frac{200^2(125-35)}{(200+70)^2 125} = 0.605$

depth of the affine slab: $d_{aff} = n_1 d = 0.605 \times 125 = 75.62mm$

dimension of nominal perimeter: $B = C + 3d_{aff} = 150 + 3 \times 75.62 = 376.9mm$

area of the nominal perimeter: $S = 4(Bd_{aff}) = 4 \times 376.9 \times 75.62 = 113993mm^2$

Flexural steel area: $A_s = 6\frac{\pi 12^2}{4} = 678.6mm^2$

Flexural steel ratio: $\rho = \frac{A_s}{Bd_{aff}} = \frac{678.6}{376.9 \times 75.6} = 2.38\%$

The nominal shear strength: $\nu_c = 0.79\sqrt[3]{2.38}\sqrt[3]{40/25}\sqrt[4]{400/125} = 1.65N/mm^2$

Punching capacity of slab: $P = P_c = S\nu_c = 113993 \times 1.65 = 188.1KN$

If Neglecting Limit on f_{cu} and ρ, then

$\nu_c = 1.78N/mm^2$

$P = 202.9KN$

2. Slab No 2 ~ No.4

The calculation for slab No.2 ~ 4 are very similar to slabs No.1, the results were give in chapter 6.

5. Slab Five

f_{cu}: $56.6N/mm^2$; load pad: 150mm square; depth: 150mm

BS8110

Method BS-One

Two possible nominal punching perimeters are considered as shown in the figure; perimeter one cuts through the local solid area and perimeter intersects with 16 ribs.

The case of Perimeter 1:

Dimension of the perimeter: $B = 150 + 3 \times 125 = 525mm$

Section area: $S = 4 \times (a+2b)d = 4 \times (200 + 2 \times 70) \times 125 = 170000mm^2$

Flexural steel area: $A_s = 5 \times \pi \times 12^2/4 = 565.5mm^2$

Flexural steel ratio: $\rho = A_s/((a+2b)d) = 565.5/((200+2 \times 70) \times 125) = 1.331\%$

As the actual concrete strength exceeds limit, take $f_{cu} = 40.0N/mm^2$

Nominal shear strength: $\nu_c = 0.79\sqrt[3]{1.331}\sqrt[3]{40/25}\sqrt[4]{400/125} = 1.359N/mm^2$

Punching Capacity: $P = S\nu_c = 231.1KN$

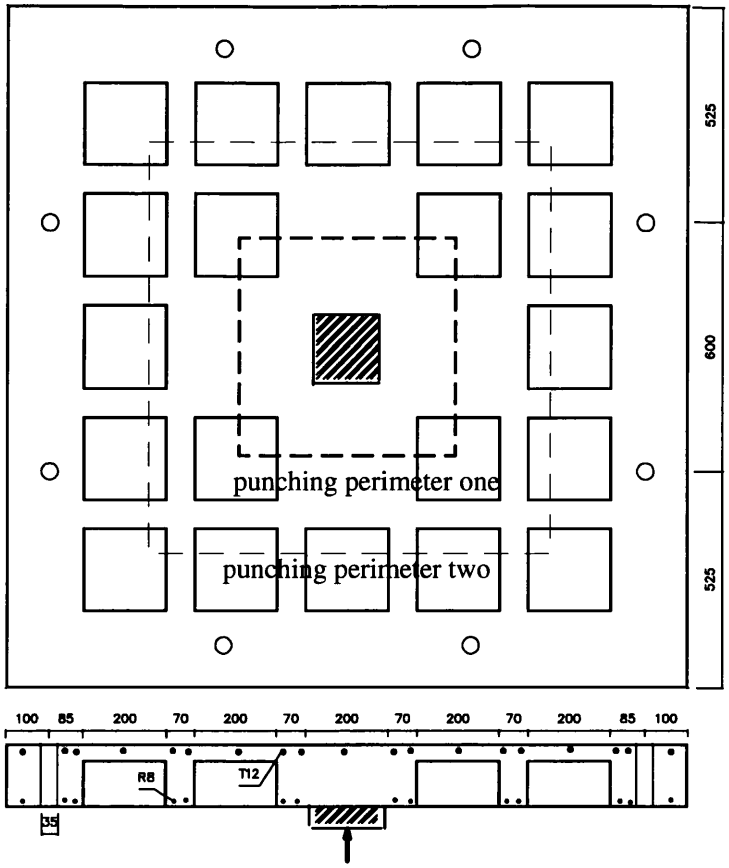

Layout of Slab Five

The case of Perimeter 2:
The width of the nominal perimeter: *B=880mm*
Number of ribs intersected with the nominal perimeter: N=16
Effective depth of slab: 125mm; width of rib: 70mm
Total area of the ribs: S = 16 A_{rib} =140000mm^2
Flexural steel ratio: $\rho=A_s/(bd)=(3\times \pi \times 12^2/4)/(70\times 125)=3.88\%$
As the actual concrete strength and steel ratio exceed 40N/mm^2 and 3% respectively, they are taken as $f_{cu}=40.0$N/mm^2,ρ=3%
Nominal shear strength: $v_c = 0.79\sqrt[3]{3.0}\sqrt[3]{40/25}\sqrt[4]{400/125} = 1.782\,N/mm^2$
Punching Capacity: $P=Sv_c=249.5\ KN > 231.1\ KN$

So the Punching Capacity: *P=231.1 KN*

If not consider the limits on f_{cu} and ρ , there are
$\upsilon_c = 0.79\sqrt[3]{1.331}\sqrt[3]{56.6/25}\sqrt[4]{400/125} = 1.526\,N/mm^2$
$P=Sv_c=259.4\ KN$

Method BS-Two
As there are no stirrups, the results are the same as that of BS-one.

ALTERNATIVE METHODS

Method One

Determine the area of the nominal perimeter:

Total area of solid section: $S_{solid}=4(a+2b)d=4\times\ (200+2\times\ 70)\times\ 125=170000mm^2$

deck area: $S_{deck}= 4\times(185\times35)=25900mm^2$

area of flexural steel: $A_s= 5\ (\pi\ \ 12^2/4) = 565.5\ mm^2$

one side area of the section: $A_T= (200+2\times\ 70)\times\ 125+ 185\times\ 35 =48975mm^2$

$\rho\ = A_s/A_T = 565.5/48975=1.155\%$

$\nu_c = 0.79\sqrt[3]{1.155}\sqrt[3]{40/25}\sqrt[4]{400/125} = 1.30\ N/mm^2$

Shear resistance of solid part: $P_{solid} = S_{solid}\nu_c = 170000\times\ 1.30 = 220.4\ KN$

Shear resistance of solid part: $P_{deck}= S_{deck}\nu_c = 25900\times\ 1.30 = 33.6\ KN$

Punching capacity of the slab: $P = P_{rib}+P_{top}= 254\ KN$

If neglecting Limit on f_{cu} and ρ, then

$\nu_c=1.46N/mm^2$

$P=258.2KN$

Method Two

$S_{solid}= 4(a+2b)d = 4\times\ (200+2\times\ 70)\times\ 125 = 170000\ mm^2$

$S_{deck}= 4\times\ (185\times\ 35) = 25900mm^2$

$A_s= 5\ (\pi\ \ 12^2/4) = 565.5\ mm^2$

$A_R= B\ d = 525\times\ 125 = 65625\ mm^2$

$\rho\ = A_s/A_R = 565.5/65625 = 0.86\%$

$\nu_c = 0.79\sqrt[3]{0.86}\sqrt[3]{40/25}\sqrt[4]{400/125} = 1.175\ N/mm^2$

$P_{solid}= S_{rib}\nu_c = 170000\times\ 1.175 = 199.8\ KN$

$P_{deck}=S_{deck}\nu_c = 25900\times\ 1.175 = 30.4\ KN$

$P = P_{rib}+P_{top}= 230.2\ KN$

If neglecting Limit on f_{cu} and ρ, then

$\nu_c=1.32N/mm^2$

$P=258.4KN$

Method Three

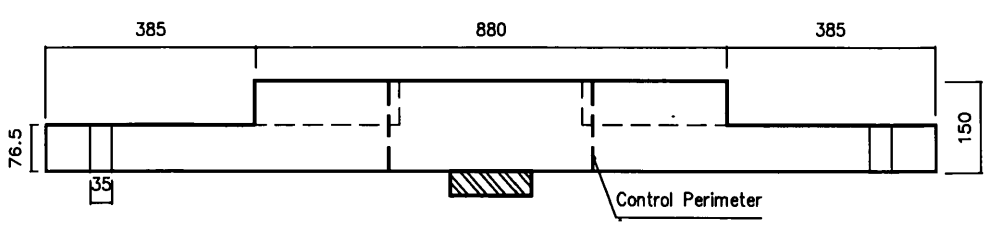

Section of the Affine Slab

$$n_1 = 1 - \frac{a^2(d-t)}{(a+b)^2 d} = 1 - \frac{200^2(125-35)}{(200+70)^2 125} = 0.605$$

$$d_{aff} = n_1 d = 0.605 \times 125 = 75.62mm$$

As this is the slab with local solid, the depth of the solid part is used to calculate the side dimension and the area of the control perimeter

$$B = C + 3d = 150 + 3 \times 125 = 525mm$$

$$S_{solid} = 4((a+b)d) = 4 \times (340 \times 125) = 170000mm^2$$

$$S_{deck} = 4((B-(a+b))d_{aff}) = 4 \times ((525-340) \times 75.6) = 55944mm^2$$

$$S = S_{solid} + S_{top} = 225944mm^2$$

The steel area and steel ratio inside the control perimeter

$$A_s = 5\frac{\pi 12^2}{4} = 565.5mm^2$$

$$\rho = \frac{A_s}{Bd} = \frac{565.5}{340 \times 125} = 1.33\%$$

$$\nu_c = 0.79\sqrt[3]{1.33}\sqrt[3]{40/25}\sqrt[4]{400/125} = 1.36N/mm^2$$

$$P = P_c = S\nu_c = 225944 \times 1.36 = 307.3KN$$

If neglect limit on f_{cu}, then

ν_c=*1.53N/mm²*

P=345.0KN

3. Slab No 6

The calculation for slab No.6 are very similar to slabs No.5, the results were give in chapter 6.

4. Slab No 7

f_{cu}:$31.2N/mm^2$; load pad:150mm square; depth:150mm

Using BS8110

Method BS-One

The width of the failure perimeter: *B=150+3× 125=525mm*

Number of ribs intersected with the perimeter; *N=8*

Total nominal area of shear: $S = 8A_{rib} = 70000mm^2$

Flexural steel ratio: $\rho = A_s/(bd) = (3 \times \pi \times 12^2/4)/(70 \times 125) = 3.88\%$

As the actual steel ratio exceeds 3%, take ρ=3%

Nominal shear strength: $\upsilon_c = 0.79\sqrt[3]{3.0}\sqrt[3]{31.2/25}\sqrt[4]{400/125} = 1.64\,N/mm^2$

Shear resistance of concrete: $P_c = S\nu_c = 70000 \times 1.64 = 114.8\,KN$

Section area of a leg: $a_{sv} = \pi\ 6^2/4 = 28.27mm^2$

There are 40 legs of link inside the control perimeter, of which 28 are reasonably in effect to carry the load, the others are too close to the load pad, so

n=28

Link strength: f_{sv}= *250 N/*mm^2
Shear resistance of stirrups: $P_{sv} = nf_{yv}a_{sv} = 28\times250\times28.27 = 197.9\,KN$
Punching Capacity of slab: $P=P_c+P_{sv}=114.8+197.9=312.7\ KN$
$P_{sv}/P = 63.3\%;\ P_c/P = 36.7\%$

if not considering the limit onρ ;
$\upsilon_c = 0.79\sqrt[3]{3.88}\sqrt[3]{31.2/25}\sqrt[4]{400/125} = 1.788\,N/mm^2$
Shear resistance of concrete: $P_c = S\,\nu_c = 70000\times\ 1.788 = 125.2\ KN$
Punching Capacity of slab: $P=P_c+P_{sv}=125.2+197.9=323.1\ KN$

check the ultimate strength:
$\nu_{max} = P/U_o d = 271.6\times10^3/((4\times150)\times125) = 3.62\,N/mm^2 < 0.8\sqrt{31.2}and5.0\,N/mm^2$
OK

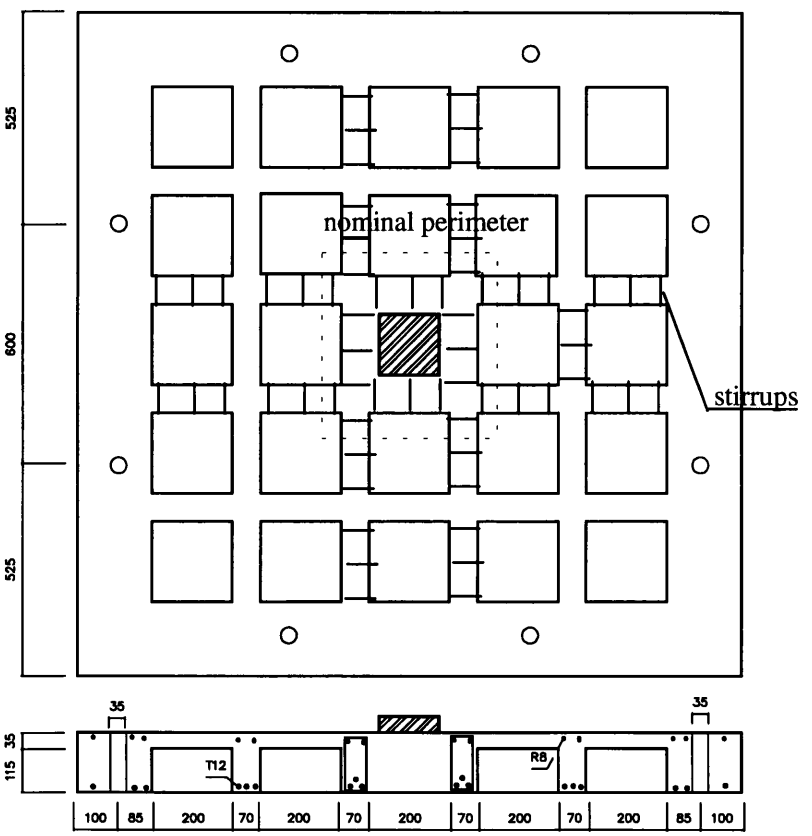

Layout of Slab Seven

Method BS-Two
Shear resistance of concrete: $P_c = S\,\nu_c = 70000\times\ 1.64 = 114.8\ KN$
Cross section area of a stirrup: $A_{sv} = 2\times\ \pi\ 6^2/4 = 56.55$mm^2
Space between stirrups: $l_{sv} = 90\ m$
Strength of stirrups: f_{sv}= *250 N/*mm^2
Nominal link shear strength provided by stirrups:
$\upsilon_{sv} = A_{sv}f_{sv}/(b\,s_v) = 56.55\times\ 250/(70\times\ 90) = 2.24$ *N/*mm^2

Shear resistance of stirrups: $P_{sv} = S \cdot a_{sv} = 70000 \times 2.24 = 156.8\,KN$
Punching Capacity of slab: $P=P_c+P_{sv}=114.8+156.8=271.6\ KN$

If not considering the limit on ρ, there are
$\upsilon_c = 0.79\sqrt[3]{3.88}\sqrt[3]{31.2/25}\sqrt[4]{400/125} = 1.788\,N/mm^2$
Shear resistance of concrete: $P_c = S\,\nu_c = 70000 \times 1.788 = 125.2\ KN$
Punching Capacity of slab: $P=P_c+P_{sv}=125.2+156.8=282.0\ KN$

ALTERNATIVE METHOD

Method One

Dimension of the nominal perimeter: $B = C + 3d = 525\ mm$
Cross section area of ribs: $S_{rib} = 8\,A_{rib} = 8 \times 70 \times 125 = 70000\ mm^2$
Width of deck in one dimension: $B_{deck} = B - 2b = 525 - 2 \times 70 = 385\ mm$
Cross section area of deck: $S_{deck} = 4(B_{top}\,t) = 4 \times (385 \times 35) = 53900 mm^2$
$A_T = a \cdot t + b \cdot d = 200 \times 35 + 70 \times 125 = 15750 mm^2$
$A_s = 3\,(\pi\ 12^2/4) = 339.3\ mm^2$
$\rho = A_s/A_T = 339.3/15750 = 2.15\%$
$\nu_c = 0.79\sqrt[3]{2.15}\sqrt[3]{31.2/25}\sqrt[4]{400/125} = 1.468\,N/mm^2$
$\upsilon_{sv} = A_{sv}f_{sv}/(b\,l_{sv}) = 56.55 \times 250/(70 \times 90) = 2.24\ N/\text{mm}^2$
$P_{rib} = S_{rib}(\nu_c + \upsilon_{sv}) = 70000 \times 3.71 = 259.6\ KN$
$P_{deck} = S_{deck}\nu_c = 53900 \times 1.468 = 79.1\ KN$
$P = P_{rib} + P_{top} = 338.7\ KN$

The results of neglecting limit on f_{cu} and ρ is the same as above.

Method Two

$$\rho = \frac{A_s}{d(a+b)} = \frac{339.3}{125 \times (200+70)} = 1.005\%$$

$\nu_c = 0.79\sqrt[3]{1.005}\sqrt[3]{31.2/25}\sqrt[4]{400/125} = 1.139\,N/mm^2$
$\upsilon_{sv} = A_{sv}f_{sv}/(b\,s_v) = 56.55 \times 250/(70 \times 90) = 2.24\ N/\text{mm}^2$
Punching capacity
$P_{rib} = S_{rib}(\nu_c + \upsilon_{sv}) = 70000 \times 3.379 = 236.6\ KN$
$P_{deck} = S_{deck}\nu_c = 53900 \times 1.139 = 61.4\ KN$
$P = P_{rib} + P_{top} = 298\ KN$

The results of neglecting limit on f_{cu} and ρ is the same as above.

Method Three

The affinity solid slab is shown below,

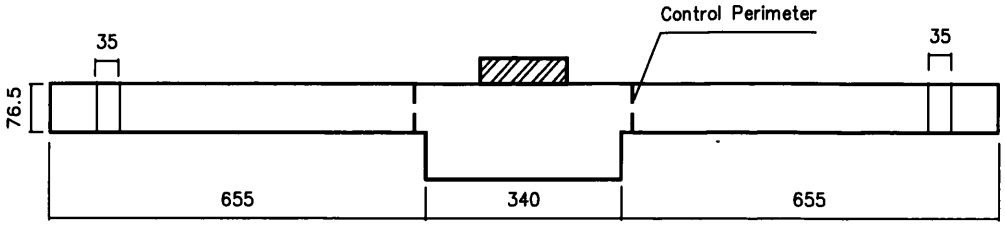

Section of the Affinity Slab

The coefficient: $n_1 = 1 - \frac{a^2(d-t)}{(a+b)^2 d} = 1 - \frac{200^2(125-35)}{(200+70)^2 125} = 0.605$

Depth of the affine slab: $d_{aff} = n_1 d = 0.605 \times 125 = 75.62mm$

The side dimension and the area of the control perimeter are

Dimension of the nominal perimeter: $B = C + 3d_{aff} = 150 + 3 \times 75.62 = 376.9mm$

Nominal shear resistance area: $S = 4(Bd_{aff}) = 4 \times 376.9 \times 75.62 = 113993mm^2$

The steel area and steel ratio inside the control perimeter

Cross section area of flexural reinforcement: $A_s = 6\frac{\pi 12^2}{4} = 678.6mm^2$

Steel content: $\rho = \frac{A_s}{Bd_{aff}} = \frac{678.6}{376.9 \times 75.6} = 2.38\%$

The nominal shear strength: $v_c = 0.79\sqrt[3]{2.38}\sqrt[3]{31.7/25}\sqrt[4]{400/125} = 1.52N/mm^2$

The concrete resistance: $P_c = Sv_c = 113993 \times 1.52 = 173.1KN$

There are totally 40 legs of link inside the control perimeter, of which 16 are reasonably to be effective, N=16

The shear resistance of the stirrups: $P_{sv} = 16A_s f_{yv} = 16 \times 28.27 \times 250 = 113.1KN$

The total shear capacity: $P = P_c + P_{sv} = 173.1 + 113.1 = 286.2KN$

The result of neglecting Limit on f_{cu} and ρ is the same as above.

5. Slab No. 8

f_{cu}:31.2 N/mm^2 ; load pad:150mm square; depth:150mm

BS8110

Method BS-One

Dimension of the failure perimeter: B=150+3×125=525mm

4 ribs intersect with the nominal perimeter: N=4

Nominal shear resistance area: $S = 4A_{rib} = 4 \times 70 \times 125 = 35000mm^2$

$\rho = A_s/(bd) = (3 \times \pi \times 12^2/4)/(70 \times 125) = 3.88\%$

As the actual steel ratio exceeds 3%, take $f_{cu} = 31.2N/mm^2$, ρ=3%

$v_c = 0.79\sqrt[3]{3.0}\sqrt[3]{31.2/25}\sqrt[4]{400/125} = 1.64N/mm^2$

Shear resistance of concrete: $P_c = S v_c = 35000 \times 1.64 = 57.4KN$

Cross section area of a leg: $a_{sv} = \pi \ 6^2/4 = 28.27 \text{mm}^2$
There are 24 legs of link inside the control perimeter, of which 16 are reasonably in effect to carry the load, so
n=16
Strength of stirrups: $f_{sv} = 250\ N/\text{mm}^2$
Shear resistance of the stirrups: $P_{sv} = nf_{sv}a_{sv} = 16 \times 250 \times 28.27 = 113.1 KN$
Punching Capacity: $P=P_c+P_{sv}=57.4+113.1=170.5\ KN$

Check the ultimate strength:
$\nu_{max} = P/U_o d = 170.5 \times 10^3/(4 \times 70 \times 125) = 4.87\ N/mm^2 \approx 0.8\sqrt{31.2} and < 5.0\ N/mm^2$
OK

if not considering the limit on ρ, there are
$\rho = A_s/(bd) = (3 \times \pi \times 12^2/4)/(70 \times 125) = 3.88\%$
$\upsilon_c = 0.79\sqrt[3]{3.88}\sqrt[3]{31.2/25}\sqrt[4]{400/125} = 1.788\ N/mm^2$
Shear resistance of concrete: $P_c = S\nu_c = 35000 \times 1.788 = 62.6\ KN$
Punching Capacity: $P=P_c+P_{sv}=62.6+113.1=175.7\ KN$

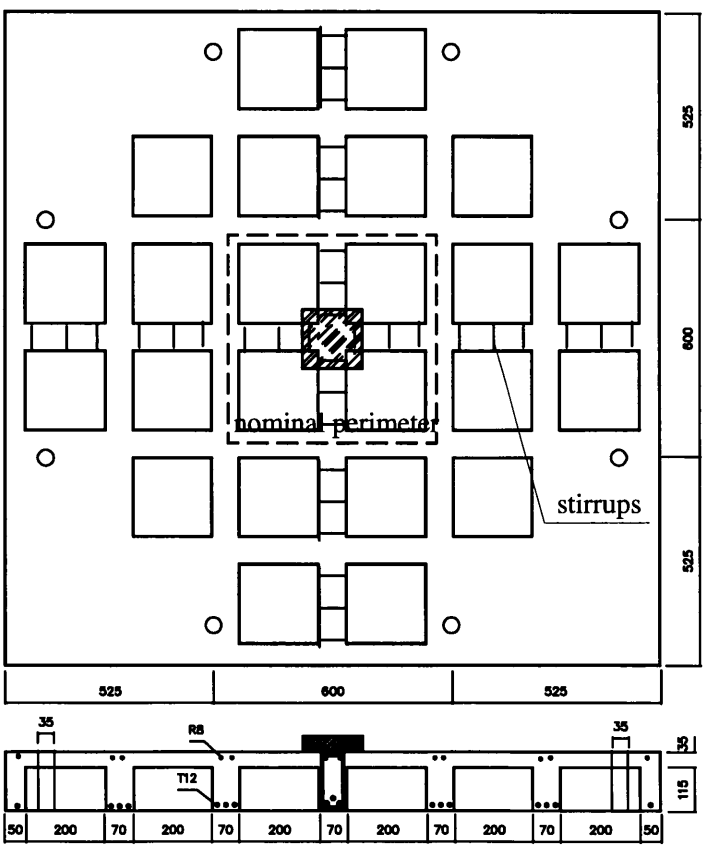

Layout of Slab Eight

Method BS-Two
Dimension of the nominal perimeter: $B = C + 3d = 525\ mm$

Area of ribs: $S_{rib}= 4A_{rib} = 4\times\ 70\times\ 125 = 35000\ mm^2$
Dimension of deck cut by the nominal perimeter: $B_{deck}= B - b = 525 -70 = 455\ mm$
Section Area of deck: $S_{deck}= 4(B_{deck}\ t) = 4\times\ (455\times\ 35) = 63700\ mm^2$
$A_s= 3\ (\pi\ \ 12^2/4) = 339.3\ mm^2$
$A_T=a\cdot t+b\cdot d= 200\times35+70\times125 = 15750 mm^2$
$\rho\ = A_s/A_T=339.3/15750=2.15\%$
$\nu_{\ c} = 0.79\sqrt[3]{2.15}\sqrt[3]{31.2/25}\sqrt[4]{400/125} = 1.468\ N/mm^2$
Section area of a stirrup: $A_{sv} = 2\times\ \pi\ \ 6^2/4 = 56.55\text{mm}^2$
Space between stirrups: $s_{sv} = 90\ mm$
Strength of stirrups: $f_{sv}= 250\ N/\text{mm}^2$
Nominal shear strength provided by stirrups:
$\upsilon_{\ sv}= A_{sv}f_{sv}\ /\ (b\ s_{sv}) = 56.55\times\ 250\ /(70\times\ 90)=2.24\ N/\text{mm}^2$
Shear resistance of ribs: $P_{rib} = S_{rib}(\nu_{\ c}+\upsilon_{\ sv})= 35000\times\ 3.71 = 129.8\ KN$
Shear resistance of deck: $P_{deck}=S_{deck}\nu_{\ c} = 63700\times\ 1.468 = 93.5\ KN$
Shear capacity of slab: $P = P_{rib}+P_{top}= 223.3\ KN$

The result of neglecting limit on f_{cu} and ρ is the same as above.

ALTERNATIVE METHODS

Method One

$B = C + 3d =525\ mm$
$S_{rib}= 4\ A_{rib} = 8\times\ 70\times\ 125 = 35000\ mm^2$
$B_{deck}= B - b = 525 - 70 = 455\ mm$
$S_{deck}= 4(B_{deck}\ t) = 4\times\ (455\times\ 35) = 63700\ mm^2$
$A_s= 3\ (\pi\ \ 12^2/4) = 339.3\ mm^2$
$A_T = a\cdot t+b\cdot d = 200\times35+70\times125 = 1570 mm^2$
$\rho\ = \dfrac{A_s}{A_T} = \dfrac{339.3}{15750} = 2.15\%$
$\nu_{\ c}= 0.79\sqrt[3]{2.15}\sqrt[3]{31.2/25}\sqrt[4]{400/125} = 1.468\ N/mm^2$
$\upsilon_{\ sv}= A_{sv}f_{sv}\ /\ (b\ s_v) = 56.55\times\ 250\ /(70\times\ 90)=2.24\ N/\text{mm}^2$
Shear resistance of the ribs: $P_{rib} = S_{rib}(\nu_{\ c}+\upsilon_{\ sv}) = 35000\times\ 3.71 = 129.8\ KN$
Shear resistance of deck: $P_{deck}=S_{deck}\nu_{\ c} = 63700\times\ 1.468 = 93.5\ KN$
Punching shear capacity of the slab: $P = P_{rib}+P_{top}= 223.3\ KN$

The result of neglecting limit on f_{cu} and ρ is the same as above.

Method Two

$B = C + 3d =525\ mm$
$S_{rib}= 4\ A_{rib} = 8\times\ 70\times\ 125 = 35000\ mm^2$
$B_{deck}= B - b = 525 - 70 = 455\ mm$
$S_{deck}= 4(B_{deck}\ t) = 4\times\ (455\times\ 35) = 63700\ mm^2$
$A_s= 3\ (\pi\ \ 12^2/4) = 339.3\ mm^2$
$\rho\ = \dfrac{A_s}{d(a+b)} = \dfrac{339.3}{125\times(200+70)} = 1.005\%$

$\nu_c = 0.79\sqrt[3]{1.005}\sqrt[3]{31.2/25}\sqrt[4]{400/125} = 1.139\ N/mm^2$

$\upsilon_{sv} = A_{sv}f_{sv}/(b\,s_v) = 56.55\times\ 250/(70\times\ 90) = 2.24\ N/mm^2$

Shear resistance of the ribs: $P_{rib} = S_{rib}(\nu_c + \upsilon_{sv}) = 35000\times\ 3.379 = 118.3\ KN$

Shear resistance of deck: $P_{deck} = S_{deck}\nu_c = 63700\times\ 1.139 = 72.6\ KN$

Punching shear capacity of the slab: $P = P_{rib} + P_{top} = 190.9\ KN$

The result of neglecting limit on f_{cu} and ρ is the same as above.

Method Two

The affinity solid slab is shown below.

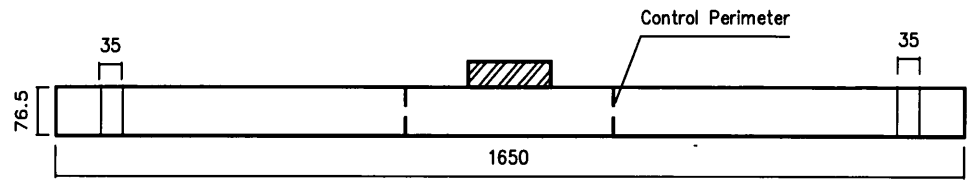

Section of the Affinity Slab

The coefficient: $n_1 = 1 - \dfrac{a^2(d-t)}{(a+b)^2 d} = 1 - \dfrac{200^2(125-35)}{(200+70)^2 125} = 0.605$

Depth of the affine slab: $d_{aff} = n_1 d = 0.605\times 125 = 75.62mm$

Dimension of the nominal perimeter: $B = C + 3d_{aff} = 150 + 3\times 75.62 = 376.9mm$

Nominal shear area: $S = 4(Bd_{aff}) = 4\times 376.9\times 75.62 = 113993mm^2$

$$A_s = 3\frac{\pi 12^2}{4} = 339.3mm^2$$

$$\rho = \frac{A_s}{Bd_{aff}} = \frac{339.3}{376.9\times 75.6} = 1.19\%$$

$$\nu_c = 0.79\sqrt[3]{1.19}\sqrt[3]{31.2/25}\sqrt[4]{400/125} = 1.21N/mm^2$$

The load contributed by concrete: $P_c = S\nu_c = 113993\times 1.21 = 138KN$

There are totally 16 legs of link inside the control perimeter, of which 8 are reasonably to be effective, N=8.

$P_{sv} = 8A_s f_{yv} = 8\times 28.27\times 250 = 56.5KN$

The total shear capacity: $P = P_c + P_{sv} = 138 + 56.5 = 194.5KN$

The result of neglecting limit on f_{cu} and ρ is the same as above.

5. Slab No. 9~12

Following the similar procedures, the calculation have been done for slabs No. 9~12. The results are listed in chapter 6.